UNIVERSIDAD AUTONOMA DE MADRID
Departamento de Bioquímica.

REGULACIÓN DE LA CADENA DE TRANSPORTE DE ELECTRONES BAJO CONDICIONES DE HIPOXIA

Eduardo Balsa Martínez

Madrid, 2012

Departamento de Bioquímica.
Facultad de Medicina
UNIVERSIDAD AUTÓNOMA DE MADRID

REGULACIÓN DE LA CADENA DE TRANSPORTE DE ELECTRONES BAJO CONDICIONES DE HIPOXIA

Memoria presentada por Eduardo Balsa Martínez
Licenciado en Biología
para optar al Grado de Doctor

Dirigida por el Doctor
Manuel Ortiz de Landázuri

Madrid, 2012

El trabajo presentado en esta Tesis Doctoral ha sido realizado en el Servicio de Inmunología del Hospital Universitario de la Princesa, bajo la dirección del Dr. Manuel O. de Landázuri.

Dn. **Eduardo Balsa Martínez** ha desarrollado bajo mi dirección el trabajo titulado "**REGULACIÓN DE LA CADENA DE TRANSPORTE DE ELECTRONES BAJO CONDICIONES DE HIPOXIA**" en el Servicio de Inmunología del Hospital Universitario de la Princesa de Madrid. Por sus aportaciones a congresos y publicaciones, así como por su interés actual, estimamos este trabajo merecedor de ser aceptado como TESIS DOCTORAL, y autorizamos su presentación en el Departamento de Biología Molecular de la Facultad de Ciencias de la Universidad Autónoma de Madrid.

En Madrid, a 03 de Septiembre de 2012

Dr. Manuel O. de Landázuri

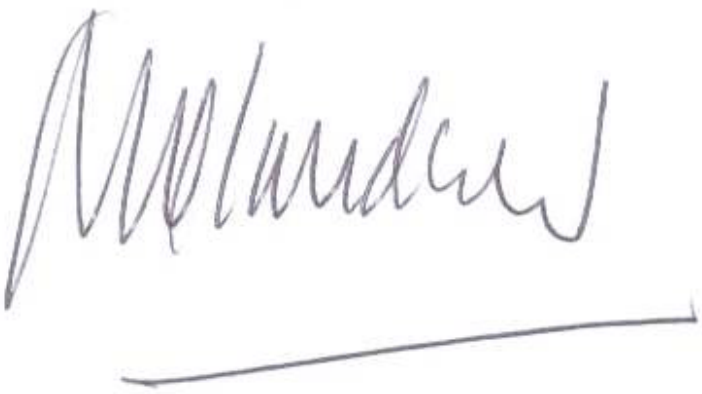

Catedrático de Inmunología de la U.A.

La primera gran virtud del hombre fue la duda y el primer gran defecto la fe **(Carl Sagan**

Agradecimientos

Agradecimientos:

Quizás esta tendría que ser la parte más larga de la tesis a causa de la infinidad de gente que me ha ayudado, directa o indirectamente, en la realización de ésta. Lamentablemente el espacio es limitado.

Gracias a Manolo por la oportunidad de unirme a su grupo y empezar a dar mis primeros pasos en el ámbito científico. Me ha apoyado y ha confiado en mi en todo momento, lo cual le hace merecedor de todo mi respeto.

Gracias a Toño, porque me acogió en su grupo como si fuese uno más. Su aportación a este trabajo, en forma de ideas, consejos y motivación ha sido superlativo. Le agradezco lo mucho que me ha ayudado a madurar profesionalmente

Muchísimas gracias a Dani. Con el fue con quien compartí mis primeras experiencias en ciencia. Le deseo de todo corazón una pronta y total recuperación, el es una de las personas que ha hecho posible que yo haya llegado hasta aquí. Muchas gracias Dani.

Gracias a Ángel, Esther y Bárbara, mis compis de "cafecito". Ellos también han supuesto una gran ayuda que ha trascendido lo profesional. También a Ali, que siempre estaba dispuesta a ayudarme en lo que fuese. Gracias a mis coleguis de los labos vecinos, A la parejita; Inés y Ainara por su positivismo y buen humor y también por soportarme día a día. A "pimpollita", la persona más buena que jamás he conocido, no cambies. A Elia, Ali izq, Elena, Cris, Pablo y Andrea, ese grupito molón de high-gueto.

Agradecer a los "cecilios" y a la propia Ceci, porque ahí es donde empezó todo. Gracias a los Resis; Carlos, por todas las aventuras que hemos vivido juntos, a Paco mi co-R, Dani, el desaparecido en Japón, a los nuevos mini-resis; Ali, Jorge, Alberto y todos los demás que quedan por llegar,,,Y por supuesto a Toñi, Pilar, Ana y Reyes que no me olvido de vosotras!

Gracias a Julián, Toño y Susana, también habéis sido de gran ayuda y os agradezco mucho vuestra aportación. Muchas dudas hubiesen quedado sin respuesta si no llega a ser por vosotros.

Gracias a los "Pacos" que siempre han estado ahí para lo que fuese, a Javi, Fran, Giulia, Cris, Hortensia, Manolo, Esteban….y muchos otros.

Gracias también a los que nos han dejado; Alfonso, Kostas, Gema, Silvia y María los cuales intuyo que se fueron para no aguantarme más.

Gracias a mi "otro" grupo, los CNICeros. Gracias a Richard, que hubiese hecho sin el, gracias por tu ayuda, consejos y mil cosas más. Gracias a las chicas; a Ana, porque es la única que se reía de mis chistes malos, a Adela, esa rubia que algún día cambiara el mundo para mejor, a

Rebe, que es el buen rollo hecho persona, a Ester, que me ayudo mucho en mis inicios con los BN, a Carmen, Marta, Andrés y demás “Genosfitos”

Gracias a los compis del “master”; Dani, Alejo, Ine, Cris, Miguel,..etc, por todas esas risas y discusiones cienti-frikis, sois unos cracks!

Por supuesto, muchísimas gracias a mi familia y sobre todo a mi madre, porque ella siempre confió en mi y me ha dado su total apoyo en mis decisiones, gracias MAMA!!!

Resumen

Resumen:

La regulación de la función mitocondrial ha resultado ser una adaptación fundamental a las fluctuaciones en las tensiones de oxígeno. Durante la hipoxia, las células activan un cambio metabólico que favorece la obtención de energía gracias a la glucólisis y atenúa la actividad mitocondrial. En este trabajo hemos identificado una nueva diana de HIF, el gen *NDUFA4L2* (NADH dehydrogenase [ubiquinone] 1 alpha subcomplex, 4-like 2). Nuestros resultados, obtenidos empleando silenciamientos de dicho gen y sirviéndonos de fibroblastos embrionarios murinos provenientes de ratones knockout para este gen, indican claramente que la inducción de NDUFA4L2 en hipoxia atenúa el consumo de oxígeno mitocondrial a través de la inhibición de la actividad del Complejo I de la cadena de transporte de electrones (ETC) , lo cual limita la producción intracelular de especies reactivas de oxígeno (ROS) en hipoxia. Así pues, la reducción en la actividad de la ETC parece ser un requisito esencial de la reprogramación que pone en marcha el factor de trascripción HIF bajo condiciones de escasez de oxigeno.

La continuación del trabajo se ha centrado en el *NDUFA4*, gen considerado parálogo a *NDUFA4L2*. Hemos descubierto que NDUFA4, el cual se pensaba era un componente del Complejo I, es en realidad un componente del Complejo IV. Análisis proteómicos, genéticos bioquímicos y evolutivos han revelado que NDUFA4 juega un papel indispensable en la función y biogénesis del Complejo IV.

Summary

The fine regulation of mitochondrial function has proved to be an essential metabolic adaptation to fluctuations in oxygen availability. During hypoxia, cells activate an anaerobic switch that favors glycolysis and attenuates the mitochondrial activity. This switch involves the hypoxia-inducible transcription factor-1 (HIF-1). We have identified a HIF-1 target gene, the mitochondrial NDUFA4L2 (NADHdehydrogenase [ubiquinone] 1 alpha subcomplex, 4-like 2). Our results, obtained employing NDUFA4L2-silenced cells and NDUFA4L2 knockout murine embryonic fibroblasts, indicate that hypoxia induced NDUFA4L2 attenuates mitochondrial oxygen consumption involving inhibition of Complex I activity, which limits the intracellular ROS production under low-oxygen conditions. Thus, reducing mitochondrial Complex I activity via NDUFA4L2 appears to be an essential element in the mitochondrial reprogramming induced by HIF-1.

We have continued the work focusing on NDUFA4, which is paralog of NDUFA4L2. Here, we show that NDUFA4, formerly considered a constituent of *NADH Dehydrogenase* (CI), is a component of the *Cytochrome c oxidase* (CIV). Proteomic, genetic, evolutionary and biochemical analyses reveal that NDUFA4 plays a role in CIV function and biogenesis, while its deletion does not perturb CI.

Abreviaturas

Abreviaturas:

Las abreviaturas corresponden a definiciones en inglés y se han mantenido para conservar la nomenclatura estándar.

AB: Acrilamida:Bisacrilamida
Acetil CoA: Acetil coenzima A
ADP: Adenosín difosfato
ATP: Adenosin-trifosfato
ATPasa: ATP sintetasa
BN: "Blue Native"
BNGE: Electroforesis en gel de "Blue Native"
ARNT: *Aryl Hydrocarbon Receptor Nuclear Translocator*. Translocador nuclear del receptor para aril hidrocarburos
bHLH: *Basic-Helix-Loop-Helix,* Motivo estructural de interacción proteína-proteína y proteína-ADN formado por un dominio básico seguido de hélice-bucle-hélice.
CI: Complejo I
CII: Complejo II
CIII: Complejo III
CIV: Complejo IV
CV: Complejo V
CAD: *C-terminal Transactivation Domain*, Dominio C-terminal de Transactivación.
ChIP: *chromatin immunoprecipitation,* Inmunoprecipitación de cromatina
CNS: *Conserved non-codind sequence,* Secuencia conservada no codificante
CREB: *cyclic AMP Response Element-Binding protein,* Proteína de unión a
CoQ: Coenzima Q
CoQ10: Coenzima Q10
COX: Citoctromo C oxidasa
CS: Citrato sintasa
Cyt b: Citocromo b
Cyt c: Citocromo c
DCF: Diclorofluoresceina
DCFH: Diclorofluorescina

DCFH2-DA: Dihidrodicluorofluoresceína diacetato

DDM: Dodecilmaltósido

DMOG: dimetil-oxo-glutarato

DMSO: Dimetilsulfóxido

DNA: Acido Desoxirribonucleico

- cDNA: Cadena codificante del DNA

- mtDNA: DNA mitocondrial

- nDNA: DNA nuclear

dNTP: Desoxinucleótido trifosfato

(d)SFB: Suero Fetal Bovino (dializado)

EGLN: *EGL [egg laying defective (Caenorhabditis elegans gene)] nine homologous protein*

EPAS: *Endothelial PAS protein,* Proteína con dominio PAS (Per-ARNT-Sim) expresada en endotelio.

EPO: *Erythropoietin*, Eritropoyetina.

FADH2: Dinucleótido de Favina y Adenina reducido

Fe-S: Grupo sulfoférrico

FMN: Mononucleótido de Flavina

FIH: *Factor Inhibiting HIF-1*, Factor inhibidor de HIF-1.

G3P: Glicerol-3-fosfato

GLUT-1: *Glucose transporter-1*, Transportador de glucosa 1.

GSK: *Glycogen synthase kinase*, Kinasa de la glucógeno sintasa.

HIF: *Hypoxia-inducible factor*, Factor inducible por hipoxia.

HRE: *Hypoxia- response element,* Elemento de respuesta a Hipoxia.

IPAS: *Inhibitory PAS Domain Protein*, Proteína inhibidora que contiene el dominio PAS.

kDa: Kilodalton

KO: *Knock-out*.

KP: Tampón fosfato potásico

LDH: *lactate deshidrogenase,* lactato deshidrogenasa

MAPK: mitogen-activated protein kinase

Mt: Mitocondria

NAD: *N-terminal Transactivation Domain*, Dominio N-terminal de Transactivación.

NAD+: Dinucleótido de nicotinamina y adenina

NADH: NAD+ reducido

NO: *Nitric oxide*, Óxido nítrico.

ODD: *Oxygen-dependent degradation domain*, Dominio de degradación dependiente de oxígeno.

OAA: Oxalacetato

8-OHDG: 8-hidroxiguanidina

OXPHOS: Fosforilación Oxidativa

PBS-T: PBS-tween

PCR: Reacción en cadena de la polimerasa

PDH: *pyruvate deshidrogenase,* piruvato deshidrogenasa

PDK: *pyruvate deshidrogenase kinase,* piruvato deshidrogenada kinasa

PTEN:Phosphatase and tensin homolog ()

PVDF: Fluoruro de polivinilideno

Q-RT-PCR: *Quantitative Real Time Polymerase Chain Reaction*. Reacción en cadena de la polimerasa a tiempo real, cuantitativa

RNA: Acido ribonucleico

- mRNA: RNA mensajero

- rRNA: RNA ribosómico

- tRNA: RNA de transferencia

RNS: Especies reactivas de nitrogeno

ROS: Especies reactivas de oxigeno

rpm: Revoluciones por minuto

SDH: Succinato Deshidrogenasa

SDS: Dodecilsulfato sódico

SDS-PAGE: Electroforesis en gel de poliacrilamida y SDS

SOD: Superóxido dismutasa

- Cu/ZnSOD: Superóxido dismutasa citoplasmática (Cu/Zn)

- MnSOD: Superóxido dismutasa mitocondrial (Mn)

TAD: *Transactivation Domain*, Dominio de Transactivación.

TEMED: N, N, N', N'-tetrametiletilendiamina

UCP: Proteina desacoplante (Uncoupling Protein)

UI: Unidades Internacionales

UV: Ultravioleta

VEGF: *Vascular Endothelial Growth Factor*, Factor de crecimiento del endotelio vascular

VHL: *von Hippel-Lindau protein,* Proteína codificada por el gen supresor de tumores causante del síndrome de von Hippel Lindau.

Indice

AGRADECIMIENTOS.....1
RESUMEN……..5
ABREVIATURAS……..……9
INDICE……..…15
INTRODUCIÓN…….……..19
1. El Oxígeno.……..…21
1.2 Oxígeno y Evolución
2. Hipoxia……..…….23
2.1 Hipoxia sistémica.
2.2 Hipoxia celular:
2.2.1 Factor de transcripción HIF.
2.2.1.1 Regulación de la estabilidad.
2.2.1.2 Regulación de la actividad transcripcional.
2.2.2 Sensores de oxígeno.
3. La mitocondria……...……28
3.1 El sistema de fosforilación oxidativa (OXPHOS):
3.1.1 El complejo I.
3.1.2 El complejo II.
3.1.3 El complejo III.
3.1.4 Complejo IV.
3.1.5 Complejo V.
3.2 Organización del sistema OXPHOS.
4. Mitocondria e Hipoxia……37
OBJETIVOS……..41
MATERIALES, MÉTODOS Y RESULTADOS.....45

Manuscrito 1: *Induction of the Mitochondrial NDUFA4L2 Protein by HIF-1a Decreases Oxygen Consumption by Inhibiting*

Complex I Activity……..……..47

Manuscrito 2: *NDUFA4 Is a Subunit of Complex IV of the Mammalian Electron Transport Chain*……81

Manuscrito 3: *Vhl Gene Inactivation Induces Cardiac HIF-Dependent Erythropoietin Gene Expresión*……..…101

Manuscrito 4: *Assembly of respiratory supercomplexes determines electron flux in the mitochondrial electron transport chain*……..……115

DISCUSIÓN……..……..……183

CONCLUSIONES……..……...193

BIBLIOGRAFÍA……197

Introducción

Introducción

1. El Oxígeno:

La palabra oxígeno proviene del griego ὀξύς, ácido, y -geno, de la raíz γεν, generar. Es un elemento químico de número atómico 8 y símbolo **O**. En su forma molecular más frecuente, O_2, es un gas a temperatura ambiente y representa aproximadamente el 20,9 % en volumen de la composición de la atmósfera terrestre actual.

La atmosfera terrestre no ha sido siempre tan abundante en oxígeno, es más, en su formación hace casi 4500 millones de años tenía unas características mucho mas reductoras. Hace 2400 millones de años se produjo un evento de oxigenación masiva en el planeta llevado a cabo por organismos unicelulares fotosintéticos que liberaron a la atmosfera grandes cantidades de oxígeno como producto de desecho metabólico. Después de que el oxígeno se incorporase y saturase los minerales fue aumentando lenta pero inexorablemente aumentando en la atmósfera durante los siguientes millones de años (figura 1). Esta acumulación de oxígeno desencadenó dos eventos se suma importancia; el primero, la oxidación del metano atmosférico (gas invernadero) a dióxido de carbono y agua, lo que provocó una glaciación de más de 300 millones de años. En segundo lugar, el aumento de los niveles de oxígeno proporcionó una nueva oportunidad para la diversificación biológica, así como enormes cambios en la naturaleza de las interacciones químicas entre las rocas, arena, arcilla y otros sustratos geológicos y el aire de la Tierra, los océanos y otras aguas superficiales.

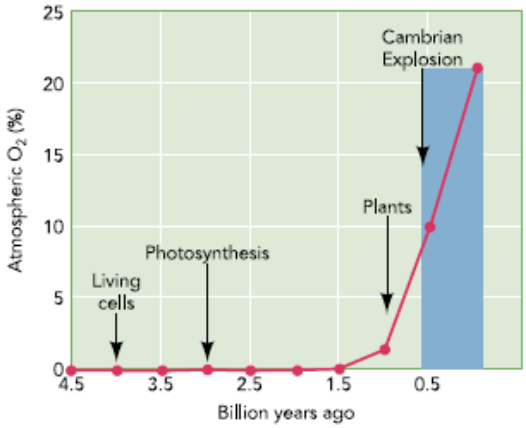

Figura 1. Niveles de oxígeno atmosférico durante la historia del planeta (Taylor & McElwain 2010).

1.2 Oxígeno y Evolución:

Los cambios en la composición de la atmósfera han estado asociados con eventos clave en la evolución de la vida en la Tierra, incluyendo el origen y la radiación de los metazoos, grandes extinciones y períodos de gigantismo vegetal y animal.

Inicialmente las altas concentraciones de oxígeno resultaron letales para la amplia mayoría de los organismos terrestres. Sin embargo, esto favoreció grupo más complejo de organismos, los eucariotas. Habiendo surgido de una simbiosis entre diferentes familias de antiguas bacterias, podían no solo soportar los efectos tóxicos del oxígeno sino también aprovechar su energía química para producir ATP de una forma mucho más eficiente que por metabolismo anaerobio.

A pesar de que la fotosíntesis en los océanos probablemente comenzó hace 3000 millones de años, no fue sino hasta hace 1000 millones de años cuando el oxígeno comenzó a acumularse significativamente en la atmosfera. Mientras que este oxígeno atmosférico continuo aumentando en los siguientes 1000 millones de años, la vida existente en la Tierra se mantuvo como simples organismos unicelulares. No fue hasta que se alcanzaron unos niveles entre el 15 y el 20% de oxígeno (hace 500-600 millones de años) cuando se empezaron a desarrollar los primeros animales y plantas y la evolución de los metazoos aumentó exponencialmente. Durante este periodo los metazoos progresaron desde simples especies acuáticas como esponjas de mar y corales a una gran diversidad de especies marinas y terrestres incluidos los *Homo sapiens*.

La alta disponibilidad de oxígeno llevó a la evolución de un increíble sistema de fosforilación oxidativa que transfería la energía química almacenada en los enlaces de carbono de las moléculas orgánicas al enlace rico en energía de la molécula de ATP, la cual es usada para catalizar la mayoría de las reacciones en los seres vivos. La energía producida por la respiración mitocondrial es suficiente para estimular el desarrollo y mantenimiento de los organismos pluricelulares, mientras que la energía producida solo por la glucólisis no sería suficiente.

Las dimensiones de las primitivas especies de metazoos eran suficientemente pequeñas para que el oxígeno pudiese difundir de la atmosfera a las miles de células del organismo, como en el caso del gusano *Caenorhabditis elegans*. Para escapar a esta limitación en el crecimiento, diversos sistemas evolucionaron para distribuir y

hacer llegar el oxígeno a todas las células del cuerpo. El último salto en la escala ocurrió en vertebrados con la aparición de un complejo sistema respiratorio, circulatorio y nerviosos diseñado, para de manera muy eficiente, capturar y distribuir el oxígeno a miles de millones de células.

2. Hipoxia

2.1 Hipoxia sistémica:

Aunque el control de la respiración en respuesta a bajadas en los niveles de oxígeno, se debe principalmente a la detección indirecta del aporte de oxígeno (medida de H^+ y CO2 en sangre en el sistema nervioso central), también existen órganos que responden directamente a la concentración de oxígeno en sangre. De este modo ante una bajada en la tensión de oxígeno en sangre, el organismo responde de forma aguda produciendo una depolarización de las células glómicas del cuerpo carotídeo con la consecuente liberación de dopamina, que actúa aumentando la frecuencia respiratoria y cardíaca. Así mismo, las células musculares de las arterias pulmonares se contraen en respuesta a bajadas en los niveles de oxígeno. Con ello, se consigue que la sangre se desplace de zonas poco oxigenadas del pulmón a zonas con un mayor nivel de oxígeno, asegurando de esta forma que los glóbulos rojos de la sangre se carguen de oxígeno de una manera óptima(Seta et al. 2002). Si el insulto hipóxico pasa a ser crónico, se producirá una respuesta caracterizada por una expresión génica. El organismo intentara aumentar los niveles de oxígeno en sangre, promoviendo tanto el transporte de hierro a los eritrocitos (mediante la inducción de la Transferrina y de su receptor) como el número de glóbulos rojos circulantes (mediante el aumento de producción de eritropoyetina por el riñón)(Jelkmann 1992). Además de estas medidas dirigidas a aumentar la concentración de oxígeno en sangre y mediada por tipos celulares concretos, la hipoxia crónica produce dos respuestas adaptativas generales en la mayoría de los tipos celulares afectados: Por un lado, se inducen genes clave de la ruta glucolítica, con el fin de mantener la producción de ATP (Firth et al. 1994) (Firth et al. 1995). Y por otra parte, se promueve la neovascularización, destinada a restablecer el flujo sanguíneo en las zonas afectadas, mediante la inducción de genes como el del factor de crecimiento vascular (VEGF) y el de su receptor (Flt-1) (Semenza 2000; Semenza 2001).

2.2 Hipoxia celular

Las células son capaces de sentir la insuficiencia en la disponibilidad de oxígeno y activar un cambio en la expresión génica que, o bien aumenta el aporte de oxígeno o promueve la supervivencia en un ambiente de escasez de oxígeno (hipoxia). En este proceso, existe un mecanismo altamente conservado desde el punto de vista evolutivo, que implica modificaciones prostraducionales dependientes de oxígeno en el factor inducible por hipoxia (HIF), llevadas a cabo por unas enzimas con actividad prolil hidroxilasas.

2.2.1 Factor de transcripción HIF:

La respuesta mejor caracterizada y más universal ante situaciones de hipoxia, es la activación de los factores de transcripción HIF (Kaelin & Ratcliffe 2008). HIF se expresa en todas las especies de metazoos existentes analizados hasta la fecha(Loenarz et al. 2011).

Estos factores, controlan la inducción dependiente de oxígeno de numerosos genes, uniéndose de manera específica a los elementos de respuesta a hipoxia (HRE), presentes en sus promotores. El factor de transcripción HIF es un heterodímero formado por una subunidad α (120 kDa) y otra β (91-94 kDa), también conocida como ARNT (Traslocador nuclear del receptor para aril hidrocarburos). Es un miembro de la familia de los factores de transcripción *basic helix-loop-helix* (bHLH)-PAS. Su región N-Terminal está evolutivamente conservada y presenta un dominio bHLH y otro dominio PAS (de alta homología con los factores **P**er, **A**RNT, **S**im) (Wang *et al.*, 1995), implicados tanto en la heterodimerización entre los miembros de la familia, como en la unión al DNA a través de residuos básicos presentes en su secuencia (Jiang et al. 1996). Además, presentan secuencias de localización nuclear (NLS) en ambos extremos. β Así mismo, la subunidad α presenta un dominio de degradación dependiente de oxígeno (ODD) que se encuentra solapando con N-TAD, y que media la estabilidad de HIF de una manera oxígeno dependiente(Pugh et al. 1997). Por otro lado, el C-TAD interactúa con el coactivador p300/CBP favoreciendo así la transcripción génica(Lando et al. 2002). Existen tres tipos de subunidades α:

·HIF-1, HIF-2 α o EPAS y HIF-3 α, estando codificadas por distintos genes y presentando una expresión diferencial en tejido(Wenger 2002).

2.2.1.1 Regulación de la estabilidad:

En normoxia la subunidad HIF- α es muy inestable, tiene una vida media de unos 5 minutos antes de ser ubiquitinada y degradada vía proteosoma. Sin embargo, en condiciones de hipoxia esta vida media se ve fuertemente incrementada(Huang et al. 1996). Existen dos regiones, dentro del dominio de degradación dependiente de oxígeno (ODD) de HIF- α, que son hidroxiladas por las prolil-hidroxilasas (PHD) en los residuos 402 y 564 de prolina en el caso de HIF-1a (405 y 531 en el caso de HIF-2 α) y reconocidas por el complejo VHL-E3 ubiquitina ligasa (Kamura et al. 1999; Jaakkola et al. 2001). En normoxia las subunidades HIF- α son hidroxiladas en los dos residuos específicos de prolina por las PHDs. Esta modificación post-traduccional a hidroxiprolinas permite el reconocimiento y unión de la proteína VHL, que poliubiquitina a HIF- α marcándolo para su posterior degradación vía proteosoma(Hon et al. 2002; Min et al. 2002; Kaelin & Ratcliffe 2008). La degradación de HIF- α puede tener lugar tanto en el núcleo como en el citoplasma(Berra et al. 2001). Sin embargo, en hipoxia, al no haber suficiente oxígeno, las PHDs no pueden realizar su función y VHL no puede unirse y ubiquitinar a la subunidad HIF- α, por lo que ésta se acumula, se transloca al núcleo y heterodimeriza con la subunidad HIF- β formando un complejo activo que se une a los elementos de respuesta a hipoxia (HRE) en los promotores de los genes diana de HIF. Curiosamente, entre estos genes diana se encuentran las PHDs, que se encargan de restablecer los niveles de HIF cuando las tensiones de oxígeno vuelven a la normalidad.

2.2.1.2 Regulación de la actividad transcripcional:

Hasta ahora hemos visto que la regulación de HIF por la hipoxia se debe a la estabilización de la subunidad α al disminuir los niveles de oxígeno. Sin embargo, tal y como ya se ha descrito, la subunidad HIF α posee dos dominios de transactivación, de los cuales, el dominio CAD está altamente conservado y su actividad transactivadora es inducida en hipoxia. Esta inducibilidad por la hipoxia se ha atribuido a una mayor capacidad del dominio CAD para unir p300 o CBP(Arany et al. 1996; Ebert & Bunn 1998). Ambas son proteínas homólogas que funcionan como coactivadoras de muchos factores de transcripición por su actividad histona acetiltransferasa (capaz de modificar la estructura de la cromatina, lo que facilita y

aumenta la actividad transcripcional de dichos factores) y su capacidad de reclutar la maquinaria basal de transcripción.

La unión de p300/CBP a HIF-α está también regulada por la hidroxilación de HIFα, pero esta vez en un residuo de asparragina. Esta asparragina, está localizada en el dominio CAD (la N803 en HIF-1α y la N851 en HIF-2α), y su hidroxilación impide la interacción de p300/CBP con dicho dominio. Esta hidroxilación es llevada a cabo por FIH, otra dioxigenasa dependiente de oxígeno, Fe^{2+} y de 2-oxoglutarato. Como ocurre con las EGLNs, la hipoxia disminuye considerablemente la actividad de FIH, permitiendo con ello la unión del coactivador p300/CBP. Y como consecuencia se produce un aumento en la actividad transcripcional de HIF(Hewitson et al. 2002; Lando et al. 2002). Es importante hacer notar que la hidroxilación en las prolinas promueve la interacción de HIFα con la proteína VHL, mientras que la hidroxilación en la asparragina impide la interacción con p300/CBP. Ambas hidroxilaciones tienen como objetivo regular negativamente HIFα, la primera promoviendo la degradación de la proteína y la segunda inhibiendo su actividad transcripcional.

En resumen, en hipoxia HIFα deja de ser hidroxilado en los residuos de prolina y asparragina, escapando a la degradación por la vía del proteosoma. HIFα estabilizado pasa al núcleo, donde interacciona con la subunidad β y el coactivador p300/CBP. Este complejo, reconoce secuencias específicas de ADN, dentro de las regiones promotoras de sus genes diana, promoviendo así su transcripción.

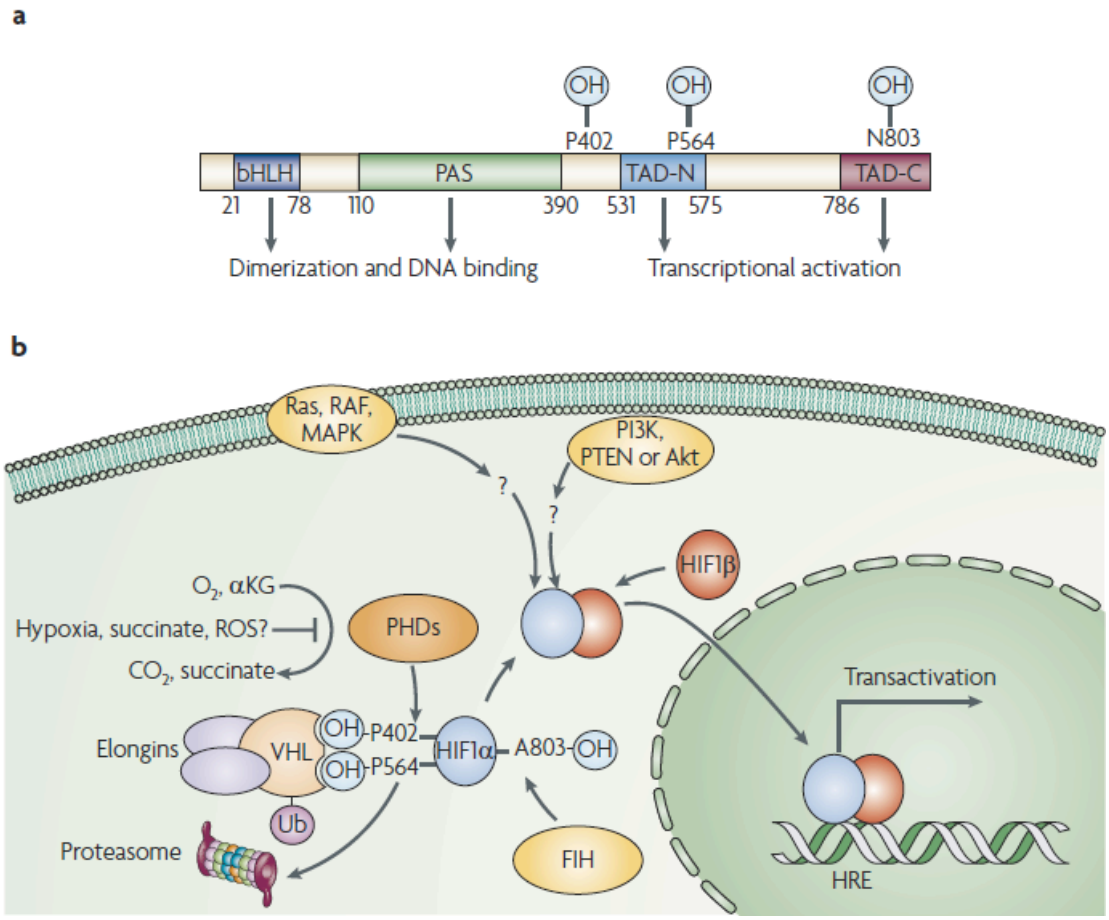

Figura 2. Mecanismo de estabilización del HIF en hipoxia. (a) Los sitios de hidroxilación en prolinas indican el domino de degradación dependiente de oxígeno. La hidroxilacion en asparragina en domino de carboxi terminal de transactivación por FIH regula la actividad de HIF pero no su estabilidad. (b) Vía clásica de degradación de HIF. La hidroxilación en la prolinas por las PHDs hacen que el complejo elongina-VHL reconozca a HIF y lo ubiquitina para su degradación en el proteasoma. Otras factores como Ras, RAF, MAPK (mitogen-activated protein kinase), fosfoinositol 3 fosfato (PI3K), PTEN o AKT pueden causar la acumulación de HIF. Intermediarios del ciclo de Krebs como el sucinato o el fumarato asiq como los ROS pueden inhibir la actividad de las PHDs, estabilizando HIF (Denko 2008).

2.2.2 Sensores de oxígeno.

El descubrimiento de las enzimas encargadas de hidroxilar a HIF, las HIF prolil hidroxilasas (PHDs) y asparaginil hidroxilasa (FIH), y la clara implicación de éstas en su regulación, tanto a nivel de estabilidad como de actividad transcripcional, ha

permitido establecer un consenso general en cuanto a la aceptación de estas enzimas como los sensores celulares de oxígeno.

Las PHD son enzimas dependientes de O2 que se han implicado directamente en la degradación de HIF (Bruick & McKnight 2001; Epstein et al. 2001). Constituyen una nueva familia de dioxigenasas (Hirsilä et al. 2003), siendo independientes de la otra familia de dioxigenasas, las hidroxilasasdel colágeno. Ensayos *in vitro* han demostrado que HIF no se hidroxila por las hidroxilasas de colágeno y sí por las PHDs.

En mamíferos se han clonado 4 isoformas diferentes de las prolil hidroxilasas, que se denominan PHD o EGLN por su alta homología con unas enzimas similares descritas *en C. Elegans* (Epstein et al. 2001). Las PHDs necesitan de O2 para hidroxilar HIF, además de hierro (II) y 2-oxoglutarato que actúan como cofactores. LA deficiencia de cualquiera de estos factores conlleva a la reducción de su actividad.

Curiosamente, la hipoxia produce un incremento de los niveles de RNA mensajero de la PHD2 y de la PHD3 mientras que la PHD1 se mantiene constante (del Peso et al. 2003) lo que sugiere que la falta de oxígeno regula a estas enzimas, tanto negativamente a nivel de actividad, como positivamente en la cantidad de enzima disponible. Diversos análisis han concluidos que es la PHD-2 la principal responsable de la degradación de HIF-1(Berra et al. 2003) considerándola entonces como el sensor de oxígeno principal.

3. La mitocondria:

Las mitocondrias son orgánulos celulares encargados de suministrar la mayor parte de la energía necesaria para la actividad celular y que están presentes en prácticamente todas las células eucariotas.

La morfología de la mitocondria es difícil de describir puesto que son estructuras muy plásticas que se deforman, se dividen y fusionan. Normalmente se las representa en forma alargada. Su tamaño oscila entre 0,5 y 1 μm de diámetro y hasta 7 μm de longitudy su número depende de las necesidades energéticas de la célula, (Cavalier-Smith 1987).

En 1967 Lynn Margulis publicó el trabajo “Origin of mitosing cells” (Sagan 1967), donde explica su Teoría de la Endosimbiosis Seriada sobre el origen de las mitocondrias y los cloroplastos. En ella, postula que las mitocondrias son el producto

de una Antigua simbiosis entre una α-Proteobacteria y una célula nucleada que había desarrollado motilidad y endocitosis.

La mitocondria se compone de dos membranas, la externa, que la separa del citoplasma, y la interna, que define el espacio intermembrana y la matriz mitocondrial. La membrana externa permite el paso de moléculas pequeñas (hasta 10 kDa) mientras la membrana interna constituye una barrera mas selectiva, siendo esta restricción de paso indispensable para el mantenimiento del gradiente de protones necesario para la síntesis de ATP. La membrana interna presenta una serie de pliegues denominados crestas que le proporcionan una gran superficie.

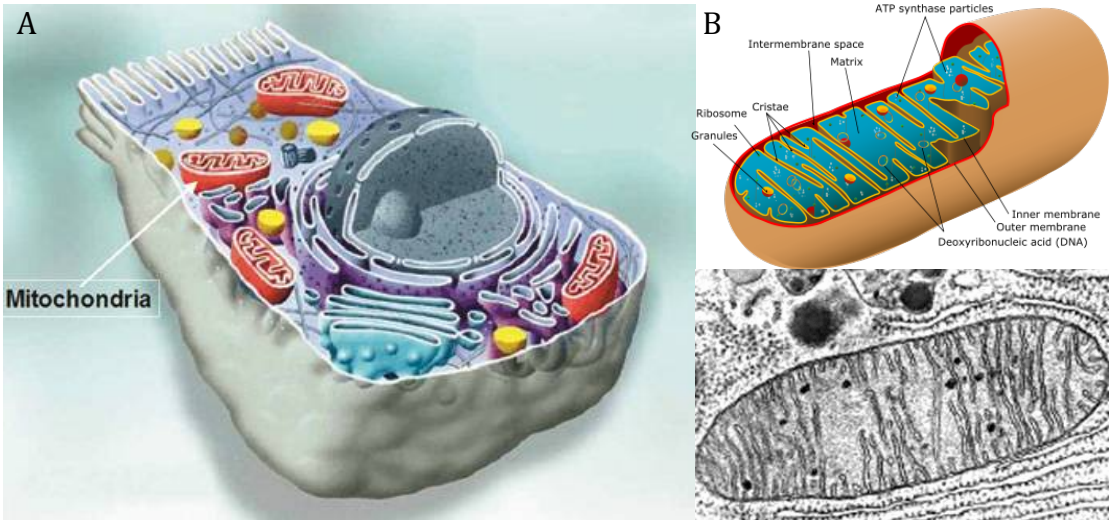

Figura 3. (a) Representación de una célula resaltando la mitocondria. (b) Dibujo simplificado de una mitocondria. Debajo se puede observar una imagen de una mitocondria real por microscopia electrónica.

Una característica peculiar es que poseen su propio genoma: el DNA mitocondrial (mtDNA)(Clayton 1982). Este segundo sistema genético celular, a pesar de contener un número muy pequeño de genes, es indispensable para la vida celular porque codifica proteínas integrales de los complejos respiratorios mitocondriales, además de los RNAs transferentes y ribosómicos. Sin embargo, las mitocondrias dependen en gran medida de proteínas codificadas en el núcleo, que son sintetizadas en los ribosomas citoplásmicos e importadas a la mitocondria.

En cuanto a la función, las mitocondrias no están solo implicadas en la producción de energía, sino que en éllas se desarrollan numerosas rutas metabólicas fundamentales como son la β-oxidación, biosíntesis de pirimidinas, aminoácidos,

fosfolípidos, nucleótidos, ácido fólico, hemo, urea y una gran variedad de metabolitos(Attardi & Schatz 1988). No obstante, la función principal de estos orgánulos es la producción de energía en forma de ATP mediante el proceso de fosforilación oxidativa (OXPHOS). Dicho proceso se nutre de la transferencia de electrones procedentes de la oxidación de ciertas moléculas orgánicas (p. ej., Glúcidos, lípidos y proteínas), en forma de NADH y $FADH_2$, hacia al oxígeno molecular produciendo agua como subproducto metabólico. En estas reacciones redox participan una serie de complejos multiproteicos (complejos I a IV), embebidos en la membrana interna mitocondrial, entre los que se sitúan dos transportadores electrónicos móviles: coenzima Q y citocromo c.

3.1 El sistema de fosforilación oxidatíva (OXPHOS):

La cadena de transporte electrónico (mtETC) (complejos I-IV) y la síntesis de ATP (complejo V) son llamados conjuntamente; sistema de fosforilación oxidativa (Sistema OXPHOS). Como ya hemos comentado anterormente, los electrones procedentes del NADH+H+ pasan secuencialmente a través del complejo I, la ubiquinona, el complejo III y el citocromo c para llegar finalmente al complejo IV, que los cederá al oxígeno molecular generando H2O. De forma alternativa, los electrones del FADH2, producto final de la succinato deshidrogenasa o complejo II, así como de otras enzimas como la glicerol- 3-P deshidrogenasa, la ETF-ubiquinona oxidorreductasa (primera enzima de la β-oxidación de los ácidos grasos) o la dihidroorotato deshidrogenasa (enzima implicada en la biosíntesis de pirimidinas), pasan a la ubiquinona y son canalizados mediante el complejo III, citocromo c y complejo IV para que lleguen finalmente hasta la reducción del oxígeno molecular.

Este transporte de electrones no es del todo eficiente y a veces el oxigeno es reducido antes de llegar al complejo IV dando lugar a especies reactivas de oxigeno (ROS). (Murphy 2009; Murphy et al. 2011)

En los complejos I, III y IV de la cadena de transporte electrónico, se produce un bombeo de protones desde la matriz mitocondrial hasta el espacio intermembrana que genera un gradiente electroquímico (de pH y electrogénico) o potencial de membrane que es aprovechado por la ATP sintasa o complejo V para impulsar la síntesis de ATP a partir de ADP y Pi, completándose de este modo el proceso de fosforilación oxidativa(MITCHELL 1961; MITCHELL & Moyle 1967).

El ATP generado en este proceso, es utilizado en los distintos tejidos para mantener las necesidades energéticas celulares. Así, aquellos tejidos que tengan mayor requerimiento de ATP serán los más afectados en el caso de producirse fallos en su generación.

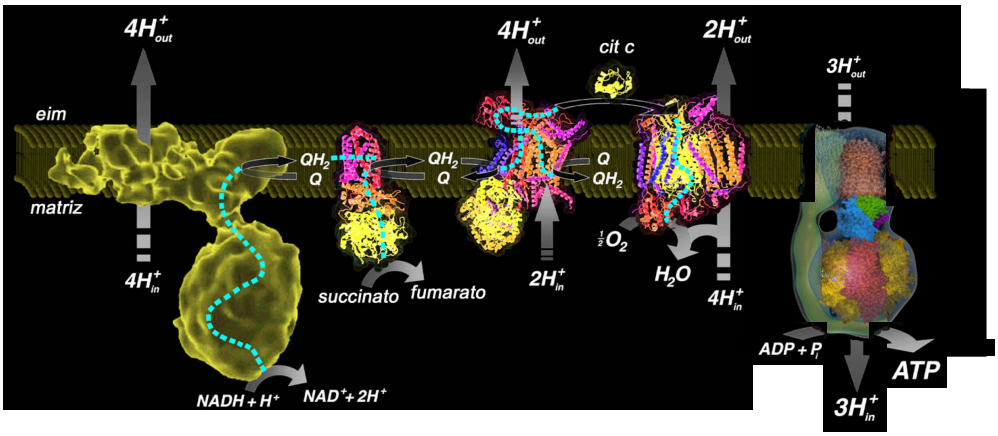

Figura 4. Modelo esquemático de la cadena de transporte de electrones mitocondrial. Están representados los complejos del I-V además de la ubiquinona y el citocromo c.

3.1.1 El complejo I:

El complejo I (NADH deshidrogenasa o NADH:ubiquinona oxidorreductasa, es el el más grande los los cinco complejos. Este complejo une y oxida NADH y transporta sus electrones a través, primero de flavoproteínas y luego de una serie de proteínas ferrosulfuradas para cedérselos últimamente a la ubiquinona. La energía liberada en este proceso es usada para la translocación de protones através de la membrana interna al espacio intermenbrana para generar gradiente electroquímico. La rección global la podemos resumir en:

NADH + ubiquinona (Q) + 5H+ (matriz) NAD+ + ubiquinol (QH2) + 4H+ (espacio intermembrana)

Se trata del complejo más grande del sistema OXPHOS, en mamíferos se estima que tiene un peso molecular de 980kDa, formado por 45 subunidades, 7 de las cuales se encuentran codificadas en el mtDNA y las 38 restantes, en el genoma nuclear. La composición y la topología del complejo I de mamíferos ha sido ampliamente

estudiada en preparaciones de corazón bovino(Walker et al. 1992; Walker 1992; Carroll 2002; Carroll et al. 2006), y las subunidades humanas codificadas en el genoma nuclear han sido identificadas por homología con las secuencias bovinas. Aunque todavía no se ha obtenido la estructura cristalina del complejo completo, se ha visto por microscopía electrónica que tiene forma de "L" (Grigorieff 1998; Sazanov et al. 2000), con dos brazos perpendiculars entre sí: un brazo hidrofóbico, embebido en la membrana interna mitocondrial donde se produce el bombeo de protones y otro brazo periférico hidrofílico, orientado hacia la matriz, que contiene el sitio de unión del NADH y los centros redox. En bacterias, existe la forma más simple de NADH:ubiquinona oxidorreductasa, con un peso molecular aproximado de 550 kDa, está formado por 14 subunidades que constituyen la estructura mínima necesaria para que el complejo sea funcional(Vogel et al. 2007). Recientemente se ha publicado la estructura cristalina de la región hidrofílica del complejo en *Thermus thermophilus* (Sazanov & Hinchliffe 2006) así como el dominio hidrofóbico de *Escherichia coli*, el cual ha permitido proponer un nuevo modelo más detallado del mecanismo de bombeo de protones(Efremov & Sazanov 2011). Durante el transcurso de la evolución, un número elevado de subunidades se han incorporado al complejo I en eucariotas, aumentando así su peso molecular a 900-1000 kDa. Aunque el papel de las subunidades supernumerarias no se conoce con exactitud, se acepta su función en el ensamblaje y/o la regulación de la actividad del complejo(Vogel et al. 2004).

3.1.2 El complejo II:

El complejo II, también denominado succinato deshidrogenasa está compuesto por cuatro subunidades, todas ellas codificadas en el genoma nuclear(Hägerhäll 1997) , tres grupos sulfoférricos, una molécula de FAD unida de forma covalente y un grupo citocromo b558(Ackrell 2000). Este complejo tiene una doble función: transformar el succinato en fumarato, en el ciclo de Krebs y transferir los electrones desde el FADH2 hasta la ubiquinona, en la cadena de transporte electrónico mitocondrial(Cecchini 2003). Este complejo II no tiene capacidad de bombeo de protones al espacio intermembrana. La rección global la podemos resumir en:

FADH2 + ubiquinona (Q) FAD + ubiquinol (QH2)

El complejo II puede ser dividido en dos fracciones: una soluble, que constituye el centro catalítico de la enzima con las subunidades de 70 kDa (flavoproteína (Fp) o SDHA) y la de 30 kDa (subunidad de Fe-S (Ip) o SDHB), y otra que sirve de anclaje a la membrana interna mitocondrial y está formada por las subunidades SDHC y SDHD. La fracción soluble presenta actividad succinato deshidrogenasa en presencia de aceptores artificiales de electrones pero no es capaz de reducir a la ubiquinona(Davis & Hatefi 1972) puesto que el sitio de unión de ésta se encuentra en las subunidades SDHC y SDHD(Oyedotun & Lemire 2001).

3.1.3 El complejo III:

El complejo III de la cadena respiratoria, también denominado ubiquinol:citocromo c oxidorreductasa o complejo bc1 mitocondrial cataliza el paso de electrones desde el ubiquinol (forma reducida de la ubiquinona) hasta el citocromo c, acoplando a esta reacción el bombeo de protones desde la matriz mitocondrial al espacio intermembrana. La rección global la podemos resumir en:

ubiquinol (QH2)+ 2cyt-c (FeIII) + 2H+(matriz) ubiquinona (Q) + 2cyt-c (FeII) + 4H+(espacio intermembrana)

En mamíferos, cada monómero del complejo bc1 contiene 11 subunidades estructurales(Schägger et al. 1986; Iwata et al. 1998) y varios grupos redox entre los que se encuentran: los citocromos b566, b562 y c1 y un centro binuclear de hierro-azufre (Fe2S2)(Berry et al. 2000). Las subunidades se han numerado según su movilidad electroforética con números romanos(Schägger et al. 1986). Sólo una de las once proteínas que componen el complejo se encuentra codificada en el mtDNA(Anderson et al. 1981), la subunidad III o CYTB, que contiene los citocromos de tipo b. La subunidad IV contiene el grupo hemo c1 (CYC1) y la V, conocida como proteína de Rieske (UQCRFS1 o RISP), el núcleo hierro-azufre. Estas tres subunidades se consideran el núcleo catalítico del complejo, responsable de la transferencia de electrones, alrededor del cual se ensamblan el resto de proteínas, cuya función todavía se desconoce, para dar lugar al holoenzima. Las subunidades I y II se consideran las proteínas centrales del complejo y se denominan Core1 y Core2 respectivamente.

3.1.4 Complejo IV:

El complejo IV o citocromo c oxidasa es el último de los complejos de la cadena de transporte electrónico y su función es la de catalizar la oxidación del citocromo c con la consiguiente reducción del oxígeno molecular para dar agua. Esta reacción está acoplada a la translocación de protones, desde la matriz mitochondrial hasta el espacio intermembrana (Zaslavsky & Gennis 2000). La rección global la podemos resumir en:

4 cyt-c (FeII) + 8 H+(matriz) + O2 4cyt-c (FeIII) + 4H+(espacio intermembrana)+ 2 H2O

En mamíferos, la citocromo c oxidasa (COX) es un complejo compuesto por 13 proteínas con un peso molecular de unos 200 kDa. Se localiza en la membrane interna de la mitocondria y sólo es activo cuando se encuentra en forma de dímero(Yoshikawa 1997). El núcleo catalítico de la enzima está formado por las tres subunidades codificadas en el mtDNA: (1) COI que contiene los grupos hemo-a y hemo-a3-CobreB (a3- CuB); (2) COII, que posee el centro cobreA (CuA) y proporciona el sitio de unión del citocromo c (Capaldi 1990; Tsukihara et al. 1995; Tsukihara et al. 1996; Tsukihara et al. 1996); (3) COIII, proteína estructural que parece tener un papel importante en el bombeo de protones. El resto de subunidades que forman parte del son codificadas en el DNA nuclear. La función de las subunidades nucleares está menos clara, pero podrían estar implicadas en el ensamblaje del complejo funcional(Mick et al. 2011), además de regular la actividad catalítica del enzima mediante la union de moduladores alostéricos(Acín-Pérez et al. 2011). La subunidad COX6A regula la actividad catalítica mediante la unión de ATP(Taanman et al. 1994; Arnold & Kadenbach 1997), la subunidad COX6B es idéntica a un péptido similar a una hormona del duodeno de porcino(Bennett et al. 1990) (Bennett, Chang et al. 1990), la proteína COX5B tiene un motivo tipo “dedo de zinc”(Tsukihara et al. 1995) y la subunidad COX4 es esencial para el ensamblaje del complejo(Li et al. 2006). También se han descrito isoformas específicas de tejido para varias de las subunidades nucleares de COX(Ewart et al. 1990; Kennaway et al. 1990), entre ellas, COX6A y COX7A presentan isoformas específicas de corazón e hígado(Grossman & Lomax 1997), COX6B2 es una isoforma específica de testículo y

también existe una isoforma específica de pulmón en el caso de COX4(Fernández-Vizarra et al. 2009).

3.1.5 Complejo V:

El complejo V (ATP sintasa, F1FO-ATPasa) es el quinto complejo enzimático del sistema OXPHOS. Su función es la de catalizar la síntesis de ATP a partir de ADP y Pi aprovechando la energía del gradiente de protones generado en el espacio intermembrana en el proceso de respiración mitocondrial.

El complejo está compuesto por 16 proteínas distintas, que forman dos dominios funcionales denominados F1 y FO, conectados entre si por un tallo(Futai et al. 1989; Boyer 1993; Lutter et al. 1993). La región F1 se localiza en la matriz mitocondrial constituyendo la fracción soluble de la enzima y se compone de cinco subunidades distintas. Esta región forma el dominio catalítico de la ATP sintasa. La región FO se encuentra anclada en la membrana interna mitocondrial y funciona como un poro de protones dirigiendo la energía liberada en la disipación del gradiente electroquímico a la parte F1 que es donde se forma el ATP. La energía se transfiere de una parte a otra mediante un mecanismo de motor rotatorio(Stock et al. 1999). Cuando disminuye el gradiente de protones, la ATP sintasa puede funcionar de modo inverso, es decir, hidroliza ATP para bombear protones al espacio intermembrana y así contribuir a mantener el potencial de membrana. La actividad hidrolítica del complejo V se regula mediante la unión de la proteína inhibitoria natural IF1(Cabezón et al. 2003).

3.2 Organización del sistema OXPHOS:

La organización del sistema de fosforilación oxidativa dentro de la membrana interna mitocondrial ha resultado ser mucho más complicada de lo que se suponía inicialmente. En 1986, el "*Modelo fluído*" proporcionó la mejor descripción de la organización del sistema OXPHOS. Este modelo postula que los complejos de la cadena difunden libremente por la membrana y la transferencia de electrones tiene lugar en función de las colisiones arbitrarias entre complejos. Dicho modelo se basa en gran parte en el hecho experimental que todos los complejos del sistema OXPHOS pueden ser purificados individualmente, manteniendo su actividad enzimática(Hackenbrock et al. 1986).

Trabajos recientes proponen una nueva teoría de organización de la ETC en supercomplejos. Mediante el análisis de geles nativos con distintos detergentes y cantidades variables de éstos, se ha observado la asociación entre algunos de los complejos de la ETC, tanto en levaduras (Cruciat et al. 2000) como en mamíferos (Schägger & Pfeiffer 2000) y plantas (Eubel et al. 2004).

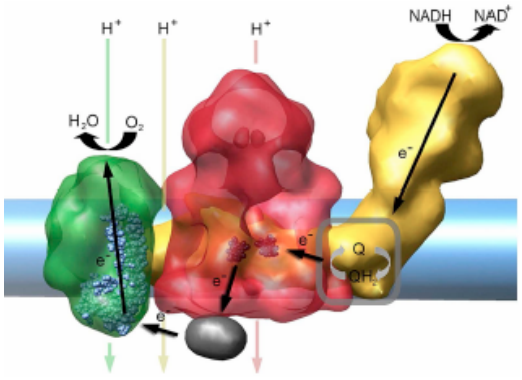

Figura 5. Supercomplejo $I_1III_2IV_1$: En la figura se aprecia el supercomplejo $I_1III_2IV_1$. Los complejos se muestran coloreados siendo el amarillo el CI, el rojo el CIII y el verde el CIV(Vonck & Schäfer 2009).

Estudios con pacientes y modelos celulares de ratón portadores de mutaciones en distintos complejos, han revelado cuáles son los complejos indispensables para el establecimiento de los respirasomas. Así, se ha observado que los complejos III y IV son esenciales para la estabilización del complejo I y que en ausencia de complejo III no es posible la formación de supercomplejos (Acín-Pérez et al. 2004; Schägger et al. 2004; Diaz et al. 2006). Por otra parte, si el complejo I no está presente, no es posible la formación de supercomplejos pero el resto de complejos pueden ensamblarse y estabilizarse.

Trabajos más recientes (Acín-Pérez et al. 2008) demuestran no solo la existencia de los supercomplejos sino su actividad respiratoria. La formación de los supercomplejos depende totalmente de la presencia de los complejos que los componen, y su ensamblaje está temporalmente retrasado con respecto a la formación de los distintos complejos individuales. También se demuestra que algunos supercomplejos contienen ubiquinona y citocromo c y lo más importante, que los supercomplejos aislados presentan capacidad para transferir electrones desde el NADH hasta el oxígeno. Algunos autores proponen la coexistencia de los complejos individuales y los supercomplejos(Boekema & Braun 2007).

Desde el punto de vista funcional, se ha propuesto que la existencia de respirosomas presenta varias ventajas entre las que destaca la canalización más

eficiente de los electrones a través de las moléculas transportadoras (D'Aurelio et al. 2006; Genova et al. 2005)

Como se forman los supercomplejos y que proteínas, si la hay, están involucradas en su ensamblaje es actualmente un activo campo de estudio que esta arrojando a la luz sus primeros datos. Se han encontrado ciertas proteínas, como Rcf1, que parecen ensamblar el supercomplejo III+ IV(Y.-C. Chen et al. 2012; Vukotic et al. 2012), y su deficiencia conlleva una importante reducción en la cantidad de dicho supercomplejo.

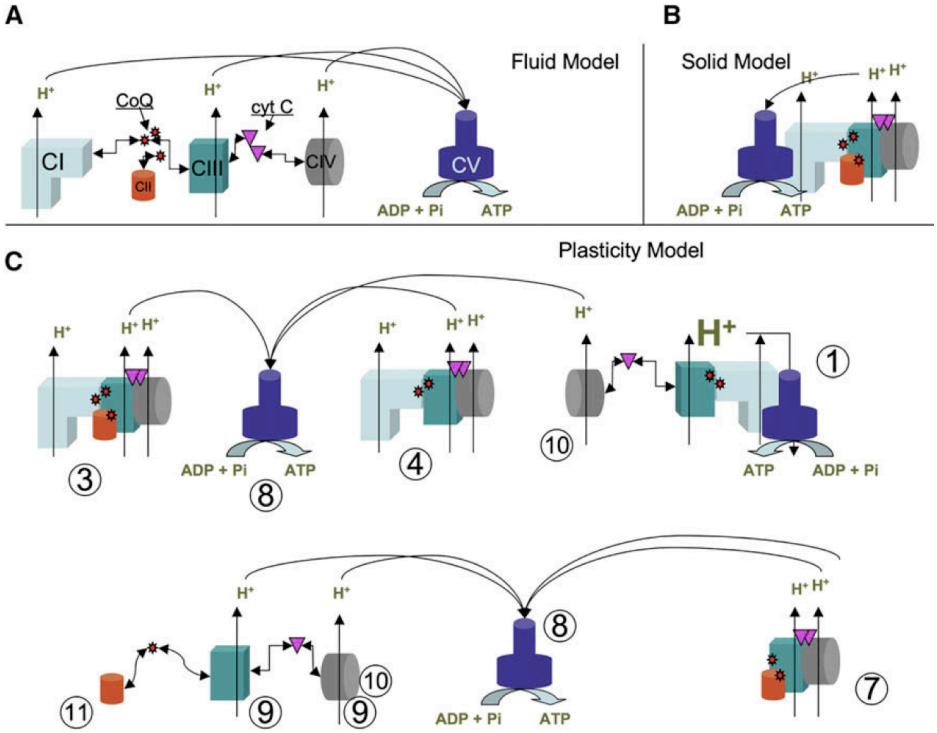

Figura 6. **Modelos de organización del sistema OXPHOS.** (a) "*Modelo Fluído*" (b) "*ModeloSólido*" (c) "*Modelo Plástico*". Representación esquemática de los complejos del sistema OXPHOS, coenzima Q esta representada por pequeñas estrellas rojas y el citocromo c por triángulos morados invertidos (Acín-Pérez et al. 2008)

4. Mitocondria e Hipoxia:

Las mitocondrias consumen más del 90% del oxigeno que respiramos(Taylor 2008), por ello, no es de extrañar que fluctuaciones en las tensiones de oxigeno tengan gran influencia en la respuesta adaptativa de estos orgánulos.

En respuesta a la hipoxia, las células activan un programa metabólico que reduce el consumo de oxígeno mitocondrial, a costa de disminuir la actividad de

fosforilación oxidativa (OXPHOS), y favorecer la captación de glucosa y aumentar la actividad glucolítica.(Aragonés et al. 2008). Esta adaptación a la hipoxia es en gran parte mediada a la expresión de una batería de genes dependientes de los factores de transcripción inducibles por hipoxia (HIFs) (Aragonés et al. 2009). Entre estos genes inducidos por HIF se encuentra el transportador de glucosa GLUT1 así como varias enzimas clave de la ruta glucolítica (Iyer et al. 1998). Los genes PDK1 y PDK3 que codifican para la piruvato deshidrogenasa kinasa también son claramente dependientes de HIF, su inducción favorece la fosforilación y consiguiente inhibición de la piruvato deshidrogenasa (PDH), con lo que se consigue disminuir la conversión de piruvato en acetil CoA que alimentaría el ciclo de Krebs. (Kim et al. 2006; Papandreou et al. 2006). Este exceso de piruvato proveniente del aumento en la tasa glucolitica es convertido a lactato por la LDH-A, otro gen diana de HIF (Iyer et al. 1998). El complejo IV de la ETC también es susceptible de modificación. HIF promueve un cambio de isoforma entre la COX4-1 hacia la COX4-2, proceso que va encaminado a maximizar la eficiencia de la respiración bajo condiciones hipóxicas(Fukuda et al. 2007).

Recientemente también se han involucrado a los microRNAs en la respuesta a hipoxia. Específicamente el miRNA 210 es inducido por HIF. Entres sus dianas se encuentras los genes mitocondriales ISCU(Tong & Rouault 2006) y COX10 (Z. Chen et al. 2010). El primero es responsable del ensamblaje de los centros ferrosulfurados que contienen algunos complejos de la ETC, como el complejo I y III. Por otra parte, COX10 es una farnesiltransferasa que resulta imprescindible para la correcta biogénesis del complejo IV. Todos estos cambios promueven un cambio encaminado a aumentar la vía anaerobia del catálisis de la glucosa y reprimen el catabolismo anaerobio, muy posiblemente para mantener unos niveles adecuados de ATP sin producir un estrés oxidativo celular. Este fino control de los ROS cobra más sentido puesto que otra de las diana de HIF2 es SOD2, enzima encargada de detoxificar la sobreproducción de especies reactivas del oxígeno. De hecho, los ratones deficientes en la subunidad HIF2 presentan numerosas patología asociadas con la homeostasis de los ROS (Scortegagna et al. 2003).

Algunos estudios proponen que HIF, a través de la inducción de BNIP3, promueve una autofagia mitocondrial selectiva (Zhang et al. 2008). En nuestras líneas celulares y a las tensiones de oxígeno y tiempos trabajados no hemos observado una

reducción significativa del contenido mitocondrial, así pues asumimos que estos efectos pueden ser específicos de la línea celular que se utilice.

Objetivos

Objetivos

En base a los estudios previos, indicados en la introducción, donde se observa una respuesta celular generalizada y encaminada a disminuir la actividad mitocondrial, hemos decidido centrarnos en el engranaje clave de la mitocondria, la cadena de transporte de electrones, e investigar los posibles eventos regulatorios que puede estar sufriendo bajo condiciones de hipoxia.

1. Dado que el complejo I es el principal aceptor de electrones de la ETC nos propusimos investigar su actividad, función y posible regulación en células sometidas a hipoxia moderada.
2. Localización, función y relevancia fisiológica de la proteína NDUFA4L2.
3. Estudio de la proteína NDUFA4, paràloga a NDUFA4L2; localización y función.

_____ *Resultados, Materiales y Métodos*

Manuscrito 1

***Induction of the Mitochondrial NDUFA4L2 Protein by HIF-1a Decreases Oxygen Consumption by Inhibiting Complex I Activity*.**

Cell Metabolism, 2011, Dec 7;14(6) 768-79.

En este articulo he sido primer coautor, contribuyendo de la misma forma. En él hemos hecho gala de multitud de técnicas para ahondar en las cuestiones e interrogantes que se nos iban planteando. Gracias a ello he conseguido adquirir bastante experiencia en cuestiones de biología molecular, bioquímica y manejo de animales.

En este articulo demostramos como la proteína NDUFA4L2, un gen diana del factor de transcripción inducible en hipoxia (HIF) es fuertemente inducida bajo condiciones de hipoxia en numerosas líneas celulares, así como en cultivos primarios y tejidos “in vivo”. Su inducción inhibe la actividad del complejo I de la cadena de transporte de electrones mitocondrial y con ello el consume de oxígeno. Esto tiene profundas implicaciones en la respuesta a la adaptación celular a las fluctuaciones de oxígeno, siendo la más importante la atenuación de la producción de radicales libres del oxígeno y el consecuente estrés oxidativo.

Cell Metabolism
Article

Induction of the Mitochondrial NDUFA4L2 Protein by HIF-1α Decreases Oxygen Consumption by Inhibiting Complex I Activity

Daniel Tello,[1,5] Eduardo Balsa,[1,5] Bárbara Acosta-Iborra,[1] Esther Fuertes-Yebra,[1] Ainara Elorza,[1] Ángel Ordóñez,[1] María Corral-Escariz,[1] Inés Soro,[1] Elia López-Bernardo,[1] Ester Perales-Clemente,[2] Antonio Martínez-Ruiz,[1] José Antonio Enríquez,[2,3] Julián Aragonés,[1] Susana Cadenas,[1,4] and Manuel O. Landázuri[1,*]

[1]Servicio de Inmunología, Hospital Universitario de La Princesa, Universidad Autónoma de Madrid, Instituto de Investigación Sanitaria Princesa (IIS-IP), Madrid, 28006, Spain

[2]Centro Nacional de Investigaciones Cardiovasculares Carlos III (CNIC), Madrid, 28029, Spain

[3]Departamento de Bioquímica y Biología Molecular y Celular, Facultad de Ciencias, Universidad de Zaragoza, Zaragoza, 50013, Spain

[4]Departamento de Biología Molecular, Facultad de Ciencias, Universidad Autónoma de Madrid, Madrid, 28049, Spain

[5]These authors contributed equally to this work

*Correspondence: mortiz.hlpr@salud.madrid.org

DOI 10.1016/j.cmet.2011.10.008

SUMMARY

The fine regulation of mitochondrial function has proved to be an essential metabolic adaptation to fluctuations in oxygen availability. During hypoxia, cells activate an anaerobic switch that favors glycolysis and attenuates the mitochondrial activity. This switch involves the hypoxia-inducible transcription factor-1 (HIF-1). We have identified a HIF-1 target gene, the mitochondrial *NDUFA4L2* (NADH dehydrogenase [ubiquinone] 1 alpha subcomplex, 4-like 2). Our results, obtained employing NDUFA4L2-silenced cells and NDUFA4L2 knockout murine embryonic fibroblasts, indicate that hypoxia-induced NDUFA4L2 attenuates mitochondrial oxygen consumption involving inhibition of Complex I activity, which limits the intracellular ROS production under low-oxygen conditions. Thus, reducing mitochondrial Complex I activity via NDUFA4L2 appears to be an essential element in the mitochondrial reprogramming induced by HIF-1.

INTRODUCTION

Aerobic organisms have developed specific systems to deliver oxygen to cells in different anatomical locations. However, insufficient oxygen supply and the ensuing hypoxia is a hallmark of different pathological situations. In response to hypoxia, cells activate a metabolic program that reduces oxygen consumption by actively lowering mitochondrial oxidative phosphorylation (OXPHOS) activity, the main oxygen-consuming process in most cell types, accompanied by an increase in glucose uptake and the rate of glycolysis (Aragonés et al., 2008; Iyer et al., 1998; Kim et al., 2006; Papandreou et al., 2006). This hypoxic adaptation is due to the expression of genes triggered by hypoxia-inducible factors (HIFs) (Aragonés et al., 2009). HIFs are master transcription factors regulated in an O_2-dependent manner by a family of prolyl hydroxylases (PHDs), which use O_2 as a substrate to hydroxylate HIF-α subunits in conditions of normoxia (Kaelin and Ratcliffe, 2008). These hydroxylated substrates are then ubiquitinated after recognition by VHL, and they are degraded by the proteasome. By contrast, PHD activity is inhibited in hypoxic conditions, and accordingly, HIF-α subunits accumulate, heterodimerize with HIF-β, and activate the expression of HIF-dependent target genes (Schofield and Ratcliffe, 2004; Semenza, 2004, 2009).

Among the genes whose expression is upregulated by HIFs are glucose transporters, like *GLUT1*, as well as key enzymes involved in glycolysis (Iyer et al., 1998). The *PDK1* and *PDK3* genes that code for pyruvate dehydrogenase (PDH) kinases are also upregulated, which results in increased phosphorylation and inactivation of PDH, the enzyme that converts pyruvate to acetyl-CoA (Kim et al., 2006; Lu et al., 2008; Papandreou et al., 2006). This process limits the substrate available for the tricarboxylic acid cycle (TCA) and thus for OXPHOS activity. Mitochondrial respiration is also regulated by additional mechanisms that maximize respiratory efficiency under conditions of reduced O_2 availability. Genes that regulate cytochrome *c* oxidase (the ETC Complex IV that reduces O_2 to H_2O) are also regulated by HIFs, including *COX4-2* isoform and the *LON* protease, which produces a switch from isoform COX4-1 to COX4-2 that optimizes the efficiency of respiration under hypoxic conditions (Fukuda et al., 2007).

Complex I (NADH:ubiquinone oxidoreductase) is the largest and least understood component of the respiratory chain. This complex catalyzes the first step in the electron transport chain (ETC), transferring electrons from NADH to a noncovalently bound flavin mononucleotide (FMN) and then, via a series of iron-sulfur clusters (FeS), to the final ubiquinone acceptor. Complex I consists of 45 different subunits that are assembled into a structure of ~1 MDa, and while 7 subunits are encoded by mitochondrial DNA, the remaining 38 are coded for by the nuclear genome (Carroll et al., 2006). The activity of the Complex I is affected by hypoxia, either through posttranslational modification (Frost et al., 2005) or the reduced expression of mitochondrial genes (Chan et al., 2009). Here we report that HIF-1 induces the expression of the NADH dehydrogenase (ubiquinone) 1 alpha subcomplex subunit 4-like 2 gene (*NDUFA4L2*, also called

NADH-ubiquinone oxidoreductase MLRQ subunit homolog [*NUOMS*]), cataloged as a component of ETC Complex I due to its high sequence identity with *NDUFA4*. It was previously described using mRNA array technology that NDUFA4L2 is overexpressed in VHL-deficient cell lines and tumors (Favier et al., 2009; Papandreou et al., 2006), as well as in neuroblastoma cells in hypoxia (Fredlund et al., 2008) and in pathophysiological conditions like rheumatoid arthritis (Andreas et al., 2009). Although the physiological function of this protein remains unclear, we show here that it is involved in lowering mitochondrial oxygen consumption and Complex I activity, thereby reducing ROS production. This provides a point in the regulation of mitochondrial activity that can reprogram Complex I activity under low-oxygen conditions.

RESULTS

Hypoxia Induces the Mitochondrial Protein NDUFA4L2 in Primary Cultures and Tumor Cells In Vitro as well as In Vivo

We hypothesized that, as the principal electron acceptor, Complex I could be a key regulatory point in the control of the ETC during hypoxia. To identify Complex I components that might be regulated by moderate hypoxia, we used an mRNA array to analyze the expression of genes in HeLa cells maintained for short periods of time (6 hr) in 1% O_2. We detected the expression of 44 genes of Complex I in the array: 40 genes encoded by nuclear DNA and 4 encoded in the mitochondria (*ND1*, *ND2*, *ND3*, and *ND6*). Of all these genes, only *NDUFA4L2* was clearly induced by hypoxia, whereas the other genes encoded by nuclear DNA remained unchanged (Table S1). By contrast and as described previously (Piruat and López-Barneo, 2005), the other mitochondrially encoded genes underwent a marked downregulation in these hypoxic conditions (Table S1). It is important to note that *NDUFA4L2* gene is strongly induced by hypoxia. In fact, it appears among the first 12 genes more induced by hypoxia in the mRNA study (Table S2).

These microarray data were validated by RT-PCR on mRNA isolated from HeLa and PC-12 cells exposed to hypoxia. Indeed, RT-PCR assays confirmed that NDUFA4L2 expression was strongly upregulated in response to hypoxia (Figure 1A), while such conditions did not change the levels of other Complex I genes encoded in the nucleus, such as *NDUFA4*, *NDUFAB1*, or *NDUFB4*, although *ND1* and *ND6* expression was downregulated (Figure S1A). Upregulation of *NDUFA4L2* expression was also observed in HUVEC and cardiomyocytes subjected to hypoxia and after treatment with PHD inhibitors such as dimethyloxaloylglycine (DMOG) and deferroxamine (Figure 1B). The efficacy of hypoxia and DMOG in these experiments was corroborated by the marked upregulation of previously recognized HIF target genes such as *PHD3*, *BNIP3*, and *GLUT1* (Figure S1B). In addition, NDUFA4L2 expression was induced in brain tissue of mice exposed to 7.5% O_2 for 18 hr (Figure 1C). An increase in NDUFA4L2 protein was also evident in response to hypoxia in different cell types and brain tissue (Figure 1D) with an antibody specific to this protein that did not recognize the homologous NDUFA4 protein (Figure S1C). Moreover, the increase in NDUFA4L2 protein induced by hypoxia was evident in cardiomyocytes when assessed by immunofluorescence (Figure 1E).

We analyzed the cellular localization of NDUFA4L2 in normoxic and hypoxic conditions. A bioinformatics approach predicted that NDUFA4L2 would be localized in mitochondria (Table S3), and this prediction was then confirmed experimentally by analyzing mitochondrial and cytoplasmic fractions from HeLa cells. NDUFA4L2 was clearly enriched in the mitochondrial fraction under hypoxic conditions (Figure 1F), and immunofluorescence showed a clear colocalization of NDUFA4L2 and cytochrome *c* in HL-1 cells (Figure 1G), as well as the colocalization of NDUFA4L2 and the mitochondria-selective dye MitoTracker in HeLa cells (Figure S1D). These results confirmed the mitochondrial location of NDUFA4L2.

HIF-1α Regulates NDUFA4L2 Induction

To investigate whether hypoxia-induced *NDUFA4L2* expression was mediated by HIF transcription factors, we first silenced HIF-1β, the common partner of HIF-1α and HIF-2α, thereby impairing the canonical HIF transcriptional response. Interference of HIF-1β expression abolished the induction of *NDUFA4L2* during hypoxia (Figure 2A), as well as the response of *PHD3* (included as a control of HIF-target gene) (Figure S2A), indicating that HIF transcriptional activity is essential for *NDUFA4L2* induction.

To study the specific role of HIF-1α and HIF-2α in the response of *NDUFA4L2* to hypoxia, we performed RNA interference assays in human renal carcinoma RCC4 cells that constitutively stabilize HIF-1α and HIF-2α through the absence of VHL. Likewise, the response of NDUFA4L2 was also assessed in RCC4/VHL cells in which VHL expression was restored, and hence both HIF-1α and HIF-2α were exclusively upregulated in response to hypoxia. In line with the role of HIF activity in *NDUFA4L2* regulation, there was a robust upregulation of *NDUFA4L2* in hypoxic RCC4/VHL cells, whereas there was marked and constitutive *NDUFA4L2* expression in normoxic RCC4 cells that was only minimally upregulated in hypoxic conditions (Figure 2B). HIF-1α interference abrogated the expression of *NDUFA4L2* in both normoxic and hypoxic RCC4 cells (Figure 2B), as well as hypoxia-driven *NDUFA4L2* expression in RCC4/VHL cells (Figure 2B). By contrast, HIF-2α interference did not affect the expression of *NDUFA4L2* in RCC4/VHL cells exposed to hypoxia, and no significant effect was observed in RCC4 cells in either normoxic or hypoxic conditions (Figure 2B). The control experiments for the interference assays showed a specific reduction of *HIF-1α* or *HIF-2α* mRNA expression (Figure S2B).

We further confirmed these data in mouse embryonic fibroblasts (MEFs) from Hif-$1\alpha^{+f/+f}$/Cre conditional mice in which HIF-1α was lost after tamoxifen treatment. As a control, we employed tamoxifen Hif-$1\alpha^{+/+}$/Cre MEFs that lacked the CRE recombination sites required for HIF-1α ablation. The hypoxic induction of *Ndufa4l2* expression as well as that of the HIF target gene *Phd3* were only abrogated in Hif-$1\alpha^{+f/+f}$/Cre conditional MEFs following tamoxifen exposure, whereas they were still expressed in Hif-$1\alpha^{+/+}$/Cre MEFs (Figures 2C and S2C). Hence, the hypoxic induction of *Ndufa4l2* appeared to be mostly mediated by HIF-1α.

To identify possible hypoxia response elements (HREs) responsible for the induction of *NDUFA4L2*, the proximal promoter region (intron 1) of *NDUFA4L2* was analyzed, identifying

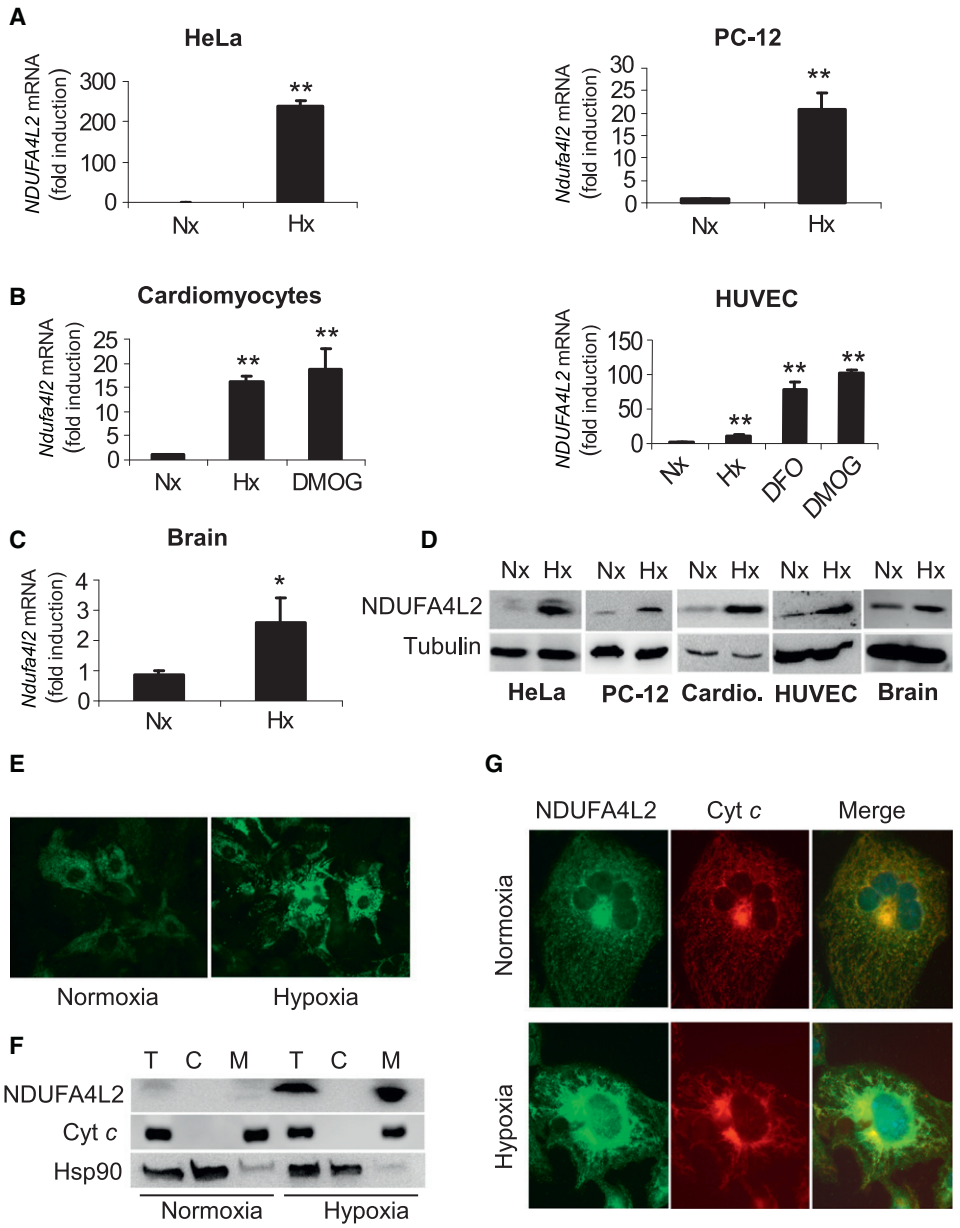

Figure 1. NDUFA4L2 Localizes to Mitochondria and Is Induced in Tumor Cells, in Primary Cultures, and In Vivo by Hypoxia

(A–C) Quantitative RT-PCR analysis of *NDUFA4L2* mRNA expression relative to the values in normoxia. HeLa, PC-12, cardiomyocytes, and HUVEC were cultured under conditions of normoxia or hypoxia (1% O_2) for 6 (HeLa) or 18 hr (PC-12, cardiomyocytes, HUVEC) (A and B). DMOG was added at 1 mM (cardiomyocytes) or 0.1 mM (HUVEC), and deferroxamine (DFO) was added at 0.2 mM in HUVEC (n = 3). Brain tissue from mice exposed to normoxic (n = 8) or hypoxic (7.5% O_2; n = 7) conditions for 18 hr is shown in (C).

(D) Immunoblot assay of NDUFA4L2 protein in HeLa, PC-12, HUVEC, or rat cardiomyocytes cultured under normoxic or hypoxic conditions (1% O_2 for cell cultures), as well as in brain tissue of mice subjected to hypoxia (7.5% O_2) for 18 hr. Tubulin is shown as a loading control. The images are representative of at least three experiments.

(E) Immunofluorescence showing the increase in NDUFA4L2 protein levels in rat cardiomyocytes exposed to normoxia or hypoxia (1% O_2) for 18 hr, with respect to those maintained in normoxic conditions. The images shown are representative of three experiments.

(F) Immunoblot assay of NDUFA4L2 in total cell (T), cytoplasmic (C), and mitochondrial (M) protein extracts from HeLa cells cultured under normoxic or hypoxic conditions (1% O_2) for 18 hr. Cytochrome *c* was assayed as a mitochondrial marker. The images shown are representative of three experiments.

(G) Immunofluorescence of HL-1 cells exposed to normoxia or hypoxia (1% O_2) for 18 hr. Images show staining for NDUFA4L2 (left panel, green) and cytochrome *c* (middle panel, red) and an overlay of the two signals (right panel). The images shown are representative of three experiments. See also Figure S1. n > 3; mean ± SEM; *p < 0.05; **p < 0.01.

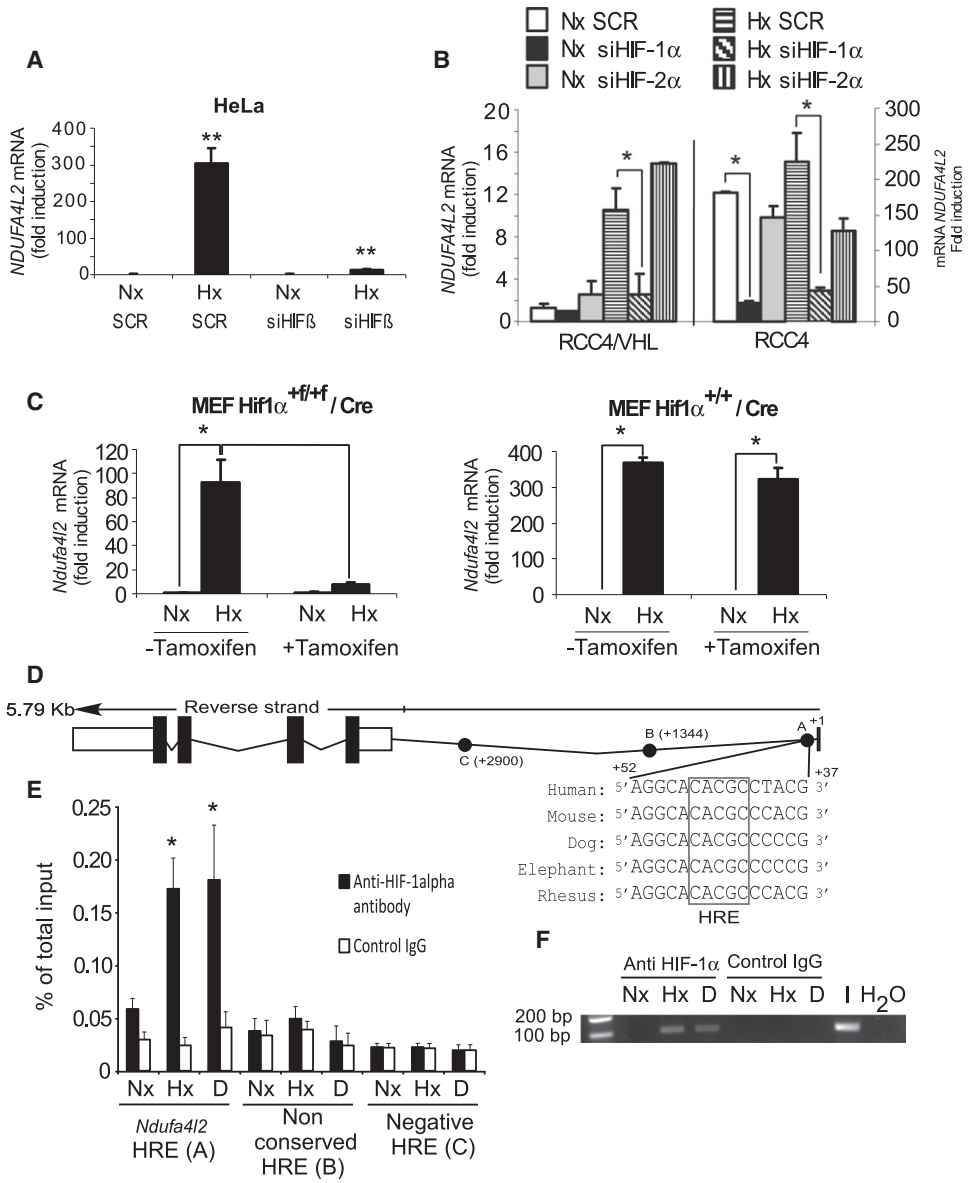

Figure 2. *NDUFA4L2* Induction Is Mediated by HIF-1α

(A) HeLa cells transfected with siRNA against HIF-β or a scramble control were cultured under normoxic or hypoxic (1% O_2) conditions for 24 hr. *NDUFA4L2* mRNA levels were quantified by real-time RT-PCR.

(B) VHL-deficient RCC4 cells or RCC4/VHL cells were transfected with siRNA against HIF-1α, HIF-2α, or a scramble control and exposed under normoxic or hypoxic conditions (1% O_2) for 24 hr. *NDUFA4L2* mRNA levels were quantified by real-time RT-PCR and are expressed relative to normoxic RCC4/VHL.

(C) Hif-1$\alpha^{+/+}$/Cre MEFs and Hif-1$\alpha^{+f/+f}$/Cre MEFs in the presence or absence of tamoxifen (1 μM) were cultured under normoxic or hypoxic conditions (1% O_2) for 18 hr. *NDUFA4L2* mRNA levels were quantified by real-time RT-PCR.

(D) Schematic representation of the human *NDUFA4L2* gene and the nucleotide sequences matching the consensus hypoxia response element (HRE) from five mammalian genes, indicating the regions A-B-C analyzed in the ChIP assay.

(E) ChIP assay of HIF-1α binding to the human *NDUFA4L2* gene in HeLa cells cultured in normoxic or hypoxic conditions (1% O_2) or exposed to DMOG (0.1 mM) for 6 hr. RT-PCR quantification is shown of regions A (putative NDUFA4L2 HRE), B (nonconserved HRE), and C (negative HRE) after immunoprecipitation with HIF-1α or a control antibody, represented as the percentage of that quantified in the total input DNA.

(F) Representative gel of DNA amplified in the ChIP assays shown in (E). See also Figure S2. n > 3; mean ± SEM; *p < 0.05; **p < 0.01.

two putative HREs at +43 and +1344 (Figure 2D). The +43 site is highly conserved between different species, unlike the +1344 site. Chromatin immunoprecipitation (ChIP) assays were performed on HeLa cells grown under normoxic or hypoxic conditions and after treatment with DMOG. To evaluate HIF-1α binding to *NDUFA4L2* regulatory sequences, quantitative PCR (qPCR) was performed using specific primers for the putative HRE site (A), the nonconserved HRE site (B), and a negative site (C). ChIP assays for *PDK1*, a well-known HIF-1α target, were also performed as a positive control (Figure S2D). HIF-1α

binding to the *NDUFA4L2* proximal promoter containing conserved HRE site (A) was strongly induced by hypoxia and DMOG treatment (Figure 2E), but not to the nonconserved HRE site (B) or the negative control region (C). The sequence amplified by qPCR had the expected size (Figure 2F). Taken together, these results suggest that *NDUFA4L2* is a direct HIF-1 target gene.

NDUFA4L2 Is Involved in the Hypoxia-Induced Decrease in Oxygen Consumption and Prevents Increases in Membrane Potential and ROS Production during Hypoxia

To test whether NDUFA4L2 is involved in the regulation of mitochondrial activity in hypoxia, we first determined the oxygen consumption in HeLa cells in which NDUFA4L2 was silenced by specific siRNA. In these experiments, *NDUFA4L2* expression was typically reduced by 80% in hypoxic conditions (Figure S3A) while *NDUFA4* mRNA levels were not affected by the siNDUFA4L2 (Figure S3B), highlighting the specificity of the interference of NDUFA4L2. Indeed, NDUFA4L2 interference reduced its protein expression in both normoxic and hypoxic conditions (Figure 3A), whereas the expression levels of proteins from other ETC complexes were unaffected by NDUFA4L2 interference (Figure S3C). Oxygen consumption decreased approximately 42% in hypoxic conditions when compared to normoxia in control HeLa cells (Figure 3B). However, oxygen consumption only decreased by 27% in hypoxic conditions when NDUFA4L2 was silenced in HeLa cells and when compared to control cells in normoxic conditions (Figure 3B). In normoxia, NDUFA4L2 silencing increased oxygen consumption by only 10%, probably due to the low normoxic levels of NDUFA4L2. We also tested whether transient overexpression of NDUFA4L2 might decrease oxygen consumption by using a pCMV-NDUFA4L2 vector to achieve expression levels similar to those obtained in hypoxia (Figures 3C and S3D). Transient overexpression of NDUFA4L2 decreased oxygen consumption in HeLa cells by approximately 20% (Figure 3D). Hence, we conclude that during hypoxia, NDUFA4L2 induction decreases oxygen consumption.

Since attenuation of mitochondrial activity in hypoxia may be a compensatory mechanism to keep mitochondrial ROS under control, we wondered whether hypoxia-driven NDUFA4L2 upregulation could also participate in this antioxidant response. Previous studies used the fluorescent dye H_2DCFDA and flow cytometry to demonstrate an increase of mitochondrial ROS production when cells are exposed to low O_2 tensions (Brunelle et al., 2005; Guzy et al., 2005; Mansfield et al., 2005). Accordingly, we observed increased H_2DCFDA fluorescence in HeLa cells exposed to hypoxia (1% O_2) that was exacerbated when NDUFA4L2 was silenced (Figure 3E). Similar data were obtained using the mitochondrial superoxide indicator MitoSOX (Figure 3F), which points to the mitochondrial origin of this increased superoxide production, probably from respiratory complexes. Increased ROS production in the absence of NDUFA4L2 during hypoxia correlated with an increased mitochondrial membrane potential in these conditions (Figure 3G). Conversely, NDUFA4L2 overexpression significantly decreased membrane potential compared to cells expressing the empty vector (Figure 3H).

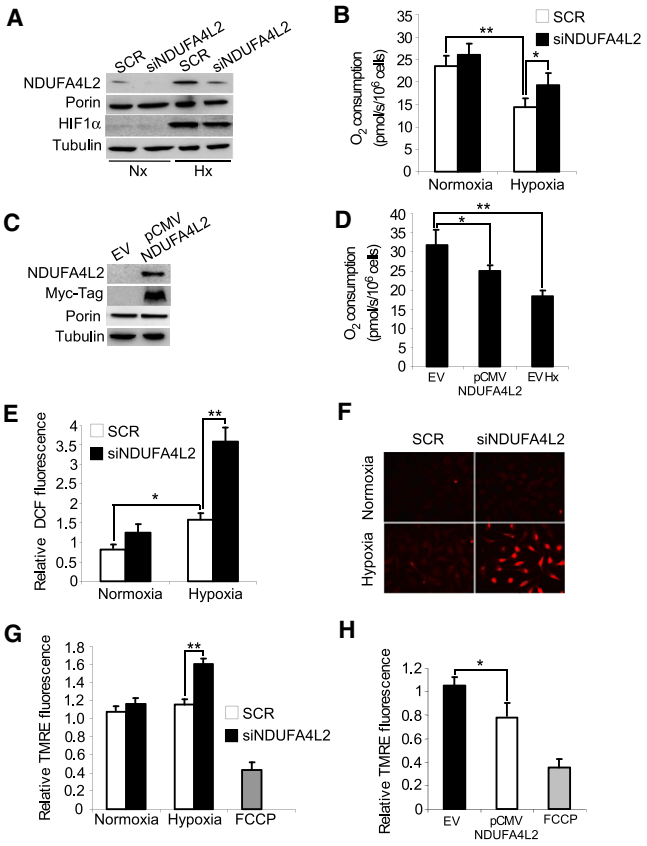

Figure 3. NDUFA4L2 Decreases Oxygen Consumption, Membrane Potential, and ROS Production in Hypoxia

(A–D) HeLa cells were transfected with a scramble control or NDUFA4L2 siRNA and exposed to normoxic or hypoxic (1% O_2) conditions for 18–24 hr. Immunoblot analysis of NDUFA4L2 and HIF-1α protein levels using tubulin and mitochondrial porin as loading controls is shown in (A). The images are representative of four independent experiments. Oxygen consumption rates were measured by high-resolution respirometry (B). HeLa cells were transfected with the empty vector (EV) or pCMV-NDUFA4L2 and then exposed to normoxic or hypoxic (1% O_2) conditions for 24 hr (C and D). Immunoblot analysis of NDUFA4L2 and myc-tagged protein levels using tubulin and mitochondrial porin as loading controls are shown (C). The images are representative of four independent experiments. Oxygen consumption rates were measured by high-resolution respirometry (D).

(E) Relative DCF fluorescence as a measure of intracellular hydrogen peroxide levels.

(F) Representative images of four independent experiments showing MitoSOX intensity as a measure of mitochondrial superoxide levels.

(G and H) Mitochondrial membrane potential was determined with the fluorescent probe TMRE and expressed relative to the control cells in normoxia. FCCP was used as a positive control of mitochondrial membrane depolarization (n > 3; mean ± SEM; *p < 0.05; **p < 0.01).

The Hypoxia-Induced Decrease in Oxygen Consumption via NDUFA4L2 Occurs through Complex I Inhibition

Given that NDUFA4L2 appears to be a mitochondrial protein involved in the downregulation of hypoxia-induced oxygen consumption, and that it likely belongs to the NDUFA4 subunit family of Complex I, we wondered whether NDUFA4L2 might be involved in actively regulating Complex I activity. We found that, when compared to normoxic conditions, Complex I activity

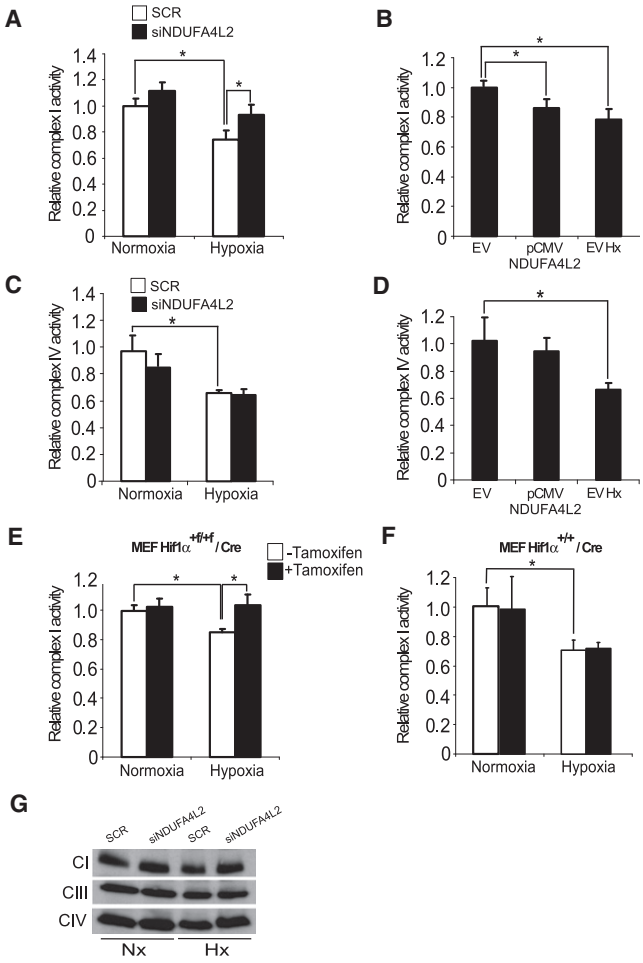

Figure 4. NDUFA4L2 Decreases Complex I Activity in Hypoxia

(A and B) Complex I activity was measured in HeLa cells transfected with a scramble control or NDUFA4L2 siRNA (A) or with the empty or pCMV-NDUFA4L2 vector (B), then exposed to normoxic or hypoxic (1% O_2) conditions for 24 hr.

(C and D) Complex IV activity was measured in HeLa cells transfected with a scramble control or NDUFA4L2 siRNA (C) and the empty or pCMV-NDUFA4L2 vector (D), then exposed to normoxic or hypoxic (1% O_2) conditions for 24 hr.

(E and F) Complex I activity was measured in Hif-1$\alpha^{+f/+f}$/Cre (E) or Hif-1$\alpha^{+/+}$/Cre MEFs (F) maintained in the presence or absence of tamoxifen (1 μM) for 48 hr and cultured under normoxic or hypoxic (1% O_2) conditions for 18 hr.

(G) Blue native PAGE (BN-PAGE) analysis of the mitochondrial OXPHOS Complex I (NDUFA9), Complex III (Core 2), and Complex IV (Col) from scramble and NDUFA4L2 siRNA HeLa cells exposed to normoxic or hypoxic (1% O_2) conditions for 24 hr ($n > 3$; mean ± SEM; *$p < 0.05$; **$p < 0.01$).

decreased ~20% in HeLa cells exposed to hypoxia (1% O_2 for 24 hr), although it did not when NDUFA4L2 expression was silenced (Figure 4A). Moreover, transient overexpression of NDUFA4L2 decreased Complex I activity in normoxic conditions (Figure 4B), demonstrating that NDUFA4L2 regulates Complex I under low-oxygen conditions.

To study the specificity of the effects of NDUFA4L2 on Complex I, we also measured Complex IV activity. Hypoxia (1% O_2 for 24 hr) induced a 38% decrease in Complex IV activity in HeLa cells (Figure 4C), but the silencing of NDUFA4L2 expression in hypoxia or its overexpression in normoxia did not affect Complex IV activity (Figures 4C and 4D). Similar results were obtained when Complex IV activity was determined spectrophotometrically (data not shown). Hence, NDUFA4L2 appears to affect ETC activity by specifically inhibiting Complex I. Since our results indicate that *NDUFA4L2* is a HIF-1α-dependent gene involved in the downregulation of Complex I activity in hypoxia, we further studied the role of HIF-1 in regulating Complex I. As expected, there was no decrease in Complex I activity following hypoxia in tamoxifen-treated Hif-1$\alpha^{+f/+f}$/Cre MEFs in which HIF-1α was ablated (Figure 4E). By contrast, a decrease in Complex I activity similar to that seen in HeLa cells was evident in tamoxifen-treated Hif-1$\alpha^{+/+}$/Cre MEFs (~20%) (Figure 4F). These results suggest that the HIF-1α-induced increase in NDUFA4L2 expression decreased oxygen consumption through the specific inhibition of mitochondrial Complex I activity.

Complex I activity can be modulated by its assembly (Vogel et al., 2005). We hypothesized that hypoxia-induced NDUFA4L2 could affect Complex I assembly. To test this possibility, we performed Blue native PAGE (BN-PAGE) in order to analyze the status of mitochondrial complexes. Neither hypoxia nor NDUFA4L2 silencing modified Complex I content, thus ruling out the involvement of NDUFA4L2 in the Complex I assembly process (Figure 4G).

Silencing of NDUFA4L2 Impairs Cell Proliferation in Hypoxia by Increasing Mitochondrial ROS Generation

While the absence of NDUFA4L2 does not significantly affect cell proliferation in normoxic conditions (Figure 5A), viable hypoxic NDUFA4L2-silenced HeLa cells proliferated at a slower rate than hypoxic control cells (Figure 5B). This slower proliferation was evident by both cell counting and by direct observation under the microscope (Figure 5C); it was also observed in other cell types such as HUVEC, UCD-Mel-N, and SKOV3 cells (Figure S4A). NDUFA4L2-silenced cells did not show either increased caspase-3 cleavage (Figure 5D) or changes in propidium iodide incorporation (Figure 5E), excluding the possibility that NDUFA4L2 silencing impaired cell proliferation by activating apoptosis. Additional studies showed that the capacity of hypoxic HeLa cells to form colonies in soft agar was affected when NDUFA4L2 was silenced, with a decrease in both the size and the number of colonies (Figure 5F). In order to investigate whether ROS overproduction in NDUFA4L2-silenced HeLa cells during hypoxia was responsible for the impairment in cell proliferation, we tested the effects of two different antioxidants, N-acetylcysteine (NAC) and MitoQ (an antioxidant targeted to mitochondria), on cell proliferation. Cell proliferation was restored when NDUFA4L2-silenced HeLa cells were treated with MitoQ in hypoxia (Figure 5G). This effect was also observed with NAC (Figure S4B), suggesting that exacerbated ROS production may be involved in the impairment of cell viability under hypoxia. Indeed, an increase in ROS production was detected in NDUFA4L2-silenced cells exposed to hypoxia using the mitochondrial superoxide indicator MitoSOX (Figure 5H). This increase was completely prevented by incubation with MitoQ (Figure 5H).

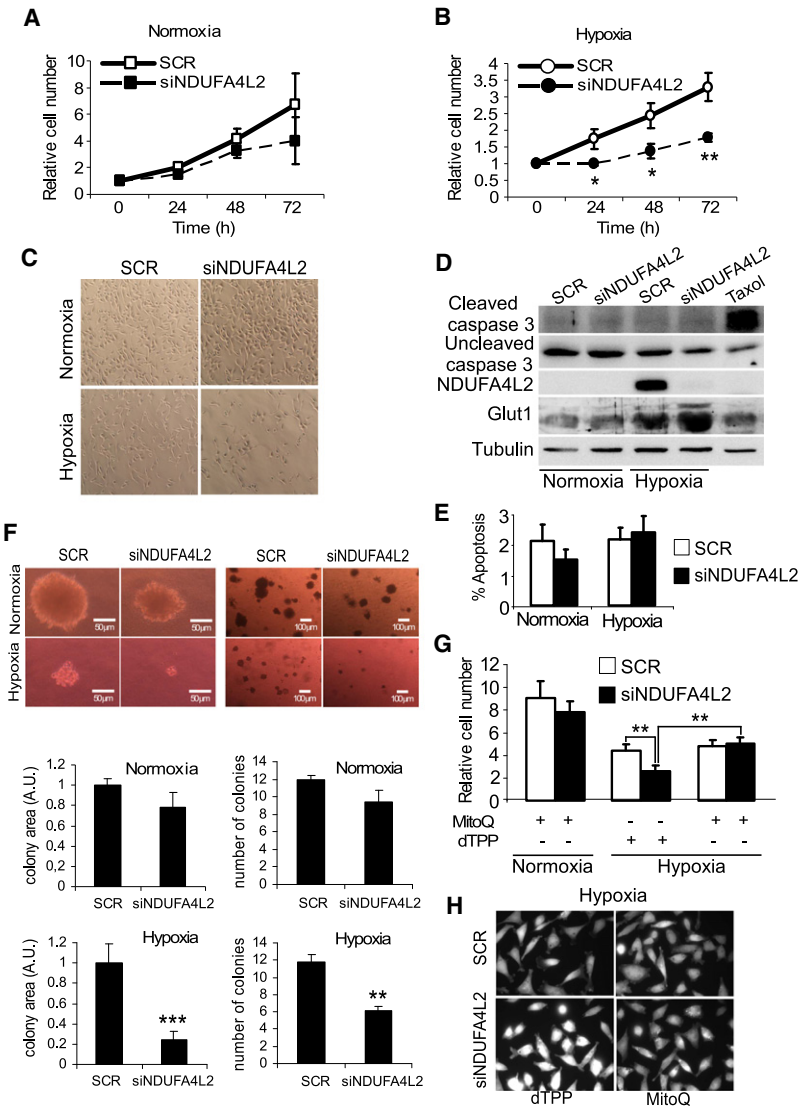

Figure 5. Reduced Hypoxic Levels of NDUFA4L2 Impair Cell Proliferation

(A and B) Growth curves of HeLa cells transfected with a scramble control or NDUFA4L2 siRNA in normoxic (A) and hypoxic (0.5% O_2) (B) conditions for different periods of time.

(C) Microscope images showing the density of HeLa cell cultures transfected with a scramble control or NDUFA4L2 siRNA and maintained under normoxic (21% O_2) or hypoxic (0.5% O_2) conditions for 72 hr.

(D) HeLa cells were transfected with either a scramble control or NDUFA4L2 siRNA and cultured under normoxic (21% O_2) or hypoxic (0.5% O_2) conditions for 72 hr, and the cell lysates were assayed in immunoblots that were probed with antibodies against NDUFA4L2, uncleaved caspase-3, and cleaved caspase-3. Glut1 was used as a positive control of hypoxic gene induction and tubulin as a loading control. Taxol was used as positive control of apoptosis.

(E) Scramble control or NDUFA4L2 siRNA HeLa cells maintained in normoxic (21% O_2) or hypoxic (0.5% O_2) conditions for 72 hr. The absolute value of apoptosis was measured by flow cytometry in cells stained with propidium iodide, as described in the Experimental Procedures.

(F) Image of colony formation by HeLa cells transfected with a scramble control or NDUFA4L2 siRNA in normoxic and hypoxic (0.5% O_2) conditions in soft agar for 15 days. Both size and number of colonies were quantified.

(G) Growth of HeLa cells transfected with a scramble control or NDUFA4L2 siRNA in normoxic and hypoxic (0.5% O_2) conditions with or without 0.5 μM MitoQ (0.5 μM dTPP was used as control of MitoQ) at 72 hr.

(H) Fluorescence microscopy images of hypoxic (0.5% O_2) cultured scramble and siNDUFA4L2 HeLa cells treated either with 0.5 μM MitoQ or 0.5 μM dTPP ($n > 3$; mean ± SEM; *$p < 0.05$; **$p < 0.01$).

Cell-cycle analysis showed that hypoxic NDUFA4L2-silenced HeLa cells had increased early S phase and decreased late S phase compared to scramble control cells (Figure S4C). Since NDUF4L2-silenced HeLa cells present ROS overproduction in hypoxia, and ROS can increase the phosphorylation of histone H2AX, a marker of cell stress (Driessens et al., 2009), we then analyzed the phosphorylation of H2AX histone. We observed increased phosho-H2AX levels in hypoxia when NDUFA4L2 was interfered (Figure S4D), suggesting that the lack of NDUFA4L2 in hypoxia produces cell stress.

It has been described that both the downregulation of the iron-sulfur cluster assembly proteins (ISCU1/2) via miR-210 and the upregulation of PDK1 are implicated in ROS control and cell viability in hypoxia (Chan et al., 2009; Chen et al., 2010; Favaro et al., 2010; Kim et al., 2006; Papandreou et al., 2006). To investigate the relative contribution of these effects to HeLa hypoxic adaptation, we performed cell proliferation assays. We only observed a decrease in ISCU1/2 protein at times over 24 hr at 0.5% (Figure S5A) but not in the milder hypoxic conditions (1% O_2). Furthermore, the overexpression of ISCU1/2 did not affect HeLa cell proliferation in hypoxia (0.5% O_2) at 72 hr (Figure S5B). In addition, HeLa cells in which PDK1 was silenced by specific siRNA (Figure S5C) showed a decrease in proliferation under hypoxia (0.5% O_2) at 72 hr (Figure S5D) similar to that observed in NDUFA4L2-silenced cells, suggesting that both NDUFA4L2 and PDK1 play an important role in ROS control and cell proliferation in our system conditions.

MEFs Obtained from NDUFA4L2 Knockout Mice Exhibit Higher Oxygen Consumption and Complex I Activity in Hypoxia Than Wild-Type MEFs

In order to gain further insight into the role of NDUFA4L2 on hypoxia-induced mitochondrial reprogramming, we generated NDUFA4L2 knockout (KO) mice. We initially planned to isolate primary cell cultures from NDUFA4L2-deficient adult mice. However, we found that homozygous *Ndufa4l2* gene inactivation results in perinatal lethality, which demonstrates an essential biological role of NDUFA4L2 in development that will be further explored in future studies. Therefore, we isolated NDUFA4L2-deficient MEFs and the corresponding wild-type controls from E12.5–14.5 embryos generated from NDUFA4L2$^{+/-}$ breeding pairs. In order to validate these MEF cultures, we analyzed the

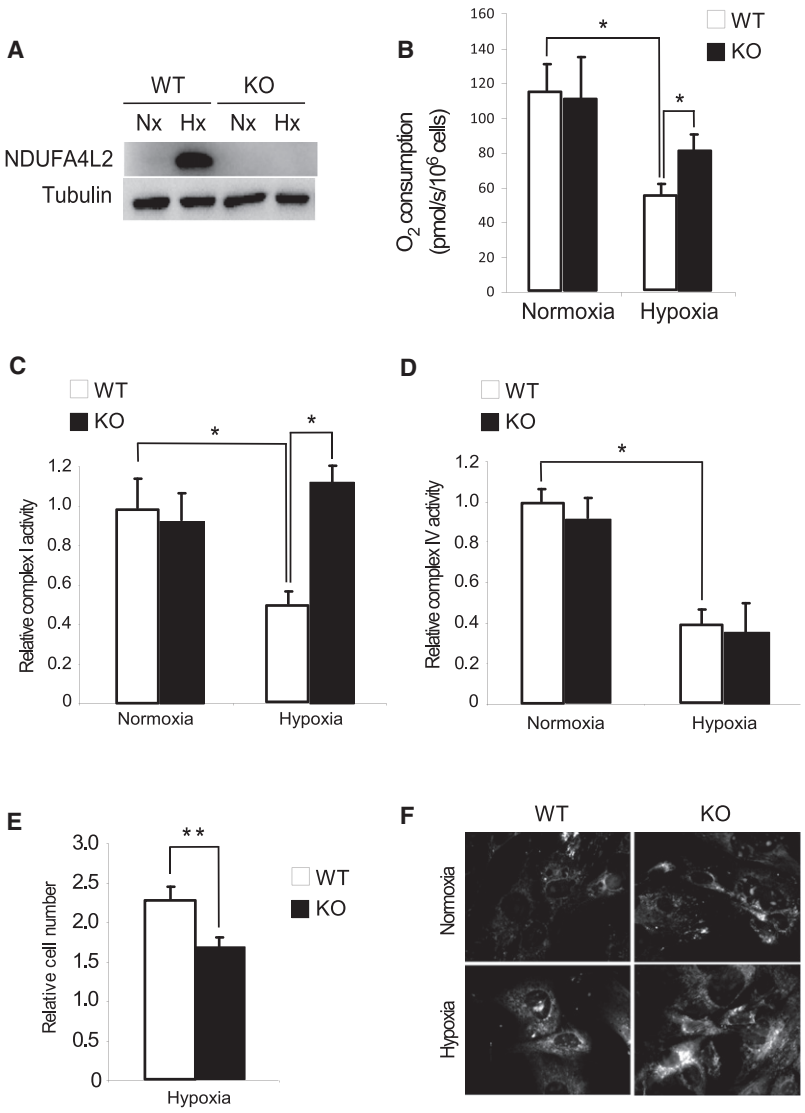

Figure 6. Analysis of NDUFA4L2-Deficient MEFs

(A–D) WT and KO MEFs were exposed to 0.5% hypoxia 24 hr prior to subsequent analysis. Immunoblot analysis showing the total deficiency of NDUFA4L2 is shown in (A). Tubulin was used as a loading control. Oxygen consumption rates were measured by high-resolution respirometry (Oxygraph 2k) (B). Complex I (C) and Complex IV (D) activities were measured spectrophotometrically and expressed relative to citrate synthase values.

(E) Relative growth rates of WT and KO NDUFA4L2 MEFs cultured in hypoxia (0.5% O_2).

(F) Representative images of three independent experiments showing MitoSOX intensity as a measure of mitochondrial superoxide levels (n > 3 mean ± SEM; *p < 0.05, **p < 0.01).

expression of NDUFA4L2. Western blot analysis confirmed that NDUFA4L2 increased in hypoxia in MEFs from wild-type mice only (Figure 6A). We determined oxygen consumption in MEFs obtained from NDUFA4L2 KO and wild-type mice (Figure 6B). Confirming results obtained in HeLa cells, MEFs from NDUFA4L2 KO mice showed increased respiration rate in hypoxia compared to wild-type mice (Figure 6B). The activity of Complex I in hypoxia was higher in MEFs from KO mice than in those from wild-type mice, confirming the results obtained in HeLa cells (Figure 6C). In contrast, the activity of Complex IV in hypoxia was similarly decreased in both types of MEFs (Figure 6D). The expression level of respiratory complexes was studied by BN-PAGE using DDM (n-dodecyl beta-D-maltoside), obtaining the same result as in HeLa cells (data not shown). In addition, MEFs from NDUFA4L2 KO mice exhibited a lower proliferation rate than those from wild-type mice when cultured under hypoxia (Figure 6E), and this lower proliferation correlated with increased ROS production under hypoxic conditions (Figure 6F).

NDUFA4 Paralogue Is Repressed under Hypoxia at the Protein Level

It is established that a COX4-2 to COX4-1 subunit substitution takes place at Complex IV during hypoxia (Fukuda et al., 2007). The paralogue proteins NDUFA4L2 and NDUFA4 derive from the same ancestral gene, share more than 65% in their amino acid sequence, and have been suggested to be part of mitochondrial Complex I (Walker et al., 1992). Since *NDUFA4* mRNA levels do not change in hypoxia up to 48 hr (Figure 7A), we investigated the fate of the protein under hypoxia. We found that NDUFA4 protein decreases in hypoxic cells while NDUFA4L2 protein expression increases in hypoxic conditions (Figure 7B). We also explored whether NDUFA4L2 levels would be responsible for the downregulation of NDUFA4. NDUFA4 protein levels decreased in hypoxia even when NDUFA4L2 was silenced (Figure 7C), and its expression in normoxia was unaffected by NDUFA4L2 overexpression (Figure 7D). NDUFA4 protein decreases to the same extent in NDUFA4L2 KO MEFs, demonstrating that both events occur independently (Figure 7E). Collectively, all these data indicate that NDUFA4L2 KO MEFs markedly repress NDUFA4 protein levels in hypoxia while Complex I activity is not affected, ruling out the possibility that Complex I activity is repressed in hypoxia via NDUFA4. These data stress the specific role of hypoxia-dependent NDUFA4L2 upregulation in Complex I activity inhibition.

DISCUSSION

The influence of fluctuations in oxygen concentration on mitochondrial activity has raised a great interest due to its broad impact on pathophysiology. Mitochondrial respiration is only compromised when the oxygen concentration drops below 0.1% O_2 because of the high affinity of mitochondrial cytochrome *c* oxidase (Complex IV) for oxygen (Aguirre et al., 2010; Gnaiger et al., 1998; Smolenski et al., 1991; Stumpe and Schrader, 1997). However, during moderate hypoxia (1%–2% O_2), cells

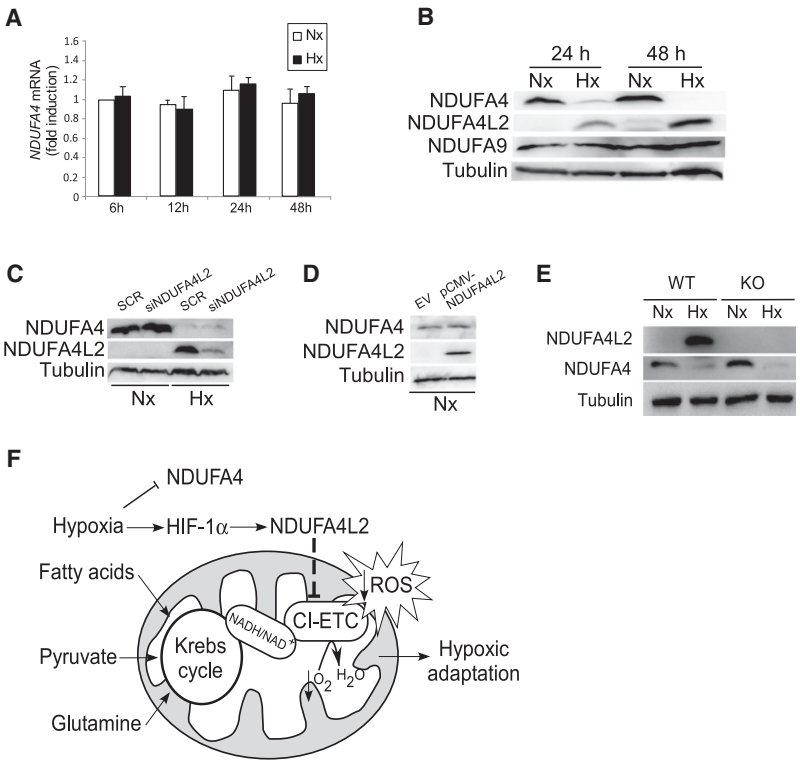

Figure 7. Opposite Regulation of NDUFA4 and NDUFA4L2 under Hypoxia

(A) HeLa cells were cultured under hypoxia (1% O_2) for 6, 12, 24, and 48 hr, and *NDUFA4* mRNA levels were analyzed.

(B) Immunoblot analysis of HeLa cells subjected to either 24 or 48 hr of hypoxia and proved against NDUFA4 and NDUFA4L2 antibodies. NDUFA9 was used as a loading control for Complex I, and tubulin was used as a total loading control.

(C and D) HeLa cells were transfected with a scramble control or NDUFA4L2 siRNA and then exposed to normoxic or hypoxic (1% O_2) conditions for 24 hr (C) or transfected with the empty or pCMV-NDUFA4L2 vector (D). Cell lysates were analyzed against NDUFA4, NDUFA4L2, and tubulin antibodies.

(E) Immunoblot analysis of MEFs WT and KO for NDUFA4L2 showing the total deficiency of NDUFA4L2 and the decrease of NDUFA4 under hypoxic (1% O_2) conditions for 24 hr. Tubulin was used as a loading control.

(F) Model showing the involvement of NDUFA4L2 induction by HIF-1α in hypoxic adaptation. HIF-1α stabilization by hypoxia upregulates NDUFA4L2, which inhibits ETC Complex I activity. As a result, oxygen consumption decreases and ROS production is abrogated, thereby allowing cells to adapt to the hypoxic conditions. In contrast, hypoxia decreases NDUFA4 protein levels ($n > 3$; mean ± SEM; $^*p < 0.05$; $^{**}p < 0.01$).

express a large number of genes, dependent on HIFs, that reprogram the metabolism to attenuate mitochondrial O_2 consumption, which also protects cells against excessive mitochondrial ROS formation (Aragonés et al., 2009; Kim et al., 2006; Papandreou et al., 2006).

At the molecular level, we show here that moderate hypoxia decreases oxygen consumption and Complex I activity via the HIF-1-dependent upregulation of NDUFA4L2. Our data indicate that *NDUFA4L2* is a HIF-1-dependent gene, emphasizing the role of HIF-1 in mitochondrial reprogramming and revealing NDUFA4L2 as an important element in metabolic adaptation to hypoxia. We have observed this induction in different cell types, as well as in tissue from animals subjected to hypoxia, suggesting a role in physiological adaptation to hypoxia. In this regard, NDUFA4L2 KO homozygous mice, which could be a presumed mouse model of Complex I gain of function based on our own data, show perinatal lethality, stressing the high relevance of this protein in vivo. Similarly, mouse models of Complex I deficiency (Kruse et al., 2008) also die shortly after birth, which indicates that Complex I activity needs to be tightly controlled to assure an adequate development early after birth.

The PHD oxygen-sensing pathway is also known to upregulate the PDH kinase isoforms PDK1, PDK3, and PDK4 (Aragonés et al., 2008; Kim et al., 2006; Lu et al., 2008; Papandreou et al., 2006). PDK overactivation reduces PDH activity, slowing down the conversion of pyruvate into acetyl-CoA and ultimately repressing the TCA cycle and the supply of NADH to the mitochondrial ETC. Therefore, PDKs could potentially cooperate with NDUFA4L2 to reduce mitochondrial Complex I activity under moderate hypoxic conditions, but it is also conceivable that NDUFA4L2 has other biological functions that cannot be accomplished by PDKs. For example, when metabolites that fuel the TCA cycle originate from pathways different from glycolysis (e.g., glutaminolysis or fatty acid oxidation), it would be necessary to reduce ETC activity in order to decrease mitochondrial function (Wheaton and Chandel, 2011). Hypoxia-induced NDUFA4L2 expression could fulfill this role, reducing oxygen consumption due to its strategic position downstream of the TCA cycle, possibly at Complex I (Figure 7F). Likewise, hypoxia induces the upregulation of microRNA-210, which represses ISCU1/2 (Chan et al., 2009; Chen et al., 2010; Favaro et al., 2010). These proteins facilitate the assembly of iron-sulfur clusters, including those in Complex I, Complex III, and aconitase, which are critical for electron transport and mitochondrial redox reactions. As a result, microRNA-210 represses mitochondrial respiration. In our model, and in line with previous studies, ISCU1/2 protein does not decrease prior to 48 hr and only under 0.5% O_2, while NDUFA4L2 becomes functional as early as 24 hr at 1% O_2. Moreover, ISCU1/2 recovery in hypoxic HeLa cells did not disturb proliferation. In this sense, it has been described that an anti-miR-210 affects HeLa cell proliferation at times longer than 48 hr and at very low oxygen tensions (0.01% O_2) (Favaro et al., 2010).

Very intriguingly, however, Complex I inhibition in HeLa cells takes place at milder hypoxia (1% O_2) (Figure 4), and this oxygen tension does not seem to be enough to decrease ISCU1/2 (Figure S5A). Furthermore, ISCU1/2 downregulation is not observed before 48 hr, but Complex I is inhibited as early as 24 hr. This opened a 24 hr window during which NDUFA4L2 could be acting before ISCU induction takes place. As demonstrated, NDUFA4L2 Complex I inhibition occurs without affecting Complex I quantity, but probably by a direct or indirect

interaction that remains to be elucidated. However, miRNA-210-targeted ISCU1/2 presumably fulfills its function by decreasing Complex I content. This early NDUFA4L2-dependent qualitative modulation followed by a later miR210-dependent quantitative repression of Complex I represents a possible model by which HIF-1 guarantees a fine control of Complex I under hypoxic conditions. In summary, we propose that, although NDUFA4L2 upregulation and miR-210-induced ISCU1/2 repression could act synergistically to decrease Complex I activity and oxygen consumption in chronic hypoxia, we should underscore that primary (1% O_2) Complex I inhibition can be only accomplished by early NDUFA4L2 induction.

Altered subunit content during hypoxia has also been reported for other ETC complexes. Thus, physiological hypoxia induces a COX4-1 to COX4-2 subunit switch, an effect mediated by HIF-1 that is thought to optimize the efficiency of respiration during conditions of reduced oxygen availability (Fukuda et al., 2007). Since we have found that NDUFA4 is downregulated at the protein level in hypoxia, we could speculate that NDUFA4L2 induction is taking over NDUFA4's place at Complex I and reducing in some way its activity. However, NDUFA4L2 KO MEFs markedly repress NDUFA4 protein levels in hypoxia, while Complex I activity is not affected, ruling out the possibility that Complex I activity is repressed in hypoxia via NDUFA4. In this regard, the role and location of NDUFA4 within Complex I are not yet well understood.

The ETC produces superoxide when single electrons are transferred to O_2 during electron transport. There are different sites of ROS production in mammalian mitochondria (Murphy, 2009), but the greatest maximum capacity of ROS production is the ubiquinone reduction site of Complex I and the outer quinone-binding site of the Q cycle in Complex III (Liu et al., 2002; Raha and Robinson, 2000; St-Pierre et al., 2002; Votyakova and Reynolds, 2001). Although superoxide production in isolated mitochondria correlates with oxygen tension (Liu et al., 2002), it is generally accepted that ROS production in cells increases during short periods of hypoxia (Brunelle et al., 2005; Guzy et al., 2005; Mansfield et al., 2005). In agreement with this, we detected increased ROS in hypoxia using the fluorescent probes DCFDA and MitoSOX. The hypoxia-induced ROS increase was exacerbated in the absence of NDUFA4L2, indicating that the expression of this protein keeps ROS production under control and hence could protect the cell against oxidative stress. Whether the effects of NDUFA4L2 on ROS production are direct or occur through the modulation of other mitochondrial proteins requires further research. However, the fact that mitochondrial membrane potential increases simultaneously with increased ROS in the absence of NDUFA4L2 suggests that both events might be closely associated, as has been demonstrated elsewhere (Korshunov et al., 1997; Votyakova and Reynolds, 2001).

Hypoxia-exposed cell cultures accumulate intracellular ROS, but most probably at lower sublethal concentrations. As shown in Figure 5, and in line with previous studies, hypoxia slows down proliferation (Gardner et al., 2001; Goda et al., 2003). However, NDUFA4L2-silenced cells and MEFs from NDUFA4L2 KO mice showed a more profound inhibition of cell proliferation in parallel to a higher ROS accumulation and DNA stress/damage (H2AX phosphorylation) than control cells or MEFs from wild-type mice. NDUFA4L2-silenced cells did not show signs of cellular apoptosis, probably because of the high-resistance nature of these tumor cells. Therefore, it is reasonable to think that the PHD-HIF system counteracts ROS overproduction that impairs cell growth.

Several in vivo and in vitro studies have revealed that the reduction of mitochondrial oxygen consumption through PHD and HIF activities prepares cells to tolerate more extreme lethal hypoxic/ischemic conditions, saving oxygen and reducing mitochondrial ROS formation. We hypothesize that NDUFA4L2 induction during hypoxia helps keep intracellular ROS production in check, consistent with the fact that NDUFA4L2 limits Complex I activity and prevents increases in membrane potential. It is therefore reasonable to speculate that NDUFA4L2 could participate in ischemic preconditioning. Indeed, several in vivo studies have shown that partial inhibition of Complex I with sublethal doses of amobarbital (a reversible inhibitor at the rotenone site of Complex I) prevents reperfusion-induced cardiac damage (Aldakkak et al., 2008; Chen et al., 2006a, 2006b).

Our studies indicate that mitochondrial Complex I activity is controlled by NDUFA4L2 during hypoxia. In conjunction with previous data on PHD- and HIF-regulated mitochondrial activity, we add further elements to the strategic armory used by HIFs to ensure that mitochondrial oxygen consumption is repressed in mild hypoxic conditions, highlighting the biological relevance of the regulation of this cellular response.

EXPERIMENTAL PROCEDURES

Cell Lines and Cultures

HeLa, RCC4, RCC4/VHL, PC-12, HL-1, neonatal rat cardiomyocytes, Hif-1$\alpha^{+/+}$/Cre or Hif-1$\alpha^{+f/+f}$/Cre MEFs, and human umbilical vein endothelial cells (HUVEC) were used. See Supplemental Experimental Procedures for details.

Microarray Analysis

Total RNA was extracted using Ultraspec reagent (Biotecx, Houston, TX). One-Color Microarray-Based Gene Expression Analysis Protocol (Agilent Technologies, Palo Alto, CA) was used to amplify and label RNA. Briefly, 200–700 ng of total RNA was reverse transcribed using T7 promoter Primer and MMLV-RT. Then cDNA was converted to aRNA using T7 RNA polymerase, which simultaneously amplifies target material and incorporates cyanine 3-labeled CTP. Samples were hybridized to Whole Human Genome Microarray 4 × 44K (G4112F, Agilent Technologies). Cy3-labeled aRNA (1.65 g) was hybridized for 17 hr at 65°C in a hybridization oven (G2545A, Agilent) set to 10 rpm in a final concentration of 1× GEx Hybridization Buffer HI-RPM, according to manufacturer's instructions (One-Color Microarray-Based Gene Expression Analysis, Agilent Technologies). Arrays were washed according to manufacturer's instructions (One-Color Microarray-Based Gene Expression Analysis, Agilent Technologies) and dried out using a centrifuge. Finally, arrays were scanned at 5 μm resolution on an Agilent DNA Microarray Scanner (G2565BA, Agilent Technologies) using the default settings for 4 × 44K format one-color arrays. Images provided by the scanner were analyzed using Feature Extraction software version 9.5.3.1 (Agilent Technologies).

In Vivo Hypoxia Experiments

Eight-week-old male C57BL/6 mice were exposed to hypoxic (7.5% O_2) or normoxic (21% O_2) conditions for 18 hr. After treatment mice were sacrificed under the same conditions to avoid tissue reoxygenation following hypoxia. The brain and heart were then excised, frozen in liquid nitrogen, and stored at −80°C. Organs were homogenized in liquid nitrogen and resuspended in RIPA buffer (1% NP40, 0.5% sodium deoxycholate, and 0.1% SDS in PBS buffer) for protein extraction or Ultraspec reagent (Biotecx, Houston, TX) for mRNA isolation.

Oxygen Consumption

Oxygen consumption was determined by high-resolution respirometry (Oxygraph-2k, Oroboros Instruments, Innsbruck, Austria). Cells were trypsinized after the indicated treatments and then resuspended at 2×10^6 cells/ml in HBSS containing 25 mM HEPES. The instrumental background flux was calculated as a linear function of the oxygen concentration, and the experimental data were corrected using DatLab software (Oroboros Instruments). The oxygen concentration in air-saturated culture medium at 37°C was 175.7 μM (Rodríguez-Juárez et al., 2007). Measurements were taken at 37°C in parallel Oxygraph-2k chambers for cells incubated in normoxic and hypoxic (1% O_2) conditions with the indicated treatments.

Mitochondria Isolation

The isolation of an enriched mitochondrial fraction from $2–5 \times 10^7$ HeLa cells was performed using the Mitochondria Isolation Kit MITOISO2 (Sigma) according to the manufacturer's instructions.

Complex I and IV Activity

The activities of Complex I and Complex IV were measured using the Complex I Enzyme Activity Microplate Assay Kit or the Complex IV Human Duplexing Microplate Assay Kit, both from MitoSciences, according to the manufacturer's instructions.

Mitochondrial Membrane Potential

Mitochondrial membrane potential was determined by incubating the cells with the fluorescent dye tetramethylrhodamine ethyl ester (TMRE; Sigma). Cells were incubated with 2.5 nM TMRE for 30 min at 37°C and subsequently analyzed by FACScan flow cytometer (Becton Dickinson, Lincoln Park, NJ).

Cell Proliferation and Apoptosis

For the cell proliferation assay, 2×10^5 HeLa, HUVEC, UCD-mel-N, and SKOV3 cells were planted in a 10 cm dish 1 day before exposure to hypoxic conditions (0.5% O_2). Either 0.1 mM NAC or 0.5 μM Mito-Q (0.5 μM DTPP was used as control of Mito-Q) was added to HeLa cells to determinate the effect of the antioxidants on NDUFA4L2-interfered cell proliferation in hypoxia. At the times indicated, the cells were trypsinized and the viable cells were counted using trypan blue. Apoptosis was determined by flow cytometry analysis of the cell cycle after DNA staining with propidium iodide (PI) and by analysis of cleaved caspase-3 with a specific antibody (Cell Signaling). Positive controls for apoptosis were performed by incubating HeLa cells with taxol (Calbiochem) at 1 μg/ml for 18 hr.

Soft Agar Assay

HeLa cells were seeded into 0.35% agar Noble (Difco) in DMEM containing 10% heat-inactivated FBS on top of a bed of 0.5% agar in 60 mm dishes at 5×10^3 cells per dish. Immobilized cells were grown for 15 days in a humidified chamber at 37°C and exposed to normoxic or hypoxic conditions (0.5% O_2). Colonies were then photographed using a DS-Fi1 camera (Nikon) and counted and measured using ImageJ software.

Analysis of ETC Complexes by Blue Native Electrophoresis Gel

Mitochondrial membrane proteins (100–150 mg) were applied and run on a 3%–13% first-dimension gradient Blue native electrophoresis gel as described elsewhere (Schägger, 1995). After electrophoresis, the complexes were electroblotted onto PVDF filters and sequentially probed with the following specific antibodies: anti-NDUFA9 (complex I), anti-core2 (complex III), anti-COI (complex IV), and anti-70 kDa subunit (complex II). All antibodies were obtained from Molecular Probes.

Ndufa4l2 Gene Inactivation in Mice

NDUFA4L2 chimeric males were obtained from Velocigene Regeneron Pharmaceuticals, Inc. (Reference number: 13661) through the KOMP repository. These chimeric mice were crossed with wild-type C57BL/6 females to generate NDUFA4L2 heterozygous mice. NDUFA4L2 heterozygous mice were used to generate NDUFA4L2-deficient embryos and the subsequent murine embryonic fibroblast isolation. The mice were bred and housed in a specific pathogen free (SPF) animal area of the animal facility at the Universidad Autónoma de Madrid (UAM).

Statistical Analysis

The data are presented as the means ± SEM of at least three independent experiments. Statistical significance *$p < 0.05$ or **$p < 0.01$ was assessed by the Wilcoxon test.

ACCESSION NUMBERS

The microarray data of HeLa cells are deposited at GEO DataSets with the accession number GSE33521.

SUPPLEMENTAL INFORMATION

Supplemental Information includes five figures, five tables, Supplemental Experimental Procedures, and Supplemental References and can be found with this article online at doi:10.1016/j.cmet.2011.10.008.

ACKNOWLEDGMENTS

This work was supported by Ministerio de Ciencia e Innovación (SAF 2007-06592, SAF 2010-14851), Comunidad Autónoma de Madrid (SAL 2006/0311), Metoxia Project-Health (F2 2009-222741), and Recava Network (RD 06/0014/0031) to M.O.L.; PS09/00101 and CP07/00143 to A.M.-R.; PI060701, PS09/00116, and CP08/00204 to S.C.; BFU2008-03407/BMC to J.A.; SAF2009-08007 to J.A.E.; and CSD2007-00020 to A.M.-R. and J.A.E. The CNIC is supported by the Instituto de Salud Carlos III-MICINN and the Pro-CNIC Foundation. We are grateful to Mike Murphy (Mitochondrial Biology Unit, MRC, Cambridge, UK) for the gift of MitoQ. We also thank Stephen Y. Chan and Joseph Loscalzo (Harvard Medical School, Boston, MA) for providing us ISCU expression vectors.

Received: April 12, 2010
Revised: July 21, 2011
Accepted: October 7, 2011
Published online: November 17, 2011

REFERENCES

Aguirre, E., Rodríguez-Juárez, F., Bellelli, A., Gnaiger, E., and Cadenas, S. (2010). Kinetic model of the inhibition of respiration by endogenous nitric oxide in intact cells. Biochim. Biophys. Acta *1797*, 557–565.

Aldakkak, M., Stowe, D.F., Chen, Q., Lesnefsky, E.J., and Camara, A.K. (2008). Inhibited mitochondrial respiration by amobarbital during cardiac ischaemia improves redox state and reduces matrix Ca2+ overload and ROS release. Cardiovasc. Res. *77*, 406–415.

Andreas, K., Häupl, T., Lübke, C., Ringe, J., Morawietz, L., Wachtel, A., Sittinger, M., and Kaps, C. (2009). Antirheumatic drug response signatures in human chondrocytes: potential molecular targets to stimulate cartilage regeneration. Arthritis Res. Ther. *11*, R15.

Aragonés, J., Schneider, M., Van Geyte, K., Fraisl, P., Dresselaers, T., Mazzone, M., Dirkx, R., Zacchigna, S., Lemieux, H., Jeoung, N.H., et al. (2008). Deficiency or inhibition of oxygen sensor Phd1 induces hypoxia tolerance by reprogramming basal metabolism. Nat. Genet. *40*, 170–180.

Aragonés, J., Fraisl, P., Baes, M., and Carmeliet, P. (2009). Oxygen sensors at the crossroad of metabolism. Cell Metab. *9*, 11–22.

Brunelle, J.K., Bell, E.L., Quesada, N.M., Vercauteren, K., Tiranti, V., Zeviani, M., Scarpulla, R.C., and Chandel, N.S. (2005). Oxygen sensing requires mitochondrial ROS but not oxidative phosphorylation. Cell Metab. *1*, 409–414.

Carroll, J., Fearnley, I.M., Skehel, J.M., Shannon, R.J., Hirst, J., and Walker, J.E. (2006). Bovine complex I is a complex of 45 different subunits. J. Biol. Chem. *281*, 32724–32727.

Chan, S.Y., Zhang, Y.Y., Hemann, C., Mahoney, C.E., Zweier, J.L., and Loscalzo, J. (2009). MicroRNA-210 controls mitochondrial metabolism during hypoxia by repressing the iron-sulfur cluster assembly proteins ISCU1/2. Cell Metab. *10*, 273–284.

Chen, Q., Hoppel, C.L., and Lesnefsky, E.J. (2006a). Blockade of electron transport before cardiac ischemia with the reversible inhibitor amobarbital protects rat heart mitochondria. J. Pharmacol. Exp. Ther. *316*, 200–207.

Chen, Q., Moghaddas, S., Hoppel, C.L., and Lesnefsky, E.J. (2006b). Reversible blockade of electron transport during ischemia protects mitochondria and decreases myocardial injury following reperfusion. J. Pharmacol. Exp. Ther. *319*, 1405–1412.

Chen, Z., Li, Y., Zhang, H., Huang, P., and Luthra, R. (2010). Hypoxia-regulated microRNA-210 modulates mitochondrial function and decreases ISCU and COX10 expression. Oncogene *29*, 4362–4368.

Driessens, N., Versteyhe, S., Ghaddhab, C., Burniat, A., De Deken, X., Van Sande, J., Dumont, J.E., Miot, F., and Corvilain, B. (2009). Hydrogen peroxide induces DNA single- and double-strand breaks in thyroid cells and is therefore a potential mutagen for this organ. Endocr. Relat. Cancer *16*, 845–856.

Favaro, E., Ramachandran, A., McCormick, R., Gee, H., Blancher, C., Crosby, M., Devlin, C., Blick, C., Buffa, F., Li, J.L., et al. (2010). MicroRNA-210 regulates mitochondrial free radical response to hypoxia and krebs cycle in cancer cells by targeting iron sulfur cluster protein ISCU. PLoS ONE *5*, e10345.

Favier, J., Brière, J.J., Burnichon, N., Rivière, J., Vescovo, L., Benit, P., Giscos-Douriez, I., De Reyniès, A., Bertherat, J., Badoual, C., et al. (2009). The Warburg effect is genetically determined in inherited pheochromocytomas. PLoS ONE *4*, e7094.

Fredlund, E., Ovenberger, M., Borg, K., and Påhlman, S. (2008). Transcriptional adaptation of neuroblastoma cells to hypoxia. Biochem. Biophys. Res. Commun. *366*, 1054–1060.

Frost, M.T., Wang, Q., Moncada, S., and Singer, M. (2005). Hypoxia accelerates nitric oxide-dependent inhibition of mitochondrial complex I in activated macrophages. Am. J. Physiol. Regul. Integr. Comp. Physiol. *288*, R394–R400.

Fukuda, R., Zhang, H., Kim, J.W., Shimoda, L., Dang, C.V., and Semenza, G.L. (2007). HIF-1 regulates cytochrome oxidase subunits to optimize efficiency of respiration in hypoxic cells. Cell *129*, 111–122.

Gardner, L.B., Li, Q., Park, M.S., Flanagan, W.M., Semenza, G.L., and Dang, C.V. (2001). Hypoxia inhibits G1/S transition through regulation of p27 expression. J. Biol. Chem. *276*, 7919–7926.

Gnaiger, E., Lassnig, B., Kuznetsov, A.V., and Margreiter, R. (1998). Mitochondrial respiration in the low oxygen environment of the cell. Effect of ADP on oxygen kinetics. Biochim. Biophys. Acta *1365*, 249–254.

Goda, N., Ryan, H.E., Khadivi, B., McNulty, W., Rickert, R.C., and Johnson, R.S. (2003). Hypoxia-inducible factor 1alpha is essential for cell cycle arrest during hypoxia. Mol. Cell. Biol. *23*, 359–369.

Guzy, R.D., Hoyos, B., Robin, E., Chen, H., Liu, L., Mansfield, K.D., Simon, M.C., Hammerling, U., and Schumacker, P.T. (2005). Mitochondrial complex III is required for hypoxia-induced ROS production and cellular oxygen sensing. Cell Metab. *1*, 401–408.

Iyer, N.V., Kotch, L.E., Agani, F., Leung, S.W., Laughner, E., Wenger, R.H., Gassmann, M., Gearhart, J.D., Lawler, A.M., Yu, A.Y., and Semenza, G.L. (1998). Cellular and developmental control of O2 homeostasis by hypoxia-inducible factor 1 alpha. Genes Dev. *12*, 149–162.

Kaelin, W.G., Jr., and Ratcliffe, P.J. (2008). Oxygen sensing by metazoans: the central role of the HIF hydroxylase pathway. Mol. Cell *30*, 393–402.

Kim, J.W., Tchernyshyov, I., Semenza, G.L., and Dang, C.V. (2006). HIF-1-mediated expression of pyruvate dehydrogenase kinase: a metabolic switch required for cellular adaptation to hypoxia. Cell Metab. *3*, 177–185.

Korshunov, S.S., Skulachev, V.P., and Starkov, A.A. (1997). High protonic potential actuates a mechanism of production of reactive oxygen species in mitochondria. FEBS Lett. *416*, 15–18.

Kruse, S.E., Watt, W.C., Marcinek, D.J., Kapur, R.P., Schenkman, K.A., and Palmiter, R.D. (2008). Mice with mitochondrial complex I deficiency develop a fatal encephalomyopathy. Cell Metab. *7*, 312–320.

Liu, Y., Fiskum, G., and Schubert, D. (2002). Generation of reactive oxygen species by the mitochondrial electron transport chain. J. Neurochem. *80*, 780–787.

Lu, C.W., Lin, S.C., Chen, K.F., Lai, Y.Y., and Tsai, S.J. (2008). Induction of pyruvate dehydrogenase kinase-3 by hypoxia-inducible factor-1 promotes metabolic switch and drug resistance. J. Biol. Chem. *283*, 28106–28114.

Mansfield, K.D., Guzy, R.D., Pan, Y., Young, R.M., Cash, T.P., Schumacker, P.T., and Simon, M.C. (2005). Mitochondrial dysfunction resulting from loss of cytochrome c impairs cellular oxygen sensing and hypoxic HIF-alpha activation. Cell Metab. *1*, 393–399.

Murphy, M.P. (2009). How mitochondria produce reactive oxygen species. Biochem. J. *417*, 1–13.

Papandreou, I., Cairns, R.A., Fontana, L., Lim, A.L., and Denko, N.C. (2006). HIF-1 mediates adaptation to hypoxia by actively downregulating mitochondrial oxygen consumption. Cell Metab. *3*, 187–197.

Piruat, J.I., and López-Barneo, J. (2005). Oxygen tension regulates mitochondrial DNA-encoded complex I gene expression. J. Biol. Chem. *280*, 42676–42684.

Raha, S., and Robinson, B.H. (2000). Mitochondria, oxygen free radicals, disease and ageing. Trends Biochem. Sci. *25*, 502–508.

Rodríguez-Juárez, F., Aguirre, E., and Cadenas, S. (2007). Relative sensitivity of soluble guanylate cyclase and mitochondrial respiration to endogenous nitric oxide at physiological oxygen concentration. Biochem. J. *405*, 223–231.

Schägger, H. (1995). Native electrophoresis for isolation of mitochondrial oxidative phosphorylation protein complexes. Methods Enzymol. *260*, 190–202.

Schofield, C.J., and Ratcliffe, P.J. (2004). Oxygen sensing by HIF hydroxylases. Nat. Rev. Mol. Cell Biol. *5*, 343–354.

Semenza, G.L. (2004). Hydroxylation of HIF-1: oxygen sensing at the molecular level. Physiology (Bethesda) *19*, 176–182.

Semenza, G.L. (2009). Regulation of oxygen homeostasis by hypoxia-inducible factor 1. Physiology (Bethesda) *24*, 97–106.

Smolenski, R.T., Schrader, J., de Groot, H., and Deussen, A. (1991). Oxygen partial pressure and free intracellular adenosine of isolated cardiomyocytes. Am. J. Physiol. *260*, C708–C714.

St-Pierre, J., Buckingham, J.A., Roebuck, S.J., and Brand, M.D. (2002). Topology of superoxide production from different sites in the mitochondrial electron transport chain. J. Biol. Chem. *277*, 44784–44790.

Stumpe, T., and Schrader, J. (1997). Phosphorylation potential, adenosine formation, and critical PO2 in stimulated rat cardiomyocytes. Am. J. Physiol. *273*, H756–H766.

Vogel, R.O., Janssen, R.J., Ugalde, C., Grovenstein, M., Huijbens, R.J., Visch, H.J., van den Heuvel, L.P., Willems, P.H., Zeviani, M., Smeitink, J.A., and Nijtmans, L.G. (2005). Human mitochondrial complex I assembly is mediated by NDUFAF1. FEBS J. *272*, 5317–5326.

Votyakova, T.V., and Reynolds, I.J. (2001). DeltaPsi(m)-Dependent and -independent production of reactive oxygen species by rat brain mitochondria. J. Neurochem. *79*, 266–277.

Walker, J.E., Arizmendi, J.M., Dupuis, A., Fearnley, I.M., Finel, M., Medd, S.M., Pilkington, S.J., Runswick, M.J., and Skehel, J.M. (1992). Sequences of 20 subunits of NADH:ubiquinone oxidoreductase from bovine heart mitochondria. Application of a novel strategy for sequencing proteins using the polymerase chain reaction. J. Mol. Biol. *226*, 1051–1072.

Wheaton, W.W., and Chandel, N.S. (2011). Hypoxia. 2. Hypoxia regulates cellular metabolism. Am. J. Physiol. Cell Physiol. *300*, C385–C393.

Supplemental Information
Cell Metabolism, *Volume 14*

Induction of the Mitochondrial NDUFA4L2 Protein by HIF-1α Decreases Oxygen Consumption by Inhibiting Complex I Activity

Daniel Tello, Eduardo Balsa, Bárbara Acosta-Iborra, Esther Fuertes-Yebra, Ainara Elorza, Ángel Ordóñez, María Corral-Escariz, Inés Soro, Elia López-Bernardo, Ester Perales-Clemente, Antonio Martínez-Ruiz, José Antonio Enríquez, Julián Aragonés, Susana Cadenas, and Manuel O. Landázuri

Supplemental Data

Figure S1

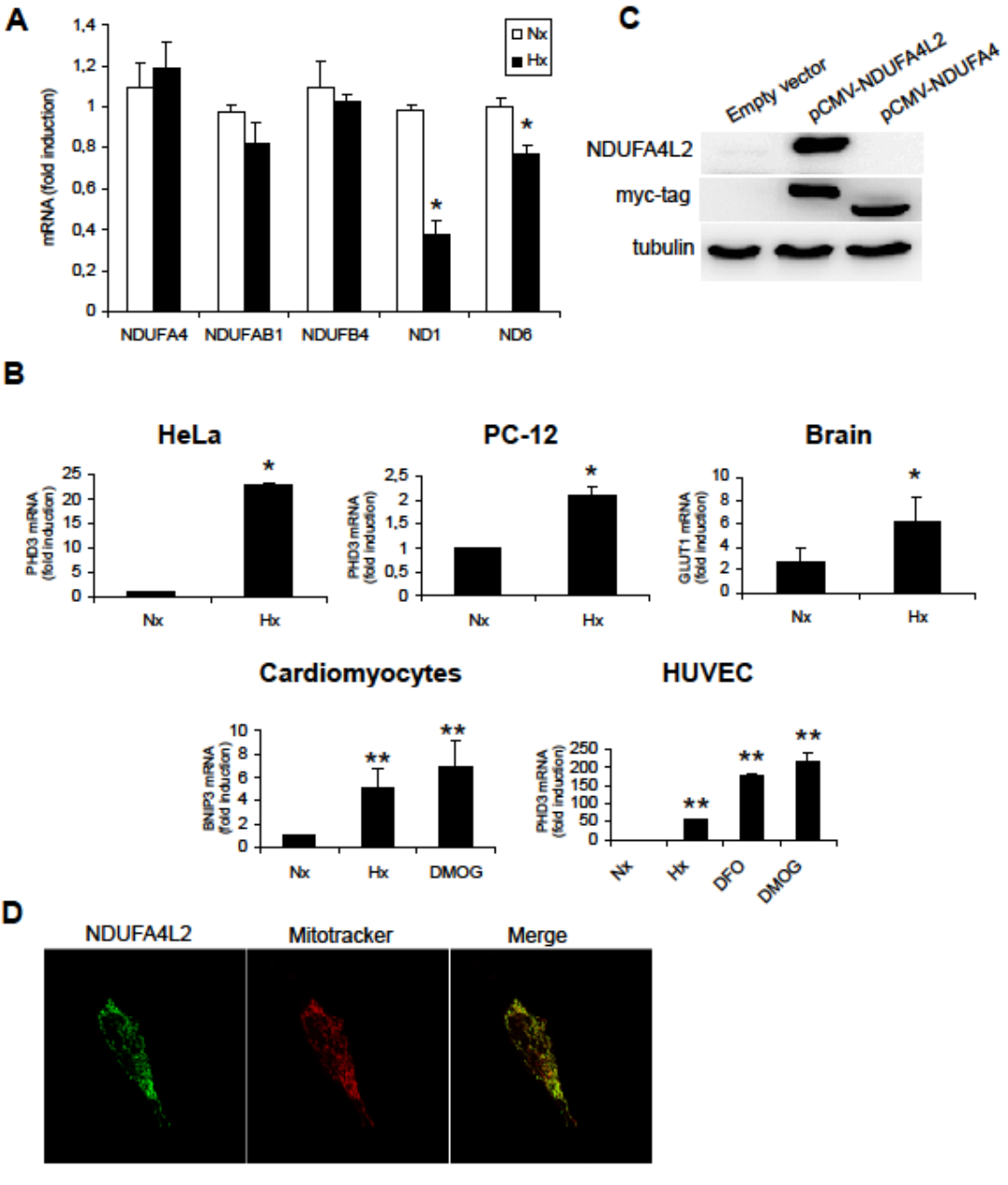

Figure S1. Related to Figure 1

(A) Quantitative RT-PCR analysis of nuclear and mitochondrial gene expression in HeLa cells cultured under normoxic or hypoxic (1% O_2) conditions for 6 h. The levels of *NDUFA4*, *NDUFAB1*, *NDUFB4*, *ND1* and *ND6* were determined by quantitative RT-PCR.

(B) Quantitative RT-PCR analysis of known HIF-1α target genes (*PHD3*, *GLUT1* and *BNIP3*) as positive controls for hypoxic gene induction in HeLa, PC-12, cadiomyocytes, HUVEC and brain tissue. Hypoxic conditions are as stated in Figure 1.

(C) Immunoblot showing the specificity of the NDUFA4L2 antibody. HeLa cells were transfected with the empty vector, pCMV-NDUFA4L2 or pCMV-NDUFA4, and the protein extracts were probed with antibodies against NDUFA4L2, myc-tag and tubulin as a loading control. The image shown is representative of 3 experiments.

(D) Confocal immunofluorescence of HeLa cells treated with either FITC goat anti-rabbit IgG to verify the presence of NDUFA4L2 (left panel, green) or mitotracker, a mitochondrial marker (middle panel, red). The right panel is an overlay of the two signals and the images shown are representative of 3 experiments. (n>3; mean ± SEM; *, $p<0.05$; **, $p<0.01$).

Figure S2

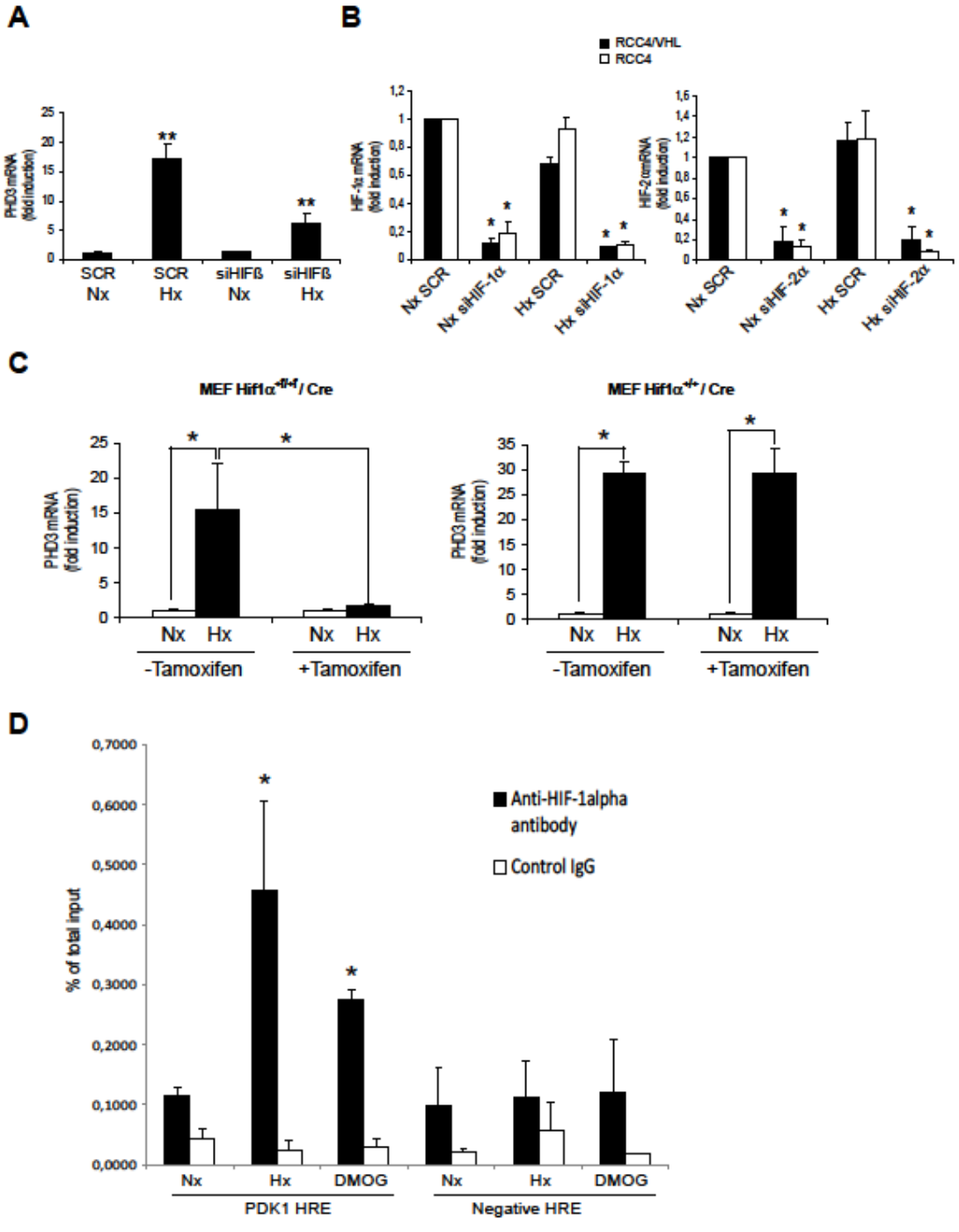
A
B
C
D
PHD3 mRNA (fold induction)
SCR Nx
SCR Hx
siHIFß Nx
siHIFß Hx
RCC4/VHL
RCC4
HIF-1α mRNA (fold induction)
HIF-2αmRNA (fold induction)
Nx SCR
Nx siHIF-1α
Hx SCR
Hx siHIF-1α
Nx siHIF-2α
Hx siHIF-2α
MEF Hif1α fl-f / Cre
MEF Hif1α +/+ / Cre
-Tamoxifen
+Tamoxifen
% of total input
Anti-HIF-1alpha antibody
Control IgG
DMOG
PDK1 HRE
Negative HRE

Figure S2. Related to Figure 2

(A) HeLa cells were transfected with a siRNA against HIFβ or a scrambled control and 24 h after transfection, the cells were seeded again and cultured under normoxic or hypoxic (1% O_2) conditions for a further 24 h. *PHD3* mRNA levels were quantified by real-time RT-PCR.

(B) VHL-deficient RCC4 cells or RCC4/VHL cells were transfected with a siRNA against HIF-1 α, HIF-2α or a scrambled control. After transfection (24 h), the cells were seeded again and cultured under normoxic or hypoxic (1% O_2) conditions for a further 24h. HIF-1α and HIF-2α mRNA levels were quantified by real-time RT-PCR.

(C) Hif1$\alpha^{+/+}$/Cre and Hif1$\alpha^{+f/+f}$/Cre MEFs were maintained in the presence or absence of tamoxifen (1μM) and cultured under normoxic or hypoxic (1% O_2) conditions for 18h. The *Phd3* mRNA levels were quantified by real-time RT-PCR.

(D) Chromatin immunoprecipitation assay of HIF-1α binding to the human *PDK1* gene. The RT-PCR quantification of regions including *PDK1* HRE (A) and a negative HRE (B) is indicated as the percentage of that in the total input chromatin DNA. (n>3; mean ± SEM; *, $p<0.05$; **, $p<0.01$).

Figure S3

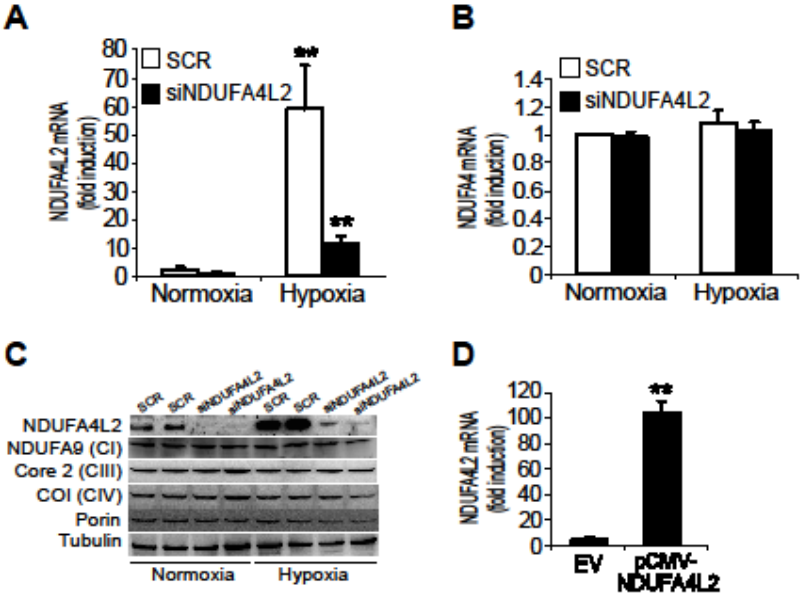
A
SCR
siNDUFA4L2
NDUFA4L2 mRNA (fold induction)
Normoxia
Hypoxia
B
SCR
siNDUFA4L2
NDUFA4 mRNA (fold induction)
Normoxia
Hypoxia
C
SCR
SCR
siNDUFA4L2
siNDUFA4L2
NDUFA4L2
NDUFA9 (CI)
Core 2 (CIII)
COI (CIV)
Porin
Tubulin
Normoxia
Hypoxia
D
NDUFA4L2 mRNA (fold induction)
EV
pCMV-NDUFA4L2

Figure S3. Related to Figures 3 and 4

(A and B) Quantitative RT-PCR analysis of *NDUFA4L2* mRNA levels (A) and *NDUFA4* mRNA levels (B) in HeLa cells transfected with a scrambled control or NDUFA4L2 siRNA followed by exposure to normoxic or hypoxic (1% O_2) conditions for 24 h.

(C) Scramble and siNDUFA4L2 HeLa cells were submitted to hypoxia 24h, (1% O_2), and cell lysate were analyzed by western blot to measure electron transport chain complexes protein levels. NDUFA9 for complex I, Core 2 for complex III and COI for complex IV. Antibody against Porin and Tubulin was used as a loading control.

(D) Quantitative RT-PCR analysis of *NDUFA4L2* mRNA levels in HeLa cells transfected either with empty vector (EV) or pCMV-NDUFA4L2. . (n>3; mean ± SEM; **, p<0.01).

Figure S4

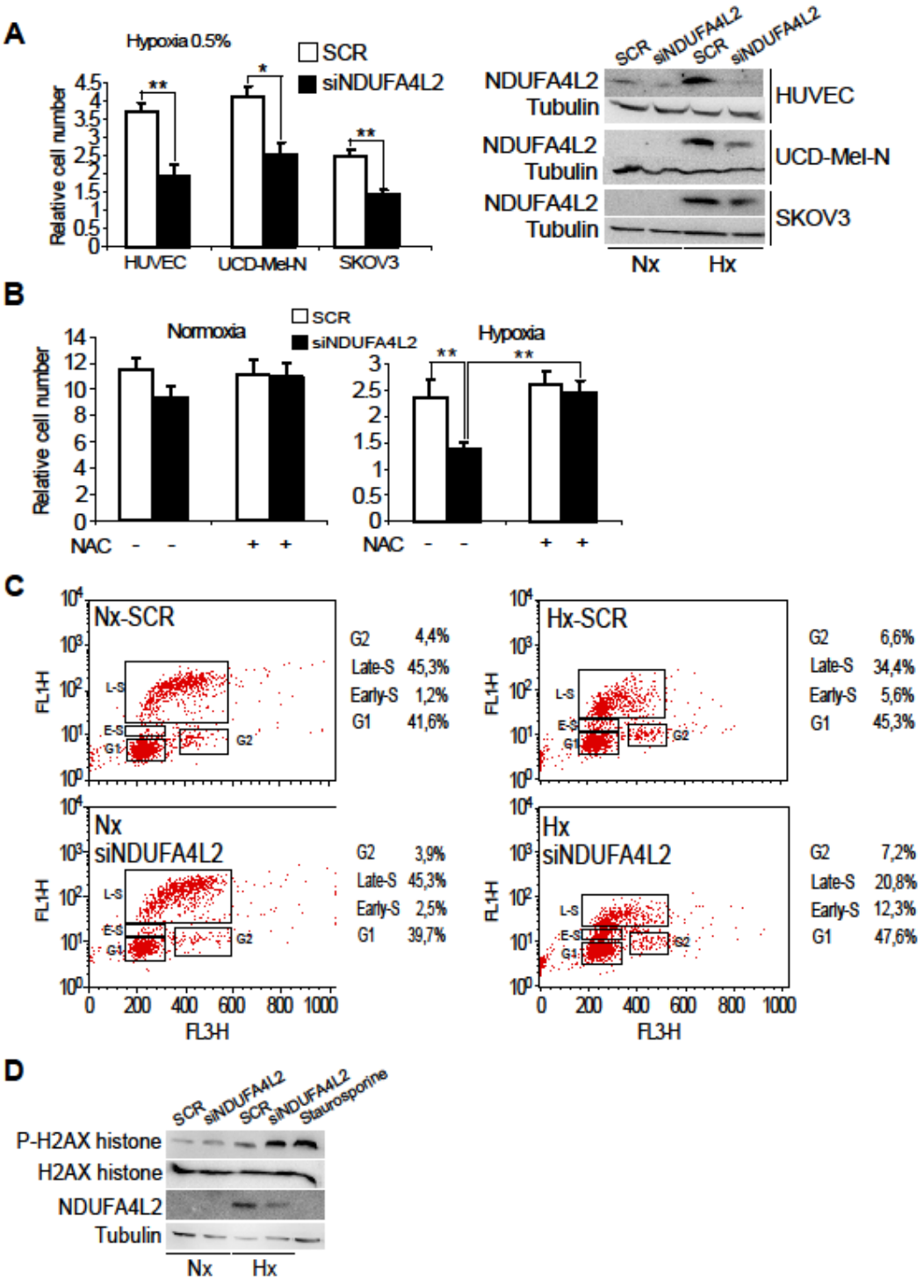
A
Hypoxia 0.5%
SCR
siNDUFA4L2
Relative cell number
HUVEC
UCD-Mel-N
SKOV3
NDUFA4L2
Tubulin
Nx
Hx
B
Normoxia
Hypoxia
NAC
C
Nx-SCR
Hx-SCR
Nx siNDUFA4L2
Hx siNDUFA4L2
FL1-H
FL3-H
L-S
E-S
G1
G2
G2 4,4%
Late-S 45,3%
Early-S 1,2%
G1 41,6%
G2 6,6%
Late-S 34,4%
Early-S 5,6%
G1 45,3%
G2 3,9%
Late-S 45,3%
Early-S 2,5%
G1 39,7%
G2 7,2%
Late-S 20,8%
Early-S 12,3%
G1 47,6%
D
Staurosporine
P-H2AX histone
H2AX histone

Figure S4. Related to Figure 5

(A) Growth of HUVEC, UCD-Mel-N and SKOV3 cells transfected with a scramble control or NDUFA4L2 siRNA in hypoxic (0.5% O_2) conditions at 72 h.

(B) Growth of HeLa cells transfected with a scramble control or NDUFA4L2 siRNA under hypoxia (0.5% O_2) with or without 0.1 mM N-acetylcysteine (NAC 72 h.

(C) Cell cycle analysis of HeLa cells transfected with a scramble control or NDUFA4L2 siRNA in normoxia and hypoxia (0.5% O_2) at 24 h.

(D) H2AX histone phosphorylation analysis in HeLa cells transfected with a scramble control or NDUFA4L2 siRNA in normoxic and hypoxic conditions (0.5% O_2) at 24 h ($n>3$; mean ± SEM; *, $p<0.05$; **, $p<0.01$).

Figure S5

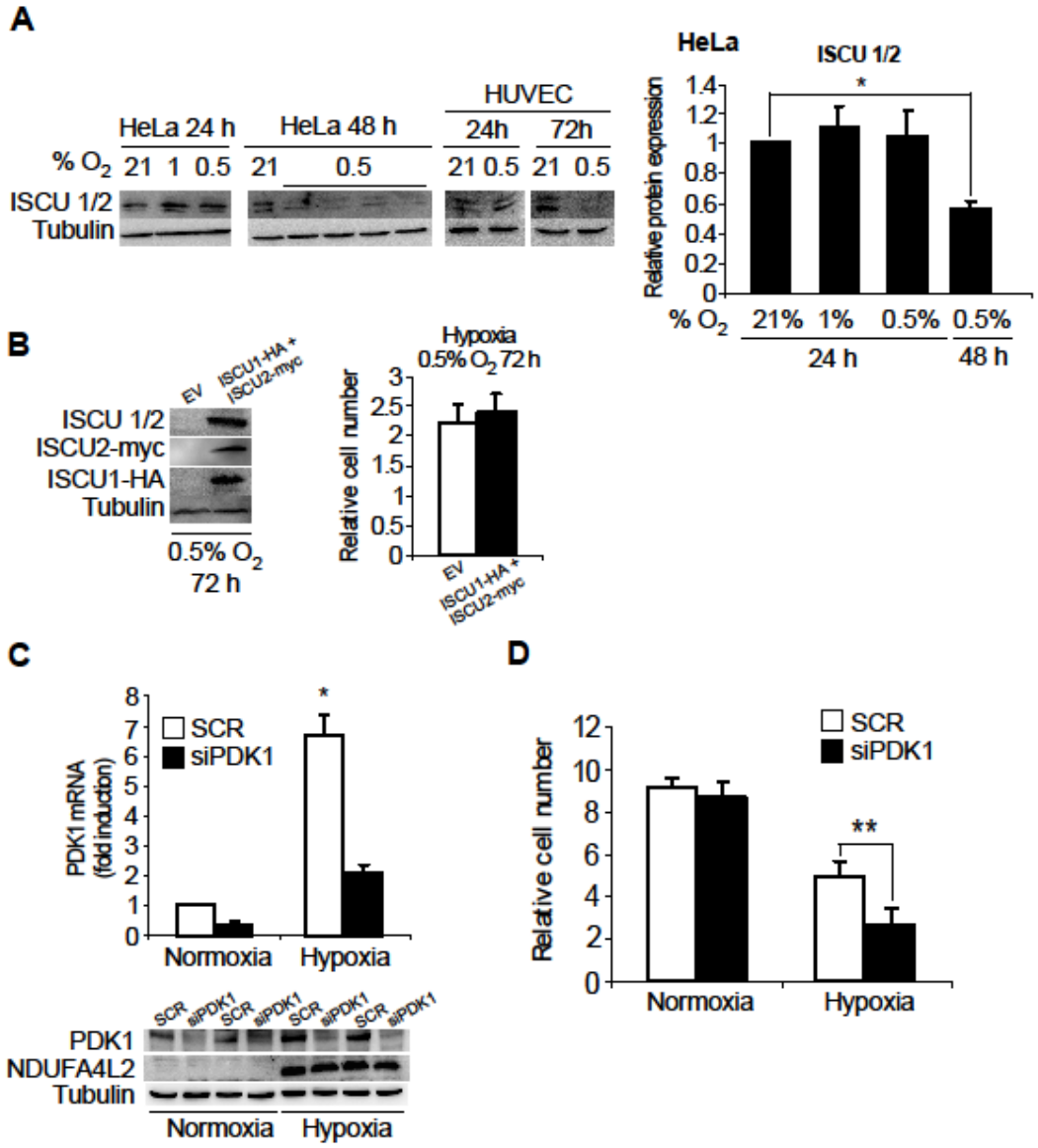
A
HeLa 24 h
HeLa 48 h
HUVEC
24h
72h
% O2 21 1 0.5 21 0.5 21 0.5 21 0.5
ISCU 1/2
Tubulin
HeLa
ISCU 1/2
Relative protein expression
% O2 21% 1% 0.5% 0.5%
24 h
48 h
B
EV
ISCU1-HA + ISCU2-myc
ISCU 1/2
ISCU2-myc
ISCU1-HA
Tubulin
0.5% O2
72 h
Hypoxia
0.5% O2 72 h
Relative cell number
C
SCR
siPDK1
PDK1 mRNA (fold induction)
Normoxia
Hypoxia
PDK1
NDUFA4L2
Tubulin
D
Relative cell number

Figure S5. Related to Figure 4

(A) ISCU 1/2 protein expression in HeLa and HUVEC cells exposed under normoxic or hypoxic (1% or 0.5%) conditions at indicated times.

(B) Growth of HeLa cells transfected with an empty vector (EV) or an expression vector encoding the ORF of ISCU1 with a 3' hemaglutinin (HA) tag (ISCU1-HA) and an expression vector encoding the ORF of ISCU2 with a 3' myc epitope (MYC) tag (ISCU2-myc) under hypoxia (0.5% O_2) at 72 h.

(C) Quantitative RT-PCR and immunoblot analysis of *PDK1* mRNA and protein levels in HeLa cells transfected with a scramble control or PDK1 siRNA followed by exposure to normoxic or hypoxic (0.5% O_2) conditions for 72 h.

(D) Growth of HeLa cells transfected with a scramble control or PDK1 siRNA in normoxic and hypoxic (0.5% O_2) conditions at 72h. ($n>3$; mean ± SEM; *, $p<0.05$; **, $p<0.01$).

Table S1. List of Complex I Genes and Hypoxia-Induced Expression Obtained in Our mRNA Array Study Performed in HeLa Cells

Gene symbol	Identifier	Average fold change	Gene symbol	Identifier	Average fold change
NDUFA4L2	**NM_020142**	**9.95**	NDUFA3	NM_004542	0.01
NDUFA1	NM_004541	0.26	NDUFB2	NM_004546	0.00
NDUFB5	NM_002492	0.23	NDUFB1	NM_004545	-0.00
NDUFA6	NM_002490	0.22	NDUFS8	NM_002496	-0.01
NDUFB8	NM_005004	0.21	NDUFA12	NM_018838	-0.01
NDUFC1	NM_002494	0.20	NDUFA5	NM_005000	-0.01
NDUFS4	NM_002495	0.19	NDUFS3	NM_004551	-0.03
NDUFV1	NM_007103	0.15	NDUFA8	NM_014222	-0.03
NDUFA7	NM_005001	0.14	NDUFA2	NM_002488	-0.06
NDUFB6	NM_182739	0.14	NDUFA11	NM_175614	-0.06
NDUFS2	NM_004550	0.14	NDUFB10	NM_004548	-0.06
NDUFB11	NM_019056	0.12	NDUFS5	NM_004552	-0.08
NDUFA12L	NM_174889	0.11	NDUFV2	NM_021074	-0.09
NDUFA4	NM_002489	0.10	NDUFB3	NM_002491	-0.09
NDUFS1	NM_005006	0.07	NDUFC2	NM_004549	-0.11
NDUFB4	NM_004547	0.06	NDUFAB1	NM_005003	-0.11
NDUFB7	NM_004146	0.06	NDUFAF1	NM_016013	-0.12
NDUFA9	NM_005002	0.05	NDUFV3	NM_021075	-0.12
NDUFS6	NM_004553	0.05	ND2	ENST00000361453	-0.76
NDUFB9	NM_005005	0.04	ND3	ENST00000361227	-1.92
NDUFA10	NM_004544	0.03	ND1	ENST00000361390	-2.72
NDUFS7	NM_024407	0.01	ND6	ENST00000361681	-2.79
NDUFA13	NM_015965	0.01			

Table S2. Genes Expressed More Strongly in Hypoxic Conditions in Our mRNA Array Study on HeLa Cells

Position	Gene symbol	Identifier	average fold increase
1	EDN2	NM_001956	12.37
2	ANGPTL4	NM_139314	12.05
3	A_23_P170719	A_23_P170719	11.92
4	GAL3ST1	NM_004861	10.98
5	IGFBP3	NM_001013398	10.88
6	THC2585656	THC2585656	10.40
7	HLXB9	NM_005515	10.32
8	THC2585656	THC2585656	10.26
9	LOC283666	BC048264	10.12
10	ZP1	NM_207341	9.98
11	**NDUFA4L2**	**NM_020142**	**9.95**
12	IGFBP3	NM_001013398	9.46

Table S3. Predicted Subcellular Location of NDUFA4L2

Program	**URL**	**Predicted localization**
HSLpred	http://www.imtech.res.in/raghava/hslpred/	Mitochondria
ProtComp V6.0	http://www.softberry.com	Mitochondria
MitoProt II - v1.101	http://www.med.tu-muenchen.de/	Mitochondria

Table S4. Primer Sequences for RT-PCR Analysis

Gene	Sequence	
	Forward	Reverse
hNDUFA4L2	5′- TTCTACCGGCAGATCAAAAGACA - 3′	5′- GGGCGAGTCGCAGCAA - 3′
mNDUFA4L2	5′- CCTGCGCAGTCCTGATGTCT - 3′	5′- GGTTGAAACGGCAAGGAACTT- 3′
rNDUFA4L2	5′- CCGCTTCTACCGGCAGATAA- 3′	5′- CCATGCCCAAGCAGATGAA- 3′
hNDUFA4	5′- TGCGTCTGGCATTGTTCAA - 3′	5′- TCCAGGGCTCTGGGTTATTTC - 3′
hNDUFAB1	5′- TTGCAGCCGGCCTTAGTG - 3′	5′- CTCTAACGTCAAAGGAGGCATGT - 3′
hNDUFAB4	5′- GCCATAAGAGCCCAGCTGAA - 3′	5′- ACGAAGCAAGGCAGGATTTTC- 3′
hND1	5′- CCCTTCGCTGACGCCATA - 3′	5′- TGGTAGATGTGGCGGCGGGTTTT - 3′
hND6	5′- GGGTTAGCGATGGAGGTAGGA - 3′	5′- CAACCACCACCCCATCATACT - 3′
hPHD3	5′- GCCGGCTGGGCAAATACTA- 3′	5′- CCGGATAGCAAGCCACCAT - 3′
mPHD3	5′- TGGACAACCCCAATGGTGAT- 3′	5′- GCAGGACCCCTCCATGTAACT - 3′
h/rBNIP3	5′- GTCTGGACGGAGTAGC- 3′	5′- GGCCGACTTGACCAAT - 3′
rGLUT1	5′- CGCAACGAGGAGAACC - 3′	5′- GCCGTGTTGACGATACC - 3′
hHIF-1α	5′- GTTTACTAAAGGACAAGTCAC- 3′	5′- TTCTGTTTGTTGAAGGGAG - 3′
hEPAS	5′- CAATCAGCTTCCTGCGAACA- 3′	5′- TTCGGCTTCGGACTCGTTT - 3′
m/rHPRT	5′- GTTAAGCAGTACAGCCCCAAA - 3′	5′- AGGGCATATCCAACAACAAACTT - 3′
hHPRT	5′- ATTGTAATGACCAGTCAACAGGG - 3′	5′- GCATTGTTTTGCCAGTGTCAA - 3′
hPDK1	5′- GTGGTTTATGTACCATCCCATCTCT - 3′	5′- TCCATAGTGGCTCTCATTGCAT- 3′

Table S5. Primer Sequences for CHIP Assays

Gene	Region	Sequence	
		Forward	Reverse
hNDUFA4L2	A	5′- CAGGTCTGTGTATGTGTGAAA - 3′	5′- CTACGCACTGTCACTGAG - 3′
hNDUFA4L2	B	5′- GGTGTATGTTAATCATGGCTCAG - 3′	5′- CAGCCAGAGGAAGTGGA - 3′
hNDUFA4L2	C	5′- CGCTAAGTTGGTGCCTG - 3′	5′- CGATTGTGGCTGGAGAGATA - 3′
hPDK1	HRE (A)	5′- CGCGTTTGGATTCCGTG - 3′	5′- CCAGTTATAATCTGCCTTCCCTATTATC - 3′
hPDK1	Non-HRE (B)	5′- AAAGGACATTCTACAACGATTCTGC - 3′	5′- CAATTGTCTGGTTACTGAAAGTCTCC - 3′

Supplemental Experimental Procedures

Cell lines and cell cultures. HeLa, SKOV3, UCD-mel-N, RCC4, RCC4/VHL, neonatal rat cardiomyocytes and Hif1$\alpha^{+/+}$/Cre or Hif1$\alpha^{+f/+f}$/Cre mouse embryo fibroblasts (MEFs) were cultured in DMEM containing 10% heat-inactivated fetal bovine serum (FBS). PC-12 cells were cultured in RPMI containing 10% heat-inactivated fetal horse serum and 5% FBS. Human umbilical vein endothelial cells (HUVEC) were cultured in 199 medium with 20% FBS and 1% ECGF. HL-1 cells were cultured in Claycomb medium containing 10% heat-inactivated FBS and supplemented with 0.1 mM norepinephrine and 2 mM glutamax. All media were also supplemented with 100 IU/ml penicillin, 100 µg/ml streptomycin and 1% HEPES buffer. Normoxic cells (21% O_2) were maintained at 37ºC in a 5% CO_2/95% air incubator. For hypoxic exposure, cell culture dishes were placed into an Invivo$_2$ 400 humidified hypoxia workstation (Ruskinn Technologies, Bridgend, UK) at 0.5% or 1% O_2. All other reagents were provided by Sigma (DFX) and Enzo (DMOG).

Quantitative RT-PCR. Total RNA extraction, cDNA synthesis, and qRT-PCR were carried out as described previously (Acosta-Iborra et al., 2009). Primer sequences are listed in *Table S4*.

ChIP assay. Chromatin immunoprecipitation and real-time PCR quantification were performed as described previously (Ortiz-Barahona et al., 2010). Primer sequences for the ChIP assay are shown in *Table S5*.

Plasmids and siRNAs. For transient overexpression, the pCMV-NDUFA4L2 and the pCMV-NDUFA4 myc-tagged open reading frame (ORF) human plasmids were purchased from Origene (Rockville, MD). An expression vector encoding the ORF of ISCU1 with a 3' hemaglutinin (HA) tag (ISCU1-HA) and an expression vector encoding the ORF of ISCU2 with a 3' myc epitope (MYC) tag (ISCU2-myc) (Tong and Rouault, 2000) were kindly provided by Stephen Y. Chan and Joseph Loscalzo. Plasmid transfection of HeLa cells was performed with lipofectamine 2000 (Invitrogen, Carlsbad, CA) according to the manufacturer's instructions. For knockdown experiments, human HIF-1β siRNA

(J-007207) and human PDK1 siRNA (J-054066) were purchased from Dharmacon, human HIF-1α siRNA (sc-44225) and human NDUFA4L2 siRNA (sc-95677) were purchased from Santa Cruz Biotechnology, and human the HIF-2α siRNA (5´-CAGCAUCUUUGAUAGCAG-3´) was provided by Eurogentec. HeLa cells were transfected with siRNAs using the lipofectamine RNAiMAX reagent (Invitrogen, Carlsbad, CA) according to the manufacturer´s instructions.

Western blot analysis. For use in standard polyacrylamide gel electrophoresis and immunoblotting, primary antibodies included polyclonal anti-NDUFA4L2 antibodies (Abcam or Proteintech), monoclonal anti-NDUFA9 antibody (Santa Cruz), monoclonal anti-Complex III subunit Core 2 antibody (Mitosciences), monoclonal anti-Complex IV subunit I antibody (Mitosciences), monoclonal anti-HIF-1α antibody (Santa Cruz), monoclonal anti-cytochrome *c* antibody (BD), monoclonal anti-porin antibody (Invitrogen), monoclonal anti-Hsp90 antibody (Santa Cruz), polyclonal anti-total Caspase-3 antibody (Cell Signaling), polyclonal anti-PDK1 antibody (Cell Signaling), polyclonal anti-IscU 1/2 antibody (Santa Cruz), monoclonal anti-myc antibody (Sigma), polyclonal anti-HA antibody (Santa Cruz), monoclonal anti-phospho H2AX antibody (Millipore), polyclonal anti-total H2AX antibody (Millipore) and monoclonal anti-tubulin antibody (Sigma) were used. Antibody binding was detected by enhanced chemiluminiscence (ECL, Amersham Biosciences) with species-specific secondary antibodies labeled with Horseradish Peroxidase (HRP) (Dako, Amersham) and visualized on a digital luminescent image analyzer (Fujifilm LAS-1000 CH).

Immunofluorescence microscopy. After specific treatment, HeLa and HL-1 cells were grown on glass coverslips in 24-well culture dishes, fixed with 3% paraformaldehyde in HBSS for 15 min at room temperature, and washed with PBS. The cells were then permeabilized with 0.5% Triton X-100 for 10 min, and non-specific binding sites were blocked by incubation with 3% BSA in PBS for 30 min. The cells were incubated with the polyclonal anti-NDUFA4L2 antiserum (Abcam) or monoclonal anti-cytochrome c (BD) for 1 h at room temperature and then washed with PBS. A secondary Alexa 488 conjugated anti-rabbit antibody

(Invitrogen) and the specific mitochondrial marker Mitotraker (Invitrogen) or Alexa 568 conjugated anti-mouse (Invitrogen) were then added to the cells for 30 min, before they were finally washed with PBS, washed briefly with distilled water, and mounted with Mowiol.

ROS measurements. Intracellular H_2O_2 and superoxide ion production were measured by staining HeLa cells with dichlorodihydrofluorescein diacetate (H_2DCFDA, Molecular Probes) and MitoSOX (Molecular Probes), respectively. DCF fluorescence was measured using a FACScan flow cytometer, while MitoSOX fluorescence was observed by fluorescence microscopy (Redondo-Horcajo et al., 2010).

Cell cycle analysis. Cell cycle was analyzed using the Click-IT EdU Flow Cytometry Assay Kit according to the manufacturer´s instructions.

Supplemental References

Acosta-Iborra, B., Elorza, A., Olazabal, I.M., Martin-Cofreces, N.B., Martin-Puig, S., Miro, M., Calzada, M.J., Aragones, J., Sanchez-Madrid, F., and Landazuri, M.O. (2009). Macrophage oxygen sensing modulates antigen presentation and phagocytic functions involving IFN-gamma production through the HIF-1 alpha transcription factor. J Immunol 182, 3155-3164.

Ortiz-Barahona, A., Villar, D., Pescador, N., Amigo, J., and Del Peso, L. (2010). Genome-wide identification of hypoxia-inducible factor binding sites and target genes by a probabilistic model integrating transcription-profiling data and in silico binding site prediction. Nucleic Acids Res 38, 2332-2345.

Redondo-Horcajo, M., Romero, N., Martinez-Acedo, P., Martinez-Ruiz, A., Quijano, C., Lourenco, C.F., Movilla, N., Enriquez, J.A., Rodriguez-Pascual, F., Rial, E., et al. (2010). Cyclosporine A-induced nitration of tyrosine 34 MnSOD in endothelial cells: role of mitochondrial superoxide. Cardiovascular research 87, 356-365.

Tong, W.H., and Rouault, T. (2000). Distinct iron-sulfur cluster assembly complexes exist in the cytosol and mitochondria of human cells. Embo J 19, 5692-5700.

Manuscrito 2

NDUFA4 Is a Subunit of Complex IV of the Mammalian Electron Transport Chain.

Cell Metabolism. (Accepted).

DOI: 10.1016/j.cmet.2012.07.015.

He sido primer autor de este trabajo y me ha ayudado a profundizar en el estudio del campo de la mitocondria, así como aprender técnicas especificas para el estudio de la función y la actividad mitocondrial.

Continuando con el trabajo anterior, en este articulo me he centrado en el estudio de la proteína NDUFA4, que es paráloga a NDUFA4L2.

El complejo I aun no ha sido cristalizado, a diferencia de los otros complejos de la cadena de transporte de electrones. Sin embargo, gracias a estudios de proteómica se ha establecido una lista de las proteínas pertenecientes a este complejo, y NDUFA4 ha sido clasificada dentro de esa lista.

Nuestro estudio, claramente ha demostrado que NDUFA4, lejos de ser una proteína perteneciente al complejo I, es en realidad un componente del complejo IV. Su ausencia impide en correcto ensamblaje y actividad del complejo IV sin que haya ninguna afectación en el complejo I. Además aportamos una explicación plausible al porque no se encontró esta proteína en el cristal del complejo IV, ya que nuestros experimentos indican que la unión NDUFA4 al complejo IV, es bastante sensible a los detergentes. Dichos detergentes se utilizan de manera rutinaria para la purificación del complejo para la cristalografía.

Dicho cambio en la adscripción de esta proteína tiene fuertes implicaciones: 1) se debe considerar a NDUFA4 como gen candidato en los escrutinios de búsqueda de patología asociadas al complejo IV y no al I. 2) Hace una llamada de atención al los protocolos de aislamiento y purificación para la obtención de cristales para cristalografía.

Please cite this article in press as: Balsa et al., NDUFA4 Is a Subunit of Complex IV of the Mammalian Electron Transport Chain, Cell Metabolism (2012), http://dx.doi.org/10.1016/j.cmet.2012.07.015

Cell Metabolism
Short Article

NDUFA4 Is a Subunit of Complex IV of the Mammalian Electron Transport Chain

Eduardo Balsa,[1,2] Ricardo Marco,[1] Ester Perales-Clemente,[1] Radek Szklarczyk,[3] Enrique Calvo,[1] Manuel O. Landázuri,[2] and José Antonio Enríquez[1,4,*]
[1]Centro Nacional de Investigaciones Cardiovasculares Carlos III (CNIC), Madrid, 28029, Spain
[2]Servicio de Inmunología, Hospital Universitario de La Princesa, Universidad Autónoma de Madrid, Instituto de Investigación Sanitaria Princesa (IIS-IP), Madrid, 28006, Spain
[3]Centre for Molecular and Biomolecular Informatics, Nijmegen Centre for Molecular Life Sciences, Radboud University Medical Centre, PO Box 9101, 6500HB, Nijmegen, The Netherlands
[4]Departamento de Bioquímica y Biología Molecular y Celular, Facultad de Ciencias, Universidad de Zaragoza, 50013, Spain
*Correspondence: jaenriquez@cnic.es
http://dx.doi.org/10.1016/j.cmet.2012.07.015

SUMMARY

The oxidative phosphorylation system is one of the best-characterized metabolic pathways. In mammals, the protein components and X-ray structures are defined for all complexes except complex I. Here, we show that NDUFA4, formerly considered a constituent of NADH Dehydrogenase (CI), is instead a component of the cytochrome *c* oxidase (CIV). Deletion of NDUFA4 does not perturb CI. Rather, proteomic, genetic, evolutionary, and biochemical analyses reveal that NDUFA4 plays a role in CIV function and biogenesis. The change in the attribution of the NDUFA4 protein requires renaming of the gene and reconsideration of the structure of CIV. Furthermore, NDUFA4 should be considered a candidate gene for CIV rather than CI deficiencies in humans.

INTRODUCTION

The OXPHOS system is one of the better and more deeply characterized metabolic pathways (Saraste, 1999). It is composed of four respiratory complexes, called complex I (NADH-ubiquinone oxidoreductase), complex II (succinate:ubiquinone oxidoreductase), complex III (ubiquinol-cytochrome *c* reductase), and complex IV (cytochrome *c* oxidase); the electron carriers ubiquinone (UQ or CoQ) and cytochrome *c* (cyt c); and the H^+-ATP synthase (complex V). All the structural protein components of the mammalian OXPHOS system are thought to be known. Complex I is composed of 45 subunits, complex II of 4, complex III of 11, complex IV of 13, and complex V of 11 proteins. In addition, a large number of assembly factors continue to be described for all the complexes, and research into assembly pathways remains a highly active field (for review, see Fernández-Vizarra et al., 2009). The biochemical organization of the complexes is also well characterized, but several key issues remain to be deciphered: the organization of cofactors in CI is not yet fully solved (Roessler et al., 2010), the interaction of this complex with CoQ is not well established (Ohnishi et al., 2005; Shinzawa-Itoh et al., 2010), and the proton translocation mechanisms in CI and IV have not been fully determined (Xu and Voth, 2008). The X-ray structures of complex II (Sun et al., 2005), III (Iwata et al., 1998), and IV (Tsukihara et al., 1995, 1996) have been solved, as well as that of the F_1 domain and the membrane-extrinsic region of complex V (Abrahams et al., 1994; Rees et al., 2009) and the complex I structure of *E. coli* (Efremov et al., 2010; Efremov and Sazanov, 2011) and Yarrowia mitochondria (Hunte et al., 2010). However, the X-ray structures of complex I in higher eukaryotes and of F_O domain of ATP synthase remain unsolved (Fernández-Vizarra et al., 2009).

This formidable accumulation of information about the OXPHOS system has turned out to be insufficient to explain the phenotypic consequences of its dysfunction, and we are consequently confronted by an impressive lack of understanding about why, where, how, and when disease will manifest if the OXPHOS system is impaired. Moreover, research into specific diseases has revealed major shortcomings in the established models of electron transport chain organization (Acín-Pérez et al., 2004). Investigation of human OXPHOS diseases teaches us that our basic knowledge of the system is far from complete and that a description of the component elements, albeit exhaustive, does not provide a functional understanding of the system as a whole. Here, we demonstrate that even aspects that were considered to be fully established, such as the number and subunit composition of the respiratory complexes, need to be revised: we provide compelling evidence that NDUFA4, a protein considered to be a complex I structural subunit (Carroll et al., 2006), is in fact an essential structural protein of complex IV.

RESULTS

Different Comigrating Pattern of NDUFA4 in Blue Native Gels

To identify interactions between mitochondrial proteins that may be revealed by their comigration on native gels, we are implementing a systematic proteomic analysis of mitochondrial protein bands in blue-native gels (Figures 1A and 1B). Thus, we compared wild-type mouse cell lines with cells from mutants with specific loss of individual respiratory complexes (CI^{KO}, $CIII^{KO}$, or CIV^{KO}) or lacking mtDNA (ρ°-cells). To maximally preserve in vivo protein interactions, we solubilized mitochondrial membranes with digitonin (Acín-Pérez et al., 2008). Since the protein composition of the mammalian respiratory

Please cite this article in press as: Balsa et al., NDUFA4 Is a Subunit of Complex IV of the Mammalian Electron Transport Chain, Cell Metabolism (2012), http://dx.doi.org/10.1016/j.cmet.2012.07.015

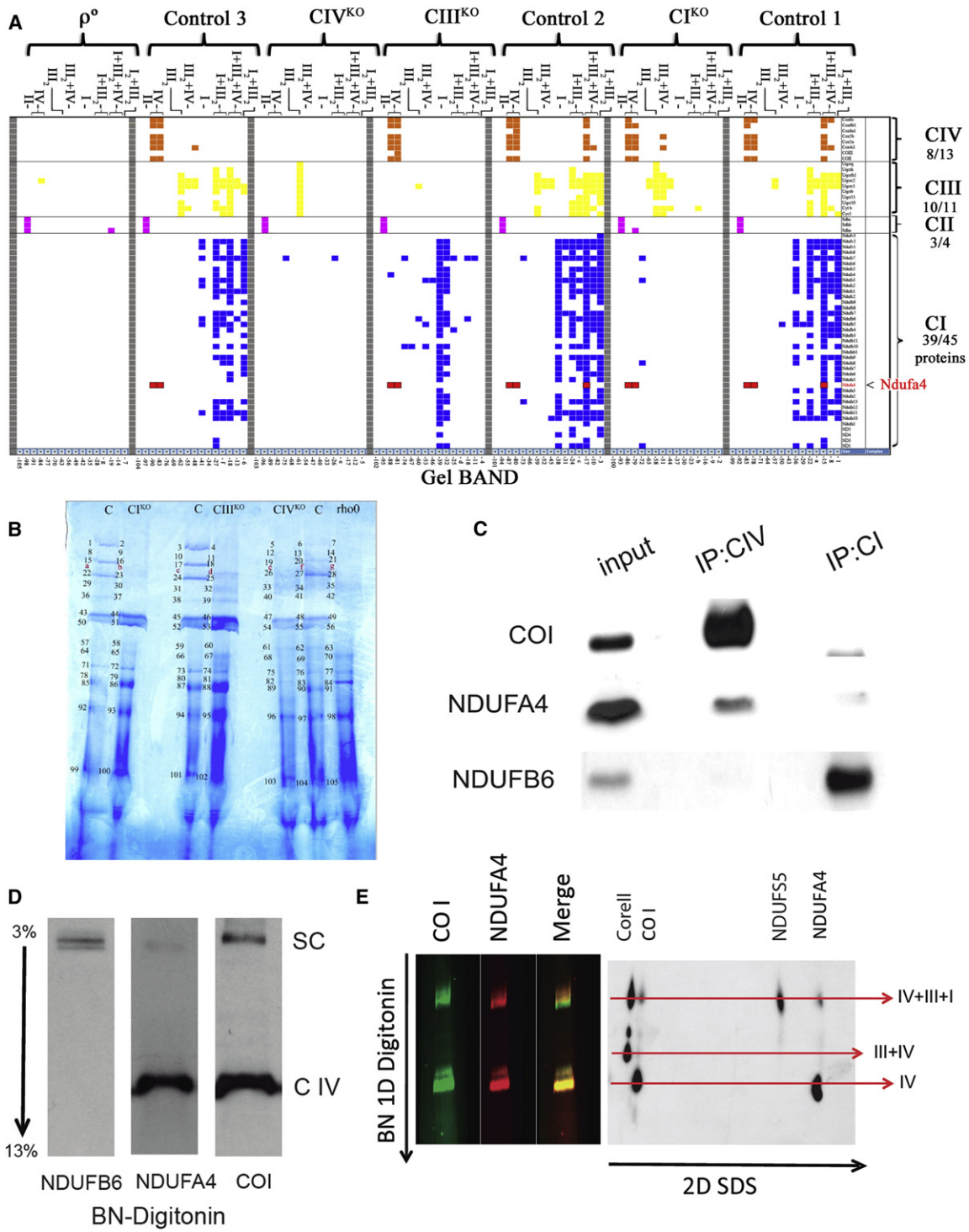

Figure 1. The NDUFA4 Protein Behaves as a Structural Component of Complex IV

(A) Scheme of retrieved peptides from MS/MS analysis of the gel slices cut from the gel shown in (B) (numbers under the graphic correspond to the gel slice number indicated in B). The position of the free complexes or supercomplexes is indicated on top for each line run on gel B and labeled as the indicated control or mutant cell line. In the scheme can be followed the distinct behavior of mitochondrial electron transport complex proteins (indicated at the right side, NDUFA4 is highlighted). Different colors identify components of individual complexes (complex I, blue; complex II, pink; complex III, yellow; complex IV, orange; NDUFA4 is shown in red).

(B) Representative Coomassie-stained blue native gel from which the bands were excised for the proteomic analysis summarized in (A). The gel was loaded with extracts from wild-type cells and cell lines depleted for specific mitochondrial electron transport complexes: control, wild-type cells; CI^{KO}, cells lacking complex I; $CIII^{KO}$, cells lacking complex III; CIV^{KO}, cells lacking complex IV; ρ°, mtDNA-less cells lacking complexes I, III, and IV.

complexes is well known (Carroll et al., 2006; Hirst et al., 2003; Iwata et al., 1998; Tsukihara et al., 1996), we examined them to determine the robustness of our approach and the level of sensitivity for highly hydrophobic mitochondrial inner membrane proteins. Our system detected 39 of the 45 CI proteins (Carroll et al., 2006; Hirst et al., 2003), 3 of the 4 CII proteins (Cecchini, 2003), 10 of the 11 CIII proteins (Iwata et al., 1998), and 8 of the 13 CIV proteins (Tsukihara et al., 1996) (Figure 1A). Our analysis also confirmed the comigration of complexes when assembled into different supercomplexes (I_2+III_2; I+III_2+IV_n; I+III_2; and III_2+ IV). Most of the proteins showed the expected distribution pattern on the BN gel, and knockout of one complex subunit not only almost abolished the detection of proteins of the same complex, but also deleted components of other complexes that associate in the same supercomplex (Figure 1A). Notably, although CI is degraded in the absence of CIII or IV, expression of CI proteins was better preserved in $CIII^{KO}$ cells, suggesting that CI is more unstable in the absence of CIV than in the absence of CIII (Figure 1A).

In departure from the expected behavior, we found NDUFA4 (unequivocally identified by three specific peptides; Figure S1), classically described as a CI subunit (Carroll et al., 2003; Hirst et al., 2003), in a distribution pattern consistent with components of CIV (Figure 1A). In control cells, NDUFA4 never occurred in positions where CI migrates alone; on the contrary, it always comigrated with CIV subunits, either at positions where CIV migrates alone, or assembled in supercomplex I+III_2+IV_n. Moreover, in CI^{KO} samples, where only four of the CI subunits are detected (NDUFS7, NDUFS3, NDUFA8, and ND1—comigrating in a previously described subcomplex [Vogel et al., 2007]), NDUFA4 was still present and comigrated with CIV. In contrast, in CIV^{KO} cells, NDUFA4 was deleted, together with all CIV proteins (Figure 1A). Moreover, in $CIII^{KO}$ cells, almost all CI subunits are detected as individual CI; but NDUFA4 again comigrated with CIV subunits. This proteomic analysis shows that NDUFA4 behaves like a CIV protein.

NDUFA4 Interacts with Proteins of Complex IV

To validate the proteomic analysis, we conducted immunoprecipitation experiments to determine whether NDUFA4 interacts directly with CIV. Endogenous NDUFA4 was specifically precipitated by antibodies targeting CIV subunits, but not by antibodies targeting CI (Figure 1C). Specific immunodetection analysis also confirmed comigration of NDUFA4 with CIV (Figure 1D), and resolving two-dimension gels showed NDUFA4 comigrating with CIV subunits (Figure 1E). Furthermore, in mouse cells lacking either ND4 or ND6, which showed a complete absence of CI when tested for several canonical proteins for this complex, NDUFA4 remained at the position of CIV (Figure 2A). In contrast, in mouse cells lacking COX10 ($COX10^{KO}$), which cannot fully assemble CIV, NDUFA4 comigrated with an immature form of CIV, and in human cells lacking COX2 ($COX2^{KO}$), which are similarly unable to form CIV, NDUFA4 was completely absent (Figure 2B). These results strongly indicate that NDUFA4 is a subunit of CIV and not CI. Furthermore, we notice that, contrary to what was found for mouse cultured cells (Diaz et al., 2006), human cells lacking CIV (see Figure S2 for a characterization of the $Cox2^{KO}$ cells) are still able to retain a significant amount of assembled CI (Figure 2C) that mainly interact with CIII. In these cells complex NDUFA4 is not detected. To ensure that CI was fully active despite the absence of NDUFA4 and CIV, we performed in-gel activity for NADH dehydrogenase (CI) or for CIV. Complex IV activity was detected in both wild-type and 80% mutant Cox2 cells, but not in 100% mutant Cox2 ones (Figure 2D). However, in-gel CI activity is easily appreciated in all tested cell lines regardless of whether they have CIV or not (Figure 2D). To determine if this NADH dehydrogenase activity was reflecting a true functional CI in vivo, we transformed $Cox2^{KO}$ cells with AOX (an alternative electron transport system present in lower eukaryotes, plants, and lower animals that can perform the overall oxidation of $CoQH_2$, instead of CIII and CIV, which are able to work in mammalian cells [Perales-Clemente et al., 2008]). The expression of AOX does not modify qualitatively the presence of CI or its in-gel activity detection (Figures 2C and 2D). It allows $Cox2^{KO}$ to respire to a robust rate and, this respiration being substantially sensitive to rotenone, a CI-specific inhibitor (Figure 2E). This demonstrates that NDUFA4 is not required to form a fully functional CI.

Targeting NDUFA4 Protein Disrupts Normal Levels of Complex IV

If NDUFA4 is a genuine CIV subunit, its downregulation is likely to affect CIV activity. To test this, we stably silenced NDUFA4 in HeLa cells and monitored the activity and stability of CI and CIV. Upon downregulation of NDUFA4, CIV levels were reduced, whereas CI and CIII showed no obvious change (Figure 3A). Two-dimensional western blot also revealed reduced levels of CIV, although no preassembled complexes were detected (Figure 3B). To confirm that the phenotype induced by NDUFA4 silencing was entirely due to the reduced expression of this protein, we performed rescue experiments, in which myc-tagged NDUFA4 was overexpressed in stably NDUFA4 interfered cells. To allow myc-NDUFA4 expression, the locus for the endogenous NDUFA4 interference was removed in the myc-NDUFA4. Exogenous NDUFA4 fully restored CIV levels (Figure 3C), confirming the role of these proteins in cytochrome *c* oxidase maintenance and function.

The protein expression changes were paralleled by changes in CIV activity, with a decrease in activity observed in shNDUFA4 HeLa cells (Figure 3D) that was restored by overexpression of myc-NDUFA4. These changes were not accompanied by significant alterations in CI activity (not shown). Culture in galactose medium, which forces cells to rely on OXPHOS-dependent generation of ATP, demonstrated that the reduced CIV activity in NDUFA4-interfered cells inhibited proliferation compared with nonsilenced counterparts (Figure 3E).

(C) Isolated mitochondria from HeLa cells were solubilized with 1% DDM and immunoprecipitated with specific antibodies against either CIV or CI. COI and NDUFA4 both coimmunoprecipitate with CIV, whereas NDUFB6 coimmunoprecipitates with CI exclusively.

(D and E) Isolated mitochondria from HeLa cells were digitonized and resolved by one-dimensional BNGE (D) or by BNGE followed by a second dimension of SDS-PAGE (E). After electrophoresis, membranes were probed with antibodies specific for CI (NDUFB6 and NDUFS5), CIII (Core II), CIV (COI), and NDUFA4.

Please cite this article in press as: Balsa et al., NDUFA4 Is a Subunit of Complex IV of the Mammalian Electron Transport Chain, Cell Metabolism (2012), http://dx.doi.org/10.1016/j.cmet.2012.07.015

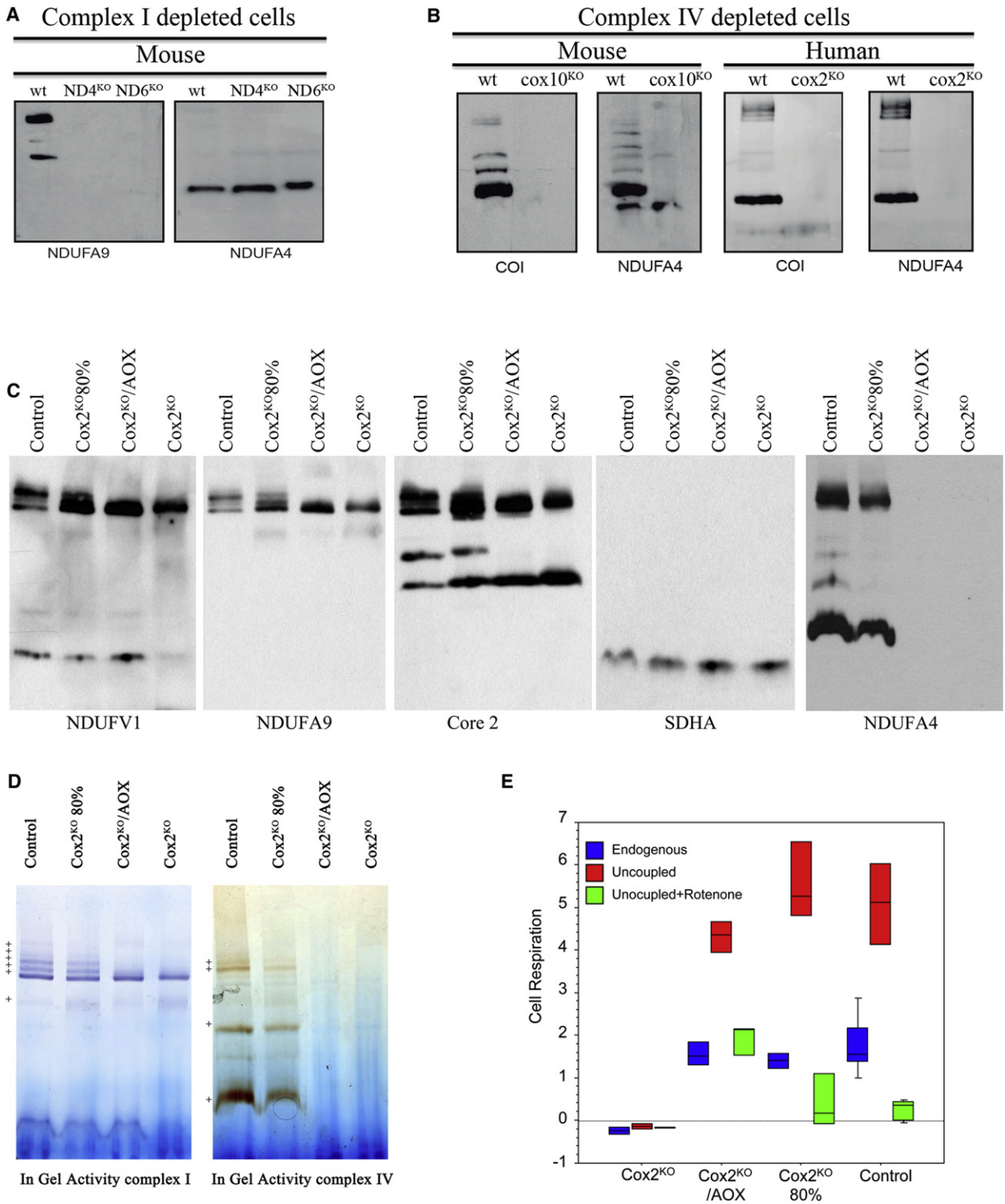

Figure 2. BNGE Analysis in Mutant Fibroblast Lines Lacking Either Complex IV or Complex I

(A) CI depleted cells: mouse fibroblasts lacking ND4 and ND6.

(B) CIV depleted cells: mouse fibroblasts lacking COX10 and human fibroblasts lacking COX2.

(C) Human cells lacking COX2 and expressing or not AOX or with 80% of the mutant Cox2 gene probed against complex I (NDUFV1, NDUFA9), complex III (Core2), complex II (SDHA), and NDUFA4. Western blots were probed with antibodies against the proteins indicated beneath the blots in (A)–(C).

(D) In-gel activity of a paralleled run gels to that of (C) above.

(E) Box plot showing oxygen consumption by the indicated intact cells under coupled or uncoupled conditions (by CCCP) and effect of CI activity inhibition by rotenone. Box plot represents data distribution by different quartile.

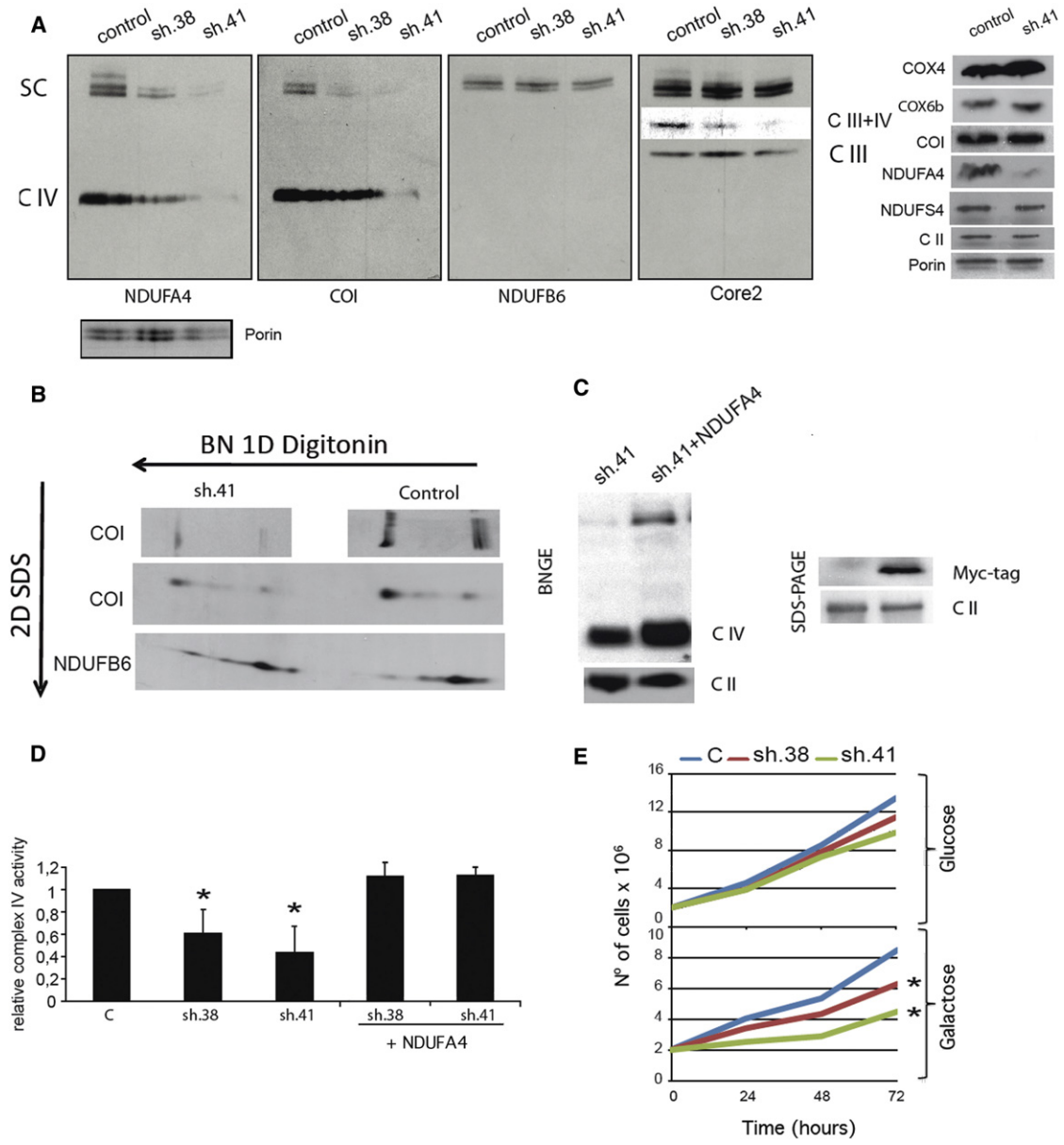

Figure 3. Complex IV Is Impaired in the Absence of NDUFA4

(A–D) NDUFA4 was stably knocked down in HeLa cells using two different NDUDA4-targeting shRNA sequences (sh.38 and sh.41). (A) Left: BNGE analysis of digitonin-isolated mitochondria, followed by western blot with antibodies against the indicated protein. Notice that on the core 2 blot, the band for CIII + CIV is a different exposure to better show that the supercomplex III + IV is also lost by the interference of NDUFA4. SC: supercomplexes. Right: western blots of SDS-PAGE analysis of control and sh.41 cells. Porin was used as a loading control. (B) Western blots of 2D electrophoresis gels (BNGE followed by SDS-PAGE) of control and sh.41 cells; membranes were probed with antibodies against the indicated proteins. (C) Left: BNGE analysis revealing restoration of CIV levels in sh.41 cells after exogenous overexpression of myc-tagged NDUFA4. Right: SDS-PAGE showing expression levels of myc-NDUFA4; CII was used as a loading control. (D) CIV activity relative to citrate synthase was measured spectrophotometrically in isolated mitochondria from control cells. Error bars indicate standard deviation of the mean. (C), NDUFA4-silenced cells (sh.38 and sh.41), and NDUFA4-silenced cells expressing myc-NDUFA4 (+NDUFA4) (E). Growth curves of control and NDUFA4-silenced HeLa cells culture in medium containing glucose or galactose. *$p < 0.05$ compared with control (Student's t test).

The Evolution of NDUFA4 Correlated with That of Complex IV

Previous evolutionary analyses of *NDUFA4* indicated its presence outside vertebrate evolutionary clade (Gabaldón et al., 2005), and more recently outside metazoa (Huynen et al., 2009), yet NDUFA4 has not been confirmed to be a genuine complex I subunit in fungi or plants (Cardol, 2011). Due to high sequence divergence rates to identify *NDUFA4* homologs in eukaryotic species, we used hidden Markov models, similar to approaches employed to establish new COX assembly factors (Szklarczyk et al., 2012). Using sensitive homology searches, we discovered that *NDUFA4* homologs' presence-absence

Please cite this article in press as: Balsa et al., NDUFA4 Is a Subunit of Complex IV of the Mammalian Electron Transport Chain, Cell Metabolism (2012), http://dx.doi.org/10.1016/j.cmet.2012.07.015

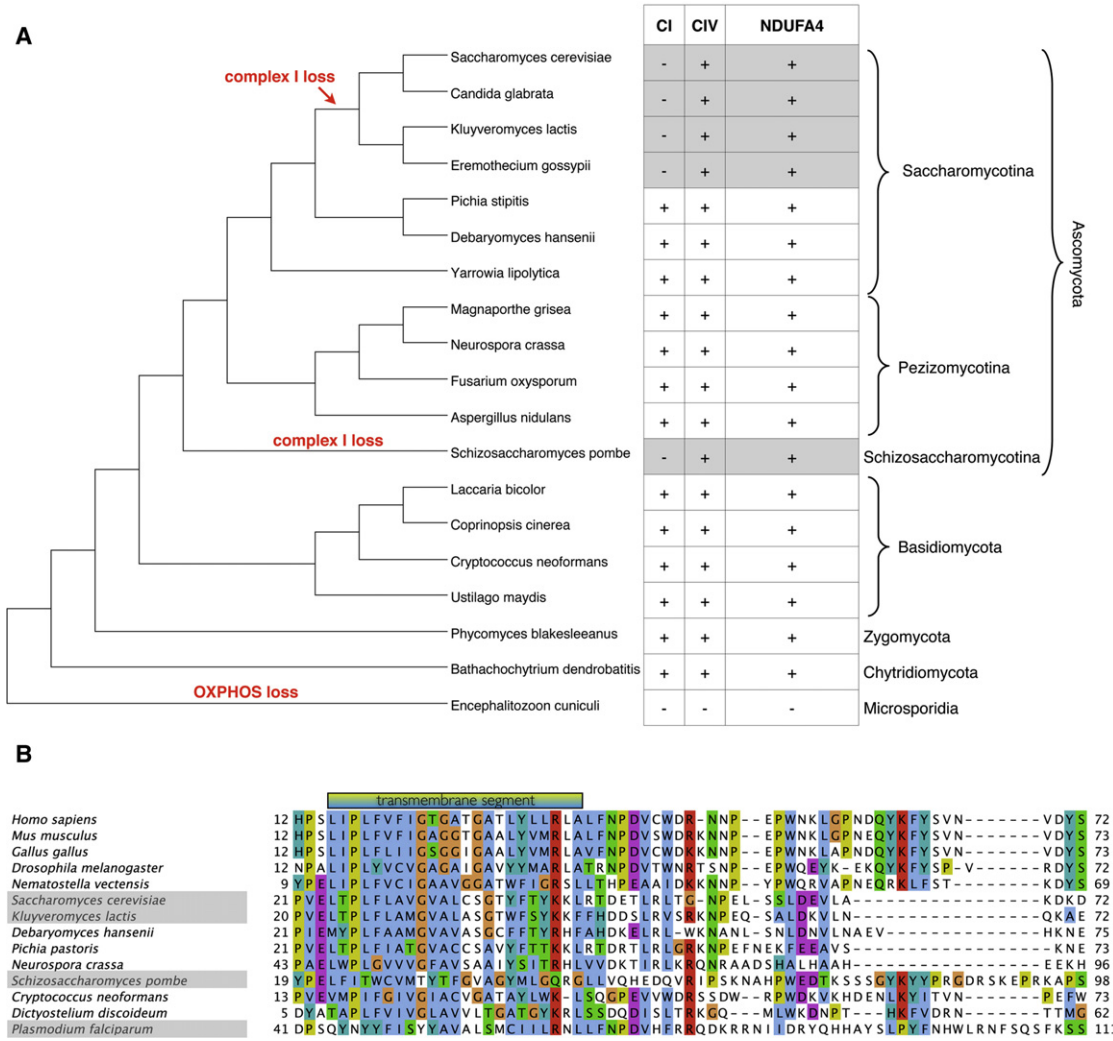

Figure 4. Sequence Evolution of NDUFA4 in Eukaryotes

(A) The analysis of NDUFA4 presence-absence patterns in fungi reveals that the NDUFA4 protein does not follow the evolutionary pattern of CI losses. Fungal species tree (Lavín et al., 2008) with indicated independent losses of respiratory chain complexes is shown. The isolated CI losses do not lead to the loss of NDUFA4, as would be expected if NDUFA4 was a CI subunit. CI, IV, and NDUFA4 presence patterns are marked in the table. Instances where CI is missing, but NDUFA4 is preserved, are marked gray.

(B) Multiple alignment of the conserved region of NDUFA4 in eukaryotes. Species without CI are marked gray. The transmembrane region (after TMHMM [Krogh et al., 2001]) that is common to all sequences is shown above the alignment. The alignment was prepared using Clustal-W with default parameters (Thompson et al., 1994). Sequence identifiers are listed in Table S1.

patterns are not congruent with evolution of complex I as previously thought. Analysis of *NDUFA4* presence-absence patterns in fungi (Figure 4A) reveals the existence of the NDUFA4 gene in all OXPHOS-encoding species. We identified *NDUFA4* in *Saccharomyces cerevisiae* and other *Saccharomycetaceae* that have lost CI (Figure 4A). The yeast's protein, encoded by a gene of unknown function, YPR010C-A, shares common features with the human NDUFA4, such as short length (81 amino acids in human and 72 in yeast) and the N-terminal transmembrane region (Figure 4B). While little is known about the gene's function in yeast, the protein has recently been copurified together with supercomplex III/IV from digitonin-solubilized mitochondria (Vukotic et al., 2012). The YPR010C-A protein sequence in *S. cerevisiae* is not divergent from CI-containing *NDUFA4* in a related fungus, *Debaryomyces hansenii*, indicating that the CI loss in the ancestor of yeast did not significantly alter the rate of sequence evolution of the gene. A high sequence divergence due to a relaxed evolutionary pressure would be expected if the gene's primary role in fungi related to CI. Also in the fission yeast *Schizosaccharomyces pombe*, species that lost CI independently from the budding yeast (Figure 4A), we identify the *NDUFA4* homolog encoded by SPBC3H7.08c gene (Figure 4B). Outside fungi, the gene can be found in CI-lacking apicomplexans, including the malaria parasite *Plasmodium falciparum* (Figure 4B). Worth noting is the loss of *NDUFA4* in *Blastocystis hominis*, a species that encodes CI in its genome, but lacks complexes III, IV, and V. Taken together, the analysis of *NDUFA4* gene evolution argues

against the gene's involvement in CI and supports the protein's role in CIV function.

DISCUSSION

Our findings are in clear conflict with the published crystal structures for cytochrome *c* oxidase. These revealed 13 distinct protein subunits, five phosphatidyl ethanolamines, three phosphatidyl glycerols and two cholates, two heme A molecules, three copper II ions, one magnesium ion, and one zinc ion, but no trace of NDUFA4. We hypothesized that NDUFA4 subunit might be lost during the purification of CIV in order to generate crystals. To obtain a high-quality crystal, samples are stringently purified using a wide range of detergents. One of the standard detergents used to purify CIV for crystallization purposes is n-dodecyl β-D-maltoside (DDM). We found that concentrations of DDM above 1.5% disrupt the interaction of NDUFA4 with CIV without affecting the remaining proteins (Figure S3). We therefore propose that this is the underlying cause for the failure of crystallization studies to detect NDUFA4 in CIV.

NDUFA4 was originally cataloged by Walker and coworkers as an accessory subunit of the mitochondrial membrane respiratory chain NADH dehydrogenase, or CI (Carroll et al., 2002, 2003, 2006; Hirst et al., 2003); however, the authors found several contradictory lines of evidence that made them doubt whether NDUFA4 was a genuine CI subunit (Hirst et al., 2003). In fact, NDUFA4 was not detected in all CI preparations and, more importantly, its presence correlated with contamination by the cytochrome *c* oxidase subunit VIB (Hirst et al., 2003). It may therefore be that the absence of NDUFA4 from CI preparations depends on detergent-mediated removal of cardiolipin, as occurs with other cytochrome *c* oxidase components, such as subunit VIB (Sedlák and Robinson, 1999). It is likely that, despite these warning signs, the established subunit composition of the other respiratory complexes based on their crystallization led to the acceptance of NDUFA4 as a CI subunit (Hirst et al., 2003). More recent evidence indicates that the expression pattern of NDUFA4 diverges notably from other CI nDNA-encoded subunits, leading to speculation that NDUFA4 may have other roles in addition to being a subunit of CI (Garbian et al., 2010). The full significance of these doubts and discrepancies is made clear in the light of our observations.

The change in the assignation of NDUFA4 from CI to CIV has important and wide implications. First, it may require redefinition of the structure of CIV. Second, it may now be necessary to consider NDUFA4 as a candidate gene for CIV deficiencies in humans, rather than for CI deficiencies. And third, it calls the attention to protocols for protein crystallization, especially from membrane protein complexes, because some proteins can be washed out during the multistep detergent-based purification of the crystals.

EXPERIMENTAL PROCEDURES

Cell Lines and Media

Mouse fibroblasts (wild-type, $COX10^{KO}$, $ND4^{KO}$, and $ND6^{KO}$), human fibroblasts (wild-type and $COX2^{KO}$), and HeLa cells were cultured in DMEM containing 10% heat-inactivated fetal bovine serum (FBS). All media were supplemented with 100 IU/ml penicillin and 100 μg/ml streptomycin. $COX10^{KO}$ and $COX2^{KO}$ fibroblasts were also supplemented with 50 mg/ml uridine. MtDNA-less mouse cells (ρ°L929) were grown in DMEM supplemented with 5% FBS, 50 mg/ml uridine, and 1 mM pyruvate (ρ° medium) and in the presence of 250 mg/ml of geneticin (G418). Medium for cells stably knocked down for NDUFA4 was supplemented with 1 μg/ml puromycin. Cells were maintained in 5% CO_2/95% air at 37°C.

shRNA and Expression Vectors

HeLa cells were stably transfected with one of two shRNA targeting sequences for NDUFA4 (sh.38 and sh.41). Specific lentivirus particles were purchased from Dharmacon. Empty vector or PCMV containing the NDUFA4 open reading frame were from OriGene and were used to transfect control HeLa cells and cells knocked down with sh.38 and sh.41 shRNAs.

Isolation of Mitochondria

Mitochondria were isolated from cultured cell lines according to Fernández-Vizarra et al., 2002, with some modifications. The following detergents were used for extracting mitochondrial membrane proteins: n-dodecyl β-D-maltoside (DDM) at 0.5%, 1%, or 3%; digitonin (DIG) at 4 g/g.

Blue Native Gel Electrophoresis and Western Blot Analysis

Mitochondrial membrane proteins (100–150 μg) were applied and run on 3%–13% first-dimension gradient BN gels as described elsewhere (Fernández-Vizarra et al., 2002). For 2D analysis, the first-dimension lane was excised from the gel, incubated for 1 hr at room temperature in 1% SDS and 1% β-mercaptoethanol, and run on a 16.5% second-dimension denaturing (SDS-PAGE) gel. After electrophoresis, the complexes were electroblotted onto PVDF membranes and sequentially probed with specific antibodies against CI (anti-NDUFB6, NDUFS5, NDUFS4, and NDUFA9), CIII (anti-core2), CIV (anti-COI), and CII (70 kDa subunit). All antibodies were from Molecular Probes. NDUFA4 antibody was purchased in Bioworld.

Protein Identification by Liquid Chromatography Coupled to Tandem Mass Spectrometry

Gel pieces from blue native gels containing the protein bands of interest were excised. After reduction with DTT (10 mM) and alkylation of Cys groups with iodoacetamide (50 mM), modified porcine trypsin (Promega) was added at a final mass ratio of 1:50 (trypsin-protein). Digestion proceeded overnight at 37°C, after which samples were vacuum-dried and dissolved in 1% acetic acid.

To identify proteins, the resulting tryptic peptide mixtures were analyzed by nanoliquid chromatography coupled to mass spectrometry. Peptides were injected onto a C-18 reversed phase (RP) nanocolumn (100 μm I.D. and 15 cm, Mediterranea Sea, Teknokroma) and analyzed on a continuous acetonitrile gradient consisting of 0%–43% B for 90 min and 50%–90% B for 1 min (B = 95% acetonitrile, 0.5% acetic acid). Peptides were eluted from the RP nanocolumn at a flow rate of ~300 nl/min to an emitter nanospray needle for real-time ionization and peptide fragmentation on an LTQ-Orbitrap mass spectrometer (Thermo Fisher, San Jose, CA). An enhanced FT-resolution spectrum (resolution = 6,000) and the MS/MS spectra of the five most-intense parent ions were analyzed during the chromatographic run (130 min). Dynamic exclusion was set at 0.5 min.

For protein identification, tandem mass spectra were extracted and charge-state deconvoluted with Proteome Discoverer 1.2.0.207 (Thermo Fisher Scientific). All MS/MS samples were analyzed by SEQUEST (Thermo Fisher Scientific, version 1.0.43.2), MASCOT (Matrixscience, version 2.1) and X! Tandem (The GPM, http://thegpm.org; version 2007.01.01.1). Search engines were set up to search MSIPI_mouse_3.67.fasta (1.0, 56,687 entries). All searches were performed assuming complete trypsin digestion. Two mixed cleavages were allowed, and errors of 15 ppm or 0.8 Da were set for full MS and MS/MS spectra searches, respectively. Oxidation of M, phosphorylation of S or T, and deamidation of Q or N were selected as dynamic modifications. All identifications were made by Decoy database search for FDR analysis. Scaffold (version Scaffold_3_00_03, Proteome Software Inc., Portland, OR) was used to validate MS/MS peptide and protein identifications. Protein probabilities were assigned by the Protein Prophet algorithm. Proteins that contained similar peptides and could not be differentiated based on MS/MS analysis alone were grouped to satisfy the principles of parsimony.

Immunocapture of Mitochondrial Complex I and IV OXPHOS Complexes

Mitochondrial CI or CIV was immunocaptured from isolated mitochondria using the CI and CIV immunoprecipitation kit (Abcam) according to the manufacturer's instructions.

Activities of Complex I and IV

CI and CIV activities were measured spectrophotometrically in mitochondrial fractions (2–5 mg protein) as described (Hofhaus et al., 1996). Both activities were expressed relative to citrate synthase activity.

Proliferation Analysis

Control, sh.38, and sh.41 HeLa cells were plated at 2×10^5 per 10 cm dish in DMEM containing either glucose or galactose. At indicated times the cells were trypsinized and the viable cells were counted.

Analysis of Genomic Presence-Absence Patterns

Homologs of the human NDUFA4 gene (Swissprot id: O00483) were retrieved with three iterations of PSI-BLAST with default parameters (Altschul et al., 1997). An alignment was build with default parameters of Clustal-W (Thompson et al., 1994) and profile and a profile-based hidden Markov model (HMM) of NDUFA4 gene were created based on the conserved part of the multiple alignment with HMMER 3.0 (http://hmmer.org) and HHSearch 1.5 (PMID: 15531603). The HMMs ware used to retrieve homologs in eukaryotes. Only statistically significant reciprocal-best hits highly indicative of orthology (Szklarczyk et al., 2012) were taken into account. The absence of the gene in *B. hominis* was confirmed at the genome level (by searching species' DNA, without prior knowledge of its gene compendium) to account for possibility of gene missing from *B. hominis* genome annotation.

Statistical Analysis

The data are presented as the means ± standard deviation of the mean of at least three independent experiments. Statistical significance ($^*p < 0.05$) was assessed by Student's t test.

SUPPLEMENTAL INFORMATION

Supplemental Information includes three figures and one table and can be found with this article online at http://dx.doi.org/10.1016/j.cmet.2012.07.015.

ACKNOWLEDGMENTS

We thank Dr. Ugalde for providing the $COXII^{KO}$ primary fibroblasts; Dr. Concepción Jimenez, Marta Roche, and Andres Gonzalez for technical assistance; and Dr. Simon Bartlett (CNIC) for English editing. This study was supported by grants from the MEC (SAF2009-08007 and CSD2007-00020) and CAM (S2010/BMD-2402). The CNIC is supported by the MEC and the Pro-CNIC Foundation. R.S. is supported by the CSBB, The Netherlands. E.B., E.P.-C., R.M., R.S., and E.C. performed experimental work and analyses. E.B., M.O.L., and J.A.E. designed the research. J.A.E. directed the work. E.B. and J.A.E. wrote the manuscript.

Received: April 16, 2012
Revised: June 18, 2012
Accepted: July 26, 2012
Published online: August 16, 2012

REFERENCES

Abrahams, J.P., Leslie, A.G., Lutter, R., and Walker, J.E. (1994). Structure at 2.8 A resolution of F1-ATPase from bovine heart mitochondria. Nature *370*, 621–628.

Acín-Pérez, R., Bayona-Bafaluy, M.P., Fernández-Silva, P., Moreno-Loshuertos, R., Pérez-Martos, A., Bruno, C., Moraes, C.T., and Enríquez, J.A. (2004). Respiratory complex III is required to maintain complex I in mammalian mitochondria. Mol. Cell *13*, 805–815.

Acín-Pérez, R., Fernández-Silva, P., Peleato, M.L., Pérez-Martos, A., and Enriquez, J.A. (2008). Respiratory active mitochondrial supercomplexes. Mol. Cell *32*, 529–539.

Altschul, S.F., Madden, T.L., Schäffer, A.A., Zhang, J., Zhang, Z., Miller, W., and Lipman, D.J. (1997). Gapped BLAST and PSI-BLAST: a new generation of protein database search programs. Nucleic Acids Res. *25*, 3389–3402.

Cardol, P. (2011). Mitochondrial NADH:ubiquinone oxidoreductase (complex I) in eukaryotes: a highly conserved subunit composition highlighted by mining of protein databases. Biochim. Biophys. Acta *1807*, 1390–1397.

Carroll, J., Shannon, R.J., Fearnley, I.M., Walker, J.E., and Hirst, J. (2002). Definition of the nuclear encoded protein composition of bovine heart mitochondrial complex I. Identification of two new subunits. J. Biol. Chem. *277*, 50311–50317.

Carroll, J., Fearnley, I.M., Shannon, R.J., Hirst, J., and Walker, J.E. (2003). Analysis of the subunit composition of complex I from bovine heart mitochondria. Mol. Cell. Proteomics *2*, 117–126.

Carroll, J., Fearnley, I.M., Skehel, J.M., Shannon, R.J., Hirst, J., and Walker, J.E. (2006). Bovine complex I is a complex of 45 different subunits. J. Biol. Chem. *281*, 32724–32727.

Cecchini, G. (2003). Function and structure of complex II of the respiratory chain. Annu. Rev. Biochem. *72*, 77–109.

Diaz, F., Fukui, H., Garcia, S., and Moraes, C.T. (2006). Cytochrome c oxidase is required for the assembly/stability of respiratory complex I in mouse fibroblasts. Mol. Cell. Biol. *26*, 4872–4881.

Efremov, R.G., and Sazanov, L.A. (2011). Structure of the membrane domain of respiratory complex I. Nature *476*, 414–420.

Efremov, R.G., Baradaran, R., and Sazanov, L.A. (2010). The architecture of respiratory complex I. Nature *465*, 441–445.

Fernández-Vizarra, E., López-Pérez, M.J., and Enriquez, J.A. (2002). Isolation of biogenetically competent mitochondria from mammalian tissues and cultured cells. Methods *26*, 292–297.

Fernández-Vizarra, E., Tiranti, V., and Zeviani, M. (2009). Assembly of the oxidative phosphorylation system in humans: what we have learned by studying its defects. Biochim. Biophys. Acta *1793*, 200–211.

Gabaldón, T., Rainey, D., and Huynen, M.A. (2005). Tracing the evolution of a large protein complex in the eukaryotes, NADH:ubiquinone oxidoreductase (Complex I). J. Mol. Biol. *348*, 857–870.

Garbian, Y., Ovadia, O., Dadon, S., and Mishmar, D. (2010). Gene expression patterns of oxidative phosphorylation complex I subunits are organized in clusters. PLoS ONE *5*, e9985.

Hirst, J., Carroll, J., Fearnley, I.M., Shannon, R.J., and Walker, J.E. (2003). The nuclear encoded subunits of complex I from bovine heart mitochondria. Biochim. Biophys. Acta *1604*, 135–150.

Hofhaus, G., Shakeley, R.M., and Attardi, G. (1996). Use of polarography to detect respiration defects in cell cultures. Methods Enzymol. *264*, 476–483.

Hunte, C., Zickermann, V., and Brandt, U. (2010). Functional modules and structural basis of conformational coupling in mitochondrial complex I. Science *329*, 448–451.

Huynen, M.A., de Hollander, M., and Szklarczyk, R. (2009). Mitochondrial proteome evolution and genetic disease. Biochim. Biophys. Acta *1792*, 1122–1129.

Iwata, S., Lee, J.W., Okada, K., Lee, J.K., Iwata, M., Rasmussen, B., Link, T.A., Ramaswamy, S., and Jap, B.K. (1998). Complete structure of the 11-subunit bovine mitochondrial cytochrome bc1 complex. Science *281*, 64–71.

Krogh, A., Larsson, B., von Heijne, G., and Sonnhammer, E.L. (2001). Predicting transmembrane protein topology with a hidden Markov model: application to complete genomes. J. Mol. Biol. *305*, 567–580.

Lavín, J.L., Oguiza, J.A., Ramírez, L., and Pisabarro, A.G. (2008). Comparative genomics of the oxidative phosphorylation system in fungi. Fungal Genet. Biol. *45*, 1248–1256.

Ohnishi, T., Johnson, J.E., Jr., Yano, T., Lobrutto, R., and Widger, W.R. (2005). Thermodynamic and EPR studies of slowly relaxing ubisemiquinone species in the isolated bovine heart complex I. FEBS Lett. *579*, 500–506.

Perales-Clemente, E., Bayona-Bafaluy, M.P., Pérez-Martos, A., Barrientos, A., Fernández-Silva, P., and Enriquez, J.A. (2008). Restoration of electron transport without proton pumping in mammalian mitochondria. Proc. Natl. Acad. Sci. USA *105*, 18735–18739.

Rees, D.M., Leslie, A.G., and Walker, J.E. (2009). The structure of the membrane extrinsic region of bovine ATP synthase. Proc. Natl. Acad. Sci. USA *106*, 21597–21601.

Roessler, M.M., King, M.S., Robinson, A.J., Armstrong, F.A., Harmer, J., and Hirst, J. (2010). Direct assignment of EPR spectra to structurally defined iron-sulfur clusters in complex I by double electron-electron resonance. Proc. Natl. Acad. Sci. USA *107*, 1930–1935.

Saraste, M. (1999). Oxidative phosphorylation at the fin de siècle. Science *283*, 1488–1493.

Sedlák, E., and Robinson, N.C. (1999). Phospholipase A(2) digestion of cardiolipin bound to bovine cytochrome c oxidase alters both activity and quaternary structure. Biochemistry *38*, 14966–14972.

Shinzawa-Itoh, K., Seiyama, J., Terada, H., Nakatsubo, R., Naoki, K., Nakashima, Y., and Yoshikawa, S. (2010). Bovine heart NADH-ubiquinone oxidoreductase contains one molecule of ubiquinone with ten isoprene units as one of the cofactors. Biochemistry *49*, 487–492.

Sun, F., Huo, X., Zhai, Y., Wang, A., Xu, J., Su, D., Bartlam, M., and Rao, Z. (2005). Crystal structure of mitochondrial respiratory membrane protein complex II. Cell *121*, 1043–1057.

Szklarczyk, R., Wanschers, B.F., Cuypers, T.D., Esseling, J.J., Riemersma, M., van den Brand, M.A., Gloerich, J., Lasonder, E., van den Heuvel, L.P., Nijtmans, L.G., and Huynen, M.A. (2012). Iterative orthology prediction uncovers new mitochondrial proteins and identifies C12orf62 as the human ortholog of COX14, a protein involved in the assembly of cytochrome c oxidase. Genome Biol. *13*, R12.

Thompson, J.D., Higgins, D.G., and Gibson, T.J. (1994). CLUSTAL W: improving the sensitivity of progressive multiple sequence alignment through sequence weighting, position-specific gap penalties and weight matrix choice. Nucleic Acids Res. *22*, 4673–4680.

Tsukihara, T., Aoyama, H., Yamashita, E., Tomizaki, T., Yamaguchi, H., Shinzawa-Itoh, K., Nakashima, R., Yaono, R., and Yoshikawa, S. (1995). Structures of metal sites of oxidized bovine heart cytochrome c oxidase at 2.8 A. Science *269*, 1069–1074.

Tsukihara, T., Aoyama, H., Yamashita, E., Tomizaki, T., Yamaguchi, H., Shinzawa-Itoh, K., Nakashima, R., Yaono, R., and Yoshikawa, S. (1996). The whole structure of the 13-subunit oxidized cytochrome c oxidase at 2.8 A. Science *272*, 1136–1144.

Vogel, R.O., Smeitink, J.A., and Nijtmans, L.G. (2007). Human mitochondrial complex I assembly: a dynamic and versatile process. Biochim. Biophys. Acta *1767*, 1215–1227.

Vukotic, M., Oeljeklaus, S., Wiese, S., Vögtle, F.N., Meisinger, C., Meyer, H.E., Zieseniss, A., Katschinski, D.M., Jans, D.C., Jakobs, S., et al. (2012). Rcf1 mediates cytochrome oxidase assembly and respirasome formation, revealing heterogeneity of the enzyme complex. Cell Metab. *15*, 336–347.

Xu, J., and Voth, G.A. (2008). Redox-coupled proton pumping in cytochrome c oxidase: further insights from computer simulation. Biochim. Biophys. Acta *1777*, 196–201.

Cell Metabolism, Volume *16*

Supplemental Information

NDUFA4 Is a Subunit of Complex IV of the Mammalian Electron Transport Chain

Eduardo Balsa, Ricardo Marco, Ester Perales-Clemente, Radek Szklarczyk, Enrique Calvo, Manuel O. Landázuri, and José Antonio Enríquez

A

NADH dehydrogenase (ubiquinone) 1 alpha Subcomplex 4 NDUFA4:
37,5% coverage

```
         10          20          30          40          50          60
MLRQILGQAK KHPSLIPLFV FIGAGGTGAA LYVMRLALFN PDVSWDRKNN PEPWNKLGPN

         70          80
EQYKFYSVNV DYSKLKKEGP DF
```

B

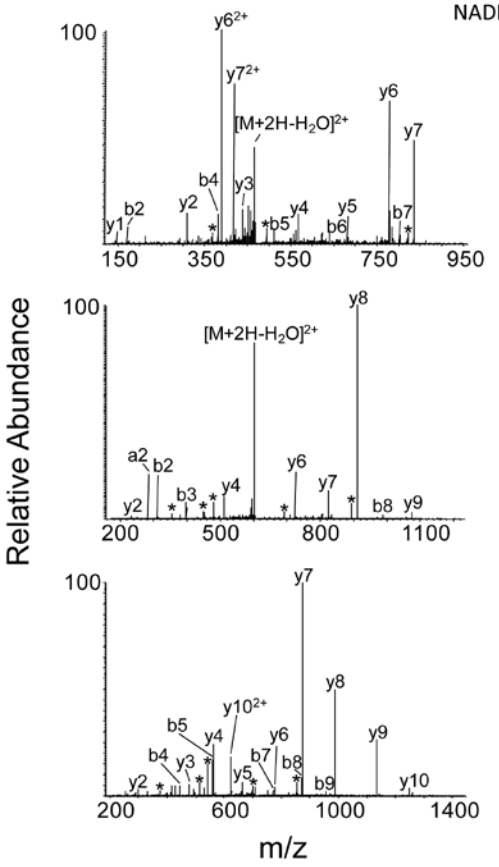

NADH dehydrogenase (ubiquinone) 1 alpha subcomplex, 4]

57-LGPNEQYK-64

B	B Ions	B+2H	B-NH3	B-H2O	AA	Y Ions	Y+2H	Y-NH3	Y-H2O	Y
1	114.1				L	948.5	474.7	931.5	930.5	8
2	171.1				G	835.4	418.2	818.4	817.4	7
3	268.2				P	778.4	389.7	761.3	760.4	6
4	382.2		365.2		N	681.3		664.3	663.3	5
5	511.3		494.2	493.2	E	567.3		550.3	549.3	4
6	639.3	320.2	622.3	621.3	Q	438.2		421.2		3
7	802.4	401.7	785.3	784.4	Y	310.2		293.1		2
8	948.5	474.7	931.5	930.5	K	147.1		130.1		1

64-FYSVNVDYSK-74

B	B Ions	B+2H	B-NH3	B-H2O	AA	Y Ions	Y+2H	Y-NH3	Y-H2O	Y
1	148.1				F	1,221.6	611.3	1,204.6	1,203.6	10
2	311.1				Y	1,074.5	537.8	1,057.5	1,056.5	9
3	398.2			380.2	S	911.4	456.2	894.4	893.4	8
4	497.2			479.2	V	824.4	412.7	807.4	806.4	7
5	611.3		594.3	593.3	N	725.3	363.2	708.3	707.3	6
6	710.4	355.7	693.3	692.3	V	611.3		594.3	593.3	5
7	825.4	413.2	808.4	807.4	D	512.2		495.2	494.2	4
8	988.4	494.7	971.4	970.4	Y	397.2		380.2	379.2	3
9	1,075.5	538.2	1,058.4	1,057.5	S	234.1		217.1	216.1	2
10	1,221.6	611.3	1,204.6	1,203.6	K	147.1		130.1		1

36-LALFNPDVSWDR-47

B	B Ions	B+2H	B-NH3	B-H2O	AA	Y Ions	Y+2H	Y-NH3	Y-H2O	Y
1	114.1				L	1,432.7	716.9	1,415.7	1,414.7	12
2	185.1				A	1,319.6	660.3	1,302.6	1,301.6	11
3	298.2				L	1,248.6	624.8	1,231.6	1,230.6	10
4	445.3				F	1,135.5	568.3	1,118.5	1,117.5	9
5	559.3		542.3		N	988.4	494.7	971.4	970.4	8
6	656.4	328.7	639.4		P	874.4	437.7	857.4	856.4	7
7	771.4	386.2	754.4	753.4	D	777.4	389.2	760.3	759.3	6
8	870.5	435.7	853.4	852.5	V	662.3		645.3	644.3	5
9	957.5	479.3	940.5	939.5	S	563.3		546.2	545.2	4
10	1,143.6	572.3	1,126.6	1,125.6	W	476.2		459.2	458.2	3
11	1,258.6	629.8	1,241.6	1,240.6	D	290.1		273.1	272.1	2
12	1,432.7	716.9	1,415.7	1,414.7	R	175.1		158.1		1

Sup. Fig 1 Balsa et al.

Figure S1 (Related to Figure 1). Identification of NDUFA4 by Mass Spectrometry

(A) NDUFA4 sequence, with the three matched peptides highlighted in color.

(B) Fragmentation spectra for the three matched NDUFA4 peptides. Singly- or doubly-charged main fragmentation series (y-carboxy and b-amino) are assigned. Asterisks mark water loss ions. Theoretical mass fragments are presented in the tables for each ion.

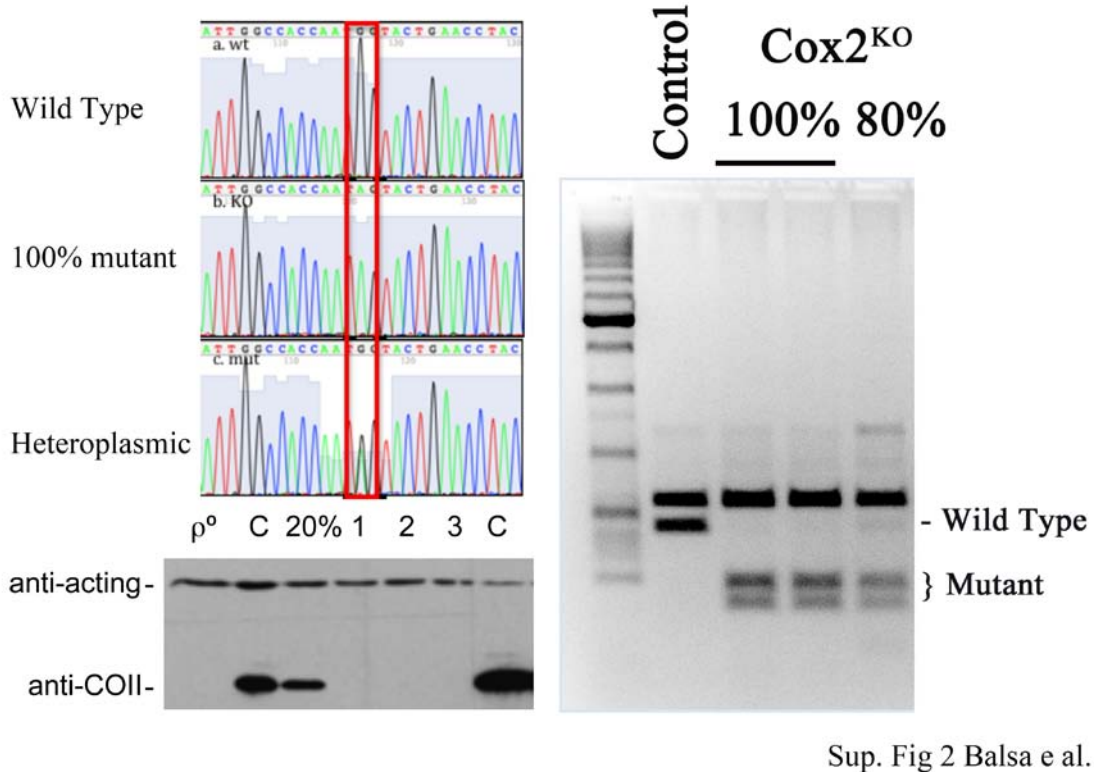

Figure S2 (Related to Figure 2). Characterization of the Human Cell Line Lacking Cox2

(A) Chromatogram showing the G7896A transition in the *Cox2* gene at human mtDNA causing a nonsense mutation (*1*).

(B) RFLP analysis to estimate the proportion of the mutant vs. wild type version of the genes in different clones.

(C) Immunodetection of COX2 protein in the different clones according with the proportion of mutant mtDNA.

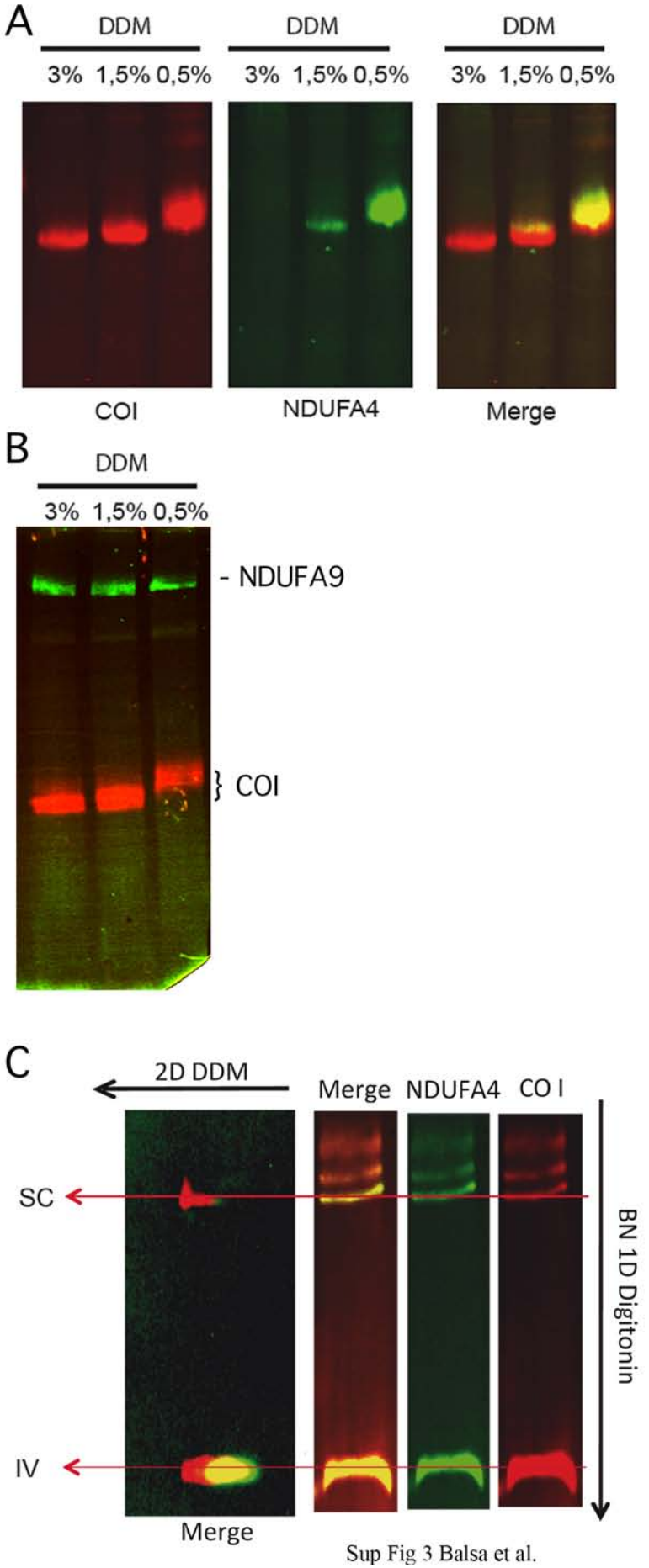

Sup Fig 3 Balsa et al.

Figure S3. DDM Detach NDUFA4 from Complex IV

(A) Isolated mitochondria from HeLa cells were treated with different concentrations of DDM (0.5% 1.5% and 3%) and extracts analyzed by BNGE. Panels show western blots for COI (complex IV; left) and NDUFA4 (center), and a merged image (right). Bound antibody signals have false colour for easer comparison.

(B) Isolated mitochondria from mouse cells were treated with different concentrations of DDM (0.5% 1.5% and 3%) and extracts analyzed by BNGE. Panel show western blots for COI and NDUFA9.

(C) Isolated mitochondria from mouse cells were treated with digitonine and analysed by 2D Digitonine BNGE /DDM:BNEG. Panels show for the 1st dimension western blots for COI (complex IV; right), NDUFA4 (center), and a merged image (right); and for the second dimension only the merged image. Bound antibody signals have false colour for easer comparison.

Table S1. Sequence Identifiers of Proteins Used in Figure 4B

Species	*Identifier type*	*Identifier*
Homo sapiens	NCBI GI	4505357
Mus musculus	NCBI GI	33563266
Gallus gallus	NCBI GI	363730012
Drosophila melanogaster	NCBI GI	24668874
Nematostella vectensis	NCBI GI	156405806
Saccharomyces cerevisiae	SGD	YPR010C-A
Kluyveromyces lactis	SWISSPROT	Q6CS34
Debaryomyces hansenii	SWISSPROT	Q6BTS4
Pichia pastoris	SWISSPROT	C4R8K6
Neurospora crassa	SWISSPROT	Q873A3
Schizosaccharomyces pombe	S. pombe annot.	SPBC3H7.08c
Cryptococcus neoformans	NCBI GI	58259629
Dictyostelium discoideum	SWISSPROT	Q54ND0
Plasmodium falciparum	NCBI GI	124809337

Supplemental References

1. Y. Campos *et al.*, Early-onset multisystem mitochondrial disorder caused by a nonsense mutation in the mitochondrial DNA cytochrome C oxidase II gene. *Annals of neurology* **50**, 409 (Sep, 2001).

Manuscrito 3

***Vhl Gene Inactivation Induces Cardiac HIF-Dependent Erythropoietin Gene Expresión*.**

PlosOne,2011, 6(7):22589

Además de los dos artículos anteriores en los que firmo como primer autor, también he ayudado a personas de mi grupo en ciertos experimentos para otros artículos, lo que me ha ayudado tener una visión más general del campo en el que trabajo.

En este articulo demostramos como la inactivación del gen VHL rápidamente resulta en una marcada esplenomegalia y eritema en la piel. Esta inactivación de VHL no solo indujo la expresión de la Epo en el riñón y el hígado sino también en el corazón, revelando de esta manera que el tejido cardiaco puede ser una fuente extra renal de EPO

OPEN ACCESS Freely available online

PLoS one

Acute *Vhl* Gene Inactivation Induces Cardiac HIF-Dependent Erythropoietin Gene Expression

Marta Miró-Murillo[2☯], Ainara Elorza[1☯], Inés Soro-Arnáiz[1☯], Lucas Albacete-Albacete[1], Angel Ordoñez[1], Eduardo Balsa[1], Alicia Vara-Vega[1], Silvia Vázquez[1], Esther Fuertes[1], Carmen Fernández-Criado[2], Manuel O. Landázuri[1], Julián Aragonés[1]*

1 Department of Immunology, Hospital of La Princesa, Sanitary Research Institute Princesa (IP), Autonomous University of Madrid, Madrid, Spain, **2** Animal Facility, Autonomous University of Madrid, Madrid, Spain

Abstract

Von Hippel Lindau (*Vhl*) gene inactivation results in embryonic lethality. The consequences of its inactivation in adult mice, and of the ensuing activation of the hypoxia-inducible factors (HIFs), have been explored mainly in a tissue-specific manner. This mid-gestation lethality can be also circumvented by using a floxed *Vhl* allele in combination with an ubiquous tamoxifen-inducible recombinase Cre-ER^{T2}. Here, we characterize a widespread reduction in *Vhl* gene expression in Vhl^{floxed}-UBC-Cre-ER^{T2} adult mice after dietary tamoxifen administration, a convenient route of administration that has yet to be fully characterized for global gene inactivation. *Vhl* gene inactivation rapidly resulted in a marked splenomegaly and skin erythema, accompanied by renal and hepatic induction of the erythropoietin (*Epo*) gene, indicative of the in vivo activation of the oxygen sensing HIF pathway. We show that acute *Vhl* gene inactivation also induced *Epo* gene expression in the heart, revealing cardiac tissue to be an extra-renal source of EPO. Indeed, primary cardiomyocytes and HL-1 cardiac cells both induce *Epo* gene expression when exposed to low O_2 tension in a HIF-dependent manner. Thus, as well as demonstrating the potential of dietary tamoxifen administration for gene inactivation studies in UBC-Cre-ER^{T2} mouse lines, this data provides evidence of a cardiac oxygen-sensing VHL/HIF/EPO pathway in adult mice.

Citation: Miró-Murillo M, Elorza A, Soro-Arnáiz I, Albacete-Albacete L, Ordoñez A, et al. (2011) Acute *Vhl* Gene Inactivation Induces Cardiac HIF-Dependent Erythropoietin Gene Expression. PLoS ONE 6(7): e22589. doi:10.1371/journal.pone.0022589

Editor: Mauricio Rojas, University of Pittsburgh, United States of America

Received December 7, 2010; **Accepted** June 29, 2011; **Published** July 21, 2011

Funding: This work was supported by grants from Ministerio de Educación y Ciencia (BFU2008-03407/BMC), RECAVA (RD06/0014/0031), CICYT (SAF2007-60592) and CAM (SAL0311/2006). The funders had no role in study design, data collection and analysis, decision to publish, or preparation of the manuscript.

Competing Interests: The authors have declared that no competing interests exist.

* E-mail: jaragones.hlpr@salud.madrid.org

☯ These authors contributed equally to this work.

Introduction

The ability of cells to respond to low O_2 supply (hypoxia) is fundamental in numerous pathological scenarios [1]. Hypoxia-inducible transcription factors (HIF) 1α, 2α and 3α, prolyl hydroxylase domain proteins (PHDs) 1, 2 and 3 and the von Hippel-Lindau (VHL) protein are essential molecular elements in the cellular response to low O_2 supply. In normoxia, PHDs hydroxylate prolyl residues in the HIFα subunits that are then recognized by VHL, a protein of the multiprotein E3 ubiquitin ligase complex that marks them for degradation by the proteasome [2,3]. In conditions of hypoxia O_2 is limited and it is insufficient to hydroxylate prolyl residues in HIFα [4,5]. As a result, these HIFα isoforms are stabilized and form a heterodimer with the HIFβ subunit, promoting the expression of many genes involved in cellular adaptation to hypoxia [6]. This includes the expression of erythropoietin (*Epo*) in the kidney and liver in order to facilitate oxygen delivery to hypoxic tissues [7,8,9,10]. Global *Vhl* gene inactivation in mice, and the ensuing HIF activation, can be used as a strategy to explore hypoxia signalling *in vivo*. However, conventional global *Vhl* gene inactivation is lethal in embryos [11], although this can be circumvented by only inducing *Vhl* gene inactivation in adult mice.

Widespread and acute gene inactivation in adult mice can be achieved through the ubiquitous expression of an inducible Cre recombinase, which can be used to eliminate the *Vhl* allelic region flanked by two loxP sites (a floxed *Vhl* allele). The nuclear activity of Cre can be induced by fusing it to a mutant form of the human estrogen receptor (ER^{T2}) that does not recognize its natural ligand (17β-estradiol) at physiological concentrations but rather, it binds the synthetic estrogen receptor ligand 4-hydroxytamoxifen (4-HT) [12]. This Cre-ER^{T2} is retained in the cytoplasm and only enters the nucleus in the presence of 4-HT, where it binds to loxP sites of the corresponding floxed alleles. Like other ubiquitous promoters, widespread Cre-ER^{T2} expression can be achieved in mice using the human ubiquitin C (UBC) promoter (UBC-Cre-ER^{T2} mice) [13]. Several means of administering tamoxifen have been described in rodents, including intraperitoneal injections and gavage [13]. However, the addition of 4-HT to powdered food or drinking water is a more convenient and less stressful means of inducing Cre recombinase activity in adult mice [14,15,16]. While the administration of tamoxifen via drinking water is hampered by its poor solubility, its delivery in food has been successfully achieved in several mouse lines [14,15,16]. However, to date, the full potential of a tamoxifen diet and its efficacy in inducing global Cre-ER^{T2} activity in different organs of a Cre-ER^{T2} transgenic mouse line (e.g. UBC-Cre-ER^{T2} mice) has not been fully explored.

Here we have successfully employed diet-based tamoxifen administration, a timesaving and convenient mean of delivering

tamoxifen in order to induce widespread inactivation of the *Vhl* gene in a Vhl^{floxed}-UBC-Cre-ER^{T2} mouse line. After validating the efficiency of tamoxifen dietary administration, we characterized VHL/HIF oxygen-sensing dependent events that were rapidly induced by global *Vhl* inactivation *in vivo* (within just a few days) in contrast to other works that have mainly studied the *in vivo* consequences of *Vhl* gene inactivation over several weeks [17,18]. This study validates the use of the tamoxifen diet in UBC-Cre-ER^{T2} mouse lines for global gene inactivation, and it identifies an oxygen-sensing VHL/HIF pathway controlling extra-renal *Epo* gene expression in cardiac tissue.

Results

Postnatal tamoxifen diet-mediated *Vhl* gene inactivation

Global *Vhl* gene inactivation results in embryonic lethality, at least in part due to placental dysfunction [11], preventing the study of the global loss of this gene in adult mice. We were interested in the short-term effects of activating the oxygen-sensing HIF pathway *in vivo*, as a result of global *Vhl* gene inactivation in adult Vhl^{floxed}-UBC-Cre-ER^{T2} mice through dietary tamoxifen administration. Since the full potential of dietary tamoxifen administration for global gene inactivation has not been explored previously, we first validated the efficacy of the tamoxifen diet in reducing *Vhl* gene expression in the Vhl^{floxed}-UBC-Cre-ER^{T2} mouse line. Age-matched Vhl^{floxed}-UBC-Cre-ER^{T2} as well as control mice Vhl^{floxed} and Vhl^{wt}-UBC-Cre-ER^{T2} were maintained for 10 days on an *ad libitum* diet of tamoxifen pellets (containing 400 mg/kg tamoxifen), before they were switched to a diet of normal chow for a further 10 days and *Vhl* gene expression was analyzed by quantitative real-time PCR in the different mouse organs. Hereinafter, the terms Vhl^{floxed}, Vhl^{wt}-UBC-Cre-ER^{T2} and Vhl^{floxed}-UBC-Cre-ER^{T2} refer to mice that have been administered a tamoxifen diet as indicated above. The tamoxifen diet significantly reduced *Vhl* gene expression in the kidney, spleen, liver, skeletal muscle, brown adipose tissue (BAT), heart, lung and brain of Vhl^{floxed}-UBC-Cre-ER^{T2} mice, reflecting widespread *Vhl* gene inactivation (Figure 1A). No differences in tamoxifen intake were observed between Vhl^{floxed}-UBC-Cre-ER^{T2} and control mice (Figure 1B). Significantly, gene inactivation was not homogeneous and expression of the *Vhl* gene was more strongly downregulated in the kidney and spleen, and less so in other tissues such as the brain and lung (Figure 1A). To further validate the specificity of *Vhl* gene inactivation, we also quantified *Vhl* gene expression in another UBC-Cre-ER^{T2} system, the $Hif1\alpha^{floxed}$-UBC-Cre-ER^{T2} mouse line and their corresponding $Hif1\alpha^{floxed}$ and $Hif1\alpha^{wt}$-UBC-Cre-ER^{T2} control mice. While there were no significant differences in tamoxifen intake between the different lines (Figure 1D), *Hif1α* gene expression was dramatically and globally reduced, while *Vhl* gene expression was not affected in tamoxifen fed $Hif1\alpha^{floxed}$-UBC-Cre-ER^{T2} mice (Figure 1C, E).

As mice were transiently exposed to a different diet, we evaluated their body weight before and after tamoxifen treatment. Baseline body weight diminished in a similar way (~10%) in Vhl^{floxed}-UBC-Cre-ER^{T2} and control mice after 10 days on the tamoxifen diet (Figure 2). However, while the body weight of control mice returned to pre-tamoxifen levels just one day after switching back to a normal diet (Figure 2), that was not the case in Vhl^{floxed}-UBC-Cre-ER^{T2} mice following tamoxifen treatment (Figure 2), suggesting that body weight was rapidly compromised by *Vhl* gene inactivation.

Gross appearance of mice shortly after acute *Vhl* inactivation

To further evaluate the efficacy of the tamoxifen diet on *Vhl* gene inactivation, we studied the biological consequences of acute *Vhl* inactivation soon after the mice returned to a normal diet (10 days). We evaluated spleen size and skin erythema as macroscopic indicators of activation of the HIF oxygen-sensing pathway *in vivo* [19]. All tamoxifen-treated Vhl^{floxed}-UBC-Cre-ER^{T2} mice analyzed exhibited marked splenomegaly when compared with controls (Figure 3 A, B). Moreover, some mice displayed obvious reddening of their paws and snouts (Figure 3 C, D). These external signs of skin erythema appeared as early as the ninth day of tamoxifen administration (data not shown), suggesting that this phenotype represents an acute manifestation of *Vhl* gene inactivation. Overall, these data confirm that dietary administration of tamoxifen is an efficient and convenient mean to induce widespread and rapid gene inactivation of floxed alleles in UBC-Cre-ER^{T2} mice and in particular, to study the short-term biological consequences of *Vhl* inactivation.

Acute *Vhl* inactivation induces cardiac *Epo* gene expression

Splenomegaly and erythema are recognized signs of activation of the oxygen-VHL/HIF/EPO pathway, and they have been reported previously in transgenic mice overexpressing EPO [20,21]. Given that the kidney and liver are the main sites of EPO production in adults [7,22,23], we investigated *Epo* gene expression in these organs in Vhl^{floxed}-UBC-Cre-ER^{T2} mice shortly after *Vhl* gene inactivation. When we analyzed renal and hepatic *Epo* gene expression in tamoxifen-treated Vhl^{floxed}-UBC-Cre-ER^{T2} mice, we found a strong induction of this gene in the kidney (~200 fold, Figure 4A) and an even stronger increase in the liver when compared to control mice (Figure 4B). The marked difference between these two organs is probably due to the very low basal levels of hepatic *Epo* gene expression, which results in more marked differences when *Vhl* is inactivated. These differences cannot simply be attributed to differences in *Vhl* inactivation, as *Vhl* is inactivated to a greater extent in the kidney than in the liver (Figure 1A). Moreover, serum EPO levels were drastically elevated in tamoxifen-treated Vhl^{floxed}-UBC-Cre-ER^{T2} when compared with tamoxifen-treated control mice (pg of EPO/ml: 150.5 ± 22.6 in Vhl^{floxed} versus 49835.5 ± 21586 in Vhl^{floxed}-UBC-Cre-ER^{T2}; $n=4$, $p<0.05$). These mice showed a remarkable reticulocytosis. Indeed, the number of circulating reticulocytes as well as splenic reticulocytes increases in Vhl^{floxed}-UBC-Cre-ER^{T2} mice (*Circulating reticulocytes* $x10^6/ml$: 603.92 ± 437 in Vhl^{floxed} versus 6391.53 ± 1381 in Vhl^{floxed}-UBC-Cre-ER^{T2}; $n=3$, $p=0.018$) (*Splenic reticulocytes* $x10^6/ml$: 32 ± 6.08 in Vhl^{floxed} versus 269.08 ± 4.4 in Vhl^{floxed}-UBC-Cre-ER^{T2}; $n=3$, $p=0.01$). However, a parallel hemocytometry showed that hematocrit is not significantly elevated in tamoxifen-treated Vhl^{floxed}-UBC-Cre-ER^{T2} when compared with control mice (*hematocrit %*: 40.8 ± 2.02 in Vhl^{floxed} versus 43 ± 5.3 in Vhl^{floxed}-UBC-Cre-ER^{T2}; $n=5$, $p=$NS). Furthermore, a follow up of Vhl^{floxed}-UBC-Cre-ER^{T2} mice revealed that they started to show anemia after a longer time period upon *Vhl* gene inactivation (*hematocrit %*: 42.62 ± 2.22 in Vhl^{floxed} versus 33.2 ± 3.8 in Vhl^{floxed}-UBC-Cre-ER^{T2}; $n=7$, $p=0.041$). In addition, the proportion of Hoechst $33342^{negative}$ $CD71^{negative}$ cells decrease in the spleens of Vhl^{floxed}-UBC-Cre-ER^{T2} (% of total number of splenic cells: 27.10 ± 5.3 in Vhl^{floxed} versus 3.22 ± 1.25 in Vhl^{floxed}-UBC-Cre-ER^{T2}; $n=3$, $p<0.01$). This possibly reflects a specific VHL-dependent effect on mature red blood cells survival that will be further explored in futures studies.

In line with other studies, baseline *Epo* gene expression was particularly weak in the heart [8], although we found a remarkable elevation in cardiac *Epo* gene expression in tamoxifen fed Vhl^{floxed}-UBC-Cre-ER^{T2} mice (Figure 4D). Given that cardiac *Vhl*

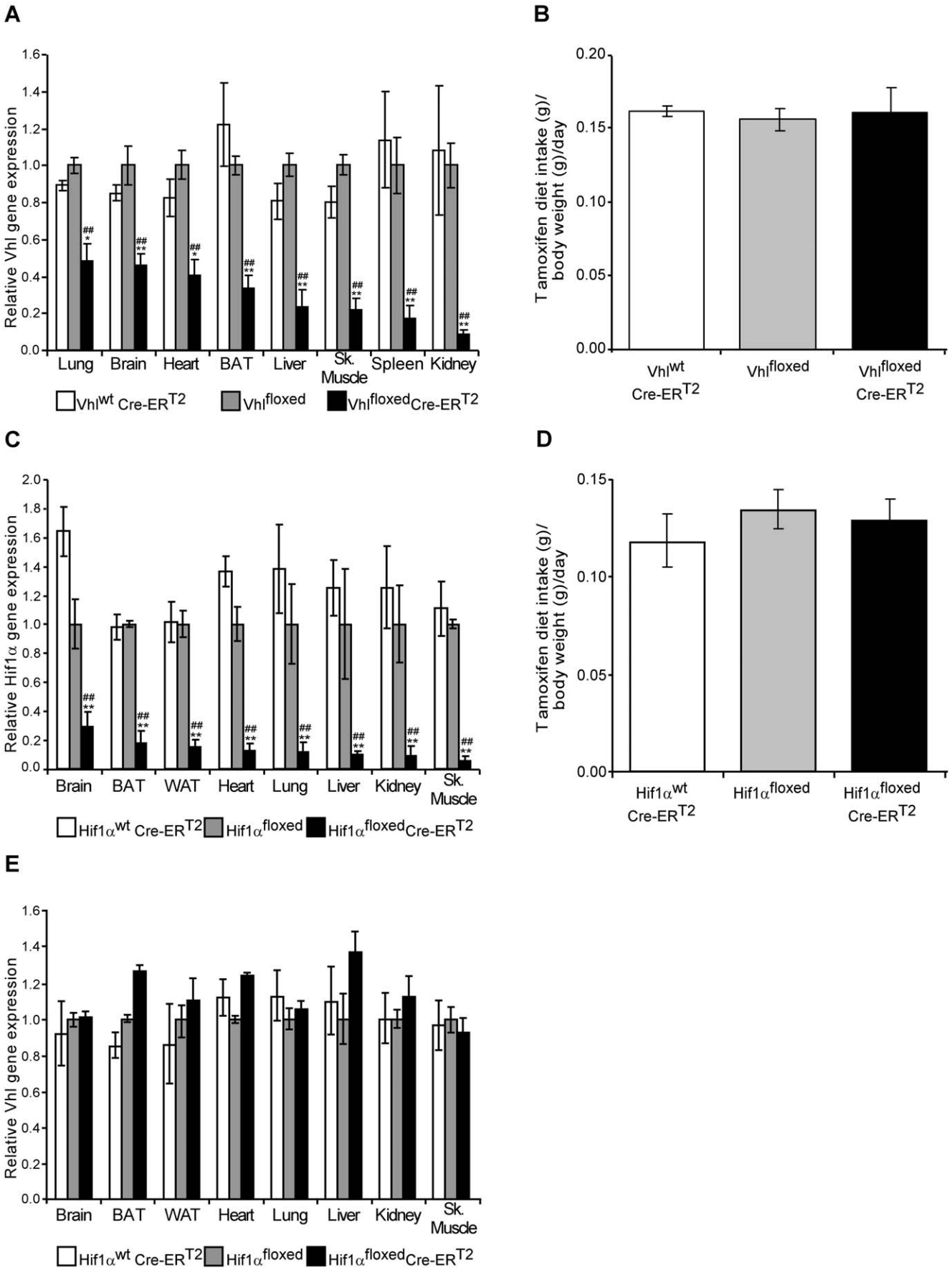
A
Relative Vhl gene expression
Lung
Brain
Heart
BAT
Liver
Sk. Muscle
Spleen
Kidney
Vhlwt Cre-ERT2
Vhlfloxed
Vhlfloxed Cre-ERT2
B
Tamoxifen diet intake (g)/ body weight (g)/day
Vhlwt Cre-ERT2
Vhlfloxed
Vhlfloxed Cre-ERT2
C
Relative Hif1α gene expression
Brain
BAT
WAT
Heart
Lung
Liver
Kidney
Sk. Muscle
Hif1αwt Cre-ERT2
Hif1αfloxed
Hif1αfloxed Cre-ERT2
D
Tamoxifen diet intake (g)/ body weight (g)/day
Hif1αwt Cre-ERT2
Hif1αfloxed
Hif1αfloxed Cre-ERT2
E
Relative Vhl gene expression
Brain
BAT
WAT
Heart
Lung
Liver
Kidney
Sk. Muscle
Hif1αwt Cre-ERT2
Hif1αfloxed
Hif1αfloxed Cre-ERT2

Figure 1. *Vhl* and *Hif1α* gene expression in tamoxifen-fed Vhl^{floxed}-UBC-Cre-ER^{T2} and Hif1α^{floxed}-UBC-Cre-ER^{T2} mice. (A) Vhl^{wt}-UBC-Cre-ER^{T2} (n = 3), Vhl^{floxed} (n = 6) and Vhl^{floxed}-UBC-Cre-ER^{T2} (n = 6) mice were placed on a tamoxifen diet for ten days followed by ten additional days on a normal diet. Gene expression was assessed by RT-PCR in the tissues indicated, the expression of the *Vhl* gene was normalized to that of *Hprt* and it was expressed as the change relative to Vhl^{floxed} mice. (B) Tamoxifen intake was measured over the 10 days of tamoxifen administration in Vhl^{wt}-UBC-Cre-ER^{T2} (n = 3), Vhl^{floxed} (n = 6) and Vhl^{floxed}-UBC-Cre-ER^{T2} (n = 6) mice. (C,E) Hif1α^{wt}-UBC-Cre-ER^{T2} (n = 4), Hif1α^{floxed} (n = 3) and Hif1α^{floxed}-UBC-Cre-ER^{T2} (n = 5) mice were administered tamoxifen as indicated above. *Hif1α* (C) or *Vhl* (E) gene expression was normalized to that of *Hprt* and expressed as the change relative to Hif1α^{floxed} mice. (D) Tamoxifen intake in Hif1α^{wt}-UBC-Cre-ER^{T2} (n = 4), Hif1α^{floxed} (n = 3) and Hif1α^{floxed}-UBC-Cre-ER^{T2} (n = 5) mice was measured as in B. Total intake per day was expressed relative to the body weight at the end of the tamoxifen treatment and the values represent the mean ± SEM. Statistical significance was assessed using a two-tailed Student's t-test, (*, $p<0.05$; **, $p<0.01$) when comparing Vhl^{wt}-UBC-Cre-ER^{T2} or Hif1α^{wt}-UBC-Cre-ER^{T2} with Vhl^{floxed}-UBC-Cre-ER^{T2} or Hif1α^{floxed}-UBC-Cre-ER^{T2} respectively; ($^{\#\#}$, $p<0.01$) when comparing Vhl^{floxed} or Hif1α^{floxed} with Vhl^{floxed}-UBC-Cre-ER^{T2} or Hif1α^{floxed}-UBC-Cre-ER^{T2} respectively.
doi:10.1371/journal.pone.0022589.g001

expression is not fully ablated in tamoxifen-treated Vhl^{floxed}-UBC-Cre-ER^{T2} mice (Figure 1A), we presumed that cardiac *Epo* gene expression could be potentially higher if *Vhl* deletion were more prominent. Expression of glucose transporter-1 (*Glut1)*, a HIF-dependent gene [24], was also elevated in the hearts of tamoxifen treated Vhl^{floxed}-UBC-Cre-ER^{T2} mice (Figure 4D). In addition, *Epo* gene expression was markedly upregulated in the brain (Figure 4C), possibly reflecting oxygen-sensing VHL/HIF-dependent EPO production in glial cells, as described previously [25]. Induction of *Epo* gene expression was stronger in cardiac tissue than in the brain, perhaps due to the weak basal expression of the *Epo* gene in the heart. These data suggest that the oxygen-sensing VHL/HIF/EPO pathway is not restricted to classical EPO-producing tissues, and they demonstrate that the heart can express EPO upon *Vhl* inactivation. To determine whether cardiomyocytes could be contributing to this VHL-dependent response, *Epo* gene expression was analyzed in isolated primary rat cardiomyocytes exposed to low oxygen tension. While weak basal expression of the *Epo* gene was observed in normoxic cardiomyocytes, hypoxia (1% O_2) augmented markedly its expression (Figure 5A). Likewise, *Glut1* expression was also induced, which indicates an effective induction of the HIF pathway in these experimental conditions (Figure 5B). We further evaluated the role of the HIF system in hypoxia-induced *Epo* gene expression in cardiac cells in the HL-1 cell line, a well-recognized cardiac cell model that retains a differentiated cardiac myocyte phenotype and maintains contractile activity [26]. We specifically silenced expression of *Hif1α*, the main HIF isoform expressed at RNA level in this cardiomyocyte cell line (data not shown and Figure 6C). *Glut1* expression was induced by hypoxia in control scramble-transfected HL-1 cells but its expression was markedly attenuated in HL-1 cells transfected with siHIF1α (Figure 6B). Similarly, hypoxia-induced *Epo* gene expression was reduced when *Hif1α* was silenced in these cells (Figure 6A). These data indicate that hypoxia-induced *Epo* gene expression is an autonomous VHL/HIF-dependent cardiomyocyte response that occurs shortly after activation of this oxygen-sensing pathway. This response provides a molecular and cellular explanation for the elevated levels of cardiac *Epo* gene expression in Vhl^{floxed}-UBC-Cre-ER^{T2} mice.

Discussion

The oxygen-sensing VHL/HIF dependent pathway plays a central role in cellular adaptation to oxygen fluctuations [27,28]. This role has primarily been explored in mouse models in which HIF is chronically overactivated following tissue-specific *Vhl* inactivation [22,25,29]. Here, we characterize the short-term *in vivo* responses following global inactivation of *Vhl* in the Vhl^{floxed}-

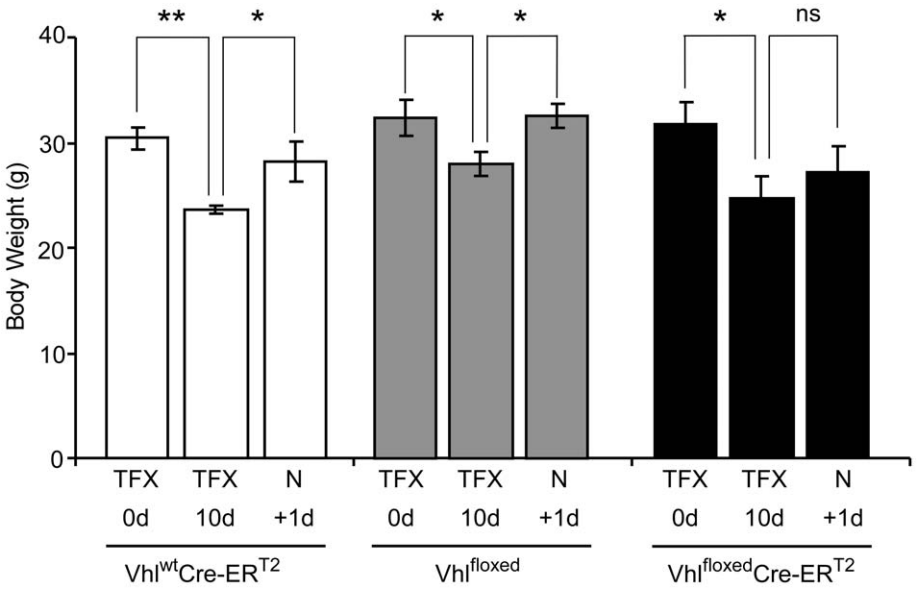

Figure 2. Body weight during and after tamoxifen diet administration in Vhl^{floxed}-UBC-Cre-ER^{T2} and control mice. Body weight of Vhl^{wt}-UBC-Cre-ER^{T2} (n = 3), Vhl^{floxed}-UBC-Cre-ER^{T2} (n = 6) control Vhl^{floxed} (n = 6) mice was measured before tamoxifen treatment (TFX 0d), at the end of 10 days on a tamoxifen diet (TFX 10d) and one day after returning to a normal diet (N +1d). Statistical significance was assessed using a two-tailed Student's t-test, (*, $p<0.05$; **, $p<0.01$; ns, no significant differences).
doi:10.1371/journal.pone.0022589.g002

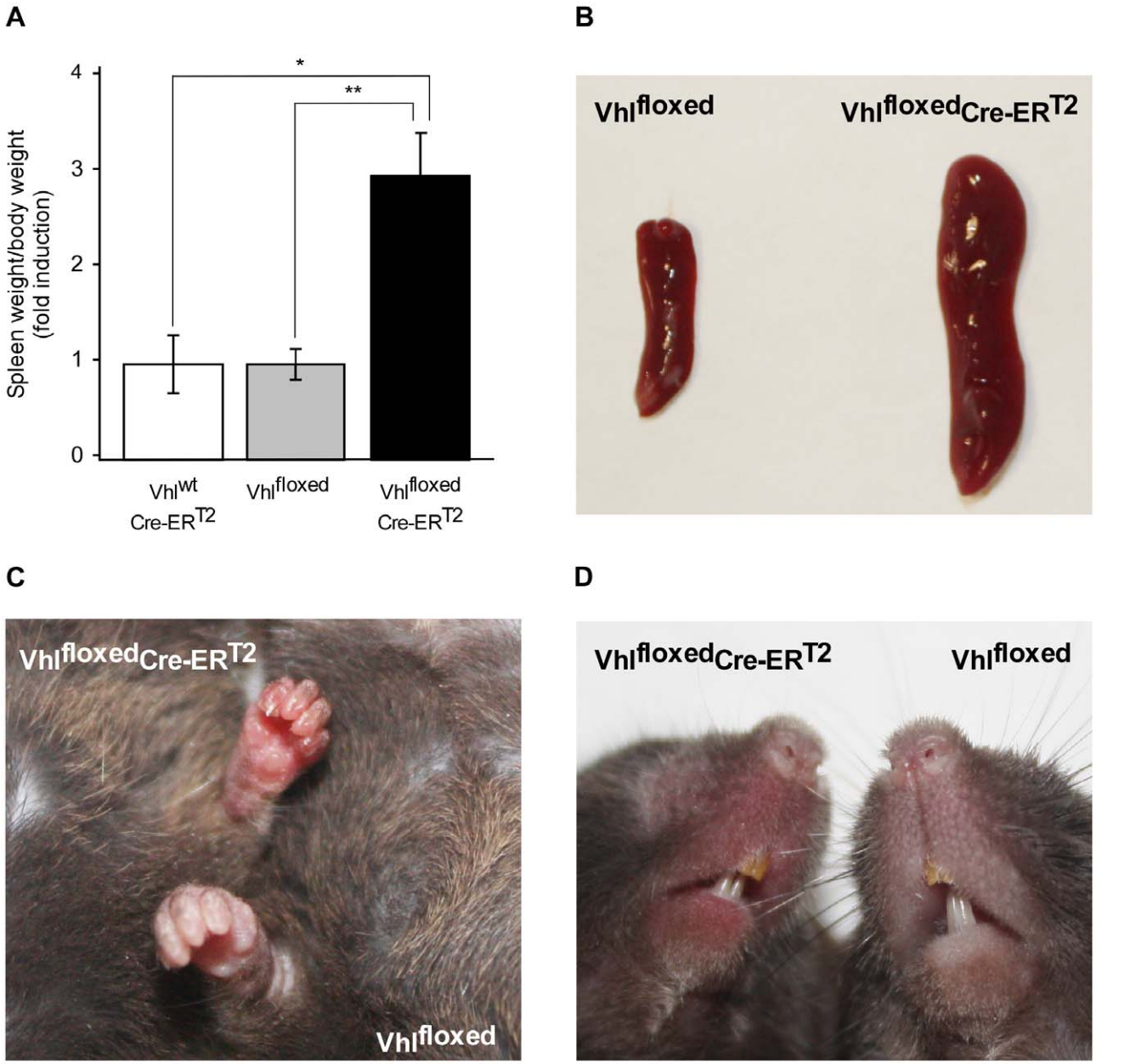

Figure 3. Gross appearance of tamoxifen-fed Vhl^{floxed}-Cre-ERT2 mice. (A) Vhl^{wt}-UBC-Cre-ER^{T2} (n = 3), Vhl^{floxed} (n = 9) and Vhl^{floxed}-UBC-Cre-ER^{T2} (n = 10) mice were administered tamoxifen as indicated in Figure 1 and the spleen/body weight ratio was then determined. Statistical significance was assessed using a two-tailed Student's t-test (*, $p<0.05$; **, $p<0.01$). Representative images of spleens (B), snouts (C) and paws (D) of Vhl^{floxed}-UBC-Cre-ER^{T2} and control Vhl^{floxed} mice are shown.
doi:10.1371/journal.pone.0022589.g003

UBC-Cre-ER^{T2} mouse line. For this purpose, we employed dietary administration of tamoxifen, a timesaving and convenient method of tamoxifen administration to induce Cre-ER^{T2} activity. The full potential for global gene inactivation was not previously explored. Indeed, dietary administration of tamoxifen has been characterized in mice with specific Cre-ER^{T2} expression in the heart, forebrain or in endothelial cells [14,15,16]. However, a comparative analysis of the efficiency of tamoxifen diet in different organs to determine its full potential to induce widespread gene inactivation has not been performed. Moreover, some of these studies have required several weeks on a tamoxifen diet. Here, we describe global gene inactivation in UBC-Cre-ER^{T2} mouse lines shortly (a few days) after tamoxifen administration.

In this first place, it appears that UBC-Cre-ER^{T2} is suitable to produce global gene inactivation in animals fed with a tamoxifen diet. However, tamoxifen-mediated *Vhl* gene inactivation was less pronounced in the Vhl^{floxed}-UBC-Cre-ER^{T2} line than *Hif1α* gene inactivation in Hif1α^{floxed}-UBC-Cre-ER^{T2} line, an effect that could not be attributed to differences in tamoxifen intake. This differential inactivation may reflect the specific efficacy of the Cre-ER^{T2} recombinase to act on the floxed region of the *Vhl* and *Hif1α* alleles. Thus, optimization of the tamoxifen diet may be necessary to achieve comparable effects in distinct UBC-Cre-ER^{T2} mouse lines. Nevertheless, the extent to which *Vhl* gene expression was reduced in these mice was sufficient to induce the activation of oxygen-sensing HIF pathways *in vivo*. Indeed, macroscopic

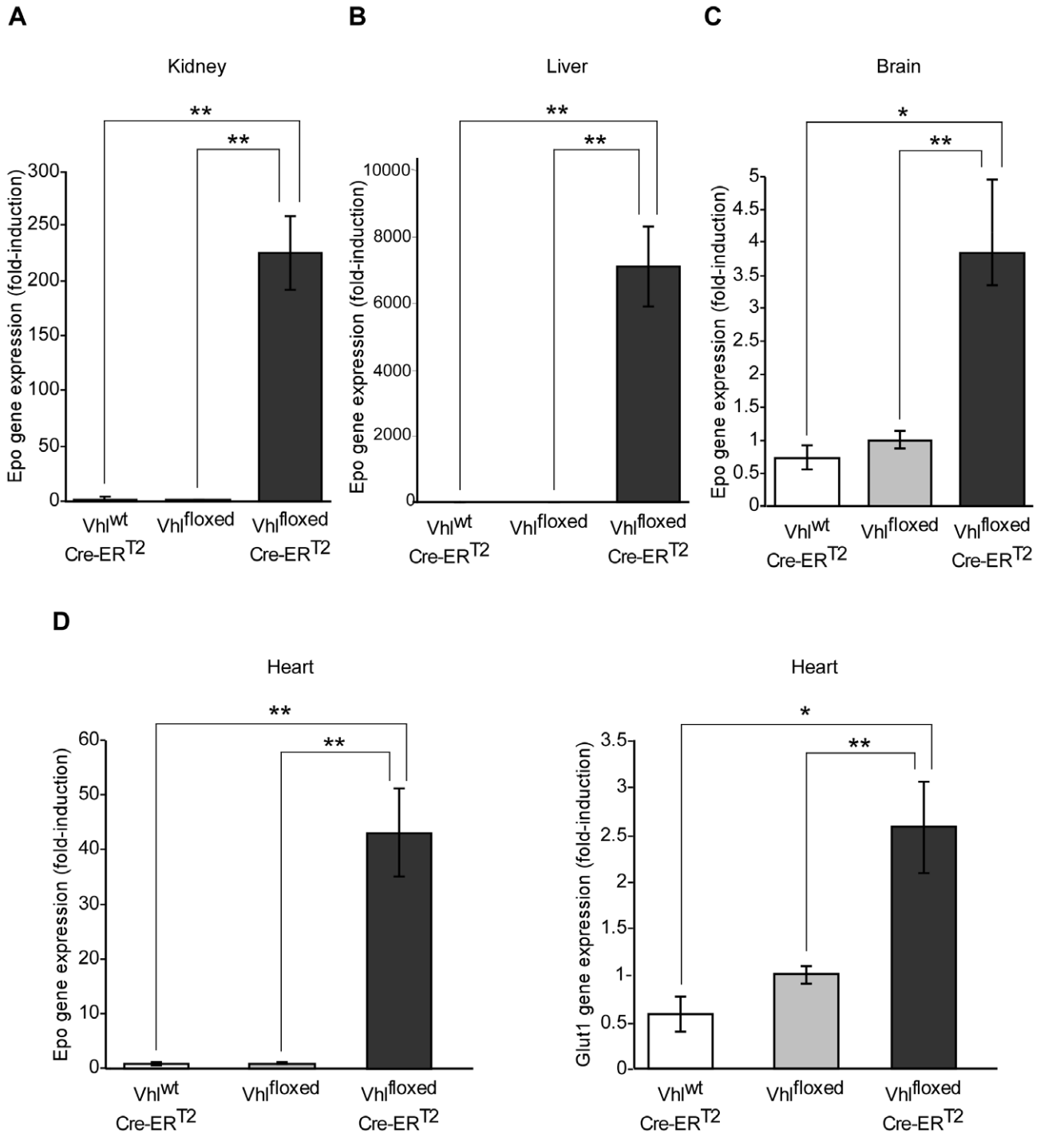

Figure 4. *Erythropoietin* gene expression in the kidney, liver, brain and heart of tamoxifen-fed Vhl^{floxed}-UBC-Cre-ER^{T2} mice. Vhl^{wt}-UBC-Cre-ER^{T2} (n = 3), Vhl^{floxed} (n = 6) and Vhl^{floxed}-UBC-Cre-ER^{T2} (n = 6) mice were administered tamoxifen as indicated in Figure 1. Gene expression was assessed by RT-PCR in the kidney (A), liver (B), brain (C) and heart (D). The expression of *Epo* and *Glut1* was normalized to that of *Hprt* and expressed as the change relative to Vhl^{floxed} mice. Statistical significance was assessed using a two-tailed Student's t-test (*, $p<0.05$; **, $p<0.01$).
doi:10.1371/journal.pone.0022589.g004

examination of tamoxifen-treated Vhl^{floxed}-UBC-Cre-ER^{T2} mice revealed marked splenomegaly, an indicator of increased activity of the oxygen-VHL/PHD/HIF sensing pathway, as seen in *Phd2* deficient and *Phd1:Phd3* double knock-out mice [19]. Tamoxifen-treated Vhl^{floxed}-UBC-Cre-ER^{T2} mice also rapidly show signs of skin erythema (Figure 3). Indeed, reddening of the paws and snouts can be apparent as early as the ninth day of tamoxifen administration (data not shown). This could reflect an increased blood flow to the skin as a consequence of local HIF-induced nitric oxide (NO) release and subsequent local vasodilatation as has been previously shown upon chronic epidermal *Vhl* deletion [30]. Boutin et al. also show that this increased cutaneous perfusion, as a consequence of epidermal *Vhl* gene inactivation, subsequently reduces liver/skin blood flow ratio leading to elevated hepatic *Epo*

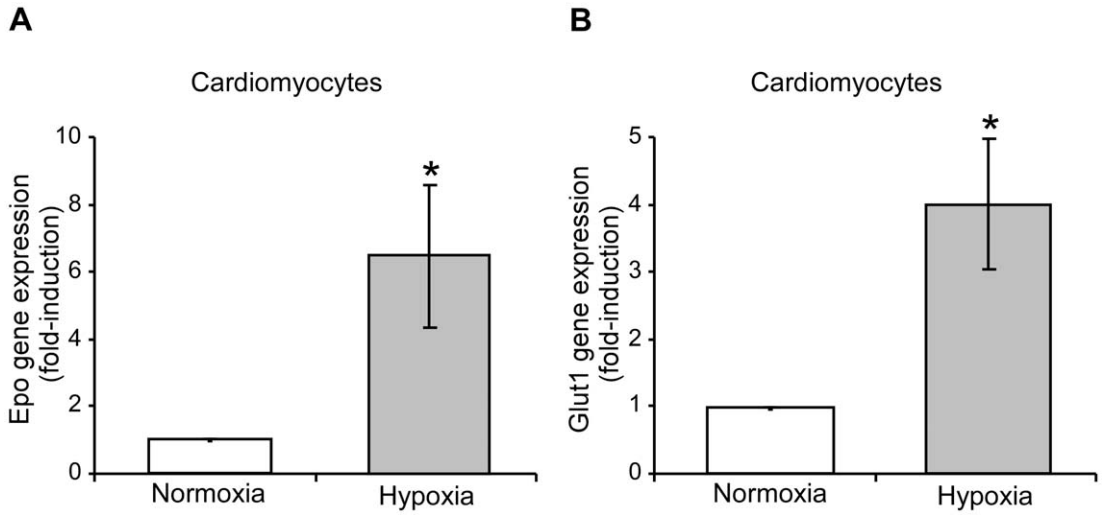

Figure 5. *Erythropoietin* and *glucose transporter-1* gene expression in isolated primary cardiomyocytes in response to hypoxia. Isolated rat cardiomyocyte cultures were subjected to basal normoxic conditions and/or hypoxia (1% O_2) for 24 hours. *Epo* (A) and *Glut1* (B) expression was then analyzed by RT-PCR and normalized to that of *Hprt*. The data from four independent experiments are expressed as the change relative to the normoxic values. Statistical significance was assessed using a two-tailed paired t-test (*, $p<0.05$).
doi:10.1371/journal.pone.0022589.g005

gene expression [30]. However, the increased hepatic *Epo* gene expression observed in tamoxifen-treated Vhl^{floxed}UBC-Cre-ER^{T2} mice is most likely a consequence of local *Vhl* gene deletion and HIF2α activation in liver.

It should be noted that other similar genetic systems have been developed to achieve inactivation of floxed alleles. Indeed, the tetracycline-dependent (Tet) system has been used for renal-specific Cre expression and subsequent inactivation of the tuberous sclerosis complex-1 (Tsc-1) when doxycycline is administered in the drinking water [31]. However, some difficulties in activating this doxycycline-dependent system in certain tissues have been reported [32,33,34]. By contrast, gene expression is significantly reduced in all the tissues analyzed from both Vhl^{floxed}-UBC-Cre-ER^{T2} and $Hif1\alpha^{floxed}$-UBC-Cre-ER^{T2} mouse lines exposed to tamoxifen diet.

Tamoxifen-treated Vhl^{floxed}-UBC-Cre-ER^{T2} mice have identified the heart as an additional site of EPO production upon *Vhl* inactivation. Indeed, the baseline expression of the *Epo* gene in the heart is weak but is elevated dramatically upon inactivation of *Vhl* gene expression. Experiments on isolated neonatal rat cardiomy-

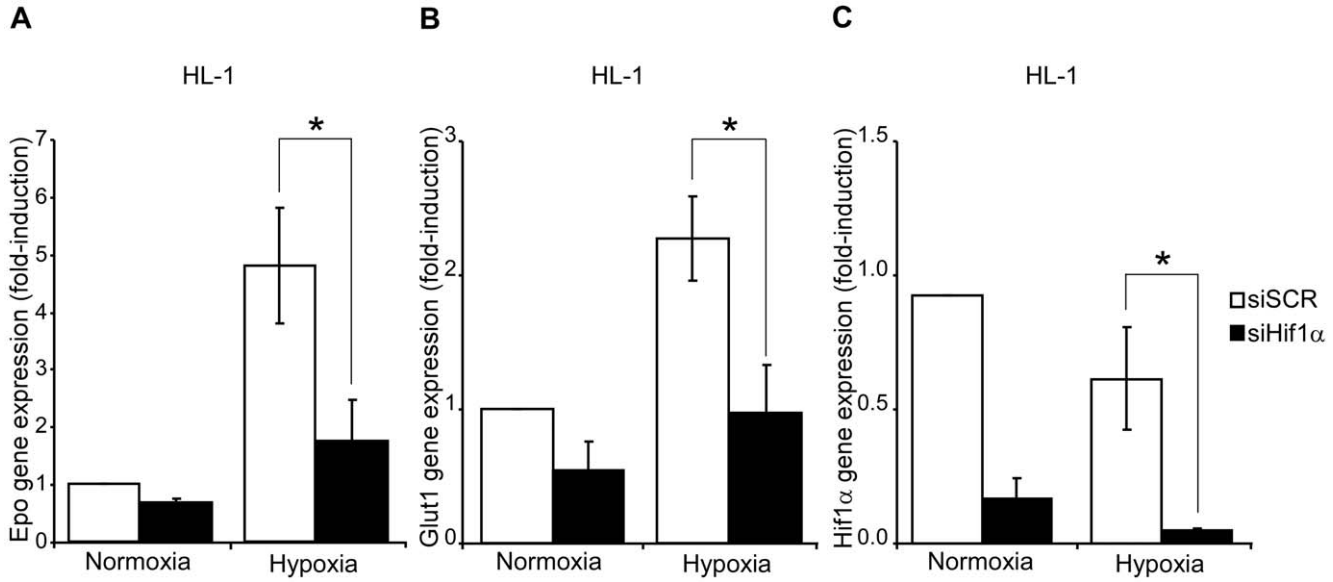

Figure 6. *Erythropoietin* and *glucose transporter-1* gene expression in HL-1 cardiomyocyte cell line in response to activation of the oxygen-sensing HIF pathway. (A,B,C) HL-1 cells were transfected with a siRNA for *Hif1α* (siHIF1α) or a scrambled siRNA control (siSCR) and 24 hours after transfection, the cells were exposed to normoxic or hypoxic (1% O_2) conditions. The expression of *Epo*, *Glut1* and *Hif1α* was measured as described above and the data from three independent experiments are expressed as the change relative to the normoxic values. Statistical significance was assessed using a two-tailed Student's t-test (*, $p<0.05$).
doi:10.1371/journal.pone.0022589.g006

ocytes revealed that EPO upregulation is an autonomous cardiomyocyte response to hypoxia that is mediated by the oxygen-sensing VHL/HIF pathway. This response is also observed in the HL-1 cardiac cell line, an experimental model suitable to study EPO production in adult cardiac cells. HL-1 is a cardiac cell line derived from the AT-1 adult mouse atrial cardiomyocyte tumor lineage, and these cells retain a differentiated cardiac myocyte phenotype and they maintain contractile activity [26]. Moreover, erythropoietin production has been demonstrated after myocardial infarction [35], which on the basis of our data could be mediated by cardiac HIF activation.

HIF1α gene expression is higher than HIF2α in HL-1 cells, which may explain the predominant contribution of HIF1α to hypoxia-induced *Epo* gene expression in these cardiac cells. However, the relative contribution of each isoform may differ *in vivo* and indeed, immunohistological studies have identified both HIF1α and HIF2α in cardiomyocytes of mice subjected to ischemia or atmospheric hypoxia [36,37,38,39,40]. Hif1α^{floxed} mice expressing Cre driven by myosin light chain 2v (MLC2v) cardiac promoter (Hif1α^{floxed}-MLC2v-Cre mice) markedly reduced HIF1α mRNA and protein expression in the heart, providing genetic evidence of *Hif1α* gene expression in cardiomyocytes [36]. Several studies have demonstrated a critical role for HIF1α in multiple cardiac oxygen-sensing pathways *in vivo* [29,36,41]. Thus, HIF1α could potentially drive cardiac *Epo* gene expression upon *Vhl* gene inactivation. However, HIF2α is the main contributor to HIF-induced *Epo* gene expression upon *Vhl* gene inactivation in the kidney, liver and glial cells [22,25,42,43]. Further studies will therefore be required to assess the relative contribution of these isoforms *in vivo*, and especially that of HIF2α to VHL/HIF-dependent cardiac EPO expression. It should be also noted that HIF1α and HIF2α are also found in cardiac stromal cells. Indeed, cardiac endothelial cells abundantly express both HIF isoforms when oxygen supply to myocardium becomes limited, as do cells in the vessel wall that are presumably smooth muscle cells, [36,37,38,39,40]. Therefore, cardiac *Epo* gene expression upon *Vhl* gene inactivation involves HIF activation in cardiomyocytes, although we cannot rule out the involvement of HIF activation in other cardiac cell types.

Elevation of cardiac *Epo* gene expression is very remarkable, although it occurs to a lesser extent than in the liver and kidney. Therefore, it is conceivable that cardiac EPO production serves a local autocrine or paracrine function when oxygen supply to cardiac tissue becomes limited. Indeed, several studies have shown that EPO protects cardiac tissue during ischemia and the ischemia-reperfusion insult, particularly by overactivating the serine threonine kinase AKT, as well as through other pathways involving sonic hedgehog [44,45,46]. Indeed, the myocardium of patients undergoing bypass is protected when pyruvate, a previously recognized suppressor of PHD activity, is used [47], which correlates with a remarkable upregulation of *Epo* gene expression [48]. However, the effect of pyruvate on *Epo* gene expression was not directly assessed in cardiac cells, nor was the direct contribution of HIF activity, as we have studied in this work. Furthermore, cardiac tolerance to ischemic damage induced by ischemic preconditioning in the heart involves HIF1α mediated upregulation of key cardioprotective molecules, such as ecto-5′-nucleotidase CD73 that generates adenosine, and the A2B adenosine receptor (A2BAR) [49]. Therefore, the cardiac oxygen-sensing VHL/HIF/EPO pathway may represent an endogenous cardioprotective response that works in tandem with other pathways (e.g. adenosine) to locally induce cardiomyocyte tolerance against ischemia or ischemia-reperfusion damage.

Materials and Methods

Ethics Statement

All the experimental procedures were approved by the Research Ethics Committee at the UAM (Autonomous University of Madrid) and they were carried out under the supervision of the Head of Animal Welfare and Health at the UAM in accordance with Spanish and European guidelines (B.O.E, 18 March 1988, and 86/609/EEC European Council Directives).

Cell culture and hypoxic conditions

The murine HL-1 cardiac cell line was cultured in Claycomb medium [26] containing 10% heat-inactivated Fetal Bovine Serum (FBS: Cambrex) and supplemented with 0.1 mM norepinephrine (Sigma) and 2 mM GLUTAMAX-I (Invitrogen). Cells were plated on gelatin (Difco) and fibronectin (Sigma) precoated surfaces, and cultured at 37°C for 16 hours. Neonatal rat cardiomyocytes were isolated from the hearts of 1 day-old Wistar rats using the Neomyt isolation system (Cellutron Life Technologies). To remove contaminating cardiac fibroblasts, dissociated cells were pre-plated for 1 hour on uncoated culture plates. The resulting suspension of cardiomyocytes was plated (2–3 million cells/60 mm plate) and cultured for 24 hours in medium supplemented with 10% FBS and 10 mM 5-bromo-2′-deoxyuridine (BrdU; Sigma, B5002), and then for an additional 24 hours in serum-free conditions. The cells were subjected to hypoxia in DMEM + 10% FBS. All media were supplemented with 100 U/ml penicillin, 100 µg/ml streptomycin and 1% HEPES buffer. Normoxic cells (21% O_2) were maintained at 37°C in an incubator with 5% CO_2. To induce hypoxia, cell culture dishes were placed into an Invivo$_2$ 400 humidified hypoxia workstation (Ruskinn Technologies, Bridgend, UK) with 1% O_2.

Mice

C;129S-*Vhlh*^{tm1Jae}/J mice (Jackson Laboratories, stock no. 4081) were used to generate the Vhl^{floxed}-UBC-Cre-ER^{T2} mice. These mice harbor two loxP sites flanking the promoter and exon 1 of the murine *Vhl* locus [50]. C;129S-*Vhlh*^{tm1Jae}/J mice were crossed with B6.Cg-Tg(UBC-Cre/ER^{T2})1Ejb/J mice (Jackson Laboratories, stock no. 008085) which ubiquitously express a tamoxifen-inducible Cre recombinase (Cre-ER^{T2}), [13]. Vhl^{floxed}-UBC-Cre-ER^{T2} mice were generated through the appropriate crosses, along with the corresponding controls, Vhl^{wt}-UBC-Cre-ER^{T2} and Vhl^{floxed}. Hif1α^{floxed}-UBC-Cre-ER^{T2} mice were generated from B6.129-Hif1a^{tm3Rsjo}/J mice (Jackson Laboratories, stock no. 007561), which harbor two loxP sites flanking exon 2 of the murine *Hif1α* locus [51]. These mice were crossed with Tg(UBC-Cre/ER^{T2})1Ejb/J mice as described above to generate Hif1α^{floxed}-UBC-Cre-ER^{T2} mice and their corresponding controls, Hif1α^{wt}-UBC-Cre-ER^{T2} and Hif1α^{floxed} mice.

The mice were bred and housed in a specific pathogen free (SPF) animal area of the animal facility at the Autonomous University of Madrid (UAM). For gene inactivation, Vhl^{wt}-UBC-Cre-ER^{T2}, Hif1α^{wt}-UBC-Cre-ER^{T2} and the corresponding control males (10–5 weeks old) were fed *ad libitum* for ten days with Teckland CRD TAM^{400}/CreER tamoxifen pellets (Harlan Teklad), which contain 400 mg tamoxifen citrate/kg. Subsequently, they were returned to a diet of standard mouse chow (Safe®, Augy, France) for an additional 10 days.

Reticulocyte counts and hematocrit measurement

The number of circulating or splenic reticulocytes was determined by counting total blood or splenic cells respectively followed by a flow cytometry analysis to determine the proportion of reticulocytes identified as CD71 positive cells (using the anti-

CD71-PE, Beckton-Dickinson) and low intracellular nucleic acid content (using the DNA dye Hoechst 33342) [52]. Similarly, splenic mature erythrocytes were identified as CD71 negative and Hoechst 33342 negative cells [52]. Hematocrit measurements were performed using a hemocytometer (apparatus SYSMEX KX-21N).

Quantitative real-time PCR analysis and primers

Mice were anaesthetized by intraperitoneal administration of ketamine (Ketolar® 50 mg/ml) and xylazine (Rompun® 20 mg/ml), and the tissues of interest were then removed and snap-frozen in liquid nitrogen. Subsequently, the tissue was homogenized in Trizol (Invitrogen) with two freeze/thaw cycles and total RNA was isolated using the RNeasy RNA extraction kit (Qiagen). cDNA was prepared by reverse transcription of RNA (1 μg) using Improm-II reverse transcriptase (Promega), and polymerase chain reaction (PCR) amplification was performed using a Power SYBR Green PCR Master Mix kit (Applied Biosystems). The following primer sets were used: mouse VHL (forward, 5′-TCAGCCCTACCCGATCTTACC-3′; reverse, 5′-ATCCCTGAAGAGCCAAAGATGA-3′); mouse HIF-1α (forward, 5′-CACCGATTCGCCATGGA-3′; reverse, 5′-TCGACGTTCAGAACTCATCTTTTTT-3′); rat HIF-1α (forward, 5′-GTCCTGTGGTGACTTGTCCTT-3′; reverse, 5′-TGGACTC TGATCATCTGACCAAA-3′); mouse erythropoietin (EPO) (forward, 5′-TCATCTGCGACAGTCGAGTTCT-3′; reverse, 5′-TTTTCACTCAGTCTGGGACCTTCT-3′); rat erythropoietin (EPO) (forward, 5′-CAAGGAGGCAGAAAATGTCACA-3′; reverse, 5′-TTTCCAAGCGTAG AAGTTGACTTTG-3′); mouse glucose transporter 1 (GLUT1) (forward, 5′-CGCAACGAGGAGAACC-3′; reverse, 5′-GCCGTG TTGACGATACC-3′); hypoxanthine-guanine phosphoribosyltransferase (HPRT) (forward, 5′-GTTAAGCAGTACAGCCCCAAA-3′; reverse, 5′-AGGGCATATCCAACAAC AAACTT-3′). The data were analyzed using StepOne Software version 2.0 (Applied Biosystems).

siRNA transfection

HL-1 cells were transfected with a siRNA targeting mouse HIF-1α (50 nM, sc-44225: Santa Cruz) or a scrambled control siRNA (sc-37007), using Lipofectamine 2000 (Invitrogen) according to the manufacturer's instructions. 24 hours after transfection the cells were exposed to normoxic or hypoxic conditions for an additional 24 hours.

Statistical analysis

The data are presented as the mean ± SEM. Statistical significance was assessed using a two-tailed Student's t-test in all figures, except in Figures 6A and B in which a two-tailed paired t-test was used.

Acknowledgments

The authors would like to thank Dr. L. del Peso, Dr. M.J. Calzada and Victoria Rodriguez for critical reading of the manuscript. The HL-1 cardiomyocyte cell line was kindly provided by Dr. Wiliam C. Claycomb (LSU Health Science Center, New Orleans, LA, USA).

Author Contributions

Conceived and designed the experiments: MM-M AE IS-A LA-A JA. Performed the experiments: MM-M AE IS-A LA-A AV-V SV. Analyzed the data: MM-M AE IS-A MOL JA. Contributed reagents/materials/analysis tools: AO EB AV-V SV EF CF-C. Wrote the paper: MM-M AE IS-A LA-A MOL JA.

References

1. Giaccia A, Siim BG, Johnson RS (2003) HIF-1 as a target for drug development. Nat Rev Drug Discov 2: 803–811.
2. Ivan M, Kondo K, Yang H, Kim W, Valiando J, et al. (2001) HIFalpha targeted for VHL-mediated destruction by proline hydroxylation: implications for O2 sensing. Science 292: 464–468.
3. Jaakkola P, Mole DR, Tian YM, Wilson MI, Gielbert J, et al. (2001) Targeting of HIF-alpha to the von Hippel-Lindau ubiquitylation complex by O2-regulated prolyl hydroxylation. Science 292: 468–472.
4. Bruick RK, McKnight SL (2001) A conserved family of prolyl-4-hydroxylases that modify HIF. Science 294: 1337–1340.
5. Epstein AC, Gleadle JM, McNeill LA, Hewitson KS, O'Rourke J, et al. (2001) C. elegans EGL-9 and mammalian homologs define a family of dioxygenases that regulate HIF by prolyl hydroxylation. Cell 107: 43–54.
6. Semenza GL (2007) Hypoxia-inducible factor 1 (HIF-1) pathway. Sci STKE 2007: cm8.
7. Eckardt KU, Kurtz A (2005) Regulation of erythropoietin production. Eur J Clin Invest 35(Suppl 3): 13–19.
8. Fandrey J, Bunn HF (1993) In vivo and in vitro regulation of erythropoietin mRNA: measurement by competitive polymerase chain reaction. Blood 81: 617–623.
9. Goldberg MA, Imagawa S, Strair RK, Bunn HF (1991) Regulation of the erythropoietin gene in Hep 3B cells. Semin Hematol 28: 35–40; discussion 40-31: .
10. Imagawa S, Goldberg MA, Bunn HF (1989) Regulation of the erythropoietin gene. Adv Exp Med Biol 271: 75–85.
11. Gnarra JR, Ward JM, Porter FD, Wagner JR, Devor DE, et al. (1997) Defective placental vasculogenesis causes embryonic lethality in VHL-deficient mice. Proc Natl Acad Sci U S A 94: 9102–9107.
12. Feil R, Wagner J, Metzger D, Chambon P (1997) Regulation of Cre recombinase activity by mutated estrogen receptor ligand-binding domains. Biochem Biophys Res Commun 237: 752–757.
13. Ruzankina Y, Pinzon-Guzman C, Asare A, Ong T, Pontano L, et al. (2007) Deletion of the developmentally essential gene ATR in adult mice leads to age-related phenotypes and stem cell loss. Cell Stem Cell 1: 113–126.
14. Casanova E, Fehsenfeld S, Lemberger T, Shimshek DR, Sprengel R, et al. (2002) ER-based double iCre fusion protein allows partial recombination in forebrain. Genesis 34: 208–214.
15. Forde A, Constien R, Grone HJ, Hammerling G, Arnold B (2002) Temporal Cre-mediated recombination exclusively in endothelial cells using Tie2 regulatory elements. Genesis 33: 191–197.
16. Kiermayer C, Conrad M, Schneider M, Schmidt J, Brielmeier M (2007) Optimization of spatiotemporal gene inactivation in mouse heart by oral application of tamoxifen citrate. Genesis 45: 11–16.
17. Ma W, Tessarollo L, Hong SB, Baba M, Southon E, et al. (2003) Hepatic vascular tumors, angiectasis in multiple organs, and impaired spermatogenesis in mice with conditional inactivation of the VHL gene. Cancer Res 63: 5320–5328.
18. Young AP, Schlisio S, Minamishima YA, Zhang Q, Li L, et al. (2008) VHL loss actuates a HIF-independent senescence programme mediated by Rb and p400. Nat Cell Biol 10: 361–369.
19. Takeda K, Aguila HL, Parikh NS, Li X, Lamothe K, et al. (2008) Regulation of adult erythropoiesis by prolyl hydroxylase domain proteins. Blood 111: 3229–3235.
20. Heinicke K, Baum O, Ogunshola OO, Vogel J, Stallmach T, et al. (2006) Excessive erythrocytosis in adult mice overexpressing erythropoietin leads to hepatic, renal, neuronal, and muscular degeneration. Am J Physiol Regul Integr Comp Physiol 291: R947–956.
21. Vogel J, Kiessling I, Heinicke K, Stallmach T, Ossent P, et al. (2003) Transgenic mice overexpressing erythropoietin adapt to excessive erythrocytosis by regulating blood viscosity. Blood 102: 2278–2284.
22. Rankin EB, Biju MP, Liu Q, Unger TL, Rha J, et al. (2007) Hypoxia-inducible factor-2 (HIF-2) regulates hepatic erythropoietin in vivo. J Clin Invest 117: 1068–1077.
23. Zanjani ED, Ascensao JL, McGlave PB, Banisadre M, Ash RC (1981) Studies on the liver to kidney switch of erythropoietin production. J Clin Invest 67: 1183–1188.
24. Chen C, Pore N, Behrooz A, Ismail-Beigi F, Maity A (2001) Regulation of glut1 mRNA by hypoxia-inducible factor-1. Interaction between H-ras and hypoxia. J Biol Chem 276: 9519–9525.
25. Weidemann A, Kerdiles YM, Knaup KX, Rafie CA, Boutin AT, et al. (2009) The glial cell response is an essential component of hypoxia-induced erythropoiesis in mice. J Clin Invest 119: 3373–3383.
26. White SM, Constantin PE, Claycomb WC (2004) Cardiac physiology at the cellular level: use of cultured HL-1 cardiomyocytes for studies of cardiac muscle cell structure and function. Am J Physiol Heart Circ Physiol 286: H823–829.

27. Mole DR, Ratcliffe PJ (2008) Cellular oxygen sensing in health and disease. Pediatr Nephrol 23: 681–694.
28. Semenza GL (2002) Involvement of hypoxia-inducible factor 1 in human cancer. Intern Med 41: 79–83.
29. Lei L, Mason S, Liu D, Huang Y, Marks C, et al. (2008) Hypoxia-inducible factor-dependent degeneration, failure, and malignant transformation of the heart in the absence of the von Hippel-Lindau protein. Mol Cell Biol 28: 3790–3803.
30. Boutin AT, Weidemann A, Fu Z, Mesropian L, Gradin K, et al. (2008) Epidermal sensing of oxygen is essential for systemic hypoxic response. Cell 133: 223–234.
31. Traykova-Brauch M, Schonig K, Greiner O, Miloud T, Jauch A, et al. (2008) An efficient and versatile system for acute and chronic modulation of renal tubular function in transgenic mice. Nat Med 14: 979–984.
32. Hochedlinger K, Yamada Y, Beard C, Jaenisch R (2005) Ectopic expression of Oct-4 blocks progenitor-cell differentiation and causes dysplasia in epithelial tissues. Cell 121: 465–477.
33. Hsiao EC, Nguyen TD, Ng JK, Scott MJ, Chang WC, et al. (2011) Constitutive Gs activation using a single-construct tetracycline-inducible expression system in embryonic stem cells and mice. Stem Cell Res Ther 2: 11.
34. Katsantoni EZ, Anghelescu NE, Rottier R, Moerland M, Antoniou M, et al. (2007) Ubiquitous expression of the rtTA2S-M2 inducible system in transgenic mice driven by the human hnRNPA2B1/CBX3 CpG island. BMC Dev Biol 7: 108.
35. Mengozzi M, Latini R, Salio M, Sfacteria A, Piedimonte G, et al. (2006) Increased erythropoietin production after myocardial infarction in mice. Heart 92: 838–839.
36. Huang Y, Hickey RP, Yeh JL, Liu D, Dadak A, et al. (2004) Cardiac myocyte-specific HIF-1alpha deletion alters vascularization, energy availability, calcium flux, and contractility in the normoxic heart. Faseb J 18: 1138–1140.
37. Jurgensen JS, Rosenberger C, Wiesener MS, Warnecke C, Horstrup JH, et al. (2004) Persistent induction of HIF-1alpha and -2alpha in cardiomyocytes and stromal cells of ischemic myocardium. Faseb J 18: 1415–1417.
38. Kim CH, Cho YS, Chun YS, Park JW, Kim MS (2002) Early expression of myocardial HIF-1alpha in response to mechanical stresses: regulation by stretch-activated channels and the phosphatidylinositol 3-kinase signaling pathway. Circ Res 90: E25–33.
39. Stroka DM, Burkhardt T, Desbaillets I, Wenger RH, Neil DA, et al. (2001) HIF-1 is expressed in normoxic tissue and displays an organ-specific regulation under systemic hypoxia. Faseb J 15: 2445–2453.
40. Wiesener MS, Jurgensen JS, Rosenberger C, Scholze CK, Horstrup JH, et al. (2003) Widespread hypoxia-inducible expression of HIF-2alpha in distinct cell populations of different organs. Faseb J 17: 271–273.
41. Cai Z, Zhong H, Bosch-Marce M, Fox-Talbot K, Wang L, et al. (2008) Complete loss of ischaemic preconditioning-induced cardioprotection in mice with partial deficiency of HIF-1 alpha. Cardiovasc Res 77: 463–470.
42. Kapitsinou PP, Liu Q, Unger TL, Rha J, Davidoff O, et al. (2010) Hepatic HIF-2 regulates erythropoietic responses to hypoxia in renal anemia. Blood 116: 3039–3048.
43. Warnecke C, Zaborowska Z, Kurreck J, Erdmann VA, Frei U, et al. (2004) Differentiating the functional role of hypoxia-inducible factor (HIF)-1alpha and HIF-2alpha (EPAS-1) by the use of RNA interference: erythropoietin is a HIF-2alpha target gene in Hep3B and Kelly cells. Faseb J 18: 1462–1464.
44. Camici GG, Stallmach T, Hermann M, Hassink R, Doevendans P, et al. (2007) Constitutively overexpressed erythropoietin reduces infarct size in a mouse model of permanent coronary artery ligation. Methods Enzymol 435: 147–155.
45. Burger D, Xenocostas A, Feng QP (2009) Molecular basis of cardioprotection by erythropoietin. Curr Mol Pharmacol 2: 56–69.
46. Ueda K, Takano H, Niitsuma Y, Hasegawa H, Uchiyama R, et al. (2010) Sonic hedgehog is a critical mediator of erythropoietin-induced cardiac protection in mice. J Clin Invest 120: 2016–2029.
47. Lu H, Dalgard CL, Mohyeldin A, McFate T, Tait AS, et al. (2005) Reversible inactivation of HIF-1 prolyl hydroxylases allows cell metabolism to control basal HIF-1. J Biol Chem 280: 41928–41939.
48. Ryou MG, Flaherty DC, Hoxha B, Sun J, Gurji H, et al. (2009) Pyruvate-fortified cardioplegia evokes myocardial erythropoietin signaling in swine undergoing cardiopulmonary bypass. Am J Physiol Heart Circ Physiol 297: H1914–1922.
49. Eckle T, Kohler D, Lehmann R, El Kasmi K, Eltzschig HK (2008) Hypoxia-inducible factor-1 is central to cardioprotection: a new paradigm for ischemic preconditioning. Circulation 118: 166–175.
50. Haase VH, Glickman JN, Socolovsky M, Jaenisch R (2001) Vascular tumors in livers with targeted inactivation of the von Hippel-Lindau tumor suppressor. Proc Natl Acad Sci U S A 98: 1583–1588.
51. Ryan HE, Lo J, Johnson RS (1998) HIF-1 alpha is required for solid tumor formation and embryonic vascularization. Embo J 17: 3005–3015.
52. Chen SY, Wang Y, Telen MJ, Chi JT (2008) The genomic analysis of erythrocyte microRNA expression in sickle cell diseases. PLoS One 3: e2360.

Manuscrito 4

Assembly of respiratory supercomplexes determines electron flux in the mitochondrial electron transport chain.

Cell (under revision).

Siguiendo en la línea de investigación de cómo se regula la cadena de transporte de electrones surge el siguiente articulo en que he ayudado en algunos experimentos.

Se han propuesto dos modelos para explicar como se organiza la cadena de transporte de electrones. El modelo fluido, que se basa en la libre difusión de los complejos por la membrana interna y sus colisiones con los transportadores, coenzima Q y citocromo C. El segundo, el modelo sólido propone que los complejos se encuentran físicamente unidos formando unas supraestructuras denominadas supercomplejos. Nuestro grupo ha sugerido un tercer modelo que hemos nombrado; modelo plástico, el cual adapta tanto al modelo fluido como al solido, siendo estos casos extremos del modelo fluido.

Proponemos que los supercomplejos son entes dinámicas que pueden ensamblarse y desensamblarse dependiendo de los requerimientos celulares. En este articulo demostramos como el ensamblaje diferencial de los complejos I/III y III/IV marca la existencia de dos fondos comunes de coenzima Q y definimos a Cox7a2l como un factor de ensamblaje de supercomplejos.

Elsevier Editorial System(tm) for Cell
Manuscript Draft

Manuscript Number: CELL-D-12-01002

Title: Assembly of respiratory supercomplexes determines electron flux in the mitochondrial electron transport chain

Article Type: Research Article

Keywords: mouse; mitochondria; Respiratory Supercomplexes; Mitochondrial Electron transport chain; plasticity model; OXPHOS

Corresponding Author: Dr. Jose A. Enriquez,

Corresponding Author's Institution: Fundacion Centro Nacional de Investigaciones Cardiovasculares CNIC

First Author: Esther Lapuente-Brun

Order of Authors: Esther Lapuente-Brun; Raquel Moreno-Loshuertos; Rebeca Acín-Pérez; Ana Latorre-Pellicer; Carmen Colás; Eduardo Balsa; Ester Perales-Clemente; Pedro M Quiros; Enrique Calvo; M. A Rodríguez-Hernández; Plácido Navas; Raquel Cruz; Ángel Carracedo; Carlos López-Otín; Acisclo Pérez-Martos; Patricio Fernández-Silva; Erika Fernández-Vizarra; Jose A. Enriquez

Abstract: Two models have been proposed for the structural organization of the mitochondrial respiratory chain: The fluid model views respiratory complexes as free-moving separate entities in the mitochondrial inner membrane, with the mobile carriers CoQ and cyt c transferring electrons between them; the solid model proposes that all respiratory chain components except for complex II assemble in a superstructure, the respirasome, and work as a unit. We recently proposed the plasticity model, in which the fluid and solid options are extreme forms. We propose that respiratory complexes associate in dynamic entities (supercomplexes) that can assemble in distinct combinations depending on cell requirements. Here, we demonstrate the role of assembly between complexes I /III and III/IV, define the existence of two CoQ pools, and identify Cox7a2l as a mammalian supercomplex assembly factor. These findings experimentally demonstrate the plasticity model.

Suggested Reviewers: Eric Shoudbridge
Department of Molecular Neurogenetics, McGill University/MNI
eric@ericpc.mni.mcgill.ca
Expert in OXPHOS

Anu Suomalainen-Wartiovaara
University of Helsinki
anu.wartiovaara@helsinki.fi

Giorgio Lenaz
University of Bologna
giorgio.lenaz@unibo.it

Opposed Reviewers: Cristina Ugalde

Hospital 12 de Octubre Madrid
cugalde@h12o.es

MINISTERIO DE CIENCIA E INNOVACIÓN
Instituto de Salud Carlos III
cnic

Professor Dr. José Antonio Enríquez
Regenerative Cardiology Department
Fundación Centro Nacional de Investigaciones Cardiovasculares Carlos III (CNIC)
C/ Melchor Fernández Almagro, 3
28029 Madrid, Spain
Tel.: + 34 914531274
Fax: + 34 914531240

May 22, 2012

Dear Faviola,

Following your indications we are submitting a single manuscript that merges the two manuscripts (CELL-D-12-00643; CELL-D-12-00641) that we submitted some weeks ago for consideration to **Cell**.

The merged manuscript, by Lapuente-Brun, *et al.*, is entitled "*Assembly of respiratory supercomplexes determines electron flux in the mitochondrial electron transport chain*".

The study links structure and function in a new paradigm for the organization of the mitochondrial electron transport chain in mammalian cells.

Over the last twelve years, a dispute has broken the consensus view, presented in the textbooks, of how the mitochondrial electron transport chain is organized in the inner mitochondrial membrane. On one side, the classical **fluid model** proposes that respiratory complexes are individual entities freely moving in the mitochondrial inner membrane, with electrons transferred between them by mobile carriers (CoQ and cyt b). On the other side, the defenders of the **solid model** have proposed that all components of the respiratory chain except for complex II are assembled in a superstructure called the respirasome and work as a single entity. The lack of definitive evidence has fed continued controversy in the debate, leaving the two positions apparently irreconcilable. In 2008, we proposed, in an article in *Molecular Cell*, the **plasticity model** as an inclusive model in which the fluid and solid proposals are extreme forms.

In the current article we present experimental evidence that confirms the plasticity model. Our principal findings are as follows:

1) Definitive genetic evidence demonstrates the physiological existence of respiratory supercomplexes in mammalian mitochondria.
2) Free and assembled complexes coexist (although complex I is generally super-assembled with other complexes).
3) Animals lacking the respirasome are healthy and fertile.
4) Complex III is organized into four structural populations, including associations with other complexes and free dimer complex, and into two functional fractions that define distinct CoQ pools, one dedicated to receiving electrons from NADH and the other to receiving electrons from FAD.
5) Complex IV is organized structurally and functionally into three populations that partner with other complexes or exist independently. One population is dedicated to the exclusive transfer of electrons from NADH to oxygen; another is dedicated to the exclusive transfer of electrons from FAD to oxygen; and a third population is able to participate in the transfer of electrons to oxygen from both NADH and FAD.
6) Complex III availability determines the proportional flux of electrons from NADH and FAD, with complex I preferentially associating with complex III.

MINISTERIO
DE CIENCIA
E INNOVACIÓN
Instituto
de Salud
Carlos III
cnic

Professor Dr. José Antonio Enríquez
Regenerative Cardiology Department
Fundación Centro Nacional de Investigaciones
Cardiovasculares Carlos III (CNIC)
C/ Melchor Fernández Almagro, 3
28029 Madrid, Spain
Tel.: + 34 914531274
Fax: + 34 914531240

7) Cox7a2l, for which we propose the new name supercomplex assembly factor I (SCAFI), is an assembly factor that determines the interaction between complexes III and IV in the respirasome (I+III+IV) or as III+IV. Definition of the three structural and functional CIV populations by SCAFI optimizes the use of combinations of substrates with differing requirements for NADH or FAD, preventing any one substrate from saturating the electron flux.

These structural and functional options determine the use of the mitochondrial electron transport chain in fasting and non-fasting settings. The relative proportions of the different supercomplexes is modified during fasting so that when more flux from FAD is required, complex I is degraded and complex III released for use by FAD dependent enzymes.

Our analysis establishes a new paradigm for the structural and functional organization of the mitochondrial electron transport chain and the regulation of bioenergetic metabolism in eukaryotic cells. The observations we describe reformulate our picture of the function, regulation and homeostasis of energy metabolism in eukaryotic cells, and clearly illustrate how a housekeeping pathway can be intricately fine-tuned for optimal performance.

We thank you in advance for your consideration and look forward to hearing from you soon.

Best regards,

Tonio

Prof. Jose A. Enriquez, Ph.D

Abstract

Two models have been proposed for the structural organization of the mitochondrial respiratory chain: The fluid model views respiratory complexes as free-moving separate entities in the mitochondrial inner membrane, with the mobile carriers CoQ and cyt c transferring electrons between them; the solid model proposes that all respiratory chain components except for complex II assemble in a superstructure, the respirasome, and work as a unit. We recently proposed the plasticity model, in which the fluid and solid options are extreme forms. We propose that respiratory complexes associate in dynamic entities (supercomplexes) that can assemble in distinct combinations depending on cell requirements. Here, we demonstrate the role of assembly between complexes I /III and III/IV, define the existence of two CoQ pools, and identify Cox7a2l as a mammalian supercomplex assembly factor. These findings experimentally demonstrate the plasticity model.

Assembly of respiratory supercomplexes determines electron flux in the mitochondrial electron transport chain

Esther Lapuente-Brun[2†], Raquel Moreno-Loshuertos[2†] Rebeca Acín-Pérez[1], Ana Latorre-Pellicer[1], Carmen Colás[1], Eduardo Balsa[1,3], Ester Perales-Clemente[1], Pedro M. Quirós[5], Enrique Calvo[1], M. A. Rodríguez-Hernández[4], Plácido Navas[4], Raquel Cruz[6], Ángel Carracedo[6], Carlos López-Otín[5], Acisclo Pérez-Martos[2], Patricio Fernández-Silva[2], Erika Fernández-Vizarra[7] and José Antonio Enríquez[1, 2] *

[1] Centro Nacional de Investigaciones Cardiovasculares Carlos III. Melchor Fernández Almagro, 3. 28029 Madrid. Spain

[2] Departamento de Bioquímica y Biología Molecular y Celular. Facultad de Ciencias. Universidad de Zaragoza. Pedro Cerbuna, 12. Zaragoza 50009. Spain

[3] Servicio de Inmunología, Hospital Universitario de La Princesa, Universidad Autónoma de Madrid, Instituto de Investigación Sanitaria Princesa (IIS-IP), Madrid, 28006, Spain.

[4] Centro Andaluz de Biología del Desarrollo, Universidad Pablo de Olavide-CSIC and Centro de Investigación Biomédica en Red de Enfermedades Raras, ISCIII, Sevilla, 41013 SPAIN.

[5]Departamento de Bioquímica y Biología Molecular, Facultad de Medicina, Instituto Universitario de Oncología (IUOPA), Universidad de Oviedo, 33006-Oviedo, Spain

[6] Grupo de Medicina Xenómica, Facultad de Medicina, CIBERER, Universidad de Santiago de Compostela C/ San Francisco s/n 15782 Santiago de Compostela, A Coruña. Spain.

[7] IIS Aragón. Unidad de Investigación Traslacional I+CS. Hospital Universitario Miguel Servet. Paseo Isabel La Católica, 1-3. Zaragoza 50009. Spain

† These authors contributed equally to this work.

* To whom correspondence should be addressed. E-mail: jaenriquez@cnic.es

Tel. +34 914531200. Fax: +34 914531240.

Running title: Functional implications of respiratory supercomplexes

Keywords: mouse/ mitochondria/ Respiratory Supercomplexes/Mitochondrial Electron transport chain

Subject Category: Cellular Metabolism; Molecular Biology of Disease

Summary

Two models have been proposed for the structural organization of the mitochondrial respiratory chain: The fluid model views respiratory complexes as free-moving separate entities in the mitochondrial inner membrane, with the mobile carriers CoQ and cyt c transferring electrons between them; the solid model proposes that all respiratory chain components except for complex II assemble in a superstructure, the respirasome, and work as a unit. We recently proposed the plasticity model, in which the fluid and solid options are extreme forms. We propose that respiratory complexes associate in dynamic entities (supercomplexes) that can assemble in distinct combinations depending on cell requirements. Here, we demonstrate the role of assembly between complexes I /III and III/IV, define the existence of two CoQ pools, and identify Cox7a2l as a mammalian supercomplex assembly factor. These findings experimentally demonstrate the plasticity model.

Highlights

- Mitochondrial Complex III is organized structurally into four groups of molecules and functionally into two fractions.
- Superassembly by complexes I and III defines distinct CoQ pools that receive electrons either from NADH or from FAD
- Complex III availability determines the relative flux of electrons from NADH and FAD
- Cox7a2l is required for the superassembly of complex IV, making it the first-identified mammalian mitochondrial respiratory supercomplex assembly factor.
- Complex IV is organized into three functional subpopulations.
- CIV superassembly prevents saturation of the mt-ETC by NADH or FAD electrons.

Introduction

Over the last twelve years, a debate has unraveled the consensus on how the mitochondrial electron transport chain is organized in the inner mitochondrial membrane. On one side, the classical fluid, or random collision, model proposes that respiratory complexes are individual entities freely moving in the mitochondrial inner membrane, with electrons transferred between them by mobile carriers (CoQ and cyt c) (Hackenbrock et al., 1986). On the other side, the defenders of the solid model propose that all components of the respiratory chain except for complex II are assembled in a superstructure called the respirasome and work as a single entity (Schagger and Pfeiffer, 2000). Several roles have been attributed to the supercomplex organization of the respiratory chain. They have been proposed to stabilize the respiratory complexes, and there is evidence indicating that complex I is stabilized by interaction with complex III or IV (Acin-Perez et al., 2004; Diaz et al., 2006; Vempati et al., 2009). Second, supercomplexes have been suggested to allow substrate channeling in order to increase electron flux; however, evidence for this role is scarce, and it has been questioned on theoretical grounds since it conflicts with the predicted pool behavior of CoQ and cytochrome c (for a review see (Genova et al., 2005; Lenaz and Genova, 2007)). The lack of solid functional and genetic evidence has fed continued controversy regarding the *in vivo* significance of supercomplexes.

We previously demonstrated that the respirasome is functional, being able to transfer electrons from NADH to oxygen (Acin-Perez et al., 2008). We have also proposed the plasticity model to resolve the apparent conflict between the fluid and solid models by incorporating them as extreme forms of a variety of structural associations adopted by respiratory complexes and in which electron flux and proton pumping can operate (Acin-Perez et al., 2008). The plasticity model accommodates observations showing that complex I is rarely found as an independent

entity, and is instead mostly associated with in supercomplexes with complex III. Some of these associations contain CoQ, cyt c, and complex IV, and are able to respire. Two abundant forms of CI/CIII-containing supercomplexes differ in their molecular mass and do not associate with complex IV.

The role of these supercomplexes is still unclear. Most complex III in liver mitochondria is associated with other complexes such as complex I, or forms additional associations such as III/IV. In contrast, although complex IV can associate with other complexes, a large fraction is found unassociated with other respiratory complexes. In all studies to date, the putative occurrence of supercomplexes has been determined by electrophoretic co-migration and stable purification through density gradients (Acin-Perez et al., 2008; Dudkina et al., 2005; Eubel et al., 2004; Schagger and Pfeiffer, 2000). In addition, 3D maps of respiratory supercomplexes have been generated by single-particle electron microscopy analysis (Dudkina et al., 2005; Schafer et al., 2007; Schafer et al., 2006) or single particle cryoelectron tomography (Dudkina et al., 2011). Despite their attractions, the major problem with the solid and plasticity models is the lack of definitive evidence for the existence of respiratory supercomplexes *in vivo*. It is also difficult to propose a role for the diverse types of associations of respiratory complexes revealed by blue-native electrophoresis, and defenders of the solid model consider that all the free complexes and all associations except those containing complexes I, III and IV are artifactual fragments of the disrupted respirasome. There is no experimental support for this conclusion, however, and we reason that since native electrophoresis detects the intact respirasome, and if we therefore assume that this structure occurs *in vivo*, then we should also regard all the other superassemblies and free complexes observed on these gels as biologically relevant entities (Acin-Perez et al., 2008).

The solid model is moreover unable to explain the pool behavior of the mobile carriers (CoQ and cyt C). Coenzyme Q (CoQ, ubiquinone) is required for the transfer of electrons from NADH- or FAD-dependent enzymes to respiratory complex III, while cytochrome c fulfills this role between complexes III and IV. For over 40 years it was generally accepted that CoQ freely diffused through the membrane, forming a single pool available to any enzyme that required it, (reviewed by (Lenaz et al., 2007)). To date there is little evidence that enzymes that feed electrons to CoQ, other than complex I, can form super-assemblies with complex III. We recently demonstrated that complex-I-containing supercomplexes include CoQ and that those containing III and IV include cytochrome c (Acin-Perez et al., 2008). A valid supercomplex model needs to explain the pool-behavior of CoQ, and also, in the case of the plasticity model, to understand the function, if any, of the I/III supercomplex.

Interaction between complexes III and IV has been postulated in all types of eukaryotic cells, from yeast and fungi to plants and animals, even in *S. cervisiae*, which lack complex I (Acin-Perez et al., 2004; Acin-Perez et al., 2008; Eubel et al., 2004; Lenaz et al., 2010; Schagger and Pfeiffer, 2000). Nonetheless, the role of complex III/IV association has not been defined and it is not clear how the components differ functionally from the more abundant free forms. Again, a valid supercomplex model has to accommodate the large number of observations supporting a pool behavior for cyt c in the transfer of electrons between complexes III and IV.

In this report we show that in mammalian cells the physical interaction between complexes I and III defines a specific CoQ pool and a subset of complex III molecules that are dedicated to transfer electrons between NADH and cytochrome c. We also show that a different subset of complex III molecules oxidizes CoQ molecules that receive electrons from complex II or other non-complex I enzymes. By modulating the relative levels of complexes I and III we demonstrate competition between these two CoQ pools for the delivery of electrons to complex

III. In addition, we identify Cox7a2l, for which we propose the new name supercomplex assembly factor I (SCAFI), as a protein required for superassembly of complexes III and IV, providing the first genetic evidence for the regulation of respiratory supercomplex assembly. Our studies further show that SCAFI is not required for cell survival in culture or *in vivo*, since mice expressing (CBA, 129, CD1, NZB) or lacking functional SCAFI (C57BL/6J and Balb/cJ) are healthy and fertile. Supercomplexes appear to allow fine-tuning of the respiratory chain in response to a combination of the respiratory substrate used and of the changing physiological requirements. Our results provide compelling functional and genetic evidence for the existence of physiological CIII+CIV and CI+CIII interactions as well as physiological CI+CIII+CIV and free CIII and CIV, and for modulation of these interactions consistent with the plasticity model.

Results

Complex I preferentially associate with complex III, defining a dedicated CoQ pool. We previously characterized a mouse mitochondrial DNA (mtDNA) mutant cell line (A22; referred to here as mutant or *M* cells) harboring a mutation in the *mt-Cytb* gene that prevents assembly of mitochondrial complex III (Acin-Perez et al., 2004). In the absence of complex III, complex I becomes unstable and is degraded. Here, we induced random suppressor mutations in A22 cells by chemical mutagenesis followed by selection for uridine autotrophy (Bayona-Bafaluy et al., 2008). Using this strategy, we induced an unidentified nuclear mutation that allows assembly of approximately 30% of the normal amount of complex III (details in supplementary material and Fig. S1). We thus had a cell line (suppressor or *S* cells) with stably and significantly reduced expression of complex III, enabling investigation of the consequences for overall respiration performance.

Polarography measurements in digitonized cells showed that the suppressor mutation restored oxygen consumption dependent on complexes I/III/IV to the level found in isogenic

control cells (*C*). Surprisingly, however, complex II/III/IV-dependent oxygen consumption in *S* cells, though restored, remained significantly lower than in controls (p=0.0024) (Fig. 1A). Spectrophotometric analysis of individual OXPHOS complexes in isolated *S* cell mitochondria revealed significantly lower than normal activities of complexes I, III and IV (CI/CS=46.9% of control, p<0.0001; CIII/CS=37.9% of control, p=0.020; CIV/CS=83.0%, p=0.0271), while complex II activity was normal or slightly increased (Fig. 1B). This observation appears to contradict the respiration rates: on the one hand, the maximal amount and activity of complex I were less than half the control values, while complex-I–dependent respiration was normal; on the other hand, maximal complex II activity and amount were normal, while complex-II–dependent respiration was significantly lower than in control cells (Fig. 1A, 1B and S1E).

To investigate electron flux through complex III we used linked spectrophotometric assays to measure the activities of complexes I plus III, II plus III or glycerol-3-phosphate dehydrogenase plus complex III (G3PDH+III). Interestingly, *S* cells showed an increase in the linked activity of complexes I and III (p=0.0252) and a reduction in the activities of the succinate dehydrogenase and glycerol-3-P-cytochrome c reductase activities (p=0.0003 and p=0.0006, respectively) (Fig. 1B, left panel). This observation strongly suggests that electron transfer to complex III through the CoQ pool is much more efficient from NADH dehydrogenase (CI) than from succinate dehydrogenase (CII). In other words, the small amount of complex III in *S* cells is more available to electrons coming from complex I than from other sources. We next measured the amount of CoQ available for electron transfer in control, mutant and suppressor cells. Since these are rodent cells, the major form of CoQ detected was CoQ_9, and levels of CoQ_{10} (the major form in humans) were much lower. In addition, while mutant cells showed a small reduction in CoQ_9, *S* cells showed no depletion in CoQ levels that could influence the availability of the carrier (Fig. S1F).

Our findings indicate that complexes I and III in *S* cells are assembled into the same supramolecular structure; moreover, no free complex III dimer was detected in *S* cells within the detection limit of the assay (Fig. 1C). This observation suggests a potential explanation for the apparently contradictory results described above: the existence of at least two functional CoQ pools in the inner mitochondrial membrane. One pool would be sequestered in supercomplexes to facilitate transfer of electrons from complex I to complex III, whereas the other would be free in the inner membrane, able to transfer electrons to free complex III from complex II and other FAD-dependent enzymes.

If this hypothesis is correct, and competition between complexes II and I also occurs at normal levels of complex III, specific depletion of complex I would result in increased electron transport via complex II/III. To test this, we used a cell line isolated in our laboratory in which complex I is partially depleted as the result of a frameshift mutation in *mt-Nd6* (Acin-Perez et al., 2003) (see also Experimental Procedures). Here we used a cell clone in which the mutation is stable at 60% heteroplasmy (Acin-Perez et al., 2003) and in which complex I activity was reduced, complex III activity was normal, and complex II showed slightly increased activity (Fig. 1D). In contrast, the combined activity of complex I+III was near normal (showing a slight, statistically non-significant reduction), whereas, as predicted, the linked activity of complex II+III was significantly increased (Fig. 1D).

These results suggested that specific depletion of complex I in the suppressor cell line would release complex III to reactivate the transfer of electrons from complex II. To test this, we had to grow *S* cells in permissive (glucose-containing) medium, in which oxidative phosphorylation is downregulated in favor of glycolysis, and the cells consequently showed a lowered overall respiratory activity. The relative amount of complex I was reduced by siRNA knockdown of NDUFS3 protein expression (Fig. 2A), resulting in three linked consequences: reduced activity

of complex I+III (Fig. 2B); a parallel increase in complex II+III activity (Fig. 2B); and release of complex III from its physical association with complex I (Fig. 2C). Thus complexes II and I also compete for the transfer of electrons to complex III in cells with abnormally low levels of complex III. This occurs because complex III associates preferentially with complex I in CoQ-containing supercomplexes (I+III or I+III+IV), establishing a preferential flux of electrons from complex I to III. These results demonstrate the existence of two functional CoQ pools in mammalian mitochondria, one for the transfer of electrons from complex I to complex III (CoQ_{NADH}) and the other for enzymes that use FAD (CoQ_{FAD}; Fig. 2D). They also indicate that the regulation of the relative abundance of complexes I and III defines the metabolic potential of mitochondria by determining the usage of CoQ.

To confirm these findings we downregulated complex III in control cells by reducing core 1 protein expression (Fig S2A). Consistent with the suppressor phenotype, reduced levels of complex III induced a specific loss of the III+IV supercomplex (Fig S2B). Also as predicted, there was a relative decrease in complex I levels and activity. More interestingly, the decrease in the activity of complex II+III was significantly greater than that observed for complex I+III (Fig. S2C). This observation confirms our interpretation of the results obtained in *S* cells, regardless the mechanism of suppression.

Lack of Cox7a2l abolishes the formation of supercomplexes containing complex IV. We previously characterized several mouse cell lines, derived from L929 cells, harboring mitochondrial DNA (mtDNA) mutations that render them deficient for a given respiratory complex (Acin-Perez et al., 2004; Acin-Perez et al., 2008; Bayona-Bafaluy et al., 2008; Moreno-Loshuertos et al., 2006; Perales-Clemente et al., 2011). High-throughput proteomic analysis of these cell lines was conducted to identify candidate participants in the formation of respiratory supercomplexes. Digitonin-treated mitochondrial samples from respiratory-deficient cell lines and from mtDNA isogenic controls were separated by blue native polyacrylamide gel

electrophoresis (BNGE). Bands corresponding to supercomplexes were identified in lanes from control cells, and these positions were excised from the lanes of control cells and respiratory-deficient cells (in which supercomplexes do not assemble due to the lack of a particular complex). We also excised gel areas corresponding to the migration positions of free complexes. The protein components in each band were then analyzed by liquid chromatography coupled to tandem mass spectrometry. We first compared isogenic controls with a cell line harboring a mutation in *mt-Nd4* that prevents assembly of complex I (Fig. S3A and S3B). Comparison of supercomplexes and free complexes identified the presence of Cox7a21 exclusively in supercomplexes of isogenic control cells. Cox7a21 is a protein of previously unknown function that is very similar in sequence to the structural complex IV subunit Cox7a2 (Fig. S3C and S3D). Cox7a2l was present in assemblies of complexes $I+III_2+IV_n$ (respirasome) and III_2+IV, but was not detected at the migration positions of free complex III_2 or complex IV (Fig. S3A). This was the case despite the fact that most complex IV migrates in the free form on BNGE, confirmed by the finding that other structural complex IV proteins such as Cox7a2 and Cox6a1 were detectable only in the free complex IV band (Fig. S3A).

During analysis of respiratory complex assembly in immortalized mouse fibroblasts derived from crosses between C57BL/6 and 129Sv strains, we observed two patterns for the incorporation of complex III into supercomplexes (SC), despite the fact that all cell lines express all individual respiratory complexes (Fig. S4A). The expected pattern (hereafter SC+ cells) included, from lower to higher molecular weight, free complex III dimer, complex III co-migrating with complex IV (III_2+IV), complex III co-migrating with complex I ($I+III_2$), the respirasome ($I+III_2+IV_n$) and complex III again co-migrating with complex I (likely I_2+III_2). However, three cell lines (hereafter SC- cells) showed a different pattern, lacking all putative co-migrations involving interaction between complexes III and IV (III_2+IV and the respirasome)

(Fig. S4A). This was confirmed by 2D BNGE plus SDS-PAGE followed by immunodetection of respiratory complexes (Fig. S4B).

To identify the genomic region responsible for the heterogeneous SC phenotype, we performed genome-wide analyses with the Affymetrix® Mouse Diversity Genotyping Array, which can interrogate more than 623,000 single nucleotide polymorphisms (SNPs). DNA samples from the three SC+ and SC- cell lines were compared. Most SNPs differentiating SC+ and SC- cells were located in chromosome 17 (274 discriminant SNPs), and very few discriminant SNPs were detected in other chromosomes (mean: 4.7, range 0-17). Mapping of chromosome 17 discriminant SNPs revealed a well-defined grouping (Fig. S4C), with most discriminant SNPs concentrated in two neighboring groups located between positions 81296164 and 86203330. Detailed examination of this zone revealed a near complete absence of non-discriminant SNPs (coded as -1 in the figure). For all discriminant SNPs, SC- cell lines were homozygous and SC+ cells were opposed allele carriers (most of them heterozygous). Among the small number of genes located in this region, we identified Cox7a21 (Fig. S4C, lower panel). Sequencing of the coding region of the Cox7a2l gene revealed that the three SC- cell lines were homozygous for a Cox7a2l version 6 bp shorter than the one found in heterozygosis in the three SC+ cell lines (Fig. S5A). The short and long forms of the gene respectively encode proteins of 111 and 113 amino acids.

Western blot analysis of the fibroblast lines with a polyclonal antibody against Cox7a2l detected two protein bands. The larger band was detected in all preparations and showed a molecular mass much higher than that expected for Cox7a2l, indicating that it was non-specific. The second immunoreactive band, corresponding to the expected size of Cox7a2l, was detected only in SC+ cell lines (Fig. S5B). Immunoprecipitation of *in vitro*-synthesized hemagglutinin epitope (HA)-tagged Cox7a21 proteins followed by western blot confirmed that the anti-

Cox7a2l antibody detects the 111 and 113 isoforms (Fig. S5B), indicating that the 111 amino-acid isoform is unstable and degraded in cells.

Investigation of the evolutionary conservation of Cox7a2l revealed that the reference sequence for the mouse Cox7a2l gene (corresponding to the C57Bl/6 genetic background) encodes the unstable, 111 amino-acid isoform (Fig. S5C), which does not support interaction between complexes III and IV. The Cox7a21 proteins of all vertebrates studied contain a conserved triplet in the region that differs between the 111 and 113 amino acid mouse proteins (Fig. S5C). The flanking amino acids of this triplet vary (VPI, VPV, LPV or IPV), but the central residue is always proline. Since proline residues often confer a specific secondary structure, it is likely that the absence of this motif in the 111 amino-acid isoform results in a misfolded, non-functional protein that is then degraded. Our proteomic study unambiguously detected the 113 isoform (Fig. S3D).

Since the analyzed fibroblast lines were derived from animals on a mixed genetic background (129sv:C57BL/6), we determined which Cox7a21 allele variant is present in the purebred strains. C57BL/6 mice contained the short allele and 129sv mice contained the long allele, both in homozygous form (Fig. 3A). Consistently, mitochondria isolated from purebred C57BL/6 mice exclusively showed the SC- phenotype, whereas mitochondria from purebred 129sv mice were SC+ (Fig. 3B). Examination of the SC phenotype in tissues derived from strain-mixed mice revealed that the SC phenotype divergence of the cell lines was also apparent in littermate source animals, with mitochondria isolated from liver and heart showing either normal formation of supercomplexes or no association between complexes III and IV (Fig. 3B). There is thus an exact correlation in cells and animals between the absence of 113 amino acid Cox7a2l and lack of interaction between complexes III and IV. To test whether this correlation signifies a causal relationship, we cloned and expressed the long and short Cox7a2l proteins in SC- cells. Expression of the short form (111 amino acids) had no effect on the phenotype of SC-

cells, whereas the long form (113 amino acids) restored the assembly of supercomplexes III_2+IV and I+III_2+IV_{1-4} (Fig. 3C and 3D).

These results demonstrate that the functional form of Cox7a2l is required for the assembly of complexes III and IV into supercomplexes in the mammalian respiratory chain. To our knowledge, these observations provide the first genetic evidence for the existence of respiratory supercomplexes in animal mitochondria and indicate that mitochondrial supercomplexes are physiologically regulated entities.

Incorporation of complex IV into supercomplexes determines the functional plasticity of the mitochondrial electron transport chain. The fact that C57BL/6J mice lack functional Cox7a2l indicates that integration of complex IV into supercomplexes is not required for health and fertility in the context of an animal facility; indeed, this mutation might be positively selected by the living conditions of inbred mouse strains. To determine if the mutation was specific to the mouse strain in our animal facility, we analyzed the *Cox7a2l* allele in four additional mouse strains and in C57BL/6J DNA samples from two independent suppliers (Harlan and Charles River). C57BL/6J mice from both sources and mice of the Balb/cJ strain all harbor the mutant (short) version of *Cox7a2l* in homozygosis, while all other strains tested (inbred: CBA, 129 and NZB; and outbred: CD1) harbor the long allele, also in homozygosis (Fig. 4A, bottom). Consistent with the allele composition, CBA, 129, CD1 and NZB mouse strains showed the expected super assembly of complex III (free dimer, III_2+IV, and I+III_2+IV), while C57BL/6J and Balb/cJ strains showed no interaction between complexes III and IV (Fig. 4A, upper panel).

To determine if super assembly between complexes III and IV influences, qualitatively or quantitatively, mitochondrial respiration capacity, we isolated liver mitochondria from the seven mouse strains and measured respiration in the presence of pyruvate plus malate (pyr+mal; to generate intramitochondrial NADH) or succinate (to feed electrons directly to FAD). With both

substrates, the respiration rate was higher in the absence of functional Cox7a2l/SCAFI and, therefore, in the absence of interaction between complexes III and IV (Fig. 4B). This difference was functionally relevant since the ATP synthesis paralleled the respiration rate (Fig 4C).

To obtain a more precise picture of the influence of SCAFI on mitochondrial respiration, we investigated whether C57BL/6J-derived immortalized skin fibroblasts showed any difference in respiration when transfected with the long or short form of the factor (Fig. S6A). In cells grown in DMEM, total cell respiration (driven by glucose, pyruvate and glutamine) was significantly higher in cells lacking functional SCAFI (Fig S6B, upper panel). In contrast, complex IV respiration driven by TMPD was similar regardless of SCAFI expression. These data indicate that cells expressing functional SCAFI do not use the full respiration potential of their complex IV content (Fig. S6B, lower panel). To test whether SCAFI expression also influenced ATP production, we permeabilized C57BL/6J-derived fibroblasts and fed them with pyr+mal or with succinate. Consistent with the results obtained with isolated liver mitochondria, respiration with either substrate was higher with permeabilized cells expressing the non-functional SCAFI allele; moreover, the rate of ATP production was maximal and identical with either substrate in cells with the non-functional SCAFI allele, and was lower in cells expressing functional SCAFI (Fig. S6C). As before, respiration as well as ATP production in cells expressing functional SCAFI was increased to the maximum rate by simultaneous addition of both substrates (Fig. S6C). These results confirm that the observations in liver mitochondria preparations were due to the presence of functional SCAFI and not to other unknown genetic elements.

Incorporation of complex IV in supercomplexes determines optimum respiration efficiency in the presence of NADH- and FADH-generating substrates. To interpret these results we reasoned that the ability of complex IV to form a supercomplex with complex III determines its availability for both (NADH- and FADH-generating) substrates. In the absence of

functional SCAFI, no complex IV will assemble in supercomplexes, and electrons from NADH or FAD will be sent via a single pool of cyt c to a single pool of complex IV (Fig. 5A). In contrast, if a fraction of complex IV interacts with complex III, two supercomplexes would be produced: I+III+IV (the respirasome) and III+IV (Fig. 5A). Since we know that supercomplexes containing complex IV also contain cyt c (Acin-Perez et al., 2008; Althoff et al., 2011), this super assembly will define three populations of complex IV: one dedicated to receiving electrons from NADH (CIV_{NADH}), another dedicated to receiving electrons from FAD-dependent enzymes (CIV_{FAD}); and a third one, which is free of interaction, able to receive electrons from both NADH and FAD (Fig. 5A). If this model is correct, simultaneous exposure of mitochondria containing functional SCAFI to both substrates (succinate and pyr+mal) would have an additive effect, whereas this additive behavior would be absent or very reduced in the absence of complex IV plus III super assembly. This is exactly what we detected both for respiration (Fig. 4B) and for mitochondrial ATP synthesis (Fig. 4C).

Thus far we have described changes to the performance of mitochondrial respiration that result from the superassembly of complex IV with complex III. The question remains, however, as to what putative advantage the presence of SCAFI confers. Since SCAFI allowed the segmentation of the mitochondrial electron transport chain by defining three populations of CIV (CIV_{NADH}, CIV_{FAD}, CIV_{BOTH}) it may to some extent prevent the saturation of the system by one substrate over the other, allowing the simultaneous oxidation of both at optimum rates. To test this possibility we isolated mitochondria from mouse liver of SCAFI+ and SCAFI- mice and we evaluated the synthesis of fumarate by the two types of mitochondria when succinate was supplied alone or in the presence of pyr+mal. In agreement with the succinate driven respiration, SCAFI- mitochondria generated fumarate from succinate at higher rates than SCAFI+ mitochondria when succinate was the only substrate (Fig. 5B). The addition of pyr+mal did not influence the rate of fumarate synthesis by SCAFI+ mitochondria (Fig 5B, upper panel). In

contrast, simultaneous addition of both substrates significantly reduced fumarate synthesis by SCAFI- mitochondria (Fig. 5B, lower panel). This demonstrates that SCAFI-mediated assembly of complex IV into supercomplexes prevents or minimizes competitive inhibition of respiration between pyruvate and succinate.

Adaptation to starvation is favoured by the reorganization of supercomplexes in SCAFI+ liver mitochondria. The proposal that there are separate routes for electron flux via NADH and FAD predicts testable physiological outcomes, given that the proportion of NADH and FAD electrons feeding the mitochondrial electron transport chain (mtETC) differs depending on the respiratory substrate and metabolic pathway. Mitochondrial fatty acid (FA) oxidation would favor the FAD route, and in this setting adjustment of the proportions of the different mtETC superassemblies would ensure efficient oxidation of the available substrate.

Adjustments could occur at two levels: (a) the proportion of complex III assembled with complex I, and (b) the proportion of complex IV assembled with complex III in the respirasome or the III+IV supercomplex. We can predict that the proportion of complex III assembled with complex I would be lower when the mitochondrial substrate is switched from glucose to fatty acids. We can further postulate that reduction in the interaction between complexes I and III would be neither beneficial nor necessary when complex IV does not assemble with complex III, since all electrons will end up in a common pool of cytochrome c, impeding optimization of the process. To test this, we analyzed respiration capacity through the FAD (succinate) and NADH (pyruvate+malate) routes in liver mitochondria isolated from CD1 and C57Bl/6J mice fed *ad libitum* or fasted for 18 h to activate FA degradation. The respiration rate in mitochondria from fed animals was higher with succinate in mitochondria from both strains (Fig 6A and 6B). Supporting the proposal of separate electron routes, simultaneous addition of both substrates was additive in CD1 mitochondria, yielding a maximum respiration not achieved with either substrate alone (Fig. 6A), but not in C57Bl/6J mitochondria (Fig. 6B). In mitochondria from

fasted animals, pyruvate respiration (NADH route) was significantly reduced in both CD1 and C57Bl/6J liver mitochondria. Succinate respiration (FAD route) was enhanced by fasting in CD1, but not in C57Bl/6J liver mitochondria (Fig. 6A). The changes induced by fasting are consistent with the predicted shift to increased use of the FAD route upon switching to FA degradation.

We measured individual and linked activities of complex III, complex II and I by spectrophotometry (Fig. 6A and 6B). In CD1 liver mitochondria, 18 h fasting reduced maximal CI and CI+CIII activities, without significantly influencing CII or CII+CIII activities (Fig. 6A), but this effect was not seen in C57Bl/6 liver mitochondria (Fig. 6B). Consistent with this, BNGE revealed that fasting reduces the proportion of CIII assembled with CI (NADH route) only in CD1 mitochondria (Fig. 6A and 6B). Decreased respiration via pyruvate+malate is therefore achieved by different mechanisms in the two mouse strains. Decreased pyruvate-dependent respiration could be consequence either of down-regulation of complex I activity or of reduced conversion of pyruvate to acetyl-coenzyme A (acetyl-CoA) through the pyruvate dehydrogenase complex (Fig. 6C). The activity of pyruvate dehydrogenase (PDH) is regulated by phosphorylation through a specific kinase/phosphatase pair (PDHK/PDHP) (Fig 6C). It is well established that starvation activates PDHK in rat liver mitochondria (Patel and Korotchkina, 2006) decreasing pyruvate/CoA conversion. An alternative way to generate intra-mitochondrial $NADH+H^+$ to measure respiration is to feed mitochondria with glutamate, which is converted to α-ketoglutarate by glutamate dehydrogenase (GDH), an enzyme not regulated by starvation (Fig. 6C). Since complex I activity is reduced in mitochondria from starved CD1 mice but not C57Bl/6 mice, glutamate-dependent respiration would be affected only in the former. This was confirmed by measurements of glutamate-driven respiration (Fig 6D), and while pyruvate- and glutamate-dependent ATP synthesis was reduced in mitochondria from starved CD1 liver, only pyruvate-dependent ATP synthesis was reduced in C57BL6 derived organelles.

These results, in a physiological *in vivo* system (adaptation to fasting), demonstrate a response predicted by our model: an increased flux via the FAD route by reducing the flux via the NADH route is achieved by decreasing the amount of supercomplexes that define the specific route for NADH derived electrons. This regulation is lost in SCAFI deficient cells.

Discussion

The debate about the organization of the mitochondrial electron transport chain (mtETC) has been sustained by the lack of solid functional and genetic evidence for the existence of supercomplexes *in vivo*. We recently proposed that the opposed views of the fluid and solid models can be reconciled in what we call the plasticity model (Acin-Perez et al., 2008). This model postulates the coexistence of several superstructures: the respirasome, comprising CI+III+IV, associations of CI+III containing CoQ, associations of complex III+IV and free complexes II, III and IV. In this scenario complex I would almost always exist in association with other complexes, whereas complex IV superassembly would be dynamically regulated. An intrinsic property of this model is that in any arrangement, from 100% free to 100% associated in supercomplexes, complex IV would be functional. The discovery of the role of SCAFI validates the plasticity model since (i) it demonstrates that CIV assembly into supercomplexes is regulated and (ii) animals whose mitochondria lack SCAFI, and therefore cannot form complex IV-containing supercomplexes, are healthy and fertile. Three independent reports recently described two related *Saccharomyces cerevisae* proteins (renamed by the three groups as rcf1 and rcf2) that might important for the assembly between complexes III and IV (Chen et al., 2012; Strogolova et al., 2012; Vukotic et al., 2012). However, in contrast with SCAFI, ablation of rcf1 and rcf2 impairs overall respiration and growth quality in non-fermentable substrates (Chen et al., 2012; Strogolova et al., 2012; Vukotic et al., 2012). This could be interpreted as support for the solid model, and therefore evidence against the fluid and the plasticity models. However, these proteins are required for assembly of the COX3 subunit into mature complex IV

and when ablated, complex IV assembly is impaired (Chen et al., 2012; Strogolova et al., 2012; Vukotic et al., 2012). Two mammalian orthologs, HIG1A and HIG2A, have been identified for rcf1. HIG1A depletion has no influence on respiratory complexes or supercomplexes (Chen et al., 2012) and has been linked to the regulation of the mitochondrial γ-secretase (Hayashi et al., 2012). HIG2A depletion induces a very moderate reduction in CI+III+IV supercomplexes but reduces complex IV to the same extent, as happens in yeast (Chen et al., 2012). These proteins can therefore be understood as factors required for complex IV function rather than supercomplex assembly factors. In contrast, SCAFI modulates the interaction between complex III and IV without affecting their assembly or stability, and is thus a true supercomplex assembly factor.

Four major advantages or roles have been attributed to the supercomplex organization of the mtETC: (1) increased efficiency of electron flux, through substrate channeling or enhanced catalysis (Schagger and Pfeiffer, 2000); (2) sequestration of reactive intermediates to prevent generation of reactive oxygen species (Schagger and Pfeiffer, 2000); (3) structural stabilization of individual respiratory complexes (Schagger, 2001; Schagger and Pfeiffer, 2000); and (4) structures in which complex I is assembled and activated (Moreno-Lastres et al., 2012). The first of these proposed roles conflicts with the well-supported pool behavior of electron transfer through complex III by CoQ and from III to IV by cytochrome c (for a review see (Genova and Lenaz, 2011)). The proposed antioxidant role, though appealing, lacks direct experimental support and requires further investigation (Lenaz et al., 2010). In contrast, the possible role in the structural stabilization of individual respiratory complexes is supported by work by ourselves and others showing that degradation of complex I is promoted by depletion of complex III (Acin-Perez et al., 2004; Stroh et al., 2004), complex IV (Diaz et al., 2006), and cytochrome c (Vempati et al., 2009). However, we recently showed that this phenomenon, consistently observed in cultured cells grown in 20% oxygen, might not occur at more physiological oxygen

concentrations (Diaz et al., 2012), indicating that its physiological significance still has to be determined. By the same token, and since complex I can be functionally assembled in the absence of supercomplex formation, a role in complex I assembly seems to be unsupported or marginal (Acin-Perez et al., 2004; Acin-Perez et al., 2008; Diaz et al., 2012).

In place of these proposals, our data demonstrate that supercomplex assembly organizes CIII into functionally separate subpopulations that define a subset of CoQ and CIII molecules dedicated to the transfer of electrons between complexes I and III. The picture is completed by the demonstration that CIV is also organized into functionally separate subpopulations that define subsets of cyt c and CIV molecules dedicated to the transfer of electrons coming from NADH or from FAD and a third, majority CIV subpopulation able to receive electrons from both donors. This organization agree with the observation that succinate oxidation follow a CoQ pool behavior and, since the more abundant form of CIV can receive electrons from both FAD and NADH and requires free cytochrome c, it is also compatible with the predominant interpretation of a pool behavior for electron transport trough cytochrome c (Genova and Lenaz, 2011).

Our results also demonstrate that the respiration capacity of mouse mitochondria is substantially modified by the organization of the respiratory complexes into dynamic superstructures. In particular, we show that this organization allows the cell to optimize the simultaneous, and more physiologically relevant, use of multiple carbon substrates whose oxidization generates variable proportions of NADH and $FADH_2$.

All these observations validate the plasticity model of mETC organization. Our results provide definitive evidence for the *in vivo* existence of dynamic superassemblies of mitochondrial respiratory complexes and reformulate the current view of the function, regulation and homeostasis of bioenergetic metabolism in eukaryotic cells. The demonstration that the mitochondrial electron transport chain has a variable and complex structural organization associated with functional differences adds a new level of regulation to our understanding of the

system. Dynamic superassembly by mETC complexes allows the cell to adapt to different carbon sources and physiological variations, and deeper understanding of these events would provide insight into the implication of the OXPHOS system in human disease.

Experimental Procedures

Cell Culture. Control cell lines were grown in DMEM (GibcoBRL) supplemented with 5% FBS (fetal bovine serum, Gibco BRL), and mutant cells (A22) were cultured in the same medium supplemented with uridine (50μg/ml). mA22 cells were obtained by random mutagenesis of A22 cells, using TMP and UV light as previously described (Acin-Perez et al., 2004; Bayona-Bafaluy et al., 2008), and positively selected by survival in the absence of uridine. When indicated, control and mA22 cells were grown in DMEM, 5% FBS lacking glucose but containing 0.9 mg/ml galactose and 0.11 mg/ml pyruvate. Cybridization experiments were performed as described (Acin-Perez et al., 2004).

Additional cell culture studies were conducted with immortalized fibroblast cell lines derived from six animals (77-82) on a mixed C57BL/6 and 129Sv nuclear background (129sv/B6). The cell line harbors an insertion of an additional C in a stretch of 6Cs at positions 13887 to 13892 of the *mt-Nd6* coding sequence, in heteroplasmic form. This frameshift mutation (13887iC) creates a stop codon 51-53 base pairs downstream of the C stretch, resulting in a 79 amino acid truncated polypeptide instead of the 172 amino acid full-length ND6 protein.

Cell Growth measurements. Growth capacity was monitored in cells plated at $5x10^4$ cells/well in 12-well test plates in 2 ml of the appropriate medium as described (Moreno-Loshuertos et al., 2006).

Mouse strains. Animal studies were approved by the local ethics committee. All animal procedures conformed to EU Directive 86/609/EEC and Recommendation 2007/526/EC regarding the protection of animals used for experimental and other scientific purposes, enforced

in Spanish law under Real Decreto 1201/2005. 129S2/SvPasCrlf, C57BL/6J, and Balb/cAnCh were from Charles Rivers. Hsd:ICR (CD1), CBA/OlaHsd, C57BL/6JOlaHsd, and NZB/OlaHsd were from Harlan. Analyses were performed in 8- to 11-week-old male mice.

DNA isolation and mutation analysis. Cells were digested with proteinase K in TE buffer (Tris 10 mM, EDTA 1 mM, pH 7.5) containing 0.5% SDS and ribonuclease A, and DNA was extracted with phenol-chloroform-isoamyl alcohol and precipitated with ethanol. DNA was isolated from liver or heart homogenates with Trizol®Reagent (Invitrogen). For microdeletion analysis the Cox7a2l genomic region was amplified with the following primers: Fwd 5´-3´: CTTTCTTGCTTTGCAGAAGGC and Rev: 5´-3´: GAAGGCCTCGTTTCAGGTGG. Amplification products (56 bp and 50 bp) were analyzed by electrophoresis on 10% polyacrylamide gels. The complete mtDNA of mA22 cells was sequenced as previously described (Gallardo et al., 2006). Primers were designed using the reference sequence (Bayona-Bafaluy et al., 2003). Assembly and identification of variations in mitochondrial DNA was performed automatically with the Staden package (Staden et al., 2000). The presence of the mt-Cytb mutation was confirmed by RFLP analysis (Acin-Perez et al., 2004).

Nuclear subunit sequencing. All nuclear-encoded subunits of mitochondrial complex III, as well as some mitochondrial chaperones, were sequenced using total cellular cDNA as template and specific oligodeoxynucleotides for each gene (Table S1). Total RNA was isolated from 5-6 $x10^6$ mA22 cells using TRIzol® Reagent (Invitrogen), and 1 µg was used to generate cDNA with the 1st Strand cDNA Synthesis Kit for RT-PCR (AMV) from Roche. All nuclear-encoded complex III subunits and chaperones were amplified by PCR, cloned in the TA Cloning® vector (Invitrogen) and automatically sequenced with M13 Fw and M13-Rev primers.

Genotyping. Cell lines were genotyped using the Affymetrix Mouse Diversity Genotyping array. Total genomic DNA (500ng) was processed according to the Affymetrix Genome-Wide Human SNP Nsp/Sty assay protocol. Image files were automatically processed for allele calling and

quality control with a modified version of the BRLMM-P algorithm, available through Affymetrix Power Tools (APT); for details, see http://www.affymetrix.com. The Affymetrix Mouse Diversity Genotyping array contains more than 623,000 SNPs, with a mean separation of 4.3 kb. Of these SNPs, 80% (498929) were monomorphic in the sample (all six cell lines showed the same genotype) and another 38457 SNPs were missing. Thus 85738 SNPs showed genetic variability in our sample and were analyzed further. To try to identify genomic regions that best discriminate between cell lines competent (SC+) and non-competent (SC-) for complex IV containing supercomplex formation, each SNP was classified as discriminant or non-discriminant. An SNP was classified as discriminant when it showed a coherent genotype within one group opposite to that shown in the other group (frequent homozygous allele versus rare allele carrier; rare homozygous allele versus frequent allele carrier). This difference was only evaluated for those SNPs genotyped in a minimum of two lines per group, to check the coherence within each phenotypic group. Data were managed and figures generated with IBM SPSS Statistics v18.

Cox7a2l constructs. Total RNA was isolated from the SC+ cell line 78 with Trizol®Reagent (Invitrogen). Total cDNA was synthesized using the Transcriptor First Stand cDNA Synthesis Kit (Roche). Cox7a2l cDNA was amplified and cloned into the pCR2.1 plasmid using the TA Cloning kit (Invitrogen) and sequenced. A second construct was prepared in which the hemagglutinin epitope was added to the C-terminus for immunoprecipitation.

The short and long Cox7a2l variants (Cox7a2l-111 and Cox7a2l-113) were subcloned into the pWPXLd lentiviral vector (Tronolab) for cell transfection, using BamHI and SpeI restriction sites (NEB), and into the pTNT™ vector (Promega) for *in vitro* protein synthesis, using NotI and XhoI restriction sites (NEB).

mRNA interference. Expression of *NDUFS3* in mA22 or *Core1* in control cells was knocked down using the "Expression Arrest™ GIPZ lentiviral shRNAmir library" developed by Thermo

Scientific Open Biosystems. Optimal multiplicity of infection (MOI) was calculated according to the manufacturer's protocol. $5x10^4$ cells per well were plated in a 24-well plate the day before transduction. The next day, medium was replaced (250 µl DMEM without FBS or antibiotics plus 8 µg/ml polybrene) and virus added at the desired MOI. After 4-6 h, an additional 1 ml of full medium was added and cells were incubated for 48 h. Cells were then examined under a fluorescence microscope every 24 h for reporter expression, and once expression reached an acceptable level, the reduction in the targeted protein content was tested by western blot.

Lentiviral vector production and cell infection. Human 293T cells ($2.5x10^6$) were plated 24 h before cotransfection with 10 µg of transfer vector (pWPXLd COX7A2L-111p or pWPXLd COX7A2L-113p), 7.5 µg of second-generation packaging plasmid (psPAX2) and 3 µg of envelope plasmid (pMD2.G). FuGENE 6 Transfection Reagent (Roche) was used. Infectious particles were collected 24h after transfection (Naldini et al., 1996). Lentiviral particles were used to transduce SC- cell lines.

Protein extraction. Cells were collected from 100mm-diameter culture plates, washed twice with PBS, pelleted and resuspended in 200µl RIPA buffer containing protease inhibitors.

***In vitro reticulocyte protein expression*.** Cox7a2l-111 and Cox7a2l-113 cloned into pTNT™ vector (Promega) were *in-vitro* synthesized using the TNT T7/SP6 Coupled Reticulocyte Lysate System (Promega).

Blue native polyacrylamide electrophoresis. Mitochondria were isolated from mouse liver and heart samples as described (Fernandez-Vizarra et al., 2002). Mitochondria were isolated from cultured cell lines according to Schägger (1995) (Schagger, 1995), with some modifications (Acin-Perez et al., 2008). Digitonin-solubilized mitochondrial proteins (100 µg) were separated on blue native gradient gels (3-13% acrylamide). After electrophoresis, the gels were further processed for western blotting or a second dimension of SDS-PAGE (Wittig et al., 2006). For proteomic analysis, the gel was submerged for 2 h at room temperature in staining solution

(0.25% Coomasie Blue R-250, 40% methanol, 10% acetic acid). After several washes in 40% methanol, 10% acetic acid, the gel was soaked in water overnight and the protein bands of interest were excised.

Immunological techniques. Synthetic proteins were immunoprecipitated using the HA epitope (Anti HA Immunoprecipitation Kit, SIGMA). Purified proteins total cell protein extracts (15 µg) were separated by 16% SDS-PAGE.

After electrophoresis, SDS-PAGE, BN-PAGE or BN-SDS-PAGE gels were electroblotted onto Hybond–P PVDF membranes (GE Lifesciences). Antibodies used were anti-cox7a2l (polyclonal, Protein Tech Group), and specific antibodies against complex I (anti-NDUFA9, MitoSciences), complex II (anti-70 kDa subunit, SDHA, Invitrogen), complex III (anti-Core2, MitoSciences) and complex IV (anti-COXIV, MitoSciences). Secondary antibodies used were peroxidase-conjugated anti-mouse or anti-rabbit (Invitrogen). Signal was detected using the EZ-ECL Chemiluminiscence Detection kit for HRP (Biological Industries).

Protein identification by liquid chromatography coupled to tandem mass spectrometry. Gel pieces from blue native gels containing the protein bands of interest were excised. After reduction with DTT (10mM) and alkylation of Cys groups with iodoacetamide (50mM), modified porcine trypsin (Promega) was added at a final mass ratio of 1:50 (trypsin-protein). Digestion proceeded overnight at 37ºC, after which samples were vacuum-dried and dissolved in 1% acetic acid.

To identify proteins, the resulting tryptic peptide mixtures were analyzed by nano-liquid chromatography coupled to mass spectrometry. Peptides were injected onto a C-18 reversed phase (RP) nano-column (100 µm I.D. and 15 cm, Mediterranea sea, Teknokroma) and analyzed on a continuous acetonitrile gradient consisting of 0-43% B for 90 min and 50-90% B for 1 min (B=95% acetonitrile, 0.5% acetic acid). Peptides were eluted from the RP nano-column at a flow rate of ~300 nL/min to an emitter nanospray needle for real-time ionization and peptide

fragmentation on an LTQ-Orbitrap mass spectrometer (Thermo Fisher, San José, CA, USA). An enhanced FT-resolution spectrum (resolution=6000) and the MS/MS spectra of the five most-intense parent ions were analyzed during the chromatographic run (130 min). Dynamic exclusion was set at 0.5 min.

For protein identification, tandem mass spectra were extracted and charge-state deconvoluted with Proteome Discoverer 1.2.0.207 (Thermo Fisher Scientific). All MS/MS samples were analyzed by SEQUEST™ (Thermo Fisher Scientific, version 1.0.43.2), MASCOT™ (Matrixscience, version 2.1) and X! Tandem (The GPM, thegpm.org; version 2007.01.01.1). Search engines were set up to search MSIPI_mouse_3.67.fasta (1.0, 56687 entries). All searches were performed assuming complete trypsin digestion. Two mixed cleavages were allowed, and errors of 15 ppm or 0.8 Da were set for full MS and MS/MS spectra searches, respectively. Oxidation on M, phosphorylation on S or T, and deamidation on Q or N were selected as dynamic modifications. All identifications were performed by Decoy database search for FDR analysis. Scaffold (version Scaffold_3_00_03, Proteome Software Inc., Portland, OR) was used to validate MS/MS peptide and protein identifications. Protein probabilities were assigned by the Protein Prophet algorithm. Proteins that contained similar peptides and could not be differentiated based on MS/MS analysis alone were grouped to satisfy the principles of parsimony.

OXPHOS performance. O_2 consumption in intact or digitonin-permeabilized cells or mouse live mitochondria (100 µg) was determined with an oxytherm Clark-type electrode (Hansatech) as previously described (Hofhaus et al., 1996) with small modifications (Acin-Perez et al., 2003). For spectrophotometric measurements of OXPHOS enzyme activity, mitochondria were isolated as described (Fernandez-Vizarra et al., 2002). Activities of citrate synthase and complexes I, II, III, I+III, II+III and IV were measured in mitochondria isolated from cultured cells or mouse liver as described (Acin-Perez et al., 2004). To measure state III O_2 consumption

driven by specific respiratory chain complexes, mouse liver mitochondria (100μg) or digitonin-permeabilized cells were placed in respiration medium containing 1mM ADP and 2mM inorganic phosphate (Hofhaus et al., 1996). Mitochondria were isolated from liver from the different mouse strains (Fernandez-Vizarra et al., 2002). C57 cells were permeabilized by incubating in the presence of 1% digitonin (1 μl per million cells) for 10 min at 37C. Substrate concentrations were as follows: 5mM pyruvate plus 5mM malate (pyr+mal); 5mM succinate plus 100nM rotenone (succinate); or 5mM pyruvate plus 5mM malate plus 5mM succinate (pyr+mal+succinate). Reactions were terminated by addition of 2mM KCN to assess any O_2 consumption not derived from the respiratory chain.

ATP synthesis driven by the different substrates in isolated mouse liver mitochondria (15-25μg mitochondrial protein) or digitonin-permeabilized cells ($2x10^6$ cells) was measured using a kinetic luminescence assay, as previously described (Vives-Bauza et al., 2007).

Fumarate production was measured spectrophomometrically at 260nm. Mitochondria (100 μg) were incubated in the measuring buffer (25 mM K_2HPO_4; 5 mM $MgCl_2$; 3 mM KCN; 2.5 mg/ml BSA) in the presence of 5mM succinate or pyr+mal+succinate, and fumarate concentration was measured after 10, 15 and 20 min. Fumarate production was calculated by subtracting the fumarate concentration at time 0.

CoQ determination. Cell samples were lysed with 1% SDS and vortexed for 1 min. A mixture of ethanol:isopropanol (95:5) was added and the samples vortexed again for 1 min. To recover CoQ, 5ml of hexane was added and the samples were centrifuged at 1000xg for 5 min at 4°C. The upper phases from two extractions were recovered and dried using a rotary evaporator. Lipid extracts were suspended in 1ml ethanol, dried in a speed-vac and stored at -20°C. Samples were suspended in a suitable volume of ethanol prior to HPLC injection. Lipid components were separated with a Beckmann 166–126 HPLC system equipped with a 15-cm Kromasil C-18 column in a column oven set to 40°C, with a flow rate of 1ml/min and a mobile phase containing

65:35 methanol/n-propanol and 1.42 mM lithium perchlorate. CoQ_6 was used as internal standard for the quantitative determination of CoQ_9 and CoQ_{10}. CoQ content was analyzed with ultraviolet (System Gold 168) and electrochemical (Coulochem III ESA) detectors, and was determined as pmol/mg protein (Brea-Calvo et al., 2006; Santos-Ocana et al., 2002).

Comparative phylogenetic analysis. Protein sequences from different vertebrate species were collected from the NCBI protein database. Sequences were aligned with the Clustawl 2.1 multiple sequence alignment package.

Statistical analysis. Differences between cell lines were assessed by analysis of variance (ANOVA). Paired differences were assessed by the post hoc Fisher's protected least significant difference test (PLSD). All tests and calculations were done with the statistical package StatView 5.0 for Macintosh (SAS Institute, Inc.).

Acknowledgements:

We thank Dr. G. Lenaz for critical reading of the manuscript, and Simon Bartlett (CNIC) for English editing. This study was supported by grants from the Ministerio de Ciencia e Innovación (SAF2 & CSD), the Instituto de Salud Carlos III-FIS, the European Union (FP7-Microenvimet & Marie Curie ERG) and the Diputación General de Aragón. EL-B is the recipient of an FPU fellowship from the Spanish Ministerio de Educación. EF-V is recipient of a Miguel Servet grant from the Instituto de Salud Carlos III. RA-P is an investigator of the Ramon y Cajal research program from the Ministerio de Economía y Competitividad. Genotyping was conducted at the Spanish National Genotyping Center (CEGEN-ISCIII). C.L-O is a Botin Foundation Investigator. The CNIC is supported by the Ministerio de Economía y Competitividad and the Pro-CNIC Foundation. All authors declare that they have no competing interests. EL-B, RM-L, RA-P, AL-P, CC & EB performed cell and mouse experiments, MAR-H & PN EP-C measured CoQ content, EP-C and EC performed the proteomics analysis, RC and AC performed genome-

wide analysis and statistics, and PMQ and CL-O generated the mouse cell lines. AP-M, PF-S, EF-V and JAE designed the experiments. JAE directed the work and wrote the manuscript.

References

Acin-Perez, R., Bayona-Bafaluy, M.P., Bueno, M., Machicado, C., Fernandez-Silva, P., Perez-Martos, A., Montoya, J., Lopez-Perez, M.J., Sancho, J., and Enriquez, J.A. (2003). An intragenic suppressor in the cytochrome c oxidase I gene of mouse mitochondrial DNA. Hum Mol Genet *12*, 329-339.

Acin-Perez, R., Bayona-Bafaluy, M.P., Fernandez-Silva, P., Moreno-Loshuertos, R., Perez-Martos, A., Bruno, C., Moraes, C.T., and Enriquez, J.A. (2004). Respiratory complex III is required to maintain complex I in mammalian mitochondria. Mol Cell *13*, 805-815.

Acin-Perez, R., Fernandez-Silva, P., Peleato, M.L., Perez-Martos, A., and Enriquez, J.A. (2008). Respiratory active mitochondrial supercomplexes. Mol Cell *32*, 529-539.

Althoff, T., Mills, D.J., Popot, J.L., and Kuhlbrandt, W. (2011). Arrangement of electron transport chain components in bovine mitochondrial supercomplex I1III2IV1. EMBO J *30*, 4652-4664.

Bayona-Bafaluy, M.P., Acin-Perez, R., Mullikin, J.C., Park, J.S., Moreno-Loshuertos, R., Hu, P., Perez-Martos, A., Fernandez-Silva, P., Bai, Y., and Enriquez, J.A. (2003). Revisiting the mouse mitochondrial DNA sequence. Nucleic Acids Res *31*, 5349-5355.

Bayona-Bafaluy, M.P., Movilla, N., Perez-Martos, A., Fernandez-Silva, P., and Enriquez, J.A. (2008). Functional genetic analysis of the mammalian mitochondrial DNA encoded peptides: a mutagenesis approach. Methods Mol Biol *457*, 379-390.

Brea-Calvo, G., Rodriguez-Hernandez, A., Fernandez-Ayala, D.J., Navas, P., and Sanchez-Alcazar, J.A. (2006). Chemotherapy induces an increase in coenzyme Q10 levels in cancer cell lines. Free radical biology & medicine *40*, 1293-1302.

Chen, Y.-C., Taylor, E.B., Dephoure, N., Heo, J.-M., Tonhato, A., Papandreou, I., Nath, N., Denko, N.C., Gygi, S.P., and Rutter, J. (2012). Identification of a Protein Mediating Respiratory Supercomplex Stability. Cell Metabolism.

Diaz, F., Enriquez, J.A., and Moraes, C.T. (2012). Cells lacking Rieske iron-sulfur protein have a reactive oxygen species-associated decrease in respiratory complexes I and IV. Mol Cell Biol *32*, 415-429.

Diaz, F., Fukui, H., Garcia, S., and Moraes, C.T. (2006). Cytochrome c oxidase is required for the assembly/stability of respiratory complex I in mouse fibroblasts. Mol Cell Biol *26*, 4872-4881.

Dudkina, N.V., Eubel, H., Keegstra, W., Boekema, E.J., and Braun, H.P. (2005). Structure of a mitochondrial supercomplex formed by respiratory-chain complexes I and III. Proc Natl Acad Sci U S A *102*, 3225-3229.

Dudkina, N.V., Kudryashev, M., Stahlberg, H., and Boekema, E.J. (2011). Interaction of complexes I, III, and IV within the bovine respirasome by single particle cryoelectron tomography. Proc Natl Acad Sci U S A *108*, 15196-15200.

Eubel, H., Heinemeyer, J., and Braun, H.P. (2004). Identification and characterization of respirasomes in potato mitochondria. Plant Physiol *134*, 1450-1459.

Fernandez-Vizarra, E., Lopez-Perez, M.J., and Enriquez, J.A. (2002). Isolation of biogenetically competent mitochondria from mammalian tissues and cultured cells. Methods *26*, 292-297.

Gallardo, M.E., Moreno-Loshuertos, R., Lopez, C., Casqueiro, M., Silva, J., Bonilla, F., Rodriguez de Cordoba, S., and Enriquez, J.A. (2006). m.6267G>A: a recurrent mutation in the human mitochondrial DNA that reduces cytochrome c oxidase activity and is associated with tumors. Human mutation *27*, 575-582.

Genova, M.L., Bianchi, C., and Lenaz, G. (2005). Supercomplex organization of the mitochondrial respiratory chain and the role of the Coenzyme Q pool: pathophysiological implications. Biofactors *25*, 5-20.

Genova, M.L., and Lenaz, G. (2011). New developments on the functions of coenzyme Q in mitochondria. Biofactors *37*, 330-354.

Hackenbrock, C.R., Chazotte, B., and Gupte, S.S. (1986). The random collision model and a critical assessment of diffusion and collision in mitochondrial electron transport. J Bioenerg Biomembr *18*, 331-368.

Hayashi, H., Nakagami, H., Takeichi, M., Shimamura, M., Koibuchi, N., Oiki, E., Sato, N., Koriyama, H., Mori, M., Gerardo Araujo, R., *et al.* (2012). HIG1, a novel regulator of mitochondrial gamma-secretase, maintains normal mitochondrial function. FASEB journal : official publication of the Federation of American Societies for Experimental Biology.

Hofhaus, G., Shakeley, R.M., and Attardi, G. (1996). Use of polarography to detect respiration defects in cell cultures. Methods Enzymol *264*, 476-483.

Lenaz, G., Baracca, A., Barbero, G., Bergamini, C., Dalmonte, M.E., Del Sole, M., Faccioli, M., Falasca, A., Fato, R., Genova, M.L., *et al.* (2010). Mitochondrial respiratory chain super-complex I-III in physiology and pathology. Biochim Biophys Acta *1797*, 633-640.

Lenaz, G., Fato, R., Formiggini, G., and Genova, M.L. (2007). The role of Coenzyme Q in mitochondrial electron transport. Mitochondrion *7 Suppl*, S8-33.

Lenaz, G., and Genova, M.L. (2007). Kinetics of integrated electron transfer in the mitochondrial respiratory chain: random collisions vs. solid state electron channeling. Am J Physiol Cell Physiol *292*, C1221-1239.

Moreno-Lastres, D., Fontanesi, F., Garcia-Consuegra, I., Martin, M.A., Arenas, J., Barrientos, A., and Ugalde, C. (2012). Mitochondrial Complex I Plays an Essential Role in Human Respirasome Assembly. Cell Metab.

Moreno-Loshuertos, R., Acin-Perez, R., Fernandez-Silva, P., Movilla, N., Perez-Martos, A., Rodriguez de Cordoba, S., Gallardo, M.E., and Enriquez, J.A. (2006). Differences in reactive oxygen species production explain the phenotypes associated with common mouse mitochondrial DNA variants. Nat Genet *38*, 1261-1268.

Naldini, L., Blomer, U., Gage, F.H., Trono, D., and Verma, I.M. (1996). Efficient transfer, integration, and sustained long-term expression of the transgene in adult rat brains injected with a lentiviral vector. Proc Natl Acad Sci U S A *93*, 11382-11388.

Patel, M.S., and Korotchkina, L.G. (2006). Regulation of the pyruvate dehydrogenase complex. Biochemical Society transactions *34*, 217-222.

Perales-Clemente, E., Fernandez-Vizarra, E., Acin-Perez, R., Movilla, N., Bayona-Bafaluy, M.P., Moreno-Loshuertos, R., Perez-Martos, A., Fernandez-Silva, P., and Enriquez, J.A. (2011). Five entry points of the mitochondrially encoded subunits in mammalian complex I assembly. Mol Cell Biol *30*, 3038-3047.

Santos-Ocana, C., Do, T.Q., Padilla, S., Navas, P., and Clarke, C.F. (2002). Uptake of exogenous coenzyme Q and transport to mitochondria is required for bc1 complex stability in yeast coq mutants. The Journal of biological chemistry *277*, 10973-10981.

Schafer, E., Dencher, N.A., Vonck, J., and Parcej, D.N. (2007). Three-dimensional structure of the respiratory chain supercomplex I1III2IV1 from bovine heart mitochondria. Biochemistry *46*, 12579-12585.

Schafer, E., Seelert, H., Reifschneider, N.H., Krause, F., Dencher, N.A., and Vonck, J. (2006). Architecture of active mammalian respiratory chain supercomplexes. The Journal of biological chemistry *281*, 15370-15375.

Schagger, H. (1995). Native electrophoresis for isolation of mitochondrial oxidative phosphorylation protein complexes. Methods Enzymol *260*, 190-202.

Schagger, H. (2001). Respiratory chain supercomplexes. IUBMB Life *52*, 119-128.

Schagger, H., and Pfeiffer, K. (2000). Supercomplexes in the respiratory chains of yeast and mammalian mitochondria. EMBO J *19*, 1777-1783.

Staden, R., Beal, K.F., and Bonfield, J.K. (2000). The Staden package, 1998. Methods Mol Biol *132*, 115-130.

Strogolova, V., Furness, A., Robb-McGrath, M., Garlich, J., and Stuart, R.A. (2012). Rcf1 and Rcf2, members of the hypoxia induced gene 1 protein family, are critical components of the mitochondrial cytochrome bc1-cytochrome c oxidase supercomplex. Mol Cell Biol.

Stroh, A., Anderka, O., Pfeiffer, K., Yagi, T., Finel, M., Ludwig, B., and Schagger, H. (2004). Assembly of respiratory complexes I, III, and IV into NADH oxidase supercomplex stabilizes complex I in Paracoccus denitrificans. The Journal of biological chemistry *279*, 5000-5007.

Vempati, U.D., Han, X., and Moraes, C.T. (2009). Lack of cytochrome c in mouse fibroblasts disrupts assembly/stability of respiratory complexes I and IV. The Journal of biological chemistry *284*, 4383-4391.

Vives-Bauza, C., Yang, L., and Manfredi, G. (2007). Assay of mitochondrial ATP synthesis in animal cells and tissues. Methods Cell Biol *80*, 155-171.

Vukotic, M., Oeljeklaus, S., Wiese, S., Vogtle, F.N., Meisinger, C., Meyer, H.E., Zieseniss, A., Katschinski, D.M., Jans, D.C., Jakobs, S., *et al.* (2012). Rcf1 Mediates Cytochrome Oxidase Assembly and Respirasome Formation, Revealing Heterogeneity of the Enzyme Complex. Cell Metab.

Wittig, I., Braun, H.P., and Schagger, H. (2006). Blue native PAGE. Nat Protoc *1*, 418-428.

Figure Legends

Figure 1.- Complexes I and III compete for delivery of electrons to complex III. A) Oxygen consumption by permeabilized control cells (*C*), mutant cells (*M*; A22 cells unable to assemble mitochondrial complex III) and suppressor cells (*S*; mutated A22 cells with limited

restoration of complex III). Oxygen consumption was measured in the presence of electron donors for complex I (glutamate + malate), complex III (succinate + G3P) and complex IV (TMPD). *M* cells only consume oxygen when complex IV substrates are added (n=6, 3 and 6 for *C*, *M* and *S* cells). Glutamate + malate respiration differed significantly between *M* cells and other cell lines ($p<0.0001$; Fisher's PLSD post-hoc test of paired differences) but did not differ between *C* and *S* cells. Succinate + G3P: $p<0.0001$ between control and mutant cells, $p=0.0024$ between *C* and *S* cells, and $p=0.0002$ between *M* and *S* cells. TMPD: $p=0.0063$ between *C* and *S* cells. B) Spectroscopic measurement in *C* and *S* cells of isolated mitochondrial complex activities, either alone (left) or in combination with complex III (right). Activities are normalized to citrate synthase (CS) and expressed as a percentage of activity in controls. $n\geq3$ for all measurements; $p<0.0001$ for CI; $p=0.0020$ for CIII; $p=0.0271$ for CIV¸ $p=0.0252$ for CI+III; $p=0.0004$ for CII+III; and $p=0.0048$ for G3PDH+III; ; Fisher's PLSD post-hoc testa of paired differences. C) Western blot of assembled supercomplexes in digitonin-permeabilized mitochondria separated by BNGE, probed with monoclonal antibodies for complexes I (anti NDUFB6), III (anti Core2), IV (anti COI) and II (anti SDHB (I30)). In *S*-cell mitochondria, supercomplexes containing complex III but lacking free complex III dimer can be observed, while other supercomplexes contain either complex IV or complex II. D) Spectroscopic measurement of isolated mitochondrial complex activities, either alone (left) or in combination with complex III (right), in *C*, *S* and heteroplasmic ND6 mutant cells (*ND6-M*; in which complex I is partially depleted). $n\geq3$ for all measurements; CI: $p<0.0001$ between *C* and *S*, $p=0.0082$ between *C* and *ND6-M*, and $p=0.0014$ between *S* and *ND6-M*; CII: $p=0.0090$ between *M* and *C* cells; CIII: $p=0.0001$ between *S* and all others; CI+III: n.s.; CII+III: $p<0.0001$ in all paired tests; ; Fisher's PLSD post-hoc test of paired differences. Data are means ± SD. Asterisks indicate significant differences with respect to control cells.

Figure 2.- Characterization of cells knocked down for complex I (NDUFS3-interfered cells). A) Immunodetection of NDUFS3 protein in *S* cells after SDS-PAGE. Actin was detected as a loading control. B) Spectrophotometric measurements of the activities of isolated complex I, complex I plus complex III, and complex II plus complex III in control and NDUFS3-interfered *S* cells (CI-Kd). The respiration capacity of *S* cells in these experiments was lower than in Figure 1 because they were in glucose medium. $n \geq 3$ in all assays; CI: $p<0.0001$ between *C* and all other cell lines and $p=0.0218$ between *S* and CI-Kd5 cell line; CI+III: $p<0.0001$ between C and both CI-Kd cell lines, $p=0.0006$ between *S* and CI-Kd2, and $p=0.0022$ between S and CI-Kd5; CII+III: $p=0.0447$ between C and CI-Kd5, $p=0.0002$ between *C* and *S*, and $p<0.0001$ between *S* and both CI-Kd lines. Data are means ± SD. Asterisks indicate significant differences with respect to control cells, tested by ANOVA and post-hoc Fisher PLSD ($p<0.05$). C) Characterization of complex III-containing supercomplexes in non-interfered and NDUFS3-interfered cells. Complex III+IV and dimeric complex III are evident in interfered clones. The small amounts of these two forms in *S* cells disappear when these cells are grown in galactose medium. D) Scheme representing the existence of two ubiquinone pools, one for NADH and the second available for FAD-containing enzymes.

Figure 3. Characterization of Cox7a2l in supercomplex-competent (SC+) and SC- cell lines and animal models. (See also Fig S4) A) PCR analysis of Cox7a2l alleles in mice on the C57BL/6 (C57) and 129S2/SvPasCrlf (129S2) backgrounds. C57 mice are homozygous for the 111 amino-acid (Short) allele, whereas 129S2 is homozygous for the 113 amino-acid (Long) allele. B) Western blot after BNGE, probed for complex III (anti Core2). Supercomplex formation in SC- cells is rescued only when cells are transfected with the long version of Cox7a2l (+113p). C) Western analysis of complex III (anti Core2) after BNGE, showing complex assembly status in mitochondrial samples from mixed background littermates (178 & 179) and tissues of purebred C57 and 129S2 mice. D) Western blot of fibroblast line 77 after

second dimension separation of blue-native-separated proteins by denaturing SDS-PAGE; blots were probed for complexes I (anti Nduaf9), II (anti SDHA), III (anti Core2) and IV (anti CoxIV). Supercomplexes formed in cells transfected with 113 amino-acid Cox7a2l are circled.

Figure 4. SCAFI depletion alters mitochondrial respiratory function. A) Genotyping (PCR) of different mouse strains for the Cox7a2l allele (lower panel) and western blot of complex III (anti Core2) after BNGE, showing complex assembly status in liver mitochondria. B) Substrate-driven rates of oxygen consumption in liver mitochondria from SCAFI-deficient (Short) and SCAFI expressing (Long) mice, compared with the rate achieved upon simultaneous addition of both substrates. ($n \geq 8$; pyr+mal, $p<0.0001$; succinate, $p<0.0001$; pyr+mal+succinate, n.s). Data are mean of means obtained with liver mitochondria from C57BL/6J (from Charles Rivers and Harlan) and Balb/cJ mice (Short), and with liver mitochondria from CBA, 129, CD1 and NZB mice (Long). C) Substrate-driven rates of ATP synthesis by liver mitochondria from SCAFI-deficient (Short) and SCAFI-expressing (Long) mice, compared with the rate achieved upon simultaneous addition of both substrates ($n \geq 8$; pyr+mal, $p<0.0222$; succinate, $p<0.0193$; pyr+mal+succinate, n.s).

Figure 5. Assembly of SC defines electron transport chain (ETC) organization alternatives for NADH- or FAD-derived electrons. A) Plasticity model of mitochondrial ETC organization, showing complex I associations with a dedicated CoQ pool (blue: the respirasome (CI+III+IV) and CI+III) coexisting with complex III+IV associations and free complexes II, III and IV. *Left:* Normal situation illustrated for CD1 mice, in which Cox7a2l/SCAFI modulates CIV-containing supercomplexes, thereby regulating the proportions of free complex III and IV and generating three states for complex IV. *Right:* Extreme situation illustrated for C57Bl6 mice, where SCAFI is absent and no complex IV-containing supercomplexes form, making all CIV available to any substrate. B) Time profile (t-t0) of fumarate production by isolated mouse liver mitochondria from SCAFI-positive mice (upper panel) and SCAFI-deficient mice (bottom panel)

in the presence of succinate or succinate and pyruvate plus malate (n=8, each measure in duplicate).

Figure 6. OXPHOS performance and supercomplex distribution in response to fasting. (A-B) *Top left panels:* Oxygen-dependent (coupled) respiration in isolated liver mitochondria from fed and starved CD1 mice (A) or C57Bl/6 mice (B) driven by pyruvate plus malate (Pyr+Mal), succinate, or both (Pyr+Mal & Succinate). *Bottom left panels:* Spectroscopic measurement of the activities of mitochondrial complexes (CI and CII), both individually and in combination with complex III (CI+III and CII+III) in mouse liver mitochondria from fed and starved CD1 mice (A) and C57Bl/6 mice (B). Activities are expressed per milligram of mitochondrial protein. *Right:* Western blots show associations complex III (anti Core2) detected after BNGE. (C) Scheme showing the sites for $NADH+H^+$ or $FADH_2$ generation in mitochondria from different substrates and the processes potentially targeted by starvation. (D) Oxygen-dependent (coupled) respiration (left) and ATP production rate (right) in isolated liver mitochondria from fed and starved CD1 or C57Bl6 mice driven by Pyr+Mal or glutamate. Asterisks represent significant differences ($p < 0.05$).

Figure 1

Click here to download high resolution image

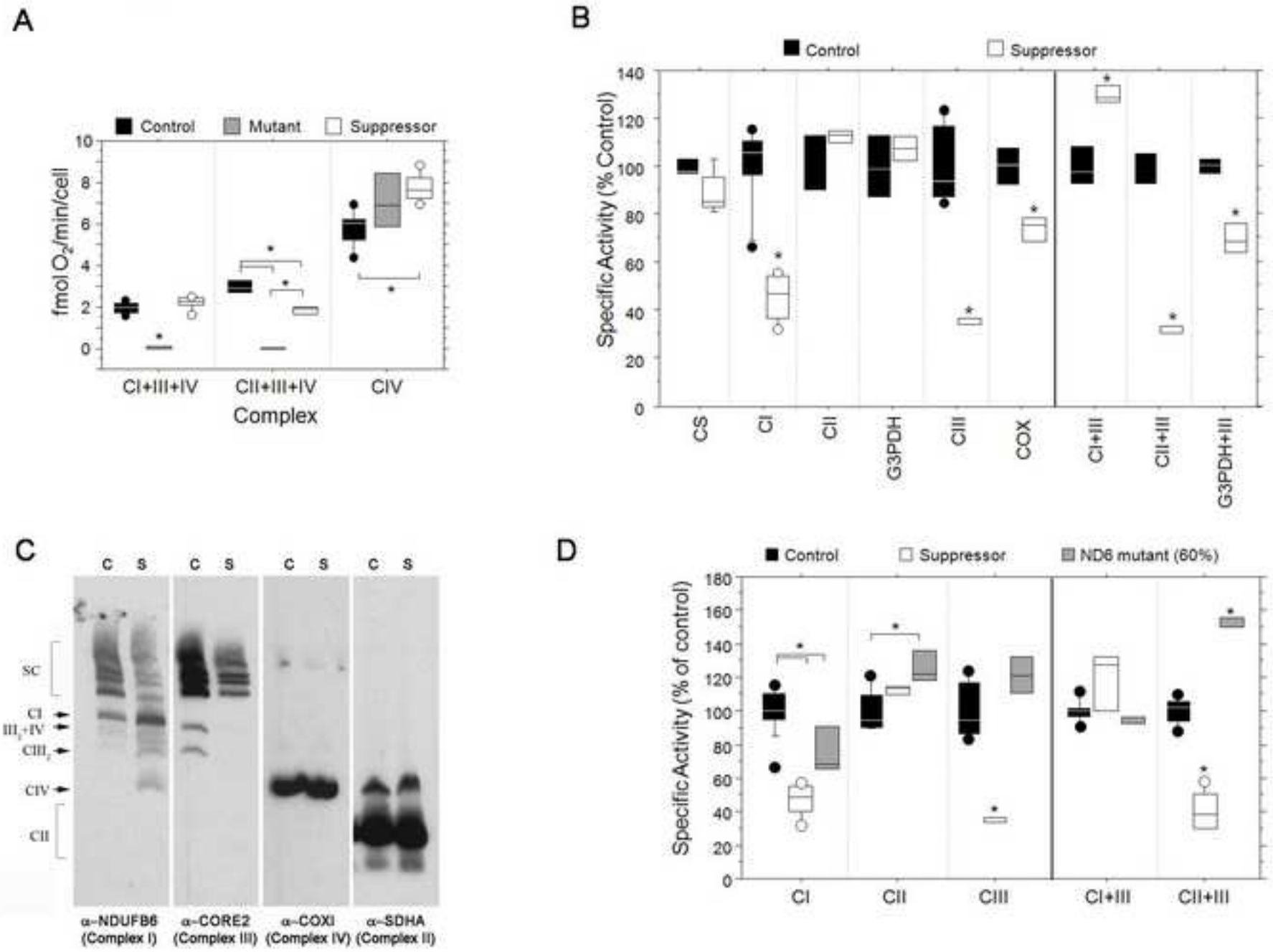

Figure 2

Click here to download high resolution image

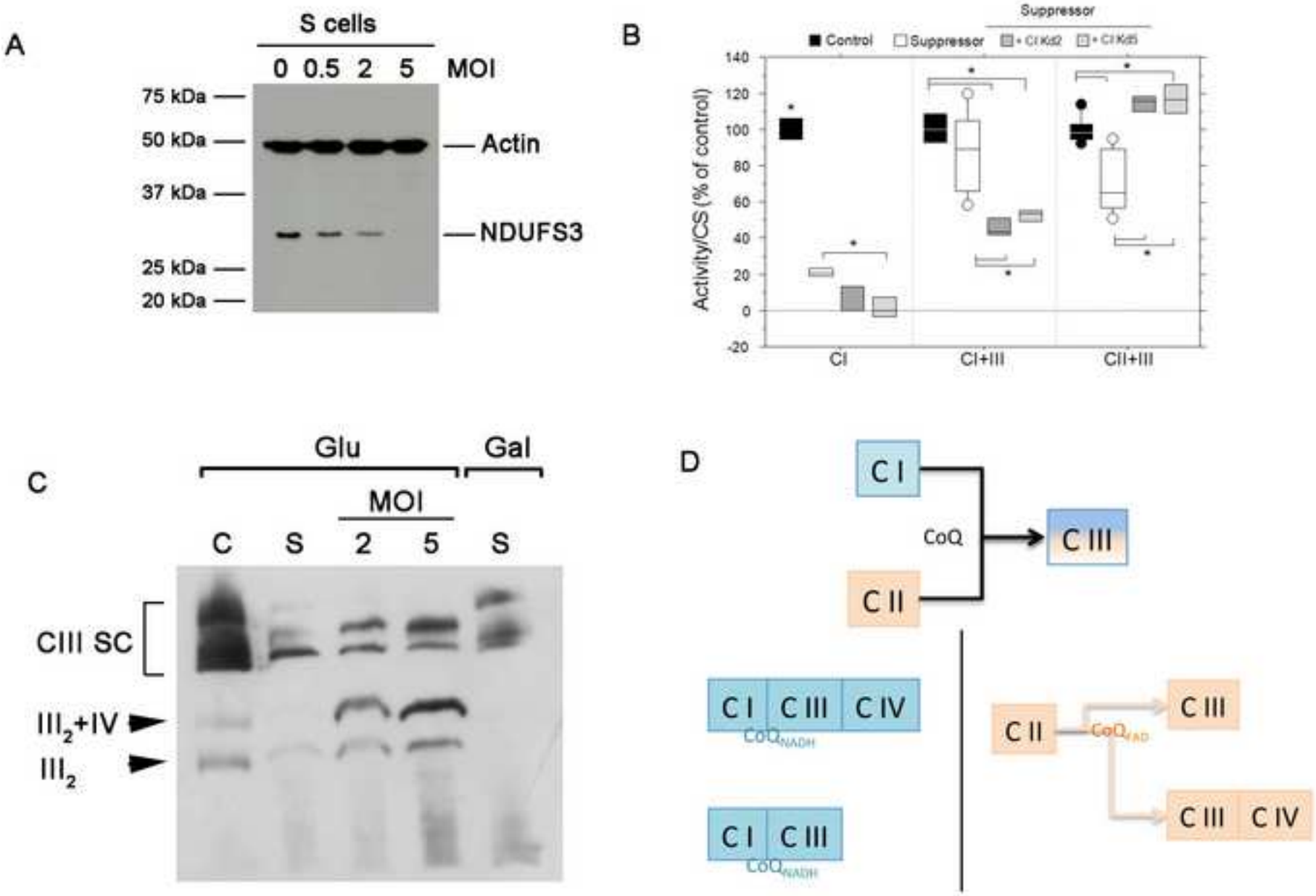

Figure 2

Figure 3

Click here to download high resolution image

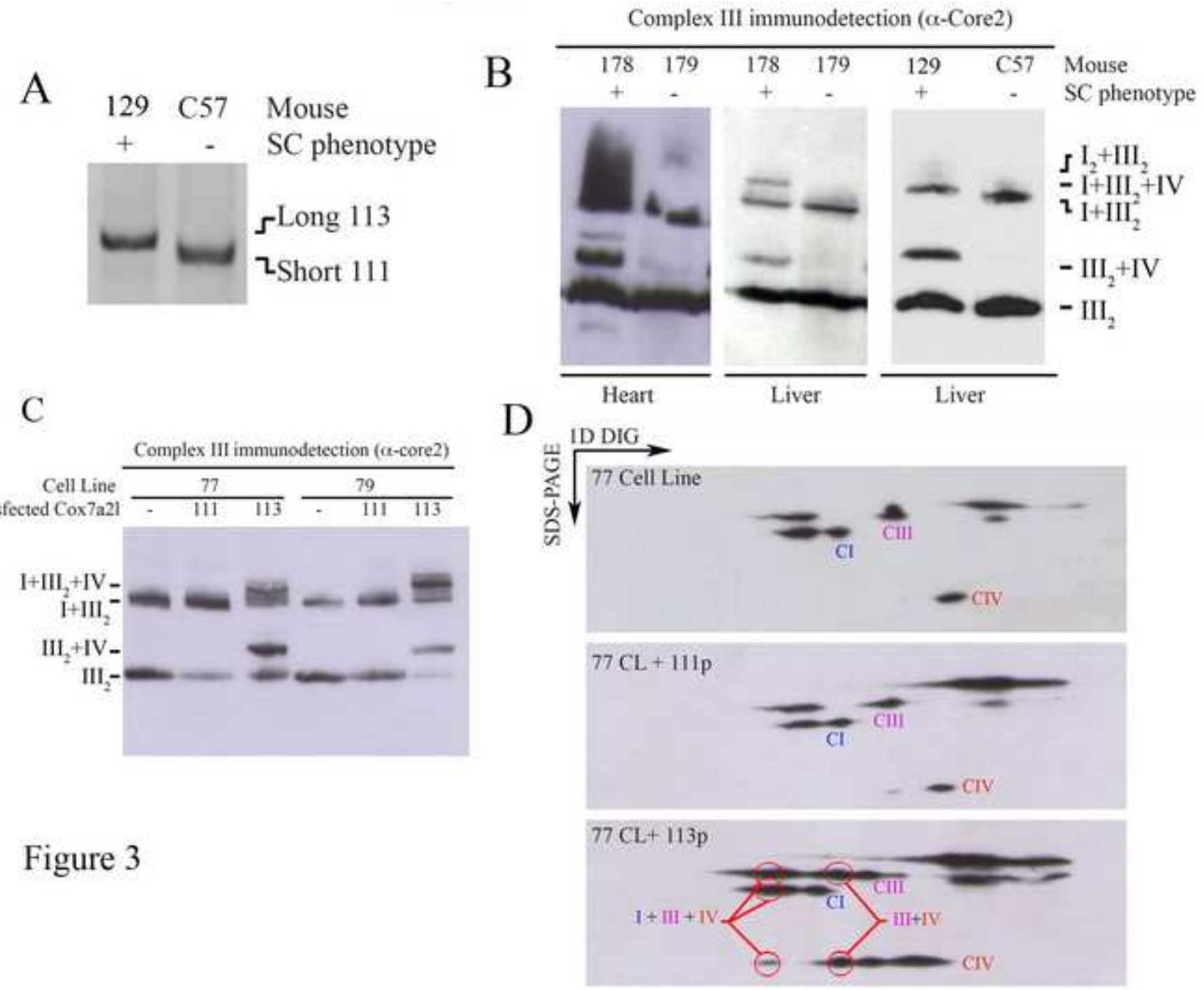

Figure 3

Figure 4

Click here to download high resolution image

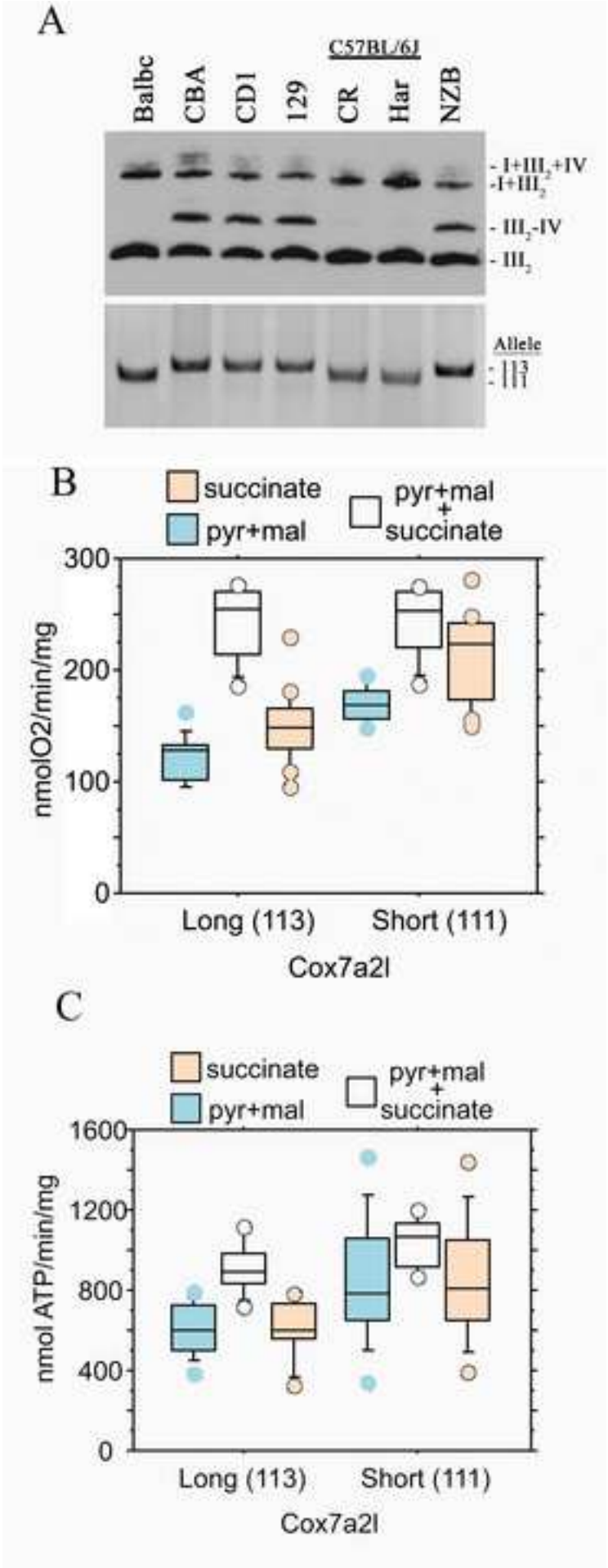

Figure 5

Click here to download high resolution image

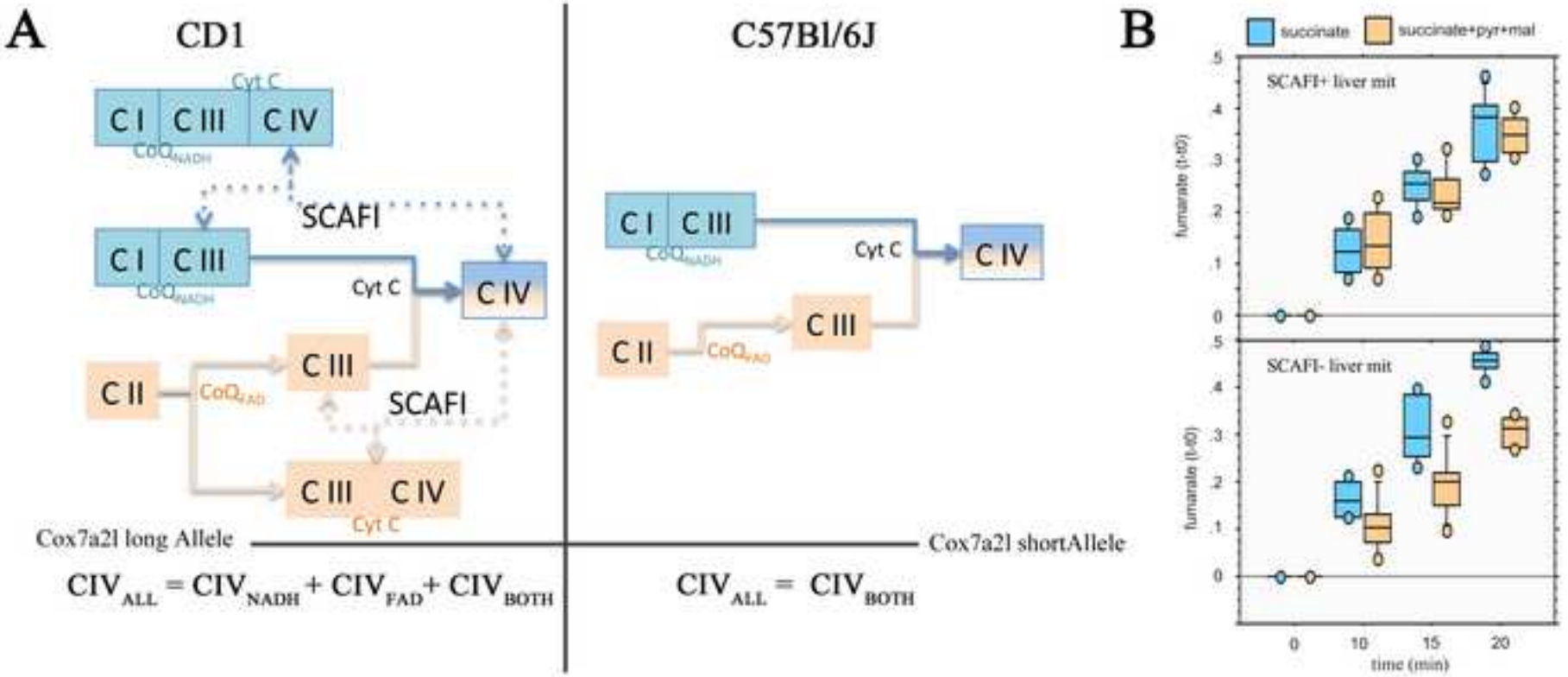

Figure 6

Click here to download high resolution image

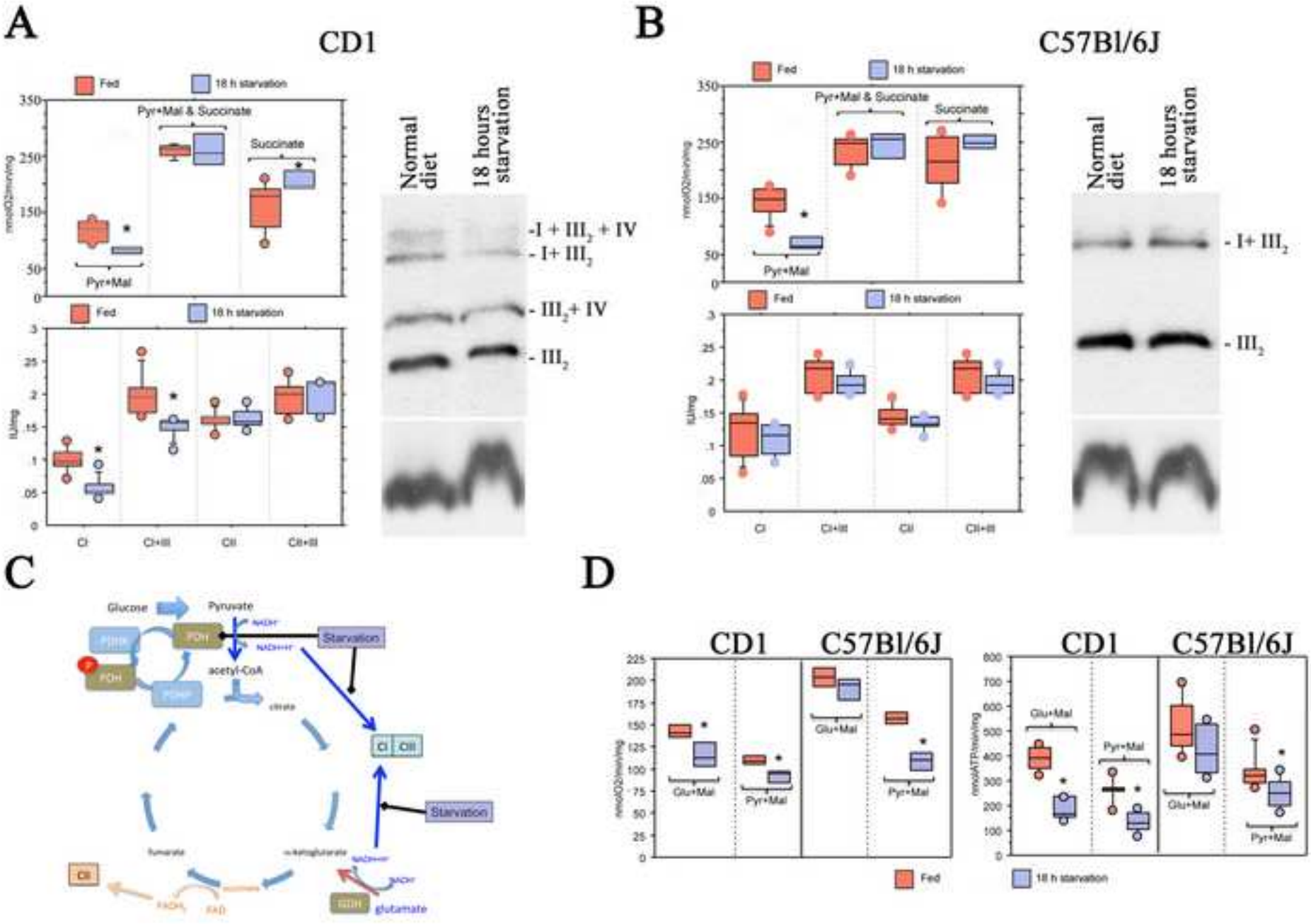

INVENTORY OF SUPPLEMENTARY MATERIAL

1.- Table S1. Primers Table

Description of the deoxyoligonucleotide primers utilized for the sequencing of the different complex III structural genes and chaperones.

2.- Characterization of the suppressor cell line:

Full explanation of the characterization of the suppressor cell line.

3.- Supplementary Figures:

- **Supplementary Figure 1.- Genetic and biochemical characterization of suppressor cells:** Linked to main figure 1
- **Supplementary Figure 2.- Characterization of complex III knocked-down cells (Core1-Kd cells):** Linked to main figure 2
- **Supplementary Figure 3. Cox7a2l is present in respiratory supercomplexes but not individual complexes:** Linked to main figure 3
- **Supplementary Figure 4. Supercomplex assembly and genotyping of six mouse fibroblast lines (77-82) from a mixed 129sv:C57BL/6 genetic background**: Linked to main figure 4
- **Supplementary Figure 5. Characterization of Cox7a2l in SC+ and SC- cell lines and in animal models:** Linked to main figure 5
- **Supplementary Figure 6.- Cox7a2l/SCAFI expression in C57Bl/6J-derived cell lines**: Linked to main figure 6

Super-assembly of respiratory complexes determines electron flux in the mitochondrial electron transport chain

Esther Lapuente-Brun[†], Raquel Moreno-Loshuertos[†] Rebeca Acín-Pérez, Ana Latorre-Pellicer, Carmen Colás, Eduardo Balsa, Ester Perales-Clemente, Pedro M. Quirós, Enrique Calvo, M. A. Rodríguez-Hernández, Plácido Navas, Raquel Cruz, Ángel Carracedo, Carlos López-Otín, Acisclo Pérez-Martos, Patricio Fernández-Silva, Erika Fernández-Vizarra and José Antonio Enríquez*

SUPPLEMENTARY MATERIAL

1.- Table S1. Primers Table

Description of the deoxyoligonucleotide primers utilized for the sequencing of the different complex III structural genes and chaperones.

2.- Characterization of the suppressor cell line:

Full explanation of the characterization of the suppressor cell line.

3.- Supplementary Figure Legends:

- **Supplementary Figure 1.- Genetic and biochemical characterization of suppressor cells:** Linked to main figure 1
- **Supplementary Figure 2.- Characterization of complex III knocked-down cells (Core1-Kd cells):** Linked to main figure 2
- **Supplementary Figure 3. Cox7a2l is present in respiratory supercomplexes but not individual complexes:** Linked to main figure 3
- **Supplementary Figure 4. Supercomplex assembly and genotyping of six mouse fibroblast lines (77-82) from a mixed 129sv:C57BL/6 genetic background**: Linked to main figure 4
- **Supplementary Figure 5. Characterization of Cox7a2l in SC+ and SC- cell lines and in animal models:** Linked to main figure 5
- **Supplementary Figure 6.- Cox7a2l/SCAFI expression in C57Bl/6J-derived cell lines**: Linked to main figure 6

1.- Table S1. Primers Table

Function	Gene	Accession number	Primer name	Primer sequence
Mitochondrial Complex III Subunits	*Uqcrc1*	NM_025407.2	Uqcrc1-F	GACGGAAGTTAGAAGATGGC
			Uqcrc1-R	CTGTGCAGACTTCCTGCCTA
	Uqcrc2	NM_025899.2	Uqcrc2-F	AGGGCAACTGCTAGAGCCAT
			Uqcrc2-R	GAGCTTTAAATACACGCATGTG
	Cyc1	NM_025567.2	Cyc1-F	GCACTAAAGGGGGCCGACAT
			Cyc1-R	CAAGCAGATACTGAACAGGG
	Uqcrfs1	NM_025710.1	RISP-F	TGGTTTGAGCAGCTGTCGCC
			RISP-R	TAGGCCCTGAGTCCACGTGT
	Uqcrb	NM_026219.1	VI-F	CGCTTCACTCTCAGGTCAAA
			VI-R	CCCACAGATCTTAACTAAAAG
	Uqcrq	NM_025352.2	Ucrq-F	GGTGTTAGGCCGTGGGAGG
			Ucrq-R	CAAGACTACAGTGTGGATTCC
	Uqcrh	NM_025641.3	VIII-F	ATCCCAAACCGGCTCCCGAC
			VIII-R	TGAGGAGGACGAATCTGCACAT
	Uqcr10	NM_197979.1	X-F	ATGTCGTCGCCGACGATCC
			X-R	TTACTCCTTGTTCTCATACTTG
	Uqcr11	NM_025650.2	XI-F	AGTATTGAGACCCTGCAGCG
			XI-R	TGAGGCCTCGGCACATGGTA
Mitochondrial Complexes Chaperones	*Bcs1l*	NM_025784	BCS1-F	CATCTGTGCTGCTTCTTTTCAAG
			BCS1-R	GCAGATCATGGCCTGGTGGGTCA
	Oxa1l	NM_026936	Oxa1-F	TTCCCGGCAAGATGGCGAG
			Oxa1-R	CAGAGTGAGCACAGAACACGTCA

2.- Characterization of the suppressor cell line:

We randomly induced suppressor mutations in A22 cells (Bayona-Bafaluy et al., 2008) by chemical mutagenesis followed by selection for uridine autotrophy. After mutagenesis, cells were cultured in selection medium (lacking uridine), which does not support growth of the original A22 cells (referred from here on as mutant or *M* cells). In this way, we isolated mA22, a cell line able to survive without uridine supplementation (hereafter suppressor or S cells). Interestingly, *S* cells were also able to grow in medium in which glucose was replaced by galactose (Fig S1A).

RFLP analysis revealed that the suppressor phenotype was not due to a reversion in the original mutation in *mt-Cytb* (Fig. S1B). Furthermore, full sequencing of *S* cell mtDNA discarded the possible role of a secondary mutation in either *mt-Cytb* or any other mtDNA-encoded gene. To directly demonstrate the nuclear origin of the suppressor mutation, we performed two cybridization assays (Acin-Perez et al., 2003; Moraes et al., 2001). First, nuclei from suppressor cells (puromycin resistant) were transferred to enucleated mutant cells (geneticin resistant); proper nucleus replacement was confirmed by geneticin sensitivity and puromycin resistance. In the second assay, mitochondria of *M* cells were replaced with mitochondria from *S* cells; the cybrids were tested for geneticin resistance and puromycin sensitivity to ensure that only mitochondria were transferred (Fig S1C). In both assays the cybrids were then cultured in galactose-containing medium. While none of 45 independent clones with the *M* nucleus was able to survive in galactose, all clones containing mutant mtDNA and the *S* nucleus survived, indicating that the suppressor genetic alteration was transferred with the nucleus and not with mtDNA. In a further test, sequencing of the entire set of cDNAs for structural complex III subunits (Uqcrc1, Uqcrc2, Cyc1, Risp, Uqcrcb, Uqcrcq, Uqcrh, Uqcr10, Uqcr), as well as the chaperones BCS1L and OXA1, did not detect any mutation that would explain the suppressor phenotype (See Table S1 for primer sequences).

The fact that *S* cells become both uridine independent and able to grow in galactose indicates that, despite the mutation in *mt-Cytb*, they have recovered OXPHOS competence. Indeed, *S* cells show normal respiration ability (Fig S1D), implying that complexes III and I are again assembled. Western blot of native gels showed that ≈11%

of the normal assembled complex III dimers were present, being able to stabilize ≈50% of fully assembled complex I (Fig S1E). *S* cells have thus recovered the ability to reduce oxygen and, despite the modest recovery in the amount of complexes I and III, their respiration capacity was even higher than that of control cells grown under the same conditions (Fig S1D).

References

Acin-Perez, R., Bayona-Bafaluy, M.P., Bueno, M., Machicado, C., Fernandez-Silva, P., Perez-Martos, A., Montoya, J., Lopez-Perez, M.J., Sancho, J., and Enriquez, J.A. (2003). An intragenic suppressor in the cytochrome c oxidase I gene of mouse mitochondrial DNA. Hum Mol Genet *12*, 329-339.

Bayona-Bafaluy, M.P., Movilla, N., Perez-Martos, A., Fernandez-Silva, P., and Enriquez, J.A. (2008). Functional genetic analysis of the mammalian mitochondrial DNA encoded peptides: a mutagenesis approach. Methods Mol Biol *457*, 379-390.

Moraes, C.T., Dey, R., and Barrientos, A. (2001). Transmitochondrial technology in animal cells. Methods Cell Biol *65*, 397-412.

3.- Supplementary Figures .-

Supplementary Figure 1.- Genetic and biochemical characterization of suppressor cells. A) Growth ratios for each cell line in medium containing galactose as the energy source versus medium containing glucose. Mutant cells (*M*) harbor a mutation in the *mt-Cytb* gene that prevents assembly of mitochondrial complex III. These cells are unable to grow in galactose-containing medium, while isogenic control cells (*C*) or suppressor cells (*S*), generated by random mutagenesis of *M* cells, do grow. n=4, 2 and 4 for *C*, *M* and *S* cells respectively; differences between *C* and *S* doubling times ratio (DT_{Gal}/DT_{Glu}) are significant according to Fisher's PLSD post-hoc test: p=0.0006. B) Chromatogram showing the G15263A transition in the *mt-Cytb* gene of *S*

cells (left) and RFLP analysis of the mutation in homoplasmy (right). C) Scheme of cybridization experiments showing the nuclear origin of the suppressor mutation. D) Endogenous (coupled) and maximal (uncoupled) rates of oxygen consumption in intact cells. *M* cells do not respire. n=4, 3 and 6 for *C*, *M* and *S* cells; paired differences between all cell lines are significant for endogenous and maximal respiratory rates according to Fisher's PLSD post-hoc test: Endogenous respiration: p=0.0001 between *C* and *S* cells and p<0.0001 between *M* and any other cell line. Maximal respiration: p=0.0003 between *C* and *S* cells and p<0.0001 between *M* and any other cell line. E) Western blot detection of the different assembled complexes after blue native gel electrophoresis (BNGE). The blot was probed with monoclonal antibodies to complexes I (anti NDUFA9), III (anti Core2), IV (anti COI) and II (anti SDHA (Fp70)). F) CoQ content in *C*, *M* and *S* cells, detected by HPLC.

Supplementary Figure 2.- Characterization of complex III knocked-down cells (Core1-Kd cells). A) Western blot of Core protein 1 after SDS-PAGE. Actin was detected as a loading control. Mock; control cells transduced with empty vector. The degree of depletion (indicated above the lanes) was quantified with Odyssey CLx. B) Characterization of complex-III-containing supercomplexes in non-interfered and Core1-Kd cells. Decreased content of complex III+IV and dimeric complex III can be observed in Core1-Kd cells. C) Spectroscopic measurement of the activities of isolated complex I and of complex I or II combined with complex III in non-interfered and Core1-Kd control cells (71.6% depletion). Complex IV activity was measured as a control. Data were normalized by CS activity and are represented as means ± SD. Asterisks indicate significant differences with respect to control cells, tested by ANOVA and post-hoc Fisher PLSD (p<0.05). n≥3 for all measurements. Fisher's PLSD post-hoc test of paired differences between cell lines is significant for all analyses

except for complex IV. Complex I: p=0.0333; Complex I+III: p=0.0298; and Complex II+III: p<0.0001.

Supplementary Figure 3. Cox7a2l is present in respiratory supercomplexes but not individual complexes. A) Determination of the protein composition of bands excised from blue native polyacrylamide gels by liquid chromatography coupled to tandem mass spectrometry. The figure shows OXPHOS proteins from complexes I to IV detected in each excised band (gel slices 1-20) from control cells and a cell line deficient for complex I (Complex I ^{KO}). Pink indicates components of complex IV (CIV), dark blue indicates CIII, orange CII, and light blue CI. The numbers of unique peptides detected for each protein in the band are indicated (# signifies more than 9 peptides). Note that Cox7a2l peptides (red arrows) are found in gel areas showing interaction of complexes III and IV. B) Example blue native polyacrylamide gel electrophoresis (BNGE) analysis of control cells and the ComplexI ^{KO} cell line. After Coomasie staining, twenty bands were excised from the control cell lanes and the corresponding migration positions in the mutant lanes. C) Amino-acid sequence of Cox7a2 and MS/MS spectra from the three identified doubly-charged Cox7a2-derived tryptic peptides. Sequences of the three matched tryptic peptides unambiguously detected by LC-MS are shown in capitals and underlined. Dots in the sequence mark trypsin cleavage sites. Numbers indicate the residue position in the protein sequence. D) Amino-acid sequence of the Cox7a2-like protein (Cox7a2l) and MS/MS spectra from the three doubly-charged Cox7a2l-derived tryptic peptides unambiguously detected by LC-MS. Tryptic peptides are highlighted as in D. The most intense signals on the MS/MS spectra in C and D correspond to the main fragmentation series (b-amino and y-carboxy). Neutral loss of water is labeled ‘o’. Accompanying series a2 ions are labeled

*. Mox indicates the oxidation of methionine in one MS/MS spectrum. Doubly-charged fragments are marked with superscript 2+.

Supplementary Figure 4. Supercomplex assembly and genotyping of six mouse fibroblast lines (77-82) from a mixed 129sv:C57BL/6 genetic background. A,B) Western blot after (A) BNGE of digitonin-permeabilized mitochondrial samples or (B) BNGE followed by second dimension denaturing SDS-PAGE. Specific antibodies detected complexes I (Nduaf9), II (SDHA), III (core2) and IV (CoxIV). Red boxes indicate supercomplex assembly; blue brackets mark individual complexes. Two phenotypes were identified (supercomplex competent, SC+, and supercomplex non-competent, SC-), with interaction between CIII and CIV lost in SC- cell lines (77, 79, 80). C) SNP differences on chromosome 17 between the SC- and SC+ genotypes. Discriminant SNPs (see text) are coded as 1, non-discriminant SNPs as -1 and monomorphic SNPs as 0. Selected regions are shown in greater detail. (Image obtained from the Ensembl website, http://www.ensembl.org/index.html.).

Supplementary Figure 5. Characterization of Cox7a2l in SC+ and SC- cell lines and in animal models. A) Cox7a2l allele analysis reveals two alleles in the mouse fibroblast lines, encoding 111 amino acid (Short 111) and 113 amino-acid (Long 113) proteins. SC- cells are homozygous for the Short 111/microdeleted allele, whereas SC+ cells contain both alleles. B) Cox7a2l immunodetection in total protein extracts; the Cox7a2l signal is lost in SC- cells. The lower gel shows immunoreactivity of the anti-Cox7a2l antibody to *in vitro* synthesized HA-tagged short (S) and long (L) Cox7a2l proteins. C) Comparative phylogenetic analysis of Cox7a2l proteins reveals high conservation of a proline residue absent in the C57BL/6 background (Image generated with the Clustawl 2.1 multiple sequence alignment package).

Supplementary Figure 6.- Cox7a2l/SCAFI expression in C57Bl/6J-derived cell lines. A) Western blot after BNGE, probed with antibody specific for complex III (anti Core2). Supercomplex formation in C57-derived cells is rescued only when cells are transfected with the 113 amino acid-long version of Cox7a2l (+113p). B) *Top:* Overall oxygen consumption in DMEM culture medium by intact C57 fibroblasts non transfected or transformed with the short (sc111) or long (sc113) form of SCAFI and compared with TMPD-driven respiration (complex IV only) in the same cells. *Bottom:* Complex IV respiration as a proportion of total respiration in C57 fibroblasts expressing functional or non-functional Cox7a2l/SCAFI (n=3). C) Substrate-driven (pyruvate or succinate) oxygen consumption and ATP synthesis rate in digitonin-permeabilized C57 fibroblasts expressing functional or non-functional SCAFI, compared with the simultaneous addition of both substrates.

Supplemental Figure 1

Click here to download high resolution image

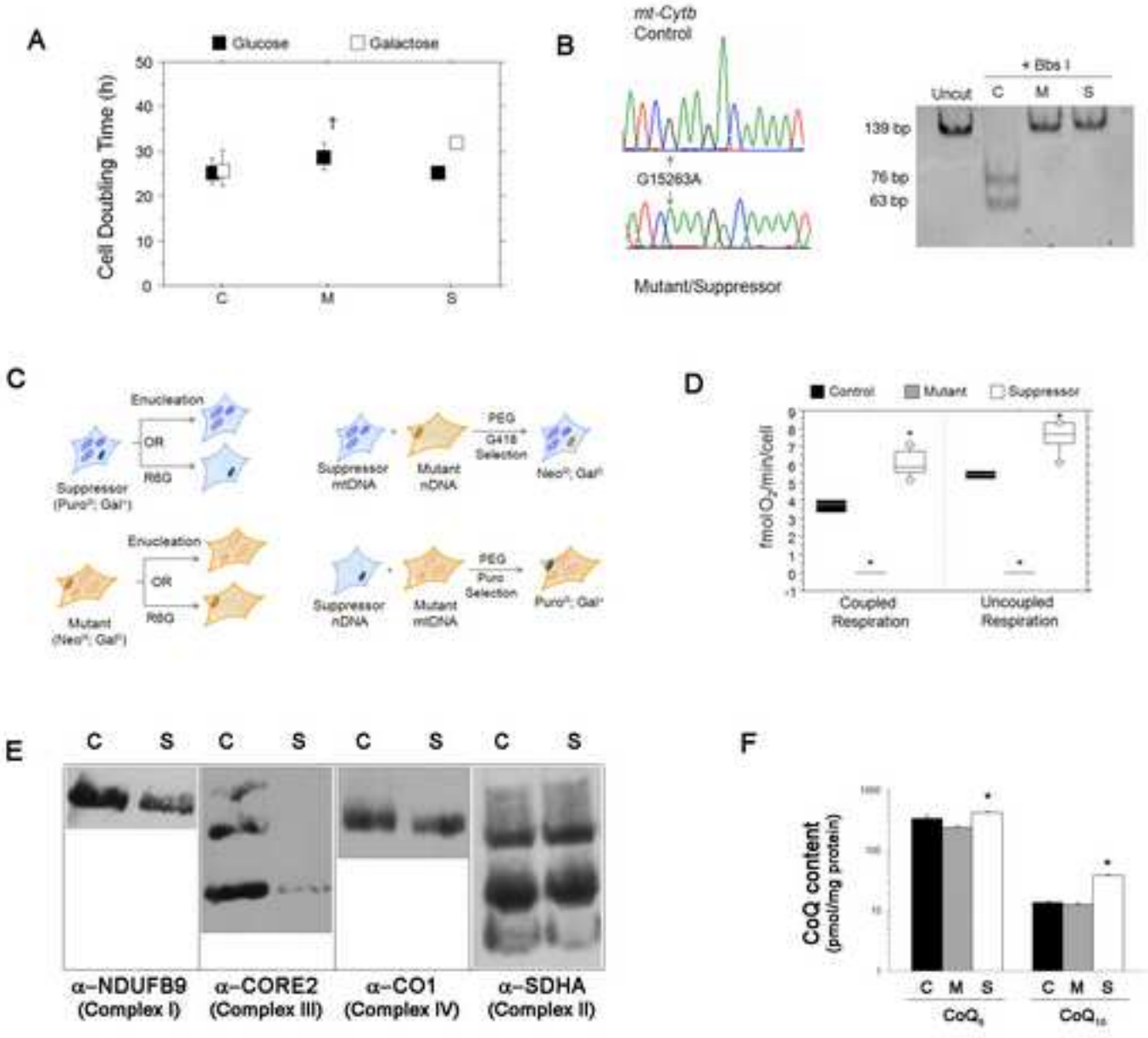

Supplemental Figure 2
Click here to download high resolution image

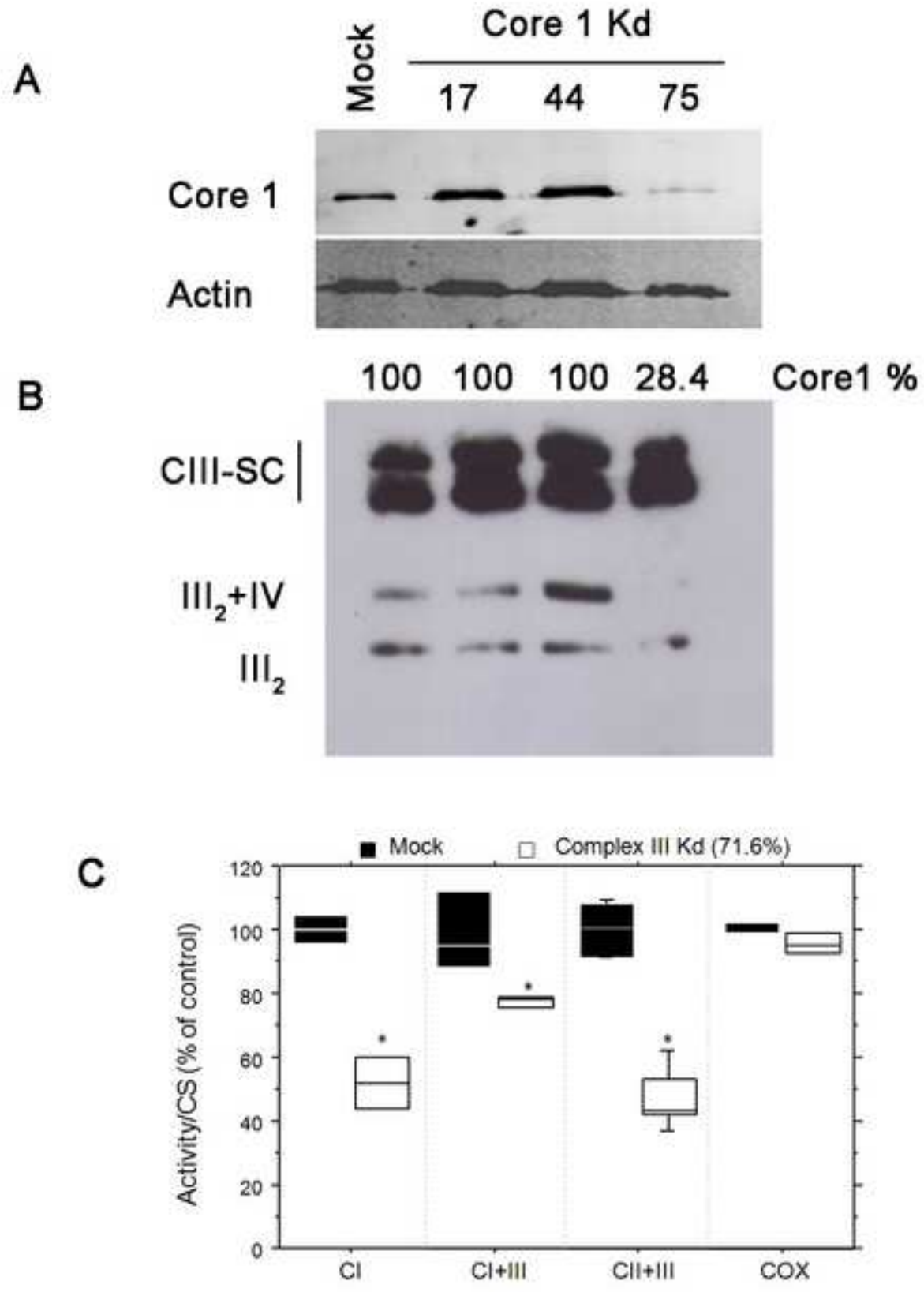

Supplemental Figure 3
Click here to download high resolution image

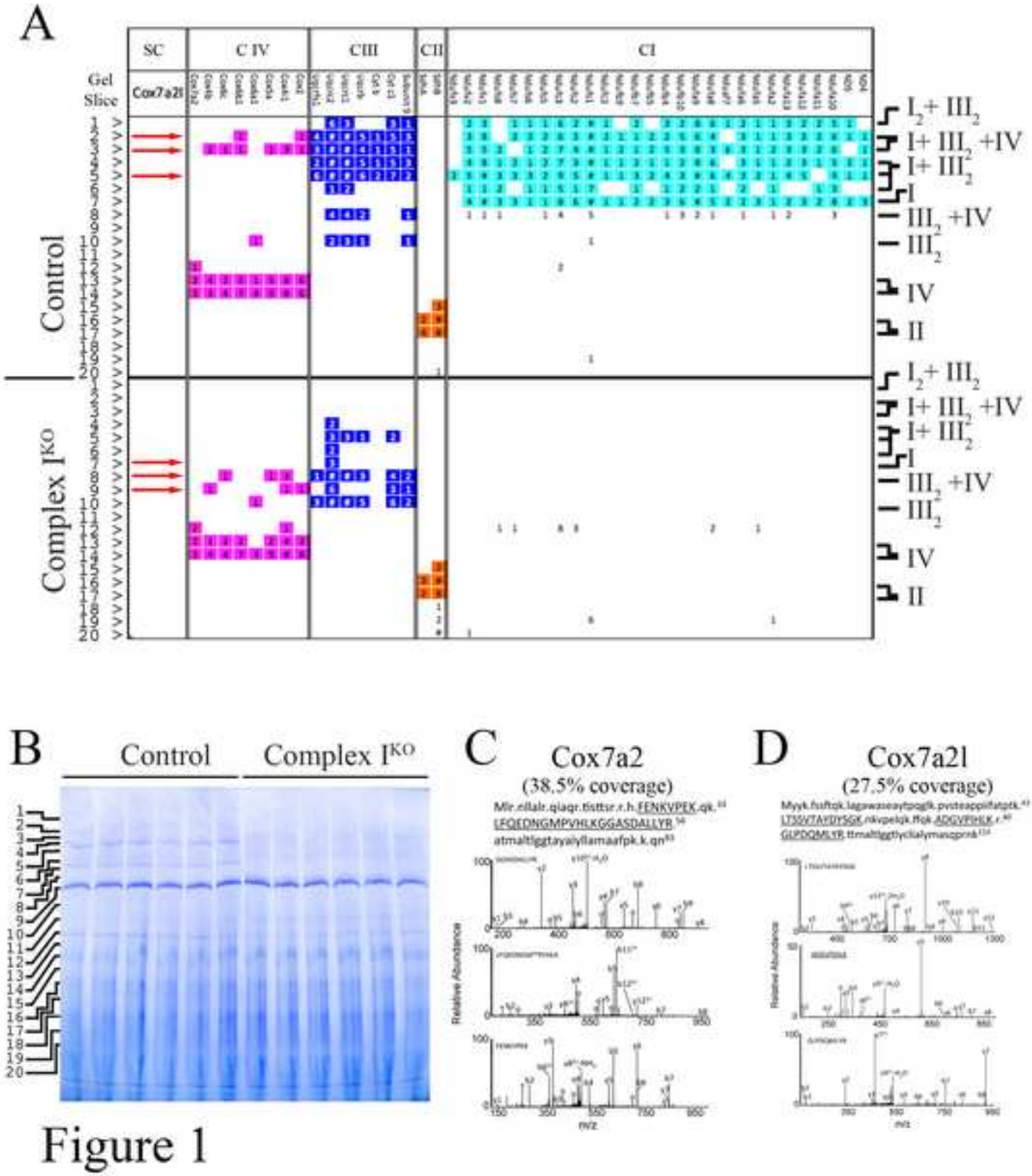

Figure 1

Supplemental Figure 4

Click here to download high resolution image

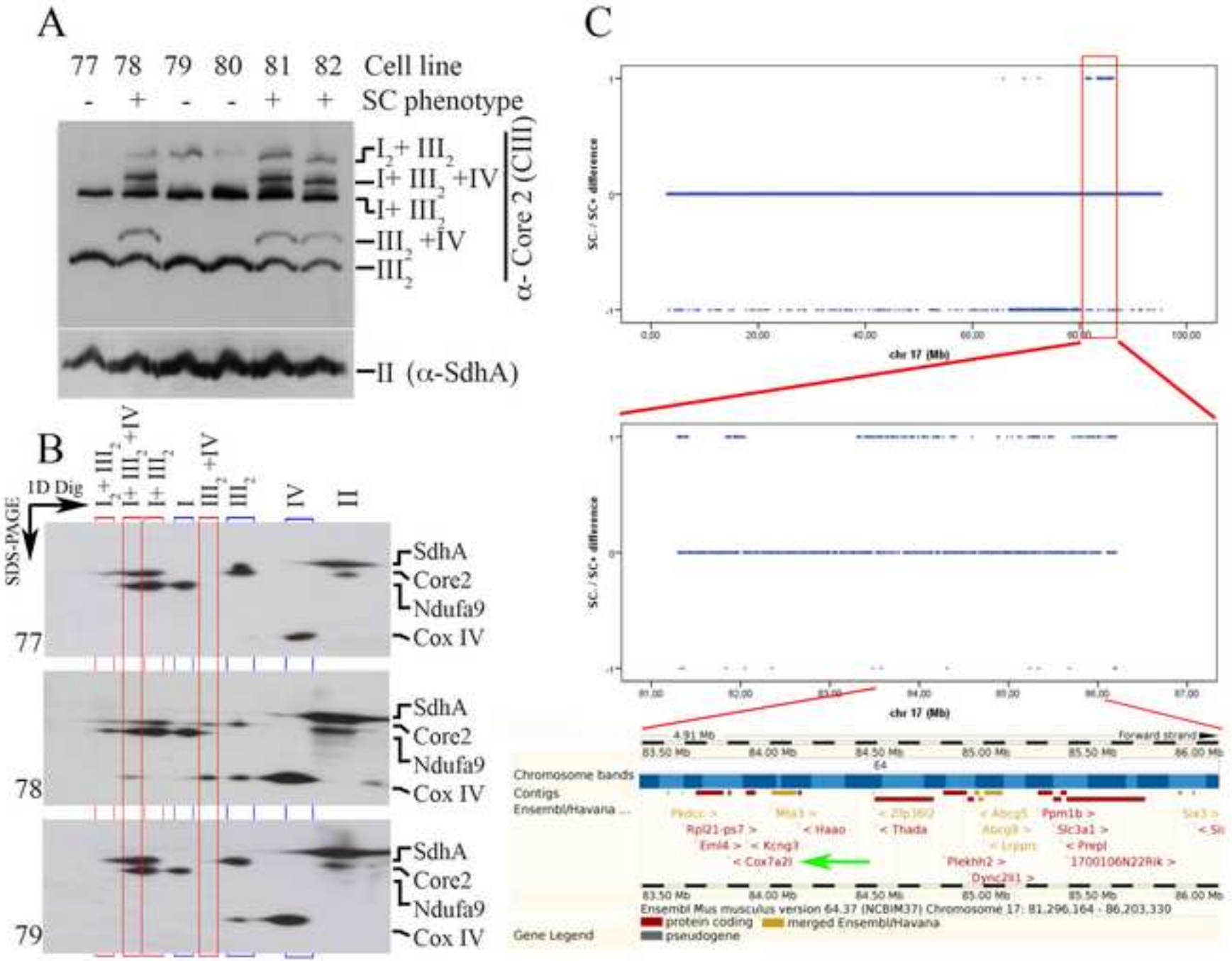

Supplemental Figure 5
Click here to download high resolution image

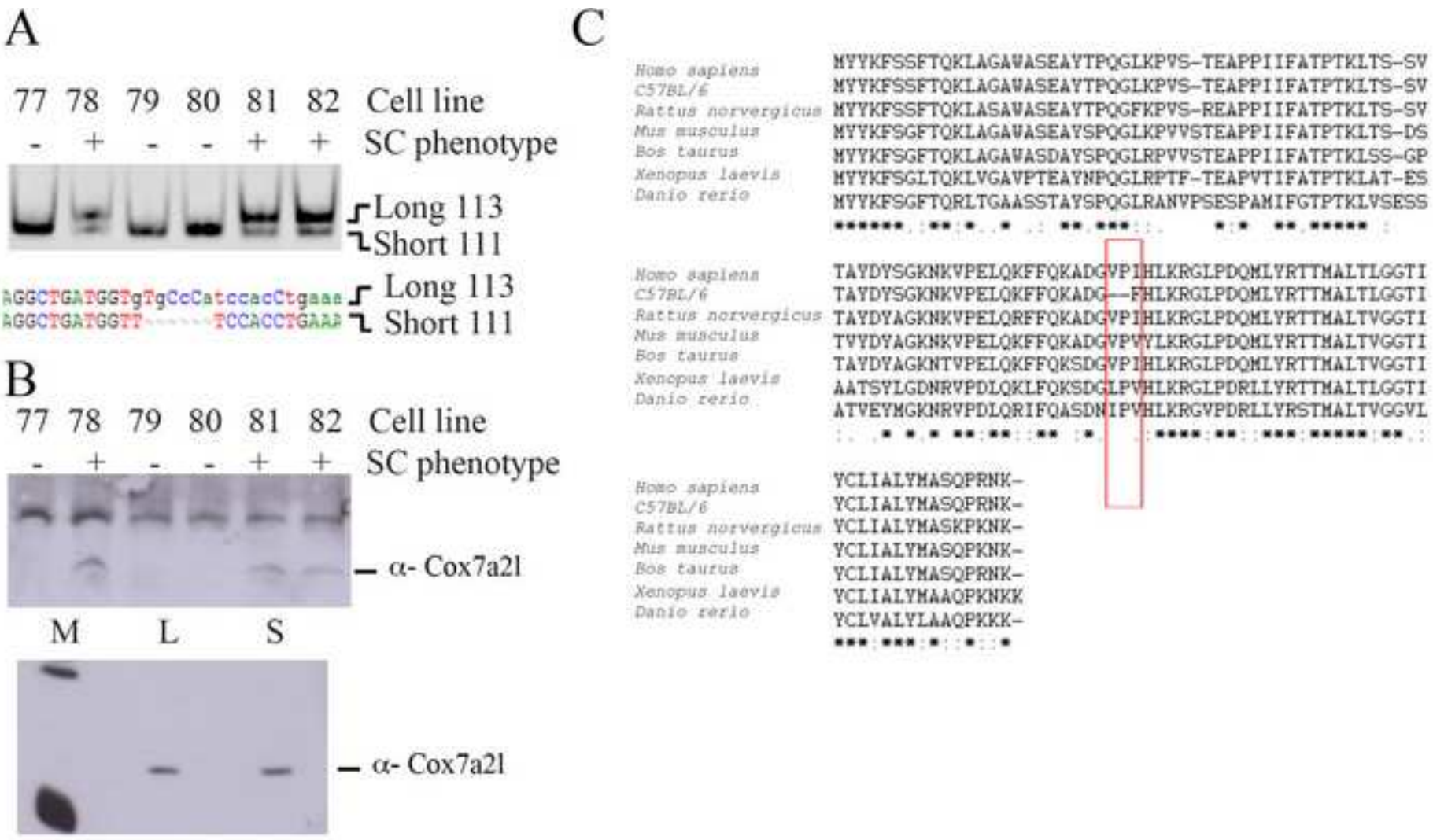

Supplemental Figure 6

Click here to download high resolution image

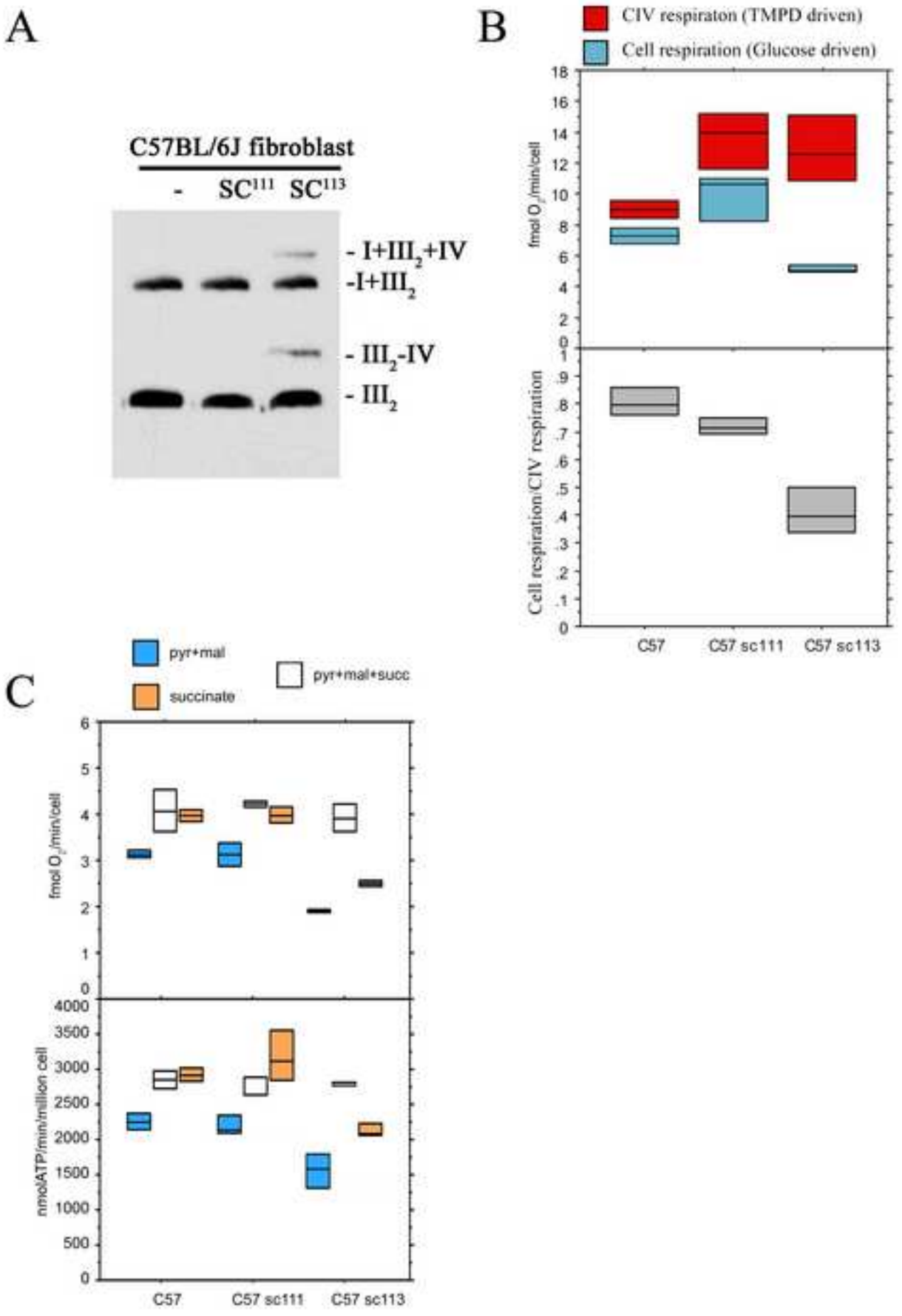

Discusión

Discusión

La influencia de la fluctuaciones en las tensiones de oxígeno sobre la actividad mitocondrial han ido ganando relevancia por sus amplias implicaciones en diversos procesos fisiopatológicos. Durante una hipoxia moderada (1-2% O_2), las células empiezan a expresar una batería de genes, dependientes de HIF, que reprograman el metabolismo atenuando el consumo de oxígeno mitocondrial, lo cual protege a la célula frente a una excesiva producción de ROS.

A nivel molecular, hemos visto que la hipoxia disminuye el consumo de oxígeno intracelular y la actividad el complejo I de la cadena de transporte de electrones gracias a la inducción, vía HIF, de la proteína NDUFA4L2. Nuestros datos claramente indican que NDUFA4L2 es un gen dependiente de HIF, lo cual resalta el papel de HIF en la reprogramación metabólica mitocondrial al mismo tiempo que revela a NDUFA4L2 como un elemento fundamental en la respuesta al estrés hipóxico. La inducción de NDUFA4L2 ha sido observada en distintas líneas celulares, cultivos primarios, así como en tejidos de animales sometidos a hipoxia, sugiriendo un papel en la fisiología de la adaptación del organismo a fluctuaciones de oxígeno.

HIF, NDUFA4L2 y el metabolismo mitocondrial:

Varias isoformas de la piruvato deshidrogenasa kinasa (PDK1, PDK3 y PDK4), también son inducidas por el eje PDH-HIF en hipoxia. Esta inducción de las PDKs tiene como función fosforilar a la PDH inhibiendo su actividad, esto reduce la conversión de piruvato a acetil-CoA, reprimiendo el ciclo de Krebs y disminuyendo la aportación de equivalentes de reducción en forma de NADH a la ETC. Así, las PDKs podrían cooperar con NDUFA4L2 para reducir la actividad mitocondrial bajo condiciones de hipoxia moderada, pero también es concebible que NDUFA4L2 tenga otras funciones biológicas que no pueden ser realizadas por las PDKs. Por ejemplo, cuando los metabolitos que alimentan el ciclo de Krebs provienen de rutas diferentes a la glucolisis (por ejemplo, la glutaminosis o la oxidación de acidos grasos), la inhibición de la PDH sería en vano, y se requeriría actuar a nivel de la ETC, justo donde NDUFA4L2 cumple su función.

También se han descrito otros mecanismos que pueden reprimir la actividad mitocondrial. Así, la hipoxia también aumenta la expresión del microRNA-210, el cual reprime ISCU1/2. Estas proteínas (Iron-sulfur cluster assembly enzyme ISCU)

están encargadas de facilitar el ensamblaje de los grupos hierro-azufre, incluidos los del complejo I, complejo III y la aconitasa. Estos grupos ferrosulfurados son críticos para el correcto transporte de los electrones y las reacciones redox en la mitocondria. Como resultado, el microRNA-210 reprime la respiración mitocondrial. En nuestro modelo, y en concordancia con estudios previos, no observamos disminución de ISCU1/2 antes de las 48 horas de hipoxia y a unas tensiones de oxigeno de 0,5%. Sin embargo NDUFA4L2 ya es funcional a las 24 horas y al 1% de O_2. Además la recuperación de los niveles de ISCU1//2 en hipoxia no afecta significativamente a la proliferación celular. De hecho, esta descrito que los efectos anti-miR-210 en la proliferación de las células HeLa, no sucede hasta las 48 horas y concentraciones de oxigeno cercanas a la anoxia (0,01% O_2).

Es sorprendente que la inhibición del complejo I sucede en condiciones de hipoxia moderada (1% de O_2), y estas tensiones de oxígeno no parecen disminuir ISCU1/2. Además la bajada de ISCU1/2 no se aprecia hasta las 48 horas, sin embargo la inhibición del complejo I sucede antes de 24 horas. Esto abre una ventana de 24 horas en la cual NDUFA4L2 podría estar actuando antes que la represión de ISCU1/2.

Hemos comprobado que, la inhibición del complejo I dependiente de NDUFA4L2 ocurre sin alterarse los niveles de este complejo, sin embargo el eje miRNA-210-ISCU1/2 claramente implica una bajada en la cantidad de complejo I. Esta modulación temprana de carácter cualitativo (llevada a cavo por NDUFA4L2), seguida de una más tardía, pero de carácter cuantitativo (llevada a cavo por ISCU1/2) representa un posible modelo por el cual HIF garantiza un fino control del complejo I bajo condiciones de hipoxia.

Como ya hemos indicado, es probable que la atenuación de la actividad del complejo I por parte de NDUFA4L2 implique interacciones indirectas. Futuros estudios para averiguar el preciso mecanismo de actuación de NDUFA4L2, y con que proteínas puede estar interaccionado serán clave a la hora de entender el mecanismo molecular y se me antojan imprescindibles si en algún momento se pretendiesen desarrollar activadores o inhibidores terapéuticos.

Otros componentes de la ETC también están implicado en la homeostasis de la actividad mitocondrial en hipoxia. En concreto el complejo IV también sufre un cambio en el contenido de sus subunidades. De este modo la hipoxia promueve el intercambio de la subunidad COX4-1 por la COX4-2, un efecto que está mediado por HIF, y se piensa esta encaminado a optimizar la eficiencia de transporte de electrones

para disminuir la producción de ROS (Fukuda et al. 2007). Ya que nuestros datos indican que NDUFA4 disminuye a nivel de proteína cuando sometemos las células a hipoxia, podíamos especular sobre un intercambio de subunidades, donde la inducción de NDUFA4L2 este tomando el lugar de NDUFA4 en el complejo I y reduciendo de algún modo su actividad. Sin embargo, los MEFs KO para NDUFA4L2 siguen reprimiendo NDUFA4 en hipoxia, mientras que la actividad del complejo I no se afecta, con lo cual descartamos que la represión del complejo I este mediada por la bajada a nivel de proteína de NDUFA4. Así pues, hemos de destacar que tanto la localización de NDUFA4 como su función dentro del complejo I aun no ha sido esclarecida.

Relación entre NDUFA4L2 y el estrés oxidativo:

La ETC es un punto de gran producción de superóxido. Esto sucede cuando los electrones saltan directamente al O_2 durante su transporte a través de los complejos. Hay diferentes sitios de producción de ROS en la mitocondrias de mamíferos (Murphy 2009). Se ha propuesto que sitio de reducción de la ubiquinona por el complejo I y el paso de cesión de los electrones de ésta a complejo III (el ciclo Q), son los lugares donde la producción de superóxido es máxima(Liu et al. 2002; Raha & Robinson 2000; St-Pierre et al. 2002; Votyakova & Reynolds 2001). Aunque la producción de superóxido en mitocondrias aisladas correlaciona con las tensiones de oxígeno (Liu et al. 2002), está generalmente aceptado que los niveles de ROS aumentan durante los primeros instantes de hipoxia (Brunelle et al. 2005; Guzy et al. 2005). En línea con los resultados obtenidos por otros grupos, nosotros también vemos una ligero aumento de los ROS en hipoxia. (usando las sondas fluorescentes DCFDA y MitoSOX). Sin embargo estos ROS aumentan de forma exacerbada cuando interferimos NDUFA4L2, lo que nos lleva a pensar que la inducción de esta proteína mantiene los niveles de ROS bajo control y protege frente al daño oxidativo. Saber si estos efectos son debidos directamente a NDUFA4L2, o ocurren indirectamente a través de la modulación de otras proteínas mitocondriales requerirá futuros experimento. Aún así, el hecho de que el potencial de membrana mitocondrial también aumenta simultáneamente con los niveles de ROS sugiere que ambos eventos están íntimamente relacionados, como ya ha sido demostrado con anterioridad (Korshunov et al. 1997; Votyakova & Reynolds 2001).

La producción de ROS bajo condiciones de hipoxia no debe llegar al niveles tóxicamente letales para la célula, en nuestros modelos celulares de estudio, puesto

que no observamos marcadores de muerte celular, pero si una inhibición de la proliferación. Por otro lado hay numerosos estudios que muestran como la hipoxia disminuye la proliferación celular (Gardner 2000; Goda et al. 2003). Es interesante la observación de que tanto las células interferidas para NDUFA4L2 como los MEFs KO muestran una inhibición en la proliferación aun mayor, que sucede en paralelo con el aumento en la acumulación de ROS y marcadores de daño oxidativo en el ADN (fosforilación de H2AX). Nosotros postulamos que las células incapaces de inducir NDUFA4L2 no pueden disminuir la actividad de la ETC, como consecuencia de ello los niveles de ROS en hipoxia se disparan. Estos ROS dañan el material genético, y esto es sentido por la célula que intentará poner en marcha mecanismos para paliarlo, reclutando la maquinaria para corregir los errores genéticos que se hayan podido producir y deteniendo el ciclo celular, de ahí que observemos una disminución en la tasa de replicación celular.

Varios estudios han revelado que la reducción en el consumo de oxigeno mitocondrial que ejerce el eje sensor de oxígeno PHDs-HIFs prepara a las células a tolerar futuras condiciones de hipoxia/isquemia más severas. Nosotros pensamos que la atenuación del complejo I y por ende de la ETC que lleva a cabo la inducción de NDUFA4L2 puede jugar un papel importante en el pre-condicionamiento isquémico. De hecho, algunos estudios han concluido que la inhibición parcial del complejo I, con dosis sub-letales de amobarbital (un inhibidor reversible del complejo I) previene del daño isquémico, el cual esta causado en gran medida por un estrés oxidativo masivo (Aldakkak et al. 2008; Q. Chen, Hoppel & Lesnefsky 2006b; Q. Chen, Moghaddas, Hoppel & Lesnefsky 2006a).

Modelos in vivo: Ratones NDUFA4L2-KO:

Un dato que nos llamó fuertemente la atención, fue el fenotipo tan radical de los ratones KO para NDUFA4L2. Jamás pudimos anticipar que dicho fenotipo implicaría una muerte del embrión a los pocos minutos de nacer. Desconocemos cual es la expresión de NDUFA4L2 en el momento del nacimiento, así que precisar en que tejidos se esta expresando se antoja imprescindible si queremos desentrañar los motivos de tal letalidad. Los ratones deficientes en NDUFA4L2, que podrían considerarse como un modelo de ganancia de función del complejo I según nuestros datos, muestran una letalidad perinatal, lo cual pone de relevancia el papel fundamental de esta proteína en condiciones *"in vivo"*. De manera similar, modelos murinos con deficiencias en complejo I también muestran letalidad al poco de

nacer(Kruse et al. 2008), lo cual indica que los parámetros fisiológicos de actividad de complejo I, al menos durante el nacimiento, han de ser controlados dentro de unos rangos concretos. Hasta el momento hemos sido incapaces de dar explicación al fenotipo letal que muestran los embriones. La hipótesis más plausible es la del estrés oxidativo. La falta total de NDUFA4L2 podría suponer una desregulación en la actividad mitocondrial con el consiguiente incremento de los niveles de ROS. Esto podría afecta negativamente de dos formas: (1) Los niveles suprafisiológicos de ROS desencadenarían una muerte celular y del tejido afectado. (2) Los ROS, que también pueden actuar como segundos mensajeros, podrían desencadenar una señalización patológica, y en último termino ser incompatible con la vida. Necesitaremos hacer un estudio más a fondo del fenotipo de estos ratones y desentrañar las causas moleculares y fisiológicas de su muerte. Desde el ámbito clínico, la comprensión de su fenotipo pueda dar luz a ciertas enfermedades mitocondriales que afectan a los infantes. En la actualidad estamos siguiendo estas vías líneas de investigación para analizar la causa de la mortalidad perinatal de los ratones KO para NDUF4L2.

Regulación inversa de NDUFA4L2 y NDUFA4 en hipoxia:

Un dato curioso es la regulación antagónica que sufren NDUFA4L2 y NDUFA4 bajo condiciones de hipoxia. Recordar que ambas proteínas son parálogas y tienen una identidad en su secuencia de aminoácidos mayor del 70%. Nuestros datos muestran que, mientras NDUFA4L2 sufre una potente inducción tanto en sus niveles de RNA mensajero como de proteína, la proteína de NDUFA4 se va reduciendo sin que haya ningún cambio en su RNA mensajero. Por los datos obtenidos parece ser que la inducción de NDUFA4L2 no influye en la bajada de NDUFA4 y al contrario, por lo que todo indica a que es un factor externo el que esta reduciendo los niveles de NDUFA4, quizás por un aumento en su degradación o bajada de su traducción. Tampoco esta claro si HIF esta detrás de esta bajada de NDUFA4. Futuros experimento inhibiendo o sobre-expresando alguno de los factores del eje PHDs-HIF nos ayudara a esclarecer esta regulación.

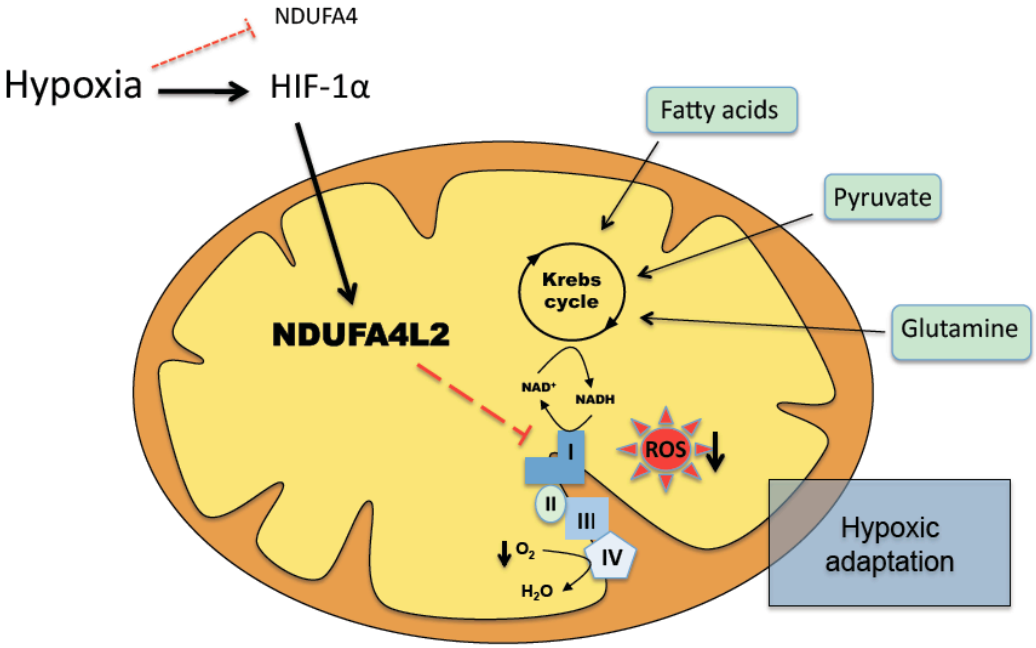

Modelo 1. La estabilización en hipoxia de HIF-1α induce la expresión de NDUFA4L2. Esto conlleva una disminución del consumo de oxígeno mitocondrial a causa de la inhibición de la actividad del complejo I. Todo este proceso esta encaminado a disminuir la producción dañina de ROS. Por otra parte la hipoxia reduce los niveles de NDUFA4.

NDUFA4 es una subunidad del complejo IV y no del complejo I:

NDUFA4 ha sido catalogada como una proteína supernumeraria estructural del complejo I(Carroll et al. 2006). Sin embargo, los autores encontraron varias evidencias contradictorias que les hacían dudar sobre si NDUFA4 era en realidad una proteína "bona fide" del complejo I. En sus estudios concluían que NDUFA4 no se pudo detectar en todas las preparaciones de complejo I y, más importante, que su presencia siempre correlacionaba con contaminaciones de ciertas subunidades del complejo IV, como es el caso de COX-VIb. Estudios más reciente muestran como el patrón de expresión de NDUFA4 es divergente si se compara con las otras subunidades del complejo I codificadas en el núcleo (Garbian et al. 2010).

Nuestros estudios demuestran claramente como, NDUFA4, es una subunidad del complejo IV y no del complejo I. Tanto ensayos de proteómica y electroforesis en SDS y nativa, como otros más funcionales interfiriendo establemente esta proteína, indican que NDUFA4, es una nueva subunidad del complejo IV que,

equivocadamente, estaba adscrita al complejo I. Experimentos con líneas mutantes especificas de los complejos apoyan esta teoría. Así pues, células mutantes del complejo I siguen manteniendo NDUFA4 a nivel del complejo IV. Al contrario, en mutantes del complejo IV, que no pueden ensamblar este complejo, NDUFA4 desaparece. Estos resultados conllevan ciertas implicaciones; (1) Se requiere una nueva redefinición tanto de la estructura del complejo I, como del complejo IV. (2) A partir de ahora se debe incluir a NDUFA4 como un gen candidato en deficiencias humanas del complejo IV. (3) Ya que el complejo IV fue cristalizado hace mas de una década, y no se encontró ni rastro de esta proteína, sería importante la repetición de ese cristal utilizando otros medios de extracción y purificación del complejo para adecuar los datos que hemos obtenido.

La purificación con detergentes afecta a la posición de NDUFA4:

Como acabamos de comentar, la estructura por cristalografía de rayos X del complejo IV fue resuelta al final de la década de los 90 (Tsukihara et al. 1996; Iwata et al. 1998). Dicha estructura reveló 13 proteinas distintas, cinco fosfatidil etanolaminas, tres fosfatidil gliceroles, dos colatos, dos grupos hemo, tres iones de cobre, uno de magnesio y uno de zinc. Lamentablemente NDUFA4 no fue hallada. Nuestra hipótesis es que NDUFA4 se debe perder durante la purificación del complejo a la hora de generar un cristal lo más limpio posible. Para la obtención de los cristales, las muestras se purifican utilizando unas condiciones bastante rigurosas a base de diversos detergentes. Uno de los detergentes comúnmente utilizados es el n-dodecil β-D maltósido. Hemos demostrado que concentraciones crecientes de este detergente hacen que NDUFA4 desaparezca del complejo IV, lo que refuerza nuestra hipótesis y da un toque de alarma a los protocolos de cristalización, ya que muchas proteínas pueden estar perdiéndose, sobre todo para aquellas con un alto índice de hidrofobicidad.

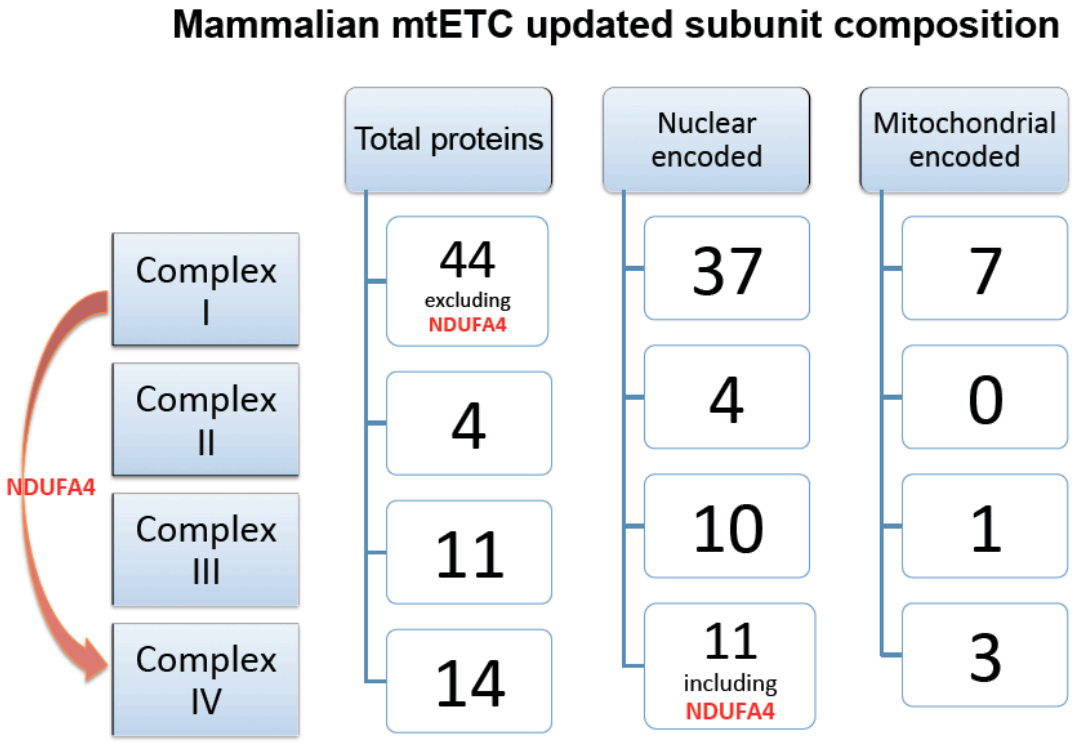

Modelo 2. Cambio en la adscripción de la proteína NDUFA4. Estando mal clasificada en el complejo I, nuestros resultados la incluirían ahora en el complejo IV.

NDUFA4 y la regulación del complejo IV en hipoxia.

Dado que el silenciamiento de NDUFA4 reduce los niveles del complejo IV, su función parece estar relacionada con la biogénesis y estabilidad de este complejo. Nuestra observación de que NDUFA4 disminuye en hipoxia junto con la actividad del complejo IV parece una correlación demasiado fuerte como para que sea pura casualidad, lo que nos hace pensar que ambos procesos están relacionados. Así pues, no es temerario pensar que la disminución en hipoxia de NDUFA4 a nivel de proteína puede ser el desencadenante de la disminución en la actividad del complejo IV que nosotros, y otros grupos, han observado (Fukuda et al. 2007). Esta especulación requerirá de futuros experimentos, que irán encaminados, primero, a determinar el factor encargado de reducir los niveles de la proteína NDUFA4 y segundo, si la disminución de la actividad y quizás de la cantidad del complejo IV son totalmente debidos a este proceso.

Conclusiones

Conclusiones

1. NDUFA4L2 es un nuevo gen diana de HIF que se localiza en la mitocondria.
2. La inducción de DUFA4L2 disminuye el consumo de oxígeno inhibiendo la actividad del complejo I.
3. NDUFA4L2 es un componente esencial en la respuesta a hipoxia ya que disminuye los niveles de ROS intracelulares.
4. Los ratones homocigotos KO de NDUFA4L2 manifiestan una letalidad perinatal.
5. NDUFA4 interacciona con proteínas del complejo IV y no con las del I.
6. El silenciamiento de NDUFA4 afecta tanto a la cantidad de complejo IV como a su actividad.
7. Se debe incluir a NFUFA4 como un gen candidato en deficiencias humanas de complejo IV.
8. Paralelamente a la inducción de NDUFA4L2, los niveles de la proteína NDUFA4 disminuyen significativamente en hipoxia.

Bibliografía

Bibliografía

Acín-Pérez, R. et al., 2011. Protein Phosphorylation and Prevention of Cytochrome Oxidase Inhibition by ATP: Coupled Mechanisms of Energy Metabolism Regulation. *Cell Metabolism*, 13(6), pp.712–719.

Acín-Pérez, R. et al., 2008. Respiratory Active Mitochondrial Supercomplexes. *Molecular Cell*, 32(4), pp.529–539.

Acín-Pérez, R. et al., 2004. Respiratory complex III is required to maintain complex I in mammalian mitochondria. *Molecular Cell*, 13(6), pp.805–815.

Ackrell, B.A., 2000. Progress in understanding structure-function relationships in respiratory chain complex II. *FEBS letters*, 466(1), pp.1–5.

Aldakkak, M. et al., 2008. Inhibited mitochondrial respiration by amobarbital during cardiac ischaemia improves redox state and reduces matrix Ca2+ overload and ROS release. *Cardiovascular Research*, 77(2), pp.406–415.

Anderson, S. et al., 1981. Sequence and organization of the human mitochondrial genome. *Nature*, 290(5806), pp.457–465.

Aragonés, J. et al., 2008. Deficiency or inhibition of oxygen sensor Phd1 induces hypoxia tolerance by reprogramming basal metabolism. *Nature genetics*, 40(2), pp.170–180.

Aragonés, J. et al., 2009. Oxygen Sensors at the Crossroad of Metabolism. *Cell Metabolism*, 9(1), pp.11–22.

Arany, Z. et al., 1996. An essential role for p300/CBP in the cellular response to hypoxia. *Proceedings of the National Academy of Sciences of the United States of America*, 93(23), pp.12969–12973.

Arnold, S. & Kadenbach, B., 1997. Cell respiration is controlled by ATP, an allosteric inhibitor of cytochrome-c oxidase. *European journal of biochemistry / FEBS*, 249(1), pp.350–354.

Attardi, G. & Schatz, G., 1988. Biogenesis of mitochondria. *Annual review of cell biology*, 4, pp.289–333.

Bennett, H.P. et al., 1990. The amino acid sequence of chymodenin, a hormone-like peptide from porcine duodenum, is identical to cytochrome C-oxidase, peptide VII. *Regulatory peptides*, 29(2-3), pp.241–250.

Berra, E. et al., 2003. HIF prolyl-hydroxylase 2 is the key oxygen sensor setting low steady-state levels of HIF-1alpha in normoxia. *The EMBO journal*, 22(16), pp.4082–4090.

Berra, E. et al., 2001. Hypoxia-inducible factor-1 alpha (HIF-1 alpha) escapes O(2)-driven proteasomal degradation irrespective of its subcellular localization: nucleus or cytoplasm. *EMBO reports*, 2(7), pp.615–620.

Berry, E.A. et al., 2000. Structure and function of cytochrome bc complexes. *Annual Review of Biochemistry*, 69, pp.1005–1075.

Boekema, E.J. & Braun, H.-P., 2007. Supramolecular structure of the mitochondrial oxidative phosphorylation system. *The Journal of biological chemistry*, 282(1), pp.1–4.

Boyer, P.D., 1993. The binding change mechanism for ATP synthase--some probabilities and possibilities. *Biochimica et biophysica acta*, 1140(3), pp.215–250.

Bruick, R.K. & McKnight, S.L., 2001. A conserved family of prolyl-4-hydroxylases that modify HIF. *Science*, 294(5545), pp.1337–1340.

Brunelle, J.K. et al., 2005. Oxygen sensing requires mitochondrial ROS but not oxidative phosphorylation. *Cell Metabolism*, 1(6), pp.409–414.

Cabezón, E. et al., 2003. The structure of bovine F1-ATPase in complex with its regulatory protein IF1. *Nature structural biology*, 10(9), pp.744–750.

Capaldi, R.A., 1990. Structure and assembly of cytochrome c oxidase. *Archives of biochemistry and biophysics*, 280(2), pp.252–262.

Carroll, J., 2002. Definition of the Nuclear Encoded Protein Composition of Bovine Heart Mitochondrial Complex I. IDENTIFICATION OF TWO NEW SUBUNITS. *Journal of Biological Chemistry*, 277(52), pp.50311–50317.

Carroll, J. et al., 2006. Bovine complex I is a complex of 45 different subunits. *The Journal of biological chemistry*, 281(43), pp.32724–32727.

Cavalier-Smith, T., 1987. Eukaryotes with no mitochondria. *Nature*, 326(6111), pp.332–333.

Cecchini, G., 2003. Function and structure of complex II of the respiratory chain. *Annual Review of Biochemistry*, 72, pp.77–109.

Chen, Q., Moghaddas, S., Hoppel, C.L. & Lesnefsky, E.J., 2006a. Reversible blockade of electron transport during ischemia protects mitochondria and decreases myocardial injury following reperfusion. *The Journal of pharmacology and experimental therapeutics*, 319(3), pp.1405–1412.

Chen, Q., Hoppel, C.L. & Lesnefsky, E.J., 2006b. Blockade of electron transport before cardiac ischemia with the reversible inhibitor amobarbital protects rat heart mitochondria. *The Journal of pharmacology and experimental therapeutics*, 316(1), pp.200–207.

Chen, Y.-C. et al., 2012. Identification of a Protein Mediating Respiratory Supercomplex Stability. *Cell Metabolism*, 15(3), pp.348–360.

Chen, Z. et al., 2010. Hypoxia-regulated microRNA-210 modulates mitochondrial function and decreases ISCU and COX10 expression. *Oncogene*, 29(30), pp.4362–4368.

Clayton, D.A., 1982. Replication of animal mitochondrial DNA. *Cell*, 28(4), pp.693–705.

Cruciat, C.M. et al., 2000. The cytochrome bc1 and cytochrome c oxidase complexes associate to form a single supracomplex in yeast mitochondria. *The Journal of biological chemistry*, 275(24), pp.18093–18098.

D'Aurelio, M. et al., 2006. Respiratory chain supercomplexes set the threshold for respiration defects in human mtDNA mutant cybrids. *Human Molecular Genetics*, 15(13), pp.2157–2169.

Davis, K.A. & Hatefi, Y., 1972. Resolution and reconstitution of complex II (succinate-ubiquinone reductase) by salts. *Archives of biochemistry and biophysics*, 149(2), pp.505–512.

del Peso, L. et al., 2003. The von Hippel Lindau/hypoxia-inducible factor (HIF) pathway regulates the transcription of the HIF-proline hydroxylase genes in response to low oxygen. *The Journal of biological chemistry*, 278(49), pp.48690–48695.

Denko, N.C., 2008. Hypoxia, HIF1 and glucose metabolism in the solid tumour. *Nature reviews. Cancer*, 8(9), pp.705–713.

Diaz, F. et al., 2006. Cytochrome c oxidase is required for the assembly/stability of respiratory complex I in mouse fibroblasts. *Molecular and Cellular Biology*, 26(13), pp.4872–4881.

Ebert, B.L. & Bunn, H.F., 1998. Regulation of transcription by hypoxia requires a multiprotein complex that includes hypoxia-inducible factor 1, an adjacent transcription factor, and p300/CREB binding protein. *Molecular and Cellular Biology*, 18(7), pp.4089–4096.

Efremov, R.G. & Sazanov, L.A., 2011. Structure of the membrane domain of respiratory complex I. *Nature*, pp.1–9.

Epstein, A.C. et al., 2001. C. elegans EGL-9 and mammalian homologs define a family of dioxygenases that regulate HIF by prolyl hydroxylation. *Cell*, 107(1), pp.43–54.

Eubel, H., Heinemeyer, J. & Braun, H.-P., 2004. Identification and characterization of respirasomes in potato mitochondria. *Plant physiology*, 134(4), pp.1450–1459.

Ewart, G. et al., 1990. Tissue specificity and defects in human cytochrome c oxidase. *Biochimica et biophysica acta*, 1018(2-3), pp.223–224.

Fernández-Vizarra, E., Tiranti, V. & Zeviani, M., 2009. Assembly of the oxidative phosphorylation system in humans: What we have learned by studying its defects. *BBA - Molecular Cell Research*, 1793(1), pp.200–211.

Firth, J.D. et al., 1994. Oxygen-regulated control elements in the phosphoglycerate kinase 1 and lactate dehydrogenase A genes: similarities with the erythropoietin 3' enhancer. *Proceedings of the National Academy of Sciences of the United States of America*, 91(14), pp.6496–6500.

Firth, J.D., Ebert, B.L. & Ratcliffe, P.J., 1995. Hypoxic regulation of lactate dehydrogenase A. Interaction between hypoxia-inducible factor 1 and cAMP response elements. *The Journal of biological chemistry*, 270(36), pp.21021–21027.

Fukuda, R. et al., 2007. HIF-1 Regulates Cytochrome Oxidase Subunits to Optimize Efficiency of Respiration in Hypoxic Cells. *Cell*, 129(1), pp.111–122.

Futai, M., Noumi, T. & Maeda, M., 1989. ATP synthase (H+-ATPase): results by combined biochemical and molecular biological approaches. *Annual Review of Biochemistry*, 58, pp.111–136.

Garbian, Y. et al., 2010. Gene Expression Patterns of Oxidative Phosphorylation Complex I Subunits Are Organized in Clusters J. Hoheisel, ed. *PLoS ONE*, 5(4), p.e9985.

Gardner, L.B., 2000. Hypoxia Inhibits G1/S Transition through Regulation of p27 Expression. *Journal of Biological Chemistry*, 276(11), pp.7919–7926.

Genova, M.L., Bianchi, C. & Lenaz, G., 2005. Supercomplex organization of the mitochondrial respiratory chain and the role of the Coenzyme Q pool: pathophysiological implications. *BioFactors (Oxford, England)*, 25(1-4), pp.5–20.

Goda, N. et al., 2003. Hypoxia-inducible factor 1alpha is essential for cell cycle arrest during hypoxia. *Molecular and Cellular Biology*, 23(1), pp.359–369.

Grigorieff, N., 1998. Three-dimensional structure of bovine NADH:ubiquinone oxidoreductase (complex I) at 22 A in ice. *Journal of Molecular Biology*, 277(5), pp.1033–1046.

Grossman, L.I. & Lomax, M.I., 1997. Nuclear genes for cytochrome c oxidase. *Biochimica et biophysica acta*, 1352(2), pp.174–192.

Guzy, R.D. et al., 2005. Mitochondrial complex III is required for hypoxia-induced ROS production and cellular oxygen sensing. *Cell Metabolism*, 1(6), pp.401–408.

Hackenbrock, C.R., Chazotte, B. & Gupte, S.S., 1986. The random collision model and a critical assessment of diffusion and collision in mitochondrial electron transport. *Journal of bioenergetics and biomembranes*, 18(5), pp.331–368.

Hägerhäll, C., 1997. Succinate: quinone oxidoreductases. Variations on a conserved theme. *Biochimica et biophysica acta*, 1320(2), pp.107–141.

Hewitson, K.S. et al., 2002. Hypoxia-inducible factor (HIF) asparagine hydroxylase is identical to factor inhibiting HIF (FIH) and is related to the cupin structural family. *The Journal of biological chemistry*, 277(29), pp.26351–26355.

Hirsilä, M. et al., 2003. Characterization of the human prolyl 4-hydroxylases that modify the hypoxia-inducible factor. *The Journal of biological chemistry*, 278(33), pp.30772–30780.

Hon, W.-C. et al., 2002. Structural basis for the recognition of hydroxyproline in HIF-1 alpha by pVHL. *Nature*, 417(6892), pp.975–978.

Huang, L.E. et al., 1996. Activation of hypoxia-inducible transcription factor depends primarily upon redox-sensitive stabilization of its alpha subunit. *The Journal of biological chemistry*, 271(50), pp.32253–32259.

Iwata, S. et al., 1998. Complete structure of the 11-subunit bovine mitochondrial cytochrome bc1 complex. *Science*, 281(5373), pp.64–71.

Iyer, N.V. et al., 1998. Cellular and developmental control of O2 homeostasis by hypoxia-inducible factor 1 alpha. *Genes & Development*, 12(2), pp.149–162.

Jaakkola, P. et al., 2001. Targeting of HIF-alpha to the von Hippel-Lindau ubiquitylation complex by O2-regulated prolyl hydroxylation. *Science*, 292(5516), pp.468–472.

Jelkmann, W., 1992. Erythropoietin: structure, control of production, and function. *Physiological reviews*, 72(2), pp.449–489.

Jiang, B.H. et al., 1996. Dimerization, DNA binding, and transactivation properties of hypoxia-inducible factor 1. *The Journal of biological chemistry*, 271(30), pp.17771–17778.

Kaelin, W.G., Jr. & Ratcliffe, P.J., 2008. Oxygen Sensing by Metazoans: The Central Role of the HIF Hydroxylase Pathway. *Molecular Cell*, 30(4), pp.393–402.

Kamura, T. et al., 1999. Rbx1, a component of the VHL tumor suppressor complex and SCF ubiquitin ligase. *Science*, 284(5414), pp.657–661.

Kennaway, N.G. et al., 1990. Isoforms of mammalian cytochrome c oxidase: correlation with human cytochrome c oxidase deficiency. *Pediatric research*, 28(5), pp.529–535.

Kim, J.-W. et al., 2006. HIF-1-mediated expression of pyruvate dehydrogenase kinase: A metabolic switch required for cellular adaptation to hypoxia. *Cell Metabolism*, 3(3), pp.177–185.

Korshunov, S.S., Skulachev, V.P. & Starkov, A.A., 1997. High protonic potential actuates a mechanism of production of reactive oxygen species in mitochondria. *FEBS letters*, 416(1), pp.15–18.

Kruse, S.E. et al., 2008. Mice with Mitochondrial Complex I Deficiency Develop a Fatal Encephalomyopathy. *Cell Metabolism*, 7(4), pp.312–320.

Lando, D. et al., 2002. FIH-1 is an asparaginyl hydroxylase enzyme that regulates the transcriptional activity of hypoxia-inducible factor. *Genes & Development*, 16(12), pp.1466–1471.

Li, Y. et al., 2006. Cytochrome c oxidase subunit IV is essential for assembly and respiratory function of the enzyme complex. *Journal of bioenergetics and biomembranes*, 38(5-6), pp.283–291.

Liu, Y., Fiskum, G. & Schubert, D., 2002. Generation of reactive oxygen species by the mitochondrial electron transport chain. *Journal of neurochemistry*, 80(5), pp.780–787.

Loenarz, C. et al., 2011. The hypoxia-inducible transcription factor pathway regulates oxygen sensing in the simplest animal, Trichoplax adhaerens. *EMBO reports*, 12(1), pp.63–70.

Lutter, R. et al., 1993. Crystallization of F1-ATPase from bovine heart mitochondria. *Journal of Molecular Biology*, 229(3), pp.787–790.

Mick, D.U., Fox, T.D. & Rehling, P., 2011. Inventory control: cytochrome c oxidase assembly regulates mitochondrial translation. *Nature Publishing Group*, 12(1), pp.14–20.

Min, J.-H. et al., 2002. Structure of an HIF-1alpha -pVHL complex: hydroxyproline recognition in signaling. *Science*, 296(5574), pp.1886–1889.

MITCHELL, P., 1961. Coupling of phosphorylation to electron and hydrogen transfer by a chemi-osmotic type of mechanism. *Nature*, 191, pp.144–148.

MITCHELL, P. & Moyle, J., 1967. Chemiosmotic hypothesis of oxidative phosphorylation. *Nature*, 213(5072), pp.137–139.

Murphy, M.P., 2009. How mitochondria produce reactive oxygen species. *Biochemical Journal*, 417(1), p.1.

Murphy, M.P. et al., 2011. Unraveling the Biological Roles of Reactive Oxygen Species. *Cell Metabolism*, 13(4), pp.361–366.

Oyedotun, K.S. & Lemire, B.D., 2001. The Quinone-binding sites of the Saccharomyces cerevisiae succinate-ubiquinone oxidoreductase. *The Journal of biological chemistry*, 276(20), pp.16936–16943.

Papandreou, I. et al., 2006. HIF-1 mediates adaptation to hypoxia by actively downregulating mitochondrial oxygen consumption. *Cell Metabolism*, 3(3), pp.187–197.

Pugh, C.W. et al., 1997. Activation of hypoxia-inducible factor-1; definition of regulatory domains within the alpha subunit. *The Journal of biological chemistry*, 272(17), pp.11205–11214.

Raha, S. & Robinson, B.H., 2000. Mitochondria, oxygen free radicals, disease and ageing. *Trends in Biochemical Sciences*, 25(10), pp.502–508.

Sagan, L., 1967. On the origin of mitosing cells. *Journal of theoretical biology*, 14(3), pp.255–274.

Sazanov, L.A. & Hinchliffe, P., 2006. Structure of the hydrophilic domain of respiratory complex I from Thermus thermophilus. *Science*, 311(5766), pp.1430–1436.

Sazanov, L.A. et al., 2000. Resolution of the membrane domain of bovine complex I into subcomplexes: implications for the structural organization of the enzyme. *Biochemistry*, 39(24), pp.7229–7235.

Schägger, H. & Pfeiffer, K., 2000. Supercomplexes in the respiratory chains of yeast and mammalian mitochondria. *The EMBO journal*, 19(8), pp.1777–1783.

Schägger, H. et al., 1986. Isolation of the eleven protein subunits of the bc1 complex from beef heart. *Methods in enzymology*, 126, pp.224–237.

Schägger, H. et al., 2004. Significance of respirasomes for the assembly/stability of human respiratory chain complex I. *The Journal of biological chemistry*, 279(35), pp.36349–36353.

Scortegagna, M. et al., 2003. Multiple organ pathology, metabolic abnormalities and impaired homeostasis of reactive oxygen species in Epas1-/- mice. *Nature genetics*, 35(4), pp.331–340.

Semenza, G.L., 2001. Hypoxia-inducible factor 1: oxygen homeostasis and disease pathophysiology. *Trends in molecular medicine*, 7(8), pp.345–350.

Semenza, G.L., 2000. Surviving ischemia: adaptive responses mediated by hypoxia-inducible factor 1. *The Journal of clinical investigation*, 106(7), pp.809–812.

Seta, K.A. et al., 2002. Responding to hypoxia: lessons from a model cell line. *Science's STKE : signal transduction knowledge environment*, 2002(146), p.re11.

St-Pierre, J. et al., 2002. Topology of superoxide production from different sites in the mitochondrial electron transport chain. *The Journal of biological chemistry*, 277(47), pp.44784–44790.

Stock, D., Leslie, A.G. & Walker, J.E., 1999. Molecular architecture of the rotary motor in ATP synthase. *Science*, 286(5445), pp.1700–1705.

Taanman, J.W., Turina, P. & Capaldi, R.A., 1994. Regulation of cytochrome c oxidase by interaction of ATP at two binding sites, one on subunit VIa. *Biochemistry*, 33(39), pp.11833–11841.

Taylor, C.T., 2008. Mitochondria and cellular oxygen sensing in the HIF pathway. *Biochemical Journal*, 409(1), pp.19–26.

Taylor, C.T. & McElwain, J.C., 2010. Ancient Atmospheres and the Evolution of Oxygen Sensing Via the Hypoxia-Inducible Factor in Metazoans. *Physiology*, 25(5), pp.272–279.

Tong, W.-H. & Rouault, T.A., 2006. Functions of mitochondrial ISCU and cytosolic ISCU in mammalian iron-sulfur cluster biogenesis and iron homeostasis. *Cell Metabolism*, 3(3), pp.199–210.

Tsukihara, T. et al., 1995. Structures of metal sites of oxidized bovine heart cytochrome c oxidase at 2.8 A. *Science*, 269(5227), pp.1069–1074.

Tsukihara, T. et al., 1996. The whole structure of the 13-subunit oxidized cytochrome c oxidase at 2.8 A. *Science*, 272(5265), pp.1136–1144.

Vogel, R. et al., 2004. Complex I assembly: a puzzling problem. *Current opinion in neurology*, 17(2), pp.179–186.

Vogel, R.O., Smeitink, J.A.M. & Nijtmans, L.G.J., 2007. Human mitochondrial complex I assembly: a dynamic and versatile process. *Biochimica et biophysica acta*, 1767(10), pp.1215–1227.

Vonck, J. & Schäfer, E., 2009. Supramolecular organization of protein complexes in the mitochondrial inner membrane. *Biochimica et biophysica acta*, 1793(1), pp.117–124.

Votyakova, T.V. & Reynolds, I.J., 2001. DeltaPsi(m)-Dependent and -independent production of reactive oxygen species by rat brain mitochondria. *Journal of neurochemistry*, 79(2), pp.266–277.

Vukotic, M. et al., 2012. Rcf1 Mediates Cytochrome Oxidase Assembly and Respirasome Formation, Revealing Heterogeneity of the Enzyme Complex. *Cell Metabolism*, pp.1–12.

Walker, J.E., 1992. The NADH:ubiquinone oxidoreductase (complex I) of respiratory chains. *Quarterly reviews of biophysics*, 25(3), pp.253–324.

Walker, J.E. et al., 1992. Sequences of 20 subunits of NADH:ubiquinone oxidoreductase from bovine heart mitochondria. Application of a novel strategy for sequencing proteins using the polymerase chain reaction. *Journal of Molecular Biology*, 226(4), pp.1051–1072.

Wenger, R.H., 2002. Cellular adaptation to hypoxia: O2-sensing protein hydroxylases, hypoxia-inducible transcription factors, and O2-regulated gene expression. *The FASEB Journal*, 16(10), pp.1151–1162.

Yoshikawa, S., 1997. Beef heart cytochrome c oxidase. *Current opinion in structural biology*, 7(4), pp.574–579.

Zaslavsky, D. & Gennis, R.B., 2000. Proton pumping by cytochrome oxidase: progress, problems and postulates. *Biochimica et biophysica acta*, 1458(1), pp.164–179.

Zhang, H. et al., 2008. Mitochondrial autophagy is an HIF-1-dependent adaptive metabolic response to hypoxia. *The Journal of biological chemistry*, 283(16), pp.10892–10903.